

Molecular Descriptor on the Basis of Structural Analysis
in Ion Mobility-Mass Spectrometry

By

Caleb Bryce Morris

Dissertation

Submitted to the Faculty of the
Graduate School of Vanderbilt University
in partial fulfillment of the requirements

for the degree of

DOCTOR OF PHILOSOPHY

in

Chemistry

May 10, 2019

Nashville, Tennessee

Approved:

John A. McLean, Ph.D.

Brian O. Bachmann, Ph.D.

Nathan D. Schley, Ph.D.

Richard F. Haglund, Ph.D.

To my wife, Heather, quick to encourage with a smile or laugh

and

To my parents, ever supportive, wise, and loving

ACKNOWLEDGEMENTS

I would like to acknowledge Dr. John A. McLean for his generosity in allowing me to work on projects that interested me. Thank-you for the opportunities you have given me to learn and grow as a scientist and teacher. You have challenged me in many ways for which I am grateful. Graduate school is a time to gain wisdom, not just knowledge. The doors you opened provided an excellent resource for both.

I would like to thank my stellar committee, Dr. John A. McLean, Dr. Brian O. Bachmann, Dr. Nathan D. Schley, and Dr. Richard F. Haglund, for their time and advice. The viewpoints each of you have brought to each meeting have been valuable in my future scientific enquiries. Your thoughtfulness, thorough questioning, and considerate advice is appreciated. I recognize you have busy schedules and am honored that you took the time to meet with me and share your insight.

I would like to thank Dr. Jody C. May for his mentorship. This experience would not have been as profitable without your guidance and advice. Your ability to relay difficult concepts has been crucial in my development as a scientist and I owe much of my success to your wisdom. Seeing your approach to challenges helped me grow as a scientist. I learned so much from our many conversations and cannot thank you enough for be willing to advise and challenge me every day.

I would like to acknowledge all the lab members past and present who have taken the time to read my horrendous first drafts and listen to my rough presentations. Your fresh perspective and support has helped me tremendously, as I was challenged to deliver scientific knowledge in a clear, concise format. I appreciate the many conversations we have had. Those discussions challenged

my knowledge and my thought process. I have learned so much from you. The kindness and generosity you show each day make this an enjoyable work environment.

I owe my family a debt of gratitude. Dad, you always took the opportunity to impart wisdom, and the example you have been continues to challenge me. I often went to you for advice, though you didn't always know it. When encountering the inevitable difficulties, I would recall your instruction. I didn't forget your teaching and found stability such wisdom provided. Mom, I know I wasn't the easiest student to teach. Your perseverance and patience are a testament to how much you cared. The educational opportunities you worked hard to provide, even when told they would come to naught, have benefitted me immensely. I can say with utmost confidence that I would never have arrived at this point without the teaching, support, and dedication you both selflessly put forth. I cannot express how important that has been to me. Thank-you from the bottom of my heart.

To my wife, your presence on this journey has been one of the most important factors in my success. Graduate school is full of ups and downs and I would not have made it through without your constant support. I appreciate your patience through my odd hours and late nights. You have sacrificed so much for me, taking care of me and our wonderful son. Thank-you is not enough.

Finally, I would like to acknowledge my sources of funding, without which such work would not be possible. This work was supported in part using the resources of the Center for Innovative Technology at Vanderbilt University. Financial support for this work was generously provided by the Vanderbilt Center for Quantitative Sciences under a CQS pilot project award, the National Institutes of Health (NIH R01GM092218 and NCI R03CA222-452-01), the U.S. Army Research Office and the Defense Advanced Research Projects Agency (DARPA) under Cooperative Agreement Number W911 NF-14-2-0022, the U.S. Environmental Protection Agency

(EPA) under Assistance Agreement No. 83573601, the NIH National Center for Advancing Translational Sciences (UH2TR000491), the Defense Threat Reduction Agency (HDTRA1-09-1-00-13 and DTRA100271 A-5196), the Defense Advanced Research Projects Agency (W911 NF-12-2-0036), the Vanderbilt Institute of Chemical Biology, and the Vanderbilt Institute for Integrative Biosystems Research and Education.. This work has not been formally reviewed by EPA and EPA does not endorse any products or commercial services mentioned in this publication. The views expressed in this document are solely those of the authors and should not be interpreted as representing the official policies, either expressed or implied, of the EPA, the Army Research Office, DARPA, or the U.S. Government.

TABLE OF CONTENTS

	Page
DEDICATION	ii
ACKNOWLEDGEMENTS	iii
LIST OF TABLES	ix
LIST OF FIGURES	x
LIST OF ABBREVIATIONS.....	xii
Chapter	
1. Fundamentals of Ion Mobility-Mass Spectrometry for the Analysis of Biomolecules	1
1.1. Statement of Thesis.....	1
1.2. Origins of Biomolecular Analysis by Ion Mobility-Mass Spectrometry	2
1.3. Biomolecular Separation and Analytical Utility of IM-MS	4
1.4. Instrumentation Considerations	9
1.4.1. Chromatography	9
1.4.2. Ion Sources.....	11
1.4.3. Time-Dispersive Ion Mobility Techniques	12
1.4.4. Mass Spectrometry Considerations.....	14
1.5. Introduction to Current Trends	15
1.6. Integrating Ion Mobility for Omic Analysis	16
1.6.1. Proteomics.....	18
1.6.2. Lipidomics	20
1.6.3. Metabolomics.....	21
1.7. Continuing Advancements in IM-MS Technology.....	26
1.8. Combining Discrete Omic Databases for Multi-Omic Experiments	32
1.9. Statement of Dissertation.....	34
1.10. Acknowledgements.....	37
1.11. References.....	38
2. An Ion Mobility Collision Cross Section Compendium.....	47
2.1. Introduction.....	47
2.2. The Collision Cross Section.....	50
2.3. Significant CCS Contributions	53
2.4. Drift Gases Represented	55
2.5. Composition of Measurements	58

2.6.	Chemical Space Represented by IM-MS Analysis	61
2.7.	CCS Coverage over Time	65
2.8.	Concluding Remarks.....	70
2.9.	Acknowledgements.....	71
2.10.	References.....	72
3.	Untargeted Molecular Discovery in Primary Metabolism: Collision Cross Section as a Molecular Descriptor in Ion Mobility-Mass Spectrometry	86
3.1.	Introduction.....	86
3.2.	Experimental Methods	88
3.2.1.	MSMLS Sample Preparation	88
3.2.2.	Collision Cross Section Measurements	89
3.2.3.	IM-MS Source and Drift Cell Conditions.....	90
3.2.4.	Nonlinear Regression Analysis.....	91
3.2.5.	Human Serum Preparation.....	91
3.2.6.	Liquid Chromatography.....	92
3.3.	Results and Discussion	92
3.3.1.	MSMLS Plate Coverage	92
3.3.2.	Mass-Mobility Correlation Analysis.....	94
3.3.3.	Metabolic Pathway Coverage	94
3.3.4.	Isomers in Metabolomics.....	95
3.3.5.	IM-MS Separation in Primary Metabolites.....	99
3.3.6.	LC-IM-MS Characterization of NIST 1950 Serum	102
3.4.	Conclusions.....	105
3.5.	Acknowledgements.....	106
3.6.	References.....	107
4.	Conformational Ordering of Biomolecules in the Gas Phase: Nitrogen Collision Cross-Sections Measured on a Prototype High Resolution Drift Tube Ion Mobility-Mass Spectrometer.....	111
4.1.	Introduction.....	111
4.2.	Experimental Methods	113
4.2.1.	Preparation of Standards	113
4.2.1.1.	Lipids	113
4.2.1.2.	Carbohydrates	114
4.2.1.3.	Peptides.....	114
4.2.1.4.	Quaternary Ammonium Salts	115
4.2.2.	Instrumentation	115
4.2.3.	Experimental Parameters	117
4.2.4.	Collision Cross-Section Calculations	118
4.3.	Results and Discussion	119
4.3.1.	Database Description and General Cross-Section Trends in Nitrogen.....	119
4.3.2.	Description of the Fits to the Empirical Data	122
4.3.3.	Extraction of Sub-Trend Information from the Data	124
4.3.4.	Comparisons between Helium and Nitrogen CCS Values	128

4.4. Conclusions.....	132
4.5. Acknowledgements.....	134
4.6. References.....	135
5. Evaluating Separation Selectivity and Collision Cross Section Measurement Reproducibility in Helium, Nitrogen, Argon, and Carbon Dioxide Drift Gases for Drift Tube Ion Mobility-Mass Spectrometry.....	138
5.1. Introduction.....	138
5.2. Methods.....	141
5.2.1. Instrumentation	141
5.2.2. Variable Pressure Experiments	143
5.2.3. Effective Length.....	144
5.2.4. Chemical Standards	144
5.3. Results and Discussion	145
5.3.1. Analyte Selection.....	145
5.3.2. Pressure Effects.....	147
5.3.3. Ion Source Temperature Effects	150
5.3.4. Ion Injection Potential.....	150
5.3.5. CCS Measurements.....	151
5.3.6. Chemical Class Behavior.....	153
5.3.7. Drift Gas Selection Criteria	156
5.4. Conclusion	158
5.5. Acknowledgements.....	159
5.6. References.....	161
6. Conclusion and Future Directions	165
6.1. Conclusion	165
6.2. Future Directions	167
6.2.1. Mathematical Descriptors in Databases.....	167
6.2.2. CCS Prediction.....	168
6.2.3. Drift Gas Selection.....	170
6.3. References.....	174
Appendix	
A. References for Adaptation of Chapters.....	175
B. Supplemental Information for Chapter 3	176
C. Supplemental Information for Chapter 4	183
D. Supplemental Information for Chapter 5	213
E. Curriculum Vitae	231

LIST OF TABLES

Table	Page
1.1. Three Key Analytical Uses of Ion Mobility	6
2.1. Three Key Analytical Uses of Ion Mobility	49
2.2. Formalized Nomenclature for CCS Reporting	52
4.1. Summary of Statistics Related to the CCS Database.....	120
4.2. TAA Salts Compared to Literature Values	121

LIST OF FIGURES

Figure	Page
1.1. Historical Developments in Ion Mobility (IM) Technologies	3
1.2. Historical Chemical Class Representation.....	5
1.3. Molecular Class Trends	8
1.4. Nesting of Analytical Timescales	10
1.5. Temporally-Dispersive Ion Mobility Techniques.....	13
1.6. IM-MS Analysis Workflow	17
1.7. IM-MS Data Acquisition and Basic Principles.....	19
1.8. Schematic Visualization of Data Acquisition	22
1.9. Example 2D IM-MS Image	25
1.10. SLIM SUPER IM-MS Instrument Schematic.....	28
1.11. Spatial Multiplexing.....	30
1.12. Mitochondrial Shuttles.....	33
2.1. Number of CCS Values Published in 40-Year Span	54
2.2. Number of CCS Values Reported Per Publication	56
2.3. Composition of CCS Values	59
2.4. Helium-Specific Conformational Space Plot.....	62
2.5. Nitrogen-Specific Conformational Space Plot.....	63
2.6. Mass Distribution of CCS Values.....	66
2.7. Historical Chemical Class Representation.....	68
3.1. Biological Category Distribution.....	93

3.2. Metabolite Pathway Coverage	96
3.3. Isomer Separation	98
3.4. Separation Strategy Comparison.....	101
3.5. NIST 1950 Human Serum Sample	103
4.1. Prototype Instrument Schematic	116
4.2. Scatter Plot of CCS Values	123
4.3. Sub-Class Analysis of Carbohydrates.....	126
4.4. Sub-Class Analysis of Lipids.....	127
4.5. Helium and Nitrogen CCS Comparison	129
5.1. Instrument Schematic of an Agilent 6560	142
5.2. Molecular Class Mass Coverage.....	146
5.3. Cesium CCS Comparison to Literature Values	148
5.4. Drift Gas CCS Plots.....	154
5.5. Class Drift Time Profiles in Multiple Drift Gases.....	155
5.6. Class Response and Separation in Multiple Drift Gases	157
6.1. Derivation of an Equation for Drift Gas CCS Relationship	169
6.2. Drift Gas Selection.....	172

ABBREVIATIONS

4P	4-parameter sigmoidal
5P	5-parameter sigmoidal
ACN	Acetonitrile
AICc	Akaike Information Criterion
AJS	Agilent Jet Stream
APCI	Atmospheric Pressure Chemical Ionization
CCS	Collision Cross Section
CID	Collision Induced Dissociation
DARPA	Defense Advanced Research Projects Agency
DGDP	2'-deoxyguanosine-5'-diphosphate
DMA	Differential Mobility Analyzers
DMS	Differential Mobility Spectrometry
DT	Drift Tube
DTIMS	Drift Tube Ion Mobility Spectrometry
EPA	Environmental Protection Agency
ESI	Electrospray Ionization
ETD	Electron Transfer Dissociation
ExPASy	Expert Protein Analysis System
FAIMS	High-field Asymmetric Waveform Ion Mobility Spectrometry
FIA	Flow Injection Analysis
GC	Gas Chromatography

GlcCer	Glycosphingolipids
HFAP	Hexakis(fluoroalkoxy)phosphazenes
HPF	High Pressure Funnel
IM	Ion Mobility
IM-MS	Ion Mobility Mass Spectrometry
IPA	Isopropanol
LC	Liquid Chromatography
LIPID MAPS	Lipid Metabolites and Pathways Strategy
LMSD	LIPID MAPS Structure Database
m/z	Mass-to-Charge Ratio
MALDI	Matrix Assisted Laser Desorption/Ionization
MS	Mass Spectrometry
MSMLS	Mass Spectrometry Metabolite Library of Standards
NIH	National Institute of Health
NMR	Nuclear Magnetic Resonance
PC	Phosphatidylcholines
PCB	Printed Circuit Board
PE	Phosphatidylethanolamines
PF	Power Fit
PS	Phosphatidylserines
R _p	Resolving Power
R _{pp}	Peak-to-Peak Resolution
SFC	Supercritical Fluid Chromatography

SLIM	Structures for Lossless Ion Manipulations
SM	Sphingomyelins
TAA	Tetraalkylammonium
TF	Trapping Funnel
TIMS	Trapped Ion Mobility Spectrometry
TOF	Time of Flight
TWIMS	Traveling Wave Ion Mobility Spectrometry
V_{Cap}	Capillary Voltage

CHAPTER 1

FUNDAMENTALS OF ION MOBILITY-MASS SPECTROMETRY FOR THE ANALYSIS OF BIOMOLECULES

1.1 Statement of Thesis

Ion mobility (IM) is an important electrophoretic technique where gas-phase ions are separated by their collision cross section (CCS). Often, it is integrated with mass spectrometry (MS), allowing separation of both ion size and mass on millisecond timescales to create a high sensitivity, high throughput analytical technique. Reproducible properties such as CCS can be utilized as metrics for identification and characterization. Molecular size and mass scale predictably in these gas-phase measurements, creating class distinctions that aid in identification of unknowns. Databases have been curated to allow improved identification of unknowns using descriptors such as mass and size and mapping IM class trends. Large databases of canonical CCS values demonstrate current trends in IM as well as new areas of exploration that will generate a significant impact. One area that has been relatively unexplored is the effect of drift gas on CCS. It has been noted that adjusting the ion mobility drift gas can affect these class distinctions. However, large scale studies had not been performed to investigate this effect across a wide mass and mobility range. This work demonstrates the value of IM as a molecular descriptor in addition to MS, establishes signposts for under-explored areas of study through a large review housing thousands of canonical CCS values, and further investigates one of these areas, exploring the effect of drift gas selection on CCS. This work seeks to demonstrate the importance of IM and its applications. A large review of the literature spanning forty years of publications will be shown to

demonstrate the trends in the IM community. It will identify new areas of study and demonstrate the need for high quality databases for characterization of unknowns. Such a database will be given, detailing the importance of IM inclusion with MS to aid in rapid identification of isomers that can be challenging to identify with MS alone. Trends in IM that can be used for characterization of unknowns will be shown along with the effect of drift gas on class separation. A study spanning a wide range of drift gases, masses, classes, mobilities, and charge states will be presented to explore the drift gas effect on CCS separation. Instrument parameters will be established to obtain reproducible CCS values and recommendations on drift gas selection will be developed. This will give future researchers the tools to investigate drift gas effect and improve fundamental IM theory.

1.2 Origins of Biomolecular Analysis by Ion Mobility-Mass Spectrometry

Ion mobility-mass spectrometry (IM-MS) is an integrated chemical separation technique which combines complementary size- and mass-selective separations into a single analytical platform. IM-MS is capable of separating individual chemical compounds on the millisecond time scale and as such is considered a high-throughput, high-sensitivity techniques which has been applied in numerous chemical analysis applications including compounds of a biological origin. Historically, IM-MS traces its roots back to experiments by Rutherford and Thomson in the late 1890s,¹ and was further improved by Tyndall in the 1920s using pure drift gases,²⁻³ before being paired with mass spectrometry in the 1960s⁴ (Figure 1.1).⁵ Electrospray ionization (ESI) and laser ionization were coupled to IM in 1968⁶⁻⁷ and 1982,⁸ respectively, with Bowers coupling matrix assisted laser desorption/ionization (MALDI) with IM-MS in the mid-1990s.⁹ From the 1990s, MALDI and ESI coupled with IM-MS saw more widespread use as they were developed and

Historical Developments in Ion Mobility (IM) Technologies

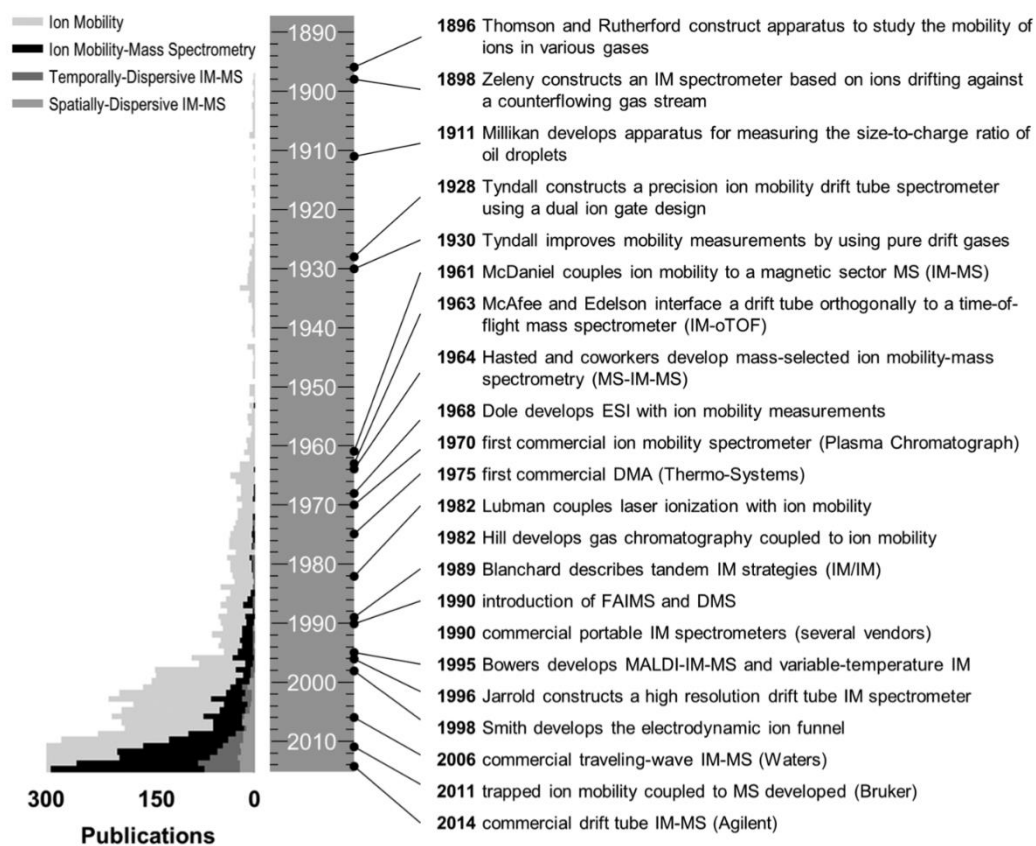


Figure 1.1 (Left) Histogram of the number of publications published per year in ion mobility and ion mobility-mass spectrometry. Note that the scale is truncated at 300 to highlight the number of publications specifically utilizing IM-MS. Further distinction is made to discriminate the frequency of publication for both time and space-dispersive IM-MS publications. (Right) Historical milestones in the development of ion mobility and IM-MS instrumentation. (Figure and legend from May, et. al.⁵)

refined for use with IM.¹⁰ These soft ionization techniques paired with IM-MS allowed for biomolecular analysis of large molecules¹¹ and the growth in the application of this technology to biomolecules is illustrated in the timeline in Figure 1.2.¹² In 2006, a commercially available ion mobility-mass spectrometer well suited for biomolecular analysis was developed by Waters Corporation, named the Synapt HDMS (traveling wave IM), which combined the soft ionization of electrospray with the rapid separation of IM and time-of-flight mass spectrometry, and supported other optional analytical capabilities including MALDI and MS imaging, as well as integration with liquid chromatography.¹³⁻¹⁵ This first commercial offering enabled a larger scientific community access to IM-MS which otherwise was only available to researchers with the capability to build their own. Other MS vendors entered the market with their own commercial IM-MS offerings, including Agilent Technologies in 2014 (drift tube IM) and Bruker Corporation in 2016 (trapped IM). With such versatile commercial instrumentation available, biomolecular analysis using IM-MS flourished and continues to be a rapidly growing field, with advances in fundamental separation techniques and broad technological application changing the analytical landscape.

1.3 Biomolecular Separation and Analytical Utility of IM-MS

IM-MS has found great utility for biomolecular separation due to its broad sample compatibility, resolution, and sensitivity. It has been used to separate and analyze a wide range of masses, from small molecules to large protein complexes.¹⁶⁻²³ The analytical importance of IM is summarized in Table 1.1.¹² Whether increasing peak capacity, reducing interference from chemical noise, or allowing for structural characterization, IM provides a broad range of analytically valuable enhancements. For example, it has been observed that biomolecular classes

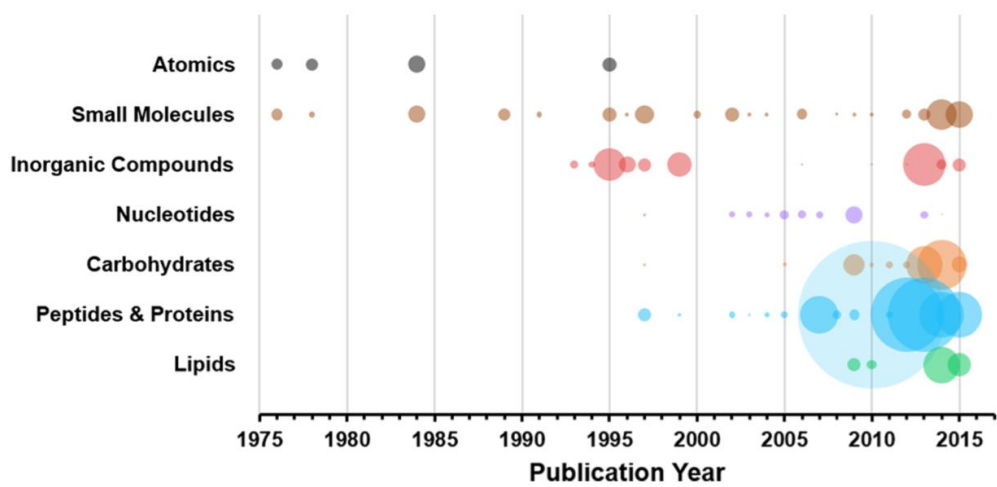


Figure 1.2 Bubble plot projecting the number of CCS values reported over time for the top 7 chemical classes represented. The size of each bubble encodes the relative number of CCS values for each respective year. (Figure and legend from May, et. al.¹²)

Table 1. Three Key Analytical Uses of Ion Mobility

analytical use of ion mobility	description	additional requirements	example application areas
1. chemical separation	partition signal from chemical noise and increase peak capacity of the analysis	none	detection of illicit compounds (e.g., drugs and explosives) and screening of exogenous metabolites (e.g., pesticides and industrial chemicals)
2. analyte identification and characterization	use CCS measurement to characterize unknowns by correlation	reference values from databases and libraries incorporating normalized drift times, reduced mobilities, and/or CCS	emerging omic and small molecule discovery initiatives
3. structural analysis	utilize the experimental CCS to infer structural information	computational methods to link theoretical structure(s) to the experimental CCS	insights into protein complex arrangements and structure

Table 1.1 from May, et. al.¹²

maintain different molecular packing efficiencies in the gas phase, which results in class-specific trend lines to develop in 2-dimensional IM-MS spectra (Figure 1.3²⁴).²⁵⁻²⁶ Notably, the canonical biochemical classes: lipids, peptides, carbohydrates, and nucleotides, align themselves into unique regions of IM-MS analytical space which reflect their conformational preferences. Within each class trend, subclass trends may also exist. Lipids have a characteristic behavior in IM-MS indicative of headgroup identity.²⁷ Lipid packing efficiency is affected by its headgroup and unsaturation within its acyl tail(s), forming differing trendlines in maps of gas phase collision cross section (CCS) versus mass. Current research is considering the effects of degree of unsaturation, double bond location, and carbon chain length on lipid packing efficiency and trendline behavior in IM.²⁸ This has made IM-MS an applicable tool for the growing field of lipidomics, where the high sensitivity and separation speeds are well suited to high throughput analyses of complex samples.²⁹⁻³⁰ Novel approaches such as ozonolysis paired with IM-MS are now being applied to lipidomics to allow for determination of double bond location in lipids.³¹⁻³² For broad scale identification of unknowns, empirically-derived databases of mass and CCS are being assembled for a variety of biomolecular compounds.^{12, 18, 23, 33-41} The IM dimension also adds valuable information beyond biomolecular class. Isobaric compounds that are unresolvable by conventional MS can be distinguished in the IM dimension due to the different conformations they adopt, whether peptides, carbohydrates, or lipids.⁴²⁻⁴⁷ Collectively, the capability to rapidly resolve biochemical based on both structure and mass differences has made IM-MS an invaluable analytical tool for biomolecular analysis.

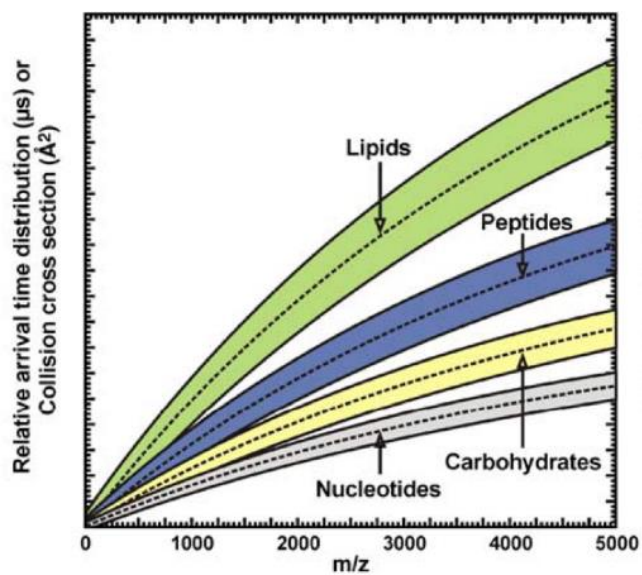


Figure 1.3 A cartoon depiction of where singly charged analytes (e.g., produced by MALDI) of different molecular classes are observed in IM–MS conformation space. (Figure and legend from Fenn, et. al.²⁴)

1.4 Instrumentation Considerations

1.4.1 Chromatography

Including a front end chromatographic separation prior to IM-MS provides added peak capacity while enhancing the analytical sensitivity by reducing ion suppression resulting from the simultaneous infusion of multiple analytes. Liquid chromatography (LC) is commonly implemented with IM-MS due to its ability to use a wide variety of flow rates, column choices, and solvents that pair well with ESI ion generation. Since the IM separation occurs post-ionization, all of the LC conditions which work in LC-MS are also compatible with IM-MS, including both normal and reversed phase LC columns and numerous solvent systems. Autosampler systems are also commonly added to facilitate automated, high throughput LC-IM-MS workflows. Other chromatographic separation techniques such as gas chromatography (GC) and supercritical fluid chromatography (SFC) have also been demonstrated with IM-MS,⁴⁸⁻⁵⁰ although these are less common due to the more limited analytical space that these techniques encompass (e.g., volatile and nonpolar analytes, respectively). Figure 1.4⁵ demonstrates the compatibility of timescales for chromatography with IM-MS. While chromatography operates on a timescale of minutes, the downstream analytical strategies such as IM operate on the order of milliseconds to microseconds, allowing further separation of the components of the chromatogram in two dimensions. Due to the capability of IM-MS to temporally nest these different separation methods, the resulting platform is versatile and selective, allowing high throughput for complex biological analyses.

Nesting of Analytical Timescales

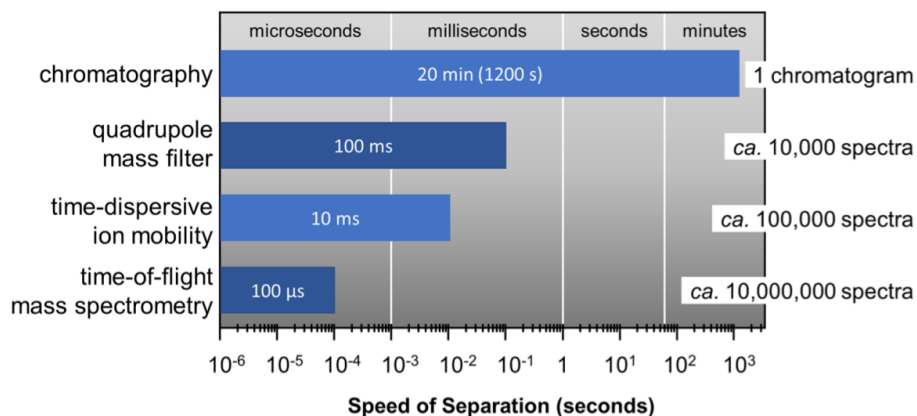


Figure 1.4 Nesting of analytical time scales based on speed of separation is shown for the analytical strategies on the left combined with the total number of potential spectra obtained through nesting the subsequent analytical separation dimensions shown to the right. (Figure and legend from May, et. al.⁵)

1.4.2 Ion Sources

Two of the most common methods for ionization of biomolecules are MALDI and ESI. These two ion sources, unlike many others, do not add significant energy to the molecule during ionization. This “soft” ionization helps to maintain the analyte’s structural integrity, which is crucial for the analysis of fragile biomolecules.⁹ MALDI typically generates low charge states in a narrow distribution, which simplifies the mass spectra. MALDI is performed on solid samples using a laser to ablate and generate ions which allows spatially-resolved mass information to be obtained. This has allowed MALDI-MS to be operated in an imaging mode for determining analyte location in tissue samples, and more recently, MALDI imaging has been coupled with IM-MS which provides a highly-dimensional separation technique that can simultaneously separate analytes based on spatial location, size, and mass.⁵¹ MALDI, however, is not conducive to direct analysis of liquid samples such as the effluent stream originating from LC. Liquid sample analysis is facilitated by ESI, which generates a continuous flow of ions from liquid-phase samples. ESI has enabled high-throughput LC-MS experiments and more recently has been used to combine LC with IM-MS. In contrast to the low charge states observed in MALDI, ESI typically generates multiply charged ions. Since mass spectrometers measure ions as a mass-to-charge ratio, higher charge states effectively increase the practical mass range accessible to a mass spectrometer, facilitating analysis of proteins and other high mass analytes alongside small molecules in a complex biological sample. For IM analysis, the various charge states generated from ESI are readily resolved into separate trendlines in mobility versus mass space, which facilitates identification of multiply charged species.

1.4.3 Time-Dispersive Ion Mobility Techniques

Two ion mobility techniques that are used in commercially available instruments are drift tube ion mobility spectrometry (DTIMS) and traveling wave ion mobility spectrometry (TWIMS) (Figure 1.5).⁵ TWIMS was the first IM technique to be used in a commercially available platform. In TWIMS, ion separations result from a series of dynamically-pulsed voltages (an electrodynamic field) which creates a traveling wave potential that transfers ions through the drift region in a mobility-selective mode. TWIMS separations are typically faster than DTIMS while accessing similar resolving powers, and because the traveling wave does not require high voltage operation, TWIMS is easier to implement on existing MS platforms. Although DTIMS combined with MS was implemented commercially several years after TWIMS, it is an older technique and considered the gold standard for CCS determination. Unlike TWIMS, DTIMS separates ions using a constant voltage gradient (a uniform electric field) which allows the measured ion drift times to be related directly to CCS via the fundamental ion mobility equation, commonly referred to as the Mason-Schamp relationship.⁵²⁻⁵³ In TWIMS, CCS values are determined via an empirical calibration relationship between TWIMS measured drift times and known CCS values obtained from DTIMS. Due to the fact that TWIMS does not require high voltages to operate, it is readily scalable to longer path lengths, which fundamentally improves instrument resolution. In contrast, high operational voltages must be utilized in order to increase the path length in DTIMS. Next generation TWIMS instruments are taking advantage of this scalability, producing high resolving power platforms based on cyclic designs.^{42,54}

Temporally-Dispersive Ion Mobility Techniques

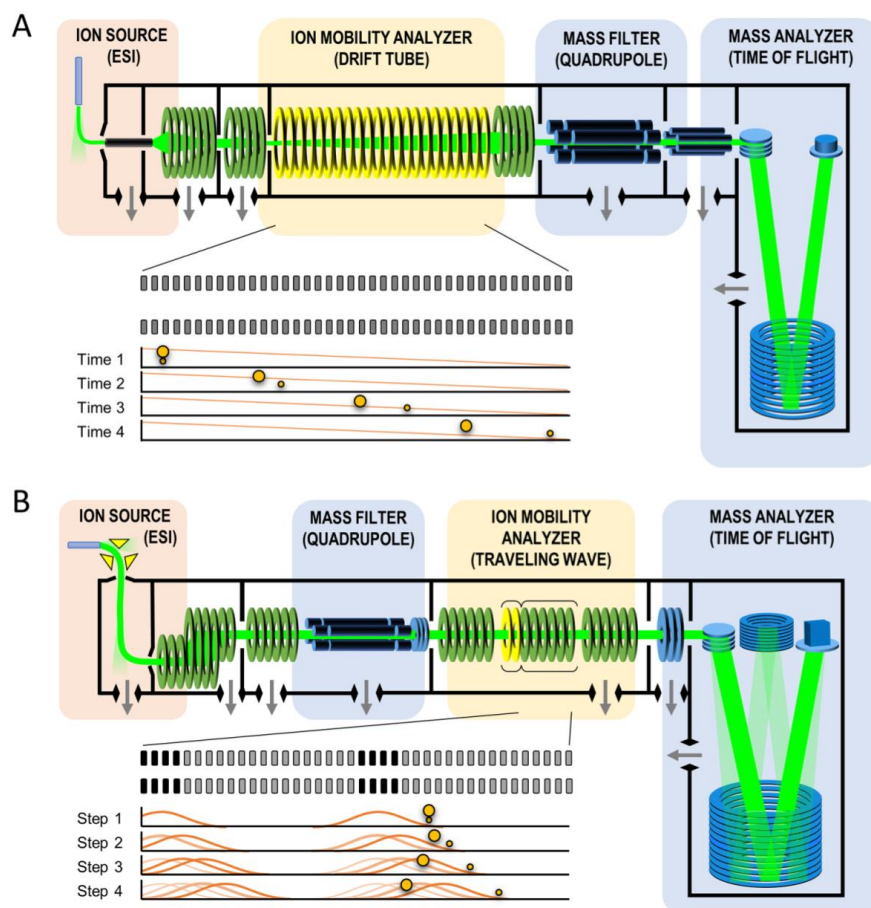


Figure 1.5 Two representative schematic diagrams for contemporary time-dispersive IM-MS instrumentation. (A) An electrostatic drift tube (DTIMS) arrangement similar to that described by Smith and co-workers. (B) An electrodynamic drift tube (TWIMS) arrangement similar to that described by Giles and co-workers. In both arrangements, hypothetical time courses are shown to illustrate the temporal separation of smaller and larger collision cross section ions. (Figure and legend from May, et. al.⁵)

1.4.4 Mass Spectrometry Considerations

When combined with IM, mass spectrometry is almost exclusively used following IM separations to provide mass measurement on mobility separated ions. In this IM-MS configuration, most of the chemical separation occurs in the mass dimension due to the high resolving power (>10,000) accessible by modern mass spectrometers, however, the added IM dimension provides improved peak capacity and the capability for resolving isomeric compounds based on structural differences.⁵⁵ IM is commonly coupled with time-of-flight (TOF) mass spectrometry due to its ability to rapidly analyze a wide mass range simultaneously and with high resolution. The timescale of the TOF is on the order of microseconds, pairing well with an upstream IM which is on the order of milliseconds per analysis. Quadrupole MS is also commonly used with IM-MS as an added mass filtering stage for tandem MS/MS experiments, which can aid in analyte identification and characterization.

Fragmentation methods have been utilized with great success in tandem mass spectrometry and continue to be used in IM-MS, where it can be initiated between the IM and MS stages (IM/MS) or prior to IM-MS either with a front-end mass filter (MS/IM-MS) or without, as is the case with in-source ion activation (/IM-MS). Collision induced dissociation (CID) is commonly used to fragment ions as it is readily implemented with existing ion optics. CID is implemented by inducing high-energy ion collisions with an inert background gas (such as nitrogen or argon) and is considered an ergodic process whereby energy is distributed across the entire analyte, causing the lowest energy bonds break first. This leads to reproducible fragmentation of ions and the analysis of CID fragmentation spectra has been used with IM-MS to identify isobaric species which exhibit different bond energies. The CID method is commonly used in proteomics to determine the amino acid sequence of peptides. While highly predictable, CID does not preserve

weak bonds such as noncovalent complexes and post-translational modifications, and is less effective at fragmenting large molecules, such as intact proteins. To address these deficiencies, electron transfer dissociation (ETD) has been used, which fragments the ion in a non-ergodic process, breaking bonds CID would not, and thus creating different but informative fragments compared to CID. ETD and CID have been used simultaneously with IM-MS for glycoproteomics.⁵⁶⁻⁵⁸ This allows a variety of fragments to be determined for a given precursor ion, with CID fragmenting the glycan portion and ETD fragmenting the peptide portion. Combining the ion drift time, precursor mass, and fragment mass information allows for confident identification of the precursor.

IM-MS holds an important role in biomolecular analysis. The ability of IM-MS to integrate with a wide variety of chromatographic techniques, ion generation methods, fragmentation methods, and mass determination ensures it will remain valuable for biomolecular analysis as it is applied to proteomics, lipidomics, metabolomics, and other biological problems requiring high sensitivity and high confidence identifications. Additionally, IM improves peak capacity compared to standalone mass spectrometers while providing separation on the order of milliseconds compared to minutes in an LC system. It can be used to identify isobaric species or as an added descriptor for the identification of unknowns. The next few sections discuss some of the applications of IM-MS to biomolecular analysis in more detail.

1.5 Introduction to Current Trends

The confident identification of small molecules continues to be one of the most difficult challenges in omic studies. While advancements in proteomics have streamlined MS-based identification efforts for peptides, metabolomic and lipidomic identification capabilities have

generally lagged behind.^{33,59-62} One reason for this is that while the structure of peptides consist of rationally-assembled amino acid building blocks which can be elucidated through ion fragmentation strategies, metabolites and lipids are not biopolymers with predicable sub-structural units. Additionally, the prevalence of isobaric species in lipidomics complicates feature identification, and metabolomics studies often encounter features of redundant mass that lack unique fragmentation patterns, further confounding attempts at identification by MS. Therefore, a combination of analytical techniques are required for high-confidence lipidomics and metabolomics. As shown in Figure 1.6, gas chromatography, liquid chromatography, or another front end separation can be readily combined with ion mobility and mass spectrometry analysis to provide highly-dimensional datasets which can be partitioned into specific omic workflows.⁶² The ion mobility provides a chemical class-specific separations based on differences in intrinsic gas-phase packing, as well as quantitative size information via the CCS measurement which can be used as a reproducible measurement for identification purposes.⁶²

1.6 Integrating Ion Mobility for Omic Analysis

IM-MS provides a fast separation of chemically unique biological groups with the added benefit of measuring collision cross section concurrently with mass-to-charge ratio.^{25,60,63} This capability is important for omics studies utilizing complex biological samples which routinely require extensive sample purification strategies to isolate molecules of interest from undesirable compounds that would otherwise make MS analysis difficult (e.g., salts, detergents, and other types of chemical noise).^{59,64} Sample preparation strategies have the potential to chemically alter molecules of interest, for example, by oxidation, reduction, conversion to a secondary metabolite, or loss of a post-translational modification in peptides. Integrating ion mobility with mass

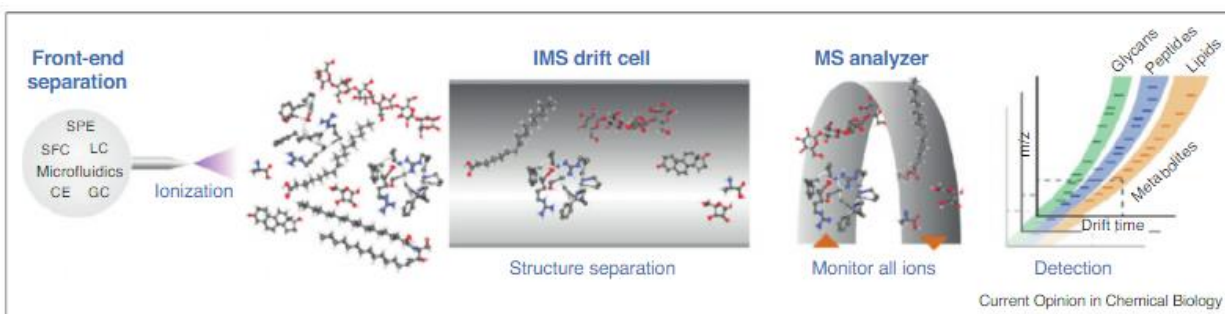


Figure 1.6 Schematic of IMMS analysis workflow with different types of front-end separation techniques. Abbreviations: SPE, solid phase extraction; SFC, super critical fluidic chromatography; LC, liquid chromatography; CE, capillary electrophoresis; GC, gas chromatography. (Figure and Caption from Zhang et al.⁶²)

spectrometry can help offset some of the burden of chemical separation and alleviate the need for extensive sample handling. In certain cases where fragmentation occurs post-mobility, either intrinsically or intentionally, IM-MS also allows the alignment of precursor and product ions which can further aid in identification.⁶¹ The following sections provide examples of how ion mobility has been integrated in proteomic, lipidomic, and metabolomic analyses. Although each analysis is discussed separately, it should be noted that ion mobility allows for simultaneous analysis of these individual omic fields via chemical class separation, providing a truly integrated multi-omic experiment.

1.6.1 Proteomics

Proteomics, the large-scale study of proteins, has been a driving force in systems biology and has increased our understanding of diseases such as lung cancer and Alzheimer's. Proteins serve as the machines for all cellular processes, thus proteomic studies are one of the most crucial tasks in systems biology. MS-based proteomics is a major component to the advancements in the field.^{65,66} Proteins encompass a large dynamic range of concentrations, necessitating separation techniques to enhance lower abundance species prior to mass analysis. Common separation methods for proteomics include gel electrophoresis, liquid chromatography, and, in a growing number of instances, ion mobility.⁶⁷⁻⁶⁹

Ion mobility has been utilized extensively in structural proteomics.^{60,70} Proteins of similar or exact mass, such as protein conformers, can be separated by ion mobility due to differences in their gas-phase size. Figure 1.7 illustrates an ion mobility separation for protein ions of different sizes but similar mass to charge ratio.⁷⁰ The majority of multiprotein complexes have been

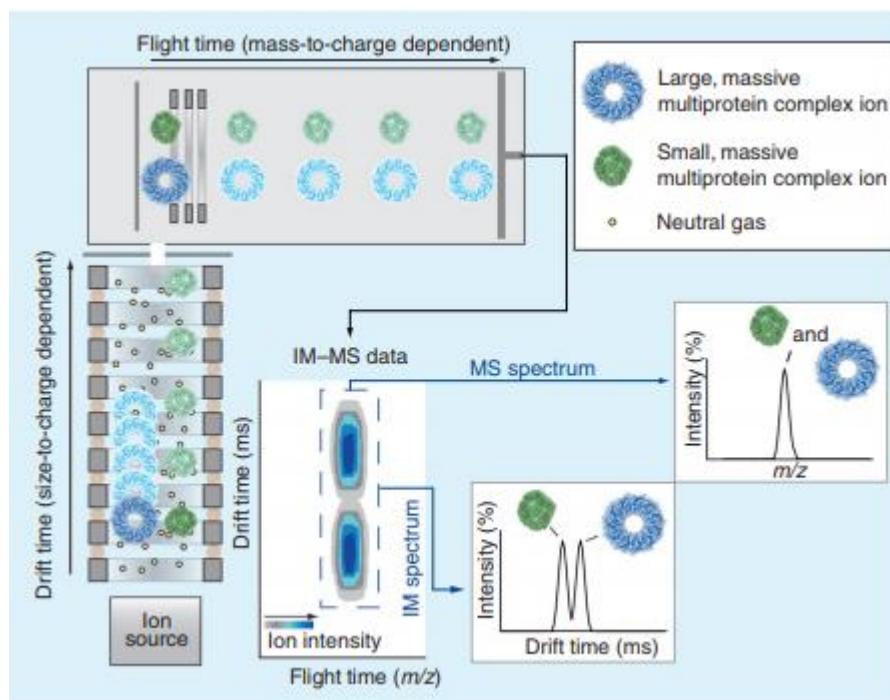


Figure 1.7 Ion mobility-mass spectrometry data acquisition and basic principles. Ions are generated at the ion source (lower left) and are allowed to drift in an ion guide filled with neutral gas molecules under the influence of an electric field. The ions migrate through this region according to their size-to-charge ratio. They are then injected into a ToF mass analyzers under vacuum for m/z analysis. The resulting data are 3D, containing ion intensity, size and mass information. The various dimensions of the data can be shown as a contour plot (middle, bottom), or 2D selections in drift time of m/z (lower right). A key for the diagram is shown (upper right). (Figure and Caption from Zhang et al.⁷⁰)

analyzed on traveling wave instruments, and it has been demonstrated that incorporation of traveling wave ion mobility can increase proteome coverage by up to 60%.⁷¹

In addition to separating proteins, ion mobility is used to probe structural information.⁷⁰ Temperature-controlled ESI sources and heated ion transfer capillaries have been used prior to IM-MS to rapidly heat proteins and monitor their controlled denaturation.⁷²⁻⁷⁴ In addition, thermally-induced protein conformational transformations as well as protein-ligand interactions are able to be observed. In these ways and others, IM-MS progresses from a separation strategy to an aid in understanding how protein clusters are formed and stabilized.^{73,74}

1.6.2 Lipidomics

Lipids comprise a large portion of the small molecules extracted from organisms. They have three major functions in biological systems: energy storage, cellular signaling, and structural functions. Lipids can be divided into eight major categories with many different chemical motifs ranging from fused cyclic molecules to long chain fatty acids. They cover a large range of m/z ratios and while mass spectrometry has been a powerful tool in lipidomics, it still falls short in some areas due to many isomeric species.^{75,76,77} Isomeric complexity makes the study of lipidomics difficult as there are many potential double bond positions, geometric (cis/trans), constitutional (linear and branched) and stereochemical orientations that a lipid can adopt which are all isobaric in mass. Identifying complex lipid structures has been a struggle in the field of lipidomics; one that ion mobility is well-suited to address.⁷⁶⁻⁷⁹ Similar to other mass spectrometry based omic fields, lipids are identified based on their fragmentation pattern obtained from tandem MS/MS experiments. As many lipids are chemically and structurally similar, lipids can be challenging to separate using LC alone, making it difficult to correlate fragment ions with their precursor ion

forms. As demonstrated by Paglia et al., ion mobility can be used to align fragmentation spectra with precursor parent ions to increase the confidence in lipid identification (Figure 1.8).⁸⁰ Additionally, ion mobility was demonstrated to be useful in separating co-eluting lipid structures with the same m/z ratios.

Ozone-induced dissociation has been recently demonstrated with IM-MS to elucidate the location of double bonds in the acyl tail region of lipids. Two separate strategies have been demonstrated: solution-phase ozonolysis of lipids prior to being introduced to the mass spectrometer,⁸¹ and gas-phase ozonolysis of lipid ions within the MS, the latter technique termed OzID. These ozonolysis strategies have been shown to be useful for locating the position of double bonds within lipids, however, one shortcoming with this approach is that it does not provide any information about the geometry of the double bond prior to ozonolysis.^{81,82} This emphasizes the strength of IM-MS analysis. Ion mobility allows for the differentiation of some geometric lipid isomers, such as *cis* versus *trans*, even when in a complex biological mixture. Groessl et al. demonstrated that collision cross section differences of 1% are sufficient for the baseline separation of lipids in DTIMS.⁷⁸ Although they discuss how it is possible to use IM for identification purposes, it is also stressed that high precision and accuracy are needed to create and populate reliable reference data libraries. As these libraries become more available, it is expected that lipidomics will experience similar growth that has been seen in the proteomics field.

1.6.3 Metabolomics

Metabolomics is the measurement of the thousands of small molecules in a biological system. Unlike genomics and proteomics, metabolomics encompasses a large amount of chemical diversity as it consists of molecules from many different biological classes, such as carbohydrates,

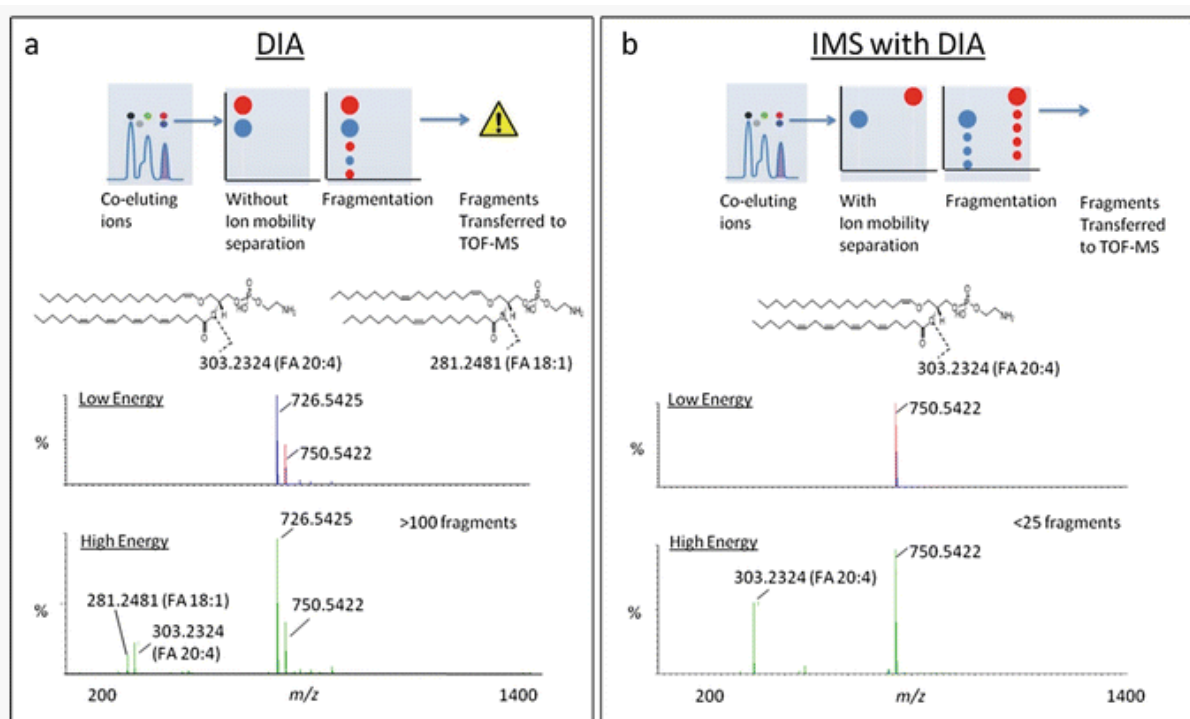


Figure 1.8 Schematic visualization of acquisition using data-independent acquisition (MSE) and MSE coupled with IM (HDMSE). Combined with IM separation, fragmentation offers unique capabilities to increase specificity and confidence in identifying complex lipid structures. (Figure and Caption from Paglia et al.⁸⁰)

amino acids, hormones, and lipids.⁸³ There are generally two approaches to mass spectrometry based metabolomics: (1) targeted analysis, in which a panel of metabolites are selected prior to data collection, and (2) untargeted analysis, in which all small molecules are analyzed simultaneously.⁸³ Both approaches have their advantages. Targeted studies allows for semi-quantitative analysis of small molecules on a curated list. Isotope standards can be analyzed concurrently with unknowns and calibrated against empirically-measured response curves (calibration curves) in order to determine the concentration of specific metabolites within a sample. While this approach provides quantitative information regarding metabolites of interest, targeted studies do not provide information for other small molecules present in the sample, and for practical reasons, generally only targets a small pool of metabolites. Untargeted approaches, on the other hand, focuses on separating and comprehensively measuring all of the small molecules present in the sample, but lacks robust means of quantifying these signals. Also, untargeted studies generally utilizes analytical methods and settings that attempt to measure a large breadth of molecules, and thus can be less sensitive to a specific class or pool of analytes.⁸³⁻⁸⁵ In addition, identifying the oftentimes thousands of metabolites detected in an untargeted study can be an arduous task. For a single m/z feature, there can be hundreds of hits in any metabolomic database, making an absolute identification difficult.⁸⁴⁻⁸⁶ In order to improve confidence in metabolite identification, multiple dimensions of analytical information are obtained in the experiment, which can include measurements from front end chromatographic separations, as well as post-ionization techniques such as ion mobility and tandem ion fragmentation information. Ion mobility in particular can help to alleviate some of the difficulties associated with confident metabolite identification.⁸⁴⁻⁸⁶

As noted in the previous section, ion mobility can improve fragmentation identification in lipidomics, and this advantage applies to metabolomics as well. With such chemical diversity found in the metabolome, ion isolation is complicated by co-eluting species, and thus aligning precursor ions with their fragments originating from ion activation experiments is challenging. Using ion mobility prior to fragmentation allows co-eluting small molecules to be further resolved following chromatography.⁸⁴⁻⁸⁶ This is demonstrated by Wickramasekara et al. in which co-eluting lipid species are classified based on the differences in their drift time (Figure 1.9).⁸⁷ In addition, the drift time extracted spectra can be used to align fragment ions to the parent ion, as they have identical drift times when conducting the fragmentation post-mobility. This capability provides more specific ion fragmentation information which can then be used with the accurate mass measurement to match unknowns to entries found in one or more databases, thus increasing the confidence in assigning metabolite identifications.

In addition to utilizing the enhanced separation and fragment alignment capabilities from IM, CCS measurements derived from IM experiments can also be used to improve metabolite validation.¹⁰⁴ CCS is linked to an intrinsic molecular property of the analyte (the microscopic cross section) and thus is considered more robust than other measurement parameters such as the chromatographic retention time. This property makes CCS useful as an additional molecular descriptor that can be used in metabolomic studies along with accurate mass and fragmentation information. Currently, there are labs attempting to use CCS in metabolite identification workflows. For example, Paglia et al. has described a robust analytical workflow incorporating CCS for both metabolite and lipid identifications, and report a ca. 2% inter-laboratory reproducibility of the TWIMS derived CCS.⁶¹ Stow et al. utilized standardized DTIMS instrumentation deployed across several laboratories to achieve an inter-laboratory CCS

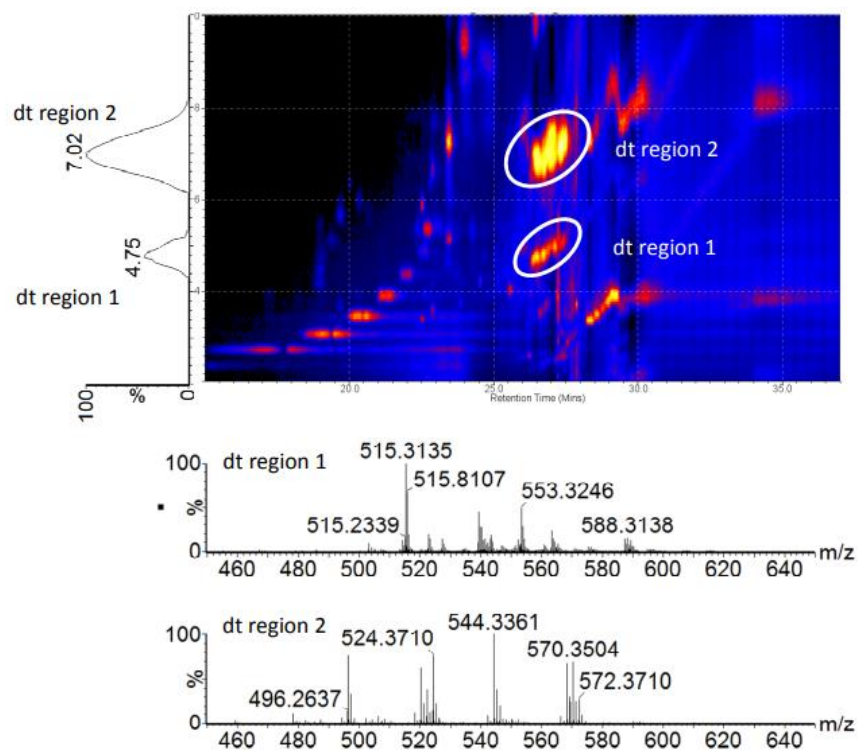


Figure 1.9 An example of a 2D image (drift time vs retention time) showing the ion mobility separation of different compound classes in rat plasma samples. The encircled regions mark the compound classes that eluted within a similar retention time window (26-28 min). Drift time-extracted spectra (bottom) show that these two clusters belong to different lipid classes, namely Lyso-PC and SM lipids (sphingosine phosphocholines) that have drift time distributions centered around 7.02 ms and 4.75 ms, respectively. (Figure and Caption from Wickramasekara et al.⁸⁷)

reproducibility of better than 0.5%, and recent work by Nichols et al. describes the utility of DTIMS CCS measurements as a molecular descriptor in untargeted studies of primary human metabolites.⁸⁸⁸⁹ As more research shifts towards incorporating CCS into metabolomic analysis, there is a need for databases to propagate likewise. Recent efforts for developing CCS databases to support metabolite identifications have included pesticides, pollutants, xenobiotics, and steroids.⁹⁰⁻⁹³ Leveraging the standardization efforts for DTIMS, Picache et al. has recently described a “Unified CCS Compendium” which compiles over 3,800 CCS measurements obtained from different studies into a single, self-consistent resource with a global average CCS precision of 0.25% RSD.⁹⁴ These and other efforts will allow rapid and reliable metabolite identification and quantification, which becomes increasingly important as the field shifts towards comprehensively characterizing individual metabolomic pathways.

1.7 Continuing Advancements in IM-MS Technology

Innovation in IM-MS instrumentation continues at a rapid pace. Various improvements have been suggested and current technologies allow for ingenious solutions for challenges encountered in biomolecular analysis. One novel instrument design approach utilizes a scalable ion optical architecture consisting of electrode pads on a printed circuit board (PCB) and driven with electrodynamic (RF) fields that confine ions to a predefined ion optical path. This approach, named by the authors as “structures for lossless ion manipulations” (SLIM), utilizes a 2-dimensional electrode geometry that is both modular and scalable such that various different experiments can be achieved on the same instrument platform.^{42, 95-98} In SLIM, two PCBs with a mirrored electrode symmetry are placed above and below one another to create the ion path of travel in between the boards, and a dynamic electric fields are used to both contains and guides the

ions through the SLIM device.⁹⁹ SLIM allows high transmission ion transfer through elevated pressure regions, and SLIM-based ion mobility separations have been demonstrated using this approach. The ability to print electrodes on a two-dimensional surface allows for various ion manipulation modules to be fabricated, including modules to move ions at 90-degree angles (elbows and tees).¹⁰⁰⁻¹⁰¹ This facilitates cyclic racetrack and serpentine geometries to be fabricated for long path-length, high-resolution ion mobility separations, and incorporation of “tee” junctions allows selection of a discrete ion mobility region for further analysis by either IM or MS techniques. An example of SLIM-based ion mobility instrumentation is shown in Figure 1.10.¹⁰² Current designs have created instruments with some of the highest IM resolution currently available.^{54, 103}

In addition to TWIMS and DTIMS, a relatively new ion mobility technique called trapped ion mobility spectrometry (TIMS) is currently available in commercial instrumentation.¹⁰⁴⁻¹⁰⁵ TIMS performs ion mobility separations by selectively releasing ions trapped in a mobility analyzer cell combining a gas flow and an opposing electric field.¹⁰⁶⁻¹⁰⁷ The ions trapped in TIMS are released slowly by lowering the electric field barrier, which allows a mobility spectrum to be obtained and subsequent MS analysis to be performed. The rate at which the electric field is lowered corresponds with IM resolution, with slower scan rates leading to higher resolution. TIMS instruments are capable of high IM resolutions and are very versatile due to its variable scan rate.¹⁰⁸ Either high throughput or high resolution scan rates may be chosen as needed, or a scan rate may be variable during analysis to allow high resolution only for certain range of mobilities, enabling targeted high resolution experiments to be conducted. This is in contrast to high resolution cyclic or racetrack IM techniques, which must discard all mobilities except a select region.

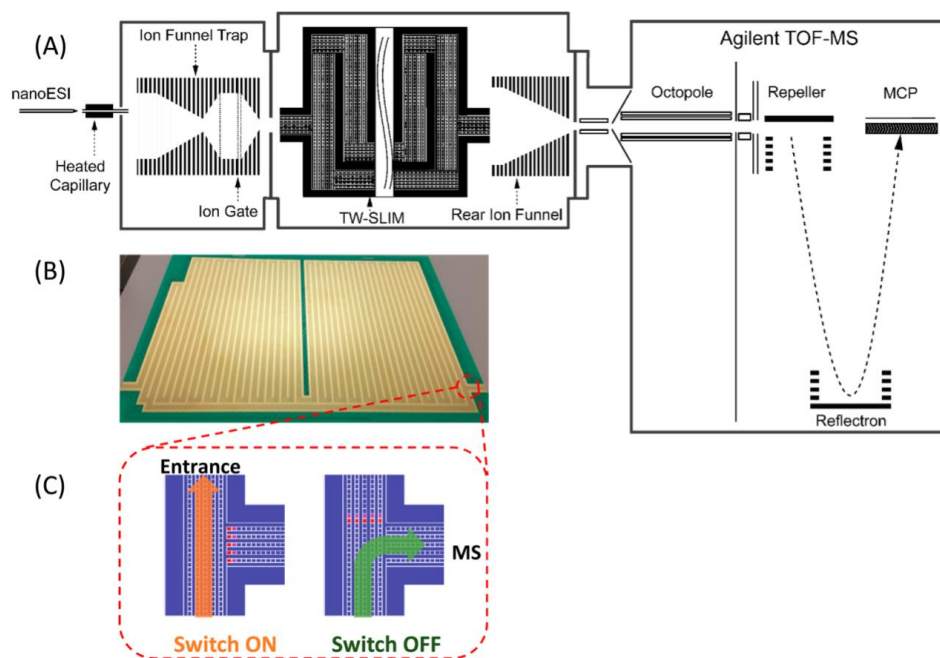


Figure 1.10 (A) Schematic diagram of the multipass SLIM SUPER IM-MS instrument used in this work; (B) photo of one of the two SLIM module surfaces; and (C) illustration of an ion switch (switch on, ion cycling; switch off, transmit ion to MS). (Figure and legend from Deng, et. al.¹⁰²)

While most efforts have focused on improving IM resolution, some approaches have sought to improve sensitivity and throughput. An example of such an approach is a multi-channel IM spectrometer shown in Figure 1.11.⁵ This instrument utilizes eight discrete ion optical paths to perform eight ion mobility separations in parallel.¹⁰⁹ Each ion channel can act independently, analyzing eight unique samples at a time, improving throughput. Alternatively, the multi-channel instrument can analyze the same sample simultaneously across the eight ion optical paths, increasing the sensitivity of the instrument. As the analytical community pushes for rapid extraction of more information from complex samples, advancements in high throughput instrument designs remain crucial.

Additional strategies for improving the mobility separation have focused on increasing the chemical selectivity of existing IM instrument by using alternate drift gases.¹⁷ The understanding and application of the effect of drift gas on IM separations and the associated CCS measurement is still in early development, but there is now mounting evidence that the use of more polarizable drift gases (e.g., CO₂, N₂O, NO₂) can increase the resolution for certain ion species.¹¹⁰⁻¹¹¹ While the hard-sphere interactions between the ion and drift gas tend to predominate the mobility of ions in the IM experiment,¹¹² long-range interactions also play a role in the observed IM separations and are exploited by varying the drift gas polarizability. Improved selectivity can occur between certain ionic species depending upon their susceptibility to long-range interactions.¹¹³ The effect on separation efficiency by varying the drift gas composition is similar to the effect of varying the solvent conditions in capillary electrophoresis to affect separation selectivity. It is common to alter the drift gas in some high-field IM techniques, such as high-field asymmetric waveform ion mobility spectrometry (FAIMS) and differential mobility spectrometry (DMS).¹¹⁴⁻¹¹⁹ In low-field IM techniques, this is less common, but there have been a number of significant examples.¹²⁰⁻¹²¹

Spatial Multiplexing

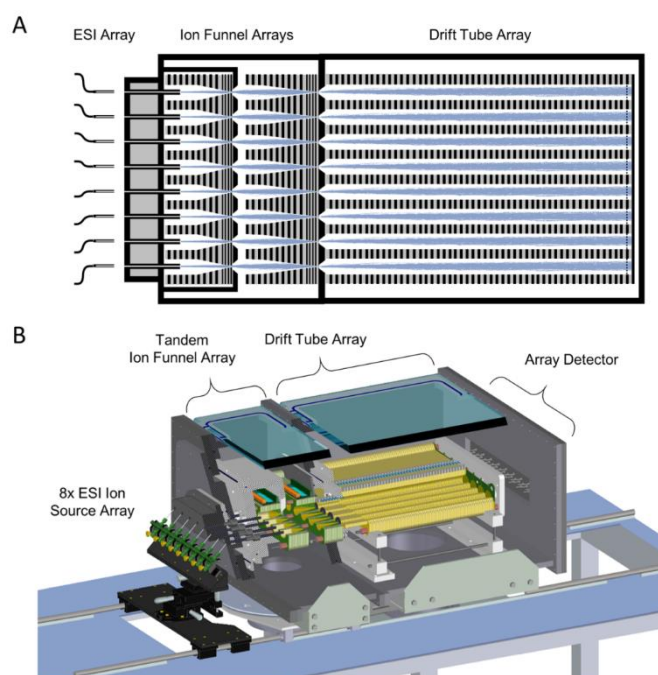


Figure 1.11 Schematic diagram illustrating a spatial multiplexing strategy for DTIMS through combining eight individual IM channels: (A) diagram showing ion simulations through the interfacing ion funnels and the drift tube array and (B) cutaway showing component details of the spatially multiplexed instrument. (Figure and legend from May, et. al.⁵)

Using an ambient pressure drift tube, Hill and coworkers showed that varying the drift gas polarizability could improve selectivity.^{110-111, 122-123} Using a reduced pressure drift tube, Yost and coworkers reported that carbon dioxide improved resolving power for several isobaric steroids.¹²⁴ Eberlin and coworkers demonstrated that replacing nitrogen with carbon dioxide in a TWIMS instrument could improve separation of a number of analytes such as carbohydrates and isomeric haloanilines.^{47, 125-127} However, it is common for observations of more polarizable drift gases to report minimal improvement to overall IM peak capacity or resolution compared to nitrogen on helium.^{113, 128-130} For example, Fjeldsted and coworkers investigated the separation of various small molecule pesticides, isomeric carbohydrates, and fluoroalkyl phosphazenes in a wide variety of drift gases, such as helium, nitrogen, argon, carbon dioxide, nitrous oxide, and sulfur hexafluoride. Generally, they observed that helium and nitrogen had the highest resolution and resolving power, with some of the more polarizable drift gases demonstrating better selectivity when comparing certain analyte pairs.¹⁷ To fully evaluate drift gas effect, a broader range of masses and biological classes needs to be reported in a variety of drift gases across multiple platforms and laboratories. The majority of CCS measurements have been reported in helium or nitrogen, hindering the evaluation of IM separation performance in alternate drift gases.¹² Normalized measurements like CCS are vital for allowing direct comparison of separations on different platforms (e.g. drift tube or traveling wave).¹⁰³ Due to the potential analytical importance of drift gas composition, there is a need for further exploration into the effect of drift gas on CCS as a method to increase IM resolution.

1.8 Combining Discrete Omic Databases for Multi-Omic Experiments

When utilized in various omics studies, ion mobility has been used primarily to partition analytes of interest from chemical noise originating from complex samples, resolve ambiguities within co-eluting features, and align precursor and fragmentation data acquired in data independent strategies. While the majority of IM-MS applications in biomolecular analysis have focused on specific omic fields (e.g., proteomics, lipidomics, metabolomics), there is increasing interest in utilizing IM-MS for untargeted, multi-omic studies which look at all molecule types simultaneously.¹³¹ A truly, multi-omic analytical workflow will facilitate the development of system maps which connect relationships between molecule types and allow perturbed pathways to be highlighted. To illustrate this concept Figure 1.12 displays work from Paglia et al. on building pathway maps to track metabolites being shuttled between mitochondria and the cytosol.¹³² An area that can benefit from this type of analysis is the microbiome field. The microbiome has experienced recent and significant attention aimed at understanding the integral role that commensal bacteria plays on human health.¹³³⁻¹³⁵ This focus, in large part, is due to advancements in sequencing of bacterial communities allowing for whole populations to be analyzed simultaneously, facilitating the comparison of healthy versus disease states.^{135,134} One challenge that remains in microbiome research is the understanding of the mechanisms that lead to disease, which can be addressed at least in part by building biochemical inventories of small molecule metabolites observed within the samples. Mass spectrometry based metabolomics nestles nicely into a potential multi-omic study. It can be applied to a variety of sample types, can measure thousands of metabolites, and requires very little sample quantities. In particular, the ability of IM-MS experiments to separate and detect multiple biological classes and chemical motifs simultaneous, can allow perturbed metabolites to be observed along with changes in the bacterial

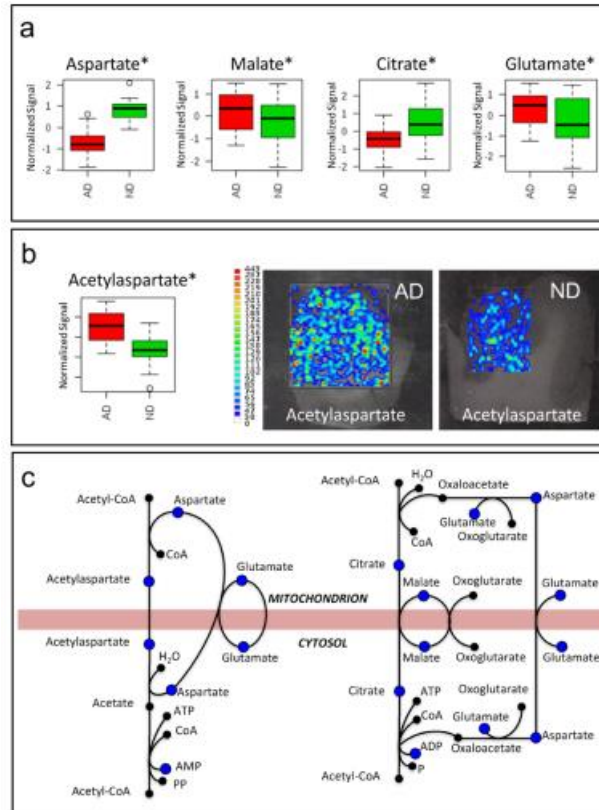


Figure 1.12 Mitochondrial shuttles. (a) Bar Charts of aspartate, malate, citrate, and glutamate obtained from normalized signals in AD (red) and ND control subjects (green). (b) Bar chart of N-acetylaspartate (NAA) obtained from normalized signals in AD (red) and control subjects (green) and MS imaging of AD and control subjects brain sections. (c) Mitochondrial shuttles and metabolites quantified in his experiment (blue dots). * $p < 0.05$ (t test). Targeted data used for bar charts were normalized by mean centering, scaled by unit variance, and log-transformed. (Figure and Caption from Paglia et al.¹³²)

community. Revealing changes in the metabolomic profile can give insight into the role that particular bacteria plays within the rich tapestry that is the microbiome.

Throughout this chapter, using the idea of using collision cross section as a tool for separation and descriptor for biomolecules has been addressed. However, this can only be useful for the field if there is a database that contains accurate collision cross sections. To date, there are several labs that are attempting to solve this problem and many labs use an in-house database. This is essential for ion mobility to expand its versatility. Similar to how Genbank¹³⁶ and The Protein Database¹³⁷ has helped normalize and improve the speed and cost of genomic and proteomic respectively, a database for collision cross sections will help to improve the speed and accuracy in which ion mobility experiments can be performed.

1.9 Statement of Dissertation

Herein, my contribution to this work is detailed. Chapter 1 was adapted from a book chapter noted in the acknowledgments section. I wrote half of the book chapter and was part of the editing process for the entire chapter. This chapter introduces IM in a methods and protocols book, describing the history, value, and effectiveness of IM to researchers not familiar with this analytical technique. In chapter 2, which was adapted from published work noted in the acknowledgments section, I searched the literature for publications with relevant data, recorded said data, brought ideas on data representation, and created figures for the publication. I created macros to give the data sheet the capability to efficiently sift through copious amounts of information and create graphs from a large number of data points and series. I also created three dimensional graphs to allow for better visualization of a large quantity of data. This work brought to light the major trends in the literature over a time span of 40 years. It allowed the community to

see both what has been done and what new areas of study are available. Chapter 3 was adapted from published work noted in the acknowledgments section. In this work, I was involved in data analysis classifying isomer groups and determining IM's effectiveness in separation of isomer pairs. I created macros that sorted through large datasets to identify and quantify the number of isomers. These macros also determined percent difference among the pairs, aiding in identification of isomers that can be separated based on current IM resolving power as well as the effect that improvements in IM resolving power will have on isomer separation and identification. I also helped create charts to visualize the results of this isomer investigation. My work demonstrated the ability of IM to enhance identification of isobaric species where mass spectrometry can struggle. It also helped demonstrate the current capabilities of IM and how improvements in mobility resolution would affect isomer coverage. In chapter 4, which was adapted from published work and noted in the acknowledgments section, I analyzed IM trends and found mathematical descriptors appropriate for each trend. I found best fit lines for data classes from multiple possible mathematical descriptors and created charts demonstrating these best fit lines as well as data inclusion bands. I was also involved in writing a portion of the manuscript. This work provided the basis for demonstrating the affect helium and nitrogen drift gases have on class as well as establishing trends that could be used for characterization of unknowns. Chapter 5 was adapted from published work and noted in the acknowledgments section. I designed the experimental method, choosing the drift gases and classes. I designed and ran the experiments on the instrument to establish experimental parameters in the different drift gases. I chose and ran the classes in each of the drift gases. I performed all the data analysis. I created figures to demonstrate the reasoning behind recommendations of instrument parameters as well as creating figures demonstrating the effects of drift gas on CCS. I wrote the manuscript and helped edit the manuscript and figures.

This work establishes instrument operating parameters for multiple drift gases to achieve reproducible CCS values. This work also gives recommendations for drift gas selection and aids researchers in identification of the appropriate drift gas for their analytical application. The reproducible CCS values can be utilized as the basis for improving fundamental IM theory and determining relative elution orders of analytes in different drift gases through future creation of predictive algorithms. This work was the first drift gas study to look at a wide range of drift gases, classes, masses, mobilities, and charge states. Chapter 6 is my own work and has not been published. This outlines future work that may be performed to improve trend fitting with mathematical descriptors for better characterization of unknowns. A method for CCS prediction in different drift gases is also noted. Such a method, if established, would allow for comparison of CCS values gathered in one drift gas with those from the literature in another drift gas. Computational analysis of these values can be time consuming and computationally expensive. This method could allow for rapid CCS prediction without the need for time intensive calculations. Finally, recommendations are made for drift gas selection for future studies. This describes the important aspects of drift gas selection to consider for enhancement of fundamental IM understanding and prediction of drift gas effect. This guide will help future investigators as they seek to describe the drift gas effect on CCS separation.

1.10 Acknowledgements

This chapter contains the invited book chapter in Ion Mobility Mass Spectrometry – Methods and Protocols, in the Methods in Molecular Biology series: “Fundamentals of Ion Mobility Mass Spectrometry for the Analysis of Biomolecules,” by Caleb B. Morris, James C. Poland, Jody C. May, and John A. McLean. Guiseppe Astarita and Guiseppe Paglia, Eds., Springer Nature (to be published in 2019).

1.11 References

1. Thomson, J. J.; Rutherford, E. *Philos. Mag. Series 5* 1896, 42 (258), 392 - 407.
2. Tyndall, A. M.; Powell, C. F. *Proc. R. Soc. Lond. A. Math. Phys. Sci.* 1930, 129 (809), 162-180.
3. Tyndall, A. M.; Starr, L. H.; Powell, C. F. *Proc. R. Soc. Lond. A. Math. Phys. Sci.* 1928, 121 (787), 172-184.
4. Barnes, W. S.; Martin, D. W.; McDaniel, E. W. *Phys. Rev. Lett.* 1961, 6 (3), 110-111.
5. May, J. C.; McLean, J. A. *Anal. Chem.* 2015, 87 (3), 1422-1436.
6. Dole, M.; Mack, L. L.; Hines, R. L.; Mobley, R. C.; Ferguson, L. D.; Alice, M. B. *J. Chem. Phys.* 1968, 49 (5), 2240-2249.
7. Dole, M.; Hines, R. L.; Mack, L. L.; Mobley, R. C.; Ferguson, L. D.; Alice, M. B. *Macromolecules* 1968, 1 (1), 96-97.
8. Lubman, D. M.; Kronick, M. N. *Anal. Chem.* 1982, 54 (9), 1546-1551.
9. von Helden, G.; Wyttenbach, T.; Bowers, M. T. *Int. J. Mass Spectrom. Ion Processes* 1995, 146-147, 349-364.
10. Wittmer, D.; Chen, Y. H.; Luckenbill, B. K.; Hill, H. H., Jr. *Anal. Chem.* 1994, 66 (14), 2348-2355.
11. Smith, R. D.; Loo, J. A.; Loo, R. R. O.; Busman, M.; Udseth, H. R. *Mass Spectrom. Rev.* 1991, 10 (5), 359-452.
12. May, J. C.; Morris, C. B.; McLean, J. A. *Anal. Chem.* 2017, 89 (2), 1032-1044.
13. Giles, K.; Williams, J. P.; Campuzano, I. *Rapid Commun. Mass Spectrom.* 2011, 25 (11), 1559-1566.
14. Giles, K.; Pringle, S. D.; Worthington, K. R.; Little, D.; L., W. J.; Bateman, R. H. *Rapid Commun. Mass Spectrom.* 2004, 18 (20), 2401-2414.
15. Pringle, S. D.; Giles, K.; Wildgoose, J. L.; Williams, J. P.; Slade, S. E.; Thalassinou, K.; Bateman, R. H.; Bowers, M. T.; Scrivens, J. H. *Int. J. Mass Spectrom.* 2007, 261 (1), 1-12.
16. Zhang, F.; Guo, S.; Zhang, M. Y.; Zhang, Z. X.; Guo, Y. L. *J. Mass Spectrom.* 2015, 50 (7), 906-913.
17. Kurulugama, R. T.; Darland, E.; Kuhlmann, F.; Stafford, G.; Fjeldsted, J. *Analyst* 2015, 14 (20), 6834-6844.

18. Paglia, G.; Williams, J. P.; Menikarachchi, L.; Thompson, J. W.; Tyldesley-Worster, R.; Halldorsson, S.; Rolfsson, O.; Moseley, A.; Grant, D.; Langridge, J.; Palsson, B. O.; Astarita, G. *Anal. Chem.* 2014, 86 (8), 3985-3993.
19. Allen, S. J.; Schwartz, A. M.; Bush, M. F. *Anal. Chem.* 2013, 85 (24), 12055-12061.
20. Campuzano, I.; Bush, M. F.; Robinson, C. V.; Beaumont, C.; Richardson, K.; Kim, H.; Kim, H. I. *Anal. Chem.* 2012, 84 (2), 1026-1033.
21. Bush, M. F.; Campuzano, I. D. G.; Robinson, C. V. *Anal. Chem.* 2012, 84 (16), 7124-7130.
22. Shah, A. R.; Agarwal, K.; Baker, E. S.; Singhal, M.; Mayampurath, A. M.; Ibrahim, Y. M.; Kangas, L. J.; Monroe, M. E.; Zhao, R.; Belov, M. E.; Anderson, G. A.; Smith, R. D. *Bioinformatics* 2010, 26 (13), 1601-1607.
23. Bush, M. F.; Hall, Z.; Giles, K.; Hoyes, J.; Robinson, C. V.; Ruotolo, B. T. *Anal. Chem.* 2010, 82 (22), 9557-9565.
24. Fenn, L. S.; McLean, J. A. *Anal. Bioanal. Chem.* 2008, 391 (3), 905-909.
25. May, J. C.; Goodwin, C. R.; Lareau, N. M.; Leaptrot, K. L.; Morris, C. B.; Kurulugama, R. T.; Mordehai, A.; Klein, C.; Barry, W.; Darland, E.; Overney, G.; Imatani, K.; Stafford, G. C.; Fjeldsted, J. C.; McLean, J. A. *Anal. Chem.* 2014, 86 (4), 2107-2116.
26. Fenn, L. S.; Kliman, M.; Mahsut, A.; Zhao, S. R.; McLean, J. A. *Anal. Bioanal. Chem.* 2009, 394 (1), 235-244.
27. Hines, K. M.; May, J. C.; McLean, J. A.; Xu, L. B. *Anal. Chem.* 2016, 88 (14), 7329-7336.
28. Leaptrot, K. L.; May, J. C.; Dodds, J. N.; McLean, J. A. *Nat. Commun.* 2019, 10, 985
29. Baker, E. S.; Burnum-Johnson, K. E.; Jacobs, J. M.; Diamond, D. L.; Brown, R. N.; Ibrahim, Y. M.; Orton, D. J.; Piehowski, P. D.; Purdy, D. E.; Moore, R. J.; Danielson, W. F.; Monroe, M. E.; Crowell, K. L.; Slyszy, G. W.; Gritsenko, M. A.; Sandoval, J. D.; LaMarche, B. L.; Matzke, M. M.; Webb-Robertson, B.-J. M.; Simons, B. C.; McMahon, B. J.; Bhattacharya, R.; Perkins, J. D.; Carithers, R. L.; Strom, S.; Self, S. G.; Katze, M. G.; Anderson, G. A.; Smith, R. D. *Mol. Cell. Proteomics* 2014, 13 (4), 1119-1127.
30. Liu, X.; Plasencia, M.; Ragg, S.; Valentine, S. J.; Clemmer, D. E. *Brief. Funct. Genomic. Proteomic.* 2004, 3 (2), 177-186.
31. Poad, B. L. J.; Zheng, X. Y.; Mitchell, T. W.; Smith, R. D.; Baker, E. S.; Blanksby, S. J. *Anal. Chem.* 2018, 90 (2), 1292-1300.
32. Harris, R. A.; May, J. C.; Stinson, C. A.; Xia, Y.; McLean, J. A. *Anal. Chem.* 2018, 90 (3), 1915-1924.

33. Valentine, S. J.; Counterman, A. E.; Clemmer, D. E. *J. Am. Soc. Mass Spectrom.* 1999, 10 (11), 1188-1211.
34. Tao, L.; McLean, J. R.; McLean, J. A.; Russell, D. H. *J. Am. Soc. Mass Spectrom.* 2007, 18 (9), 1727-1728.
35. Dilger, J. M.; Valentine, S. J.; Glover, M. S.; Ewing, M. A.; Clemmer, D. E. *Int. J. Mass Spectrom.* 2012, 330–332 (0), 35-45.
36. Dilger, J. M.; Valentine, S. J.; Glover, M. S.; Clemmer, D. E. *J. Am. Soc. Mass Spectrom.* 2013, 24 (5), 768-779.
37. Paglia, G.; Angel, P.; Williams, J. P.; Richardson, K.; Olivos, H. J.; Thompson, J. W.; Menikarachchi, L.; Lai, S.; Walsh, C.; Moseley, A.; Plumb, R. S.; Grant, D. F.; Palsson, B. O.; Langridge, J.; Geromanos, S.; Astarite, G. *Anal. Chem.* 2015, 87 (2), 1137-1144.
38. Viehland, L. A.; Mason, E. A. *At. Data Nucl. Data Tables* 1995, 60 (1), 37-95.
39. Ellis, H. W.; Thackston, M. G.; McDaniel, E. W.; Mason, E. A. *At. Data Nucl. Data Tables* 1984, 31 (1), 113-151.
40. Ellis, H. W.; McDaniel, E. W.; Albritton, D. L.; Viehland, L. A.; Lin, S. L.; Mason, E. A. *At. Data Nucl. Data Tables* 1978, 22 (3), 179-217.
41. Ellis, H. W.; Pai, R. Y.; McDaniel, E. W.; Mason, E. A.; Viehland, L. A. *At. Data Nucl. Data Tables* 1976, 17 (3), 177-210.
42. Deng, L. L.; Ibrahim, Y. M.; Baker, E. S.; Aly, N. A.; Hamid, A. M.; Zhang, X.; Zheng, X. Y.; Garimella, S. V. B.; Webb, I. K.; Prost, S. A.; Sandoval, J. A.; Norheim, R. V.; Anderson, G. A.; Tolmachev, A. V.; Smith, R. D. *ChemistrySelect* 2016, 1 (10), 2396-2399.
43. Dodds, J. N.; May, J. C.; McLean, J. A. *Anal. Chem.* 2017, 89 (1), 952-959.
44. Dwivedi, P.; Bendiak, B.; Clowers, B. H.; Hill Jr, H. H. *J. Am. Soc. Mass Spectrom.* 2007, 18 (7), 1163-1175.
45. Fenn, L. S.; McLean, J. A. *Phys. Chem. Chem. Phys.* 2011, 13 (6), 2196-2205.
46. Groessl, M.; Graf, S.; Knochenmuss, R. *Analyst* 2015, 14 (20), 6904-6911.
47. Lalli, P. M.; Corilo, Y. E.; Fasciotti, M.; Riccio, M. F.; de Sa, G. F.; Daroda, R. J.; Souza, G. H. M. F.; McCullagh, M.; Bartberger, M. D.; Eberlin, M. N.; Campuzano, I. D. G. *J. Mass Spectrom.* 2013, 48 (9), 989-997.
48. Gerhardt, N.; Schwolow, S.; Rohn, S.; Perez-Cacho, P. R.; Galan-Soldevilla, H.; Arce, L.; Weller, P. *Food Chem.* 2019, 278, 720-728.

49. Donato, P.; Giuffrida, D.; Oteri, M.; Inferrera, V.; Dugo, P.; Mondello, L. *Food Anal. Methods* 2018, 11 (12), 3331-3341.
50. Hill, H. H.; Stlouis, R. H.; Morrissey, M. A.; Shumate, C. B.; Siems, W. F.; McMinn, D. G. J. *High Resolut. Chromatogr.* 1992, 15 (7), 417-422.
51. McLean, J. A.; Ridenour, W. B.; Caprioli, R. M. J. *Mass Spectrom.* 2007, 42 (8), 1099-1105.
52. Mason, E. A.; McDaniel, E. W. *Transport Properties of Ions in Gases*. Wiley: New York, 1988
53. Mason, E. A.; McDaniel, E. W. *The Mobility and Diffusion of Ions in Gases*. Wiley: New York, 1973
54. Deng, L. L.; Ibrahim, Y. M.; Hamid, A. M.; Garimella, S. V. B.; Webb, I. K.; Zheng, X. Y.; Prost, S. A.; Sandoval, J. A.; Norheim, R. V.; Anderson, G. A.; Tolmachev, A. V.; Baker, E. S.; Smith, R. D. *Anal. Chem.* 2016, 88 (18), 8957-8964.
55. May, J. C.; McLean, J. A., *Advanced Multidimensional Separations in Mass Spectrometry: Navigating the Big Data Deluge*. In *Annual Review of Analytical Chemistry*, Vol 9, Bohn, P. W.; Pemberton, J. E., Eds. *Annu. Rev. Anal. Chem.*: Palo Alto, 2016; Vol. 9, pp 387-409.
56. Kolli, V.; Schumacher, K. N.; Dodds, E. D. *Analyst* 2017, 142 (24), 4691-4702.
57. Lermyte, F.; Verschueren, T.; Brown, J. M.; Williams, J. P.; Valkenburg, D.; Sobott, F. *Methods* 2015, 89, 22-29.
58. Williams, J. P.; Pringle, S.; Richardson, K.; Gethings, L.; Vissers, J. P. C.; De Cecco, M.; Houel, S.; Chakraborty, A. B.; Yu, Y. Q.; Chen, W. B.; Brown, J. M., *Rapid Commun. Mass Spectrom.* 2013, 27 (21), 2383-2390.
59. Ruotolo, B. L.; Benesch, J. L. P.; Sandercock, A. M.; Hyung, S.; Robinson, C. *Nat. Protoc.*, 2008, 3, 1139-1152
60. McLean, J. A.; Ruotolo, B. T.; Gillig, K. J.; Russel, D. H. *Int. J. Mass Spectrom.* 2005, 240, 3, 301-315
61. Paglia, G.; Astarita, G. *Nat. Protoc.*, 2017, 12, 797-813
62. Zhang, X.; Quinn, K.; Cruickshank-Quinn, C.; Reisdorph, R.; Reisdorph, N. *Curr. Opin. Chem. Biol.* 2018, 42, 60-66
63. May, J. C.; Goodwin, C. R.; McLean, J. A. *Curr. Opin. Biotechnol.* 2015, 31, 117-121

64. Dunn, W. B.; Broadhurst, D.; Begley, P.; Zelena, E.; Francis-McIntyre, S.; Anderson, N.; Brown, M.; Knowles, J. D.; Halsall, A.; Haselden, J. N.; Nicholls, A. W.; Wilson, I. D.; Kell, D. B.; Goodacre, R. *Nat. Protoc.* 2011, 6, 1060-1083
65. Taguchi, F.; Solomon, B.; Gregorc, V.; Roder, H.; Gray, R.; Kashara, K.; Nisho, M.; Brahmer, J.; Spreafico, A.; Ludovini, V.; Massion, P. P.; Dziadziuszko, R.; Schiller, J.; Grigorieva, J.; Tsypin, M.; Hunsucker, S. W.; Caprioli, R.; Duncan, M. W.; Hirsch, F. R.; Bunn, P. A.; Carbone, D. P. *J. Natl. Cancer Inst.* 2007, 99 (11), 838-846
66. Mori, H.; Takio, K.; Ogawara, M.; Selkoe, D. J. *J. Biochem. Chem.* 1992, 17082-17086
67. Djidja, M. C.; Francese, S.; Loadman, P. M.; Sutton, C. W.; Scriven, P.; Claude, E.; Snel, M. F.; Franck, J.; Salzert, M.; Clench, M. R. *Proteomics*, 2009, 9 (10), 2750-2763
68. Moon, M. H.; Myung, S.; Plasencia, M.; Hilderbrand, A. E.; Clemmer, D. E. *J. Proteome Res.* 2003, 2 (6), 589-597
69. Thalassinou, K.; Grabenauer, M.; Slade, S. E.; Hilton, G. R.; Bowers, M. T.; Scrivens, J. H. *Anal. Chem.* 2009 81 (1), 248-254
70. Zhong, Y.; Hyung, S.; Ruotolo, B. T. *Expert Rev. Proteomics.* 2012, 9 (1), 47-58
71. Shliha, P. V.; Bond, N. J.; Gatto, L.; Liley, K. S. *J. Proteome Res.* 2013, 12 (6), 2323-2339
72. Clemmer, D. E.; Jarrold, M. F. *J. Mass Spectrom.* 1997, 32, 577-592
73. Wang, G.; Abzalimov, R. R.; Kaltashov, I. A. *Anal. Chem.* 2011, 83 (8), 2870-2876
74. El-Baba, T. J.; Woodall, D. W.; Raab, S. A.; Fuller, D. R.; Langanowsky, A.; Russell, D. H.; Clemmer, D. E. *J. Am. Chem. Soc.* 2017, 139, 18, 6306-6309
75. Han, X.; Yang, K.; Gross, R. W. *Mass Spectrom. Rev.* 2011, 31 (1), 134-178
76. Kliman, M.; May, J. C.; McLean, J. A. *Biochim. Biophys. Acta* 2011, 1811 (11), 935-945
77. Paglia, G.; Kliman, M.; Claude, E.; Geromanos, S.; Astarita G. *Anal. Bioanal. Chem.* 2015, 407 (17), 4995-5007
78. Grossel, M.; Graf, S.; Knochenmuss, R. *Analyst* 2015, 140
79. Di Giovanni, J. P.; Barkley, R. M.; Jones, D. N. M.; Hankins, J. A.; Murphy, R. C. *J. Am. Soc. Mass Spectrom.* 2018, 29 (6), 1231-1241
80. Paglia, G.; Shrestha, B.; Astarita G. (2017) *Ion-Mobility Mass Spectrometry for Lipidomics Application. Lipidomics. Neuromethods*, vol 125. Humana Press, New York, NY

81. Thomas, M. C.; Mitchell, T. W.; Harman, D. G.; Deeley, J. M.; Murphy, R. C.; Blanksby, S. J. *Anal. Chem.* 2007, 79 (13), 5013-5022
82. Sun, C.; Zhao, Y.; Curtis, J. M. J. *Chromatogr. A* 2014, 1351, 37-45
83. Dettmer, K.; Aronov, P. A.; Hammock, B. D. *Mass Spectrom. Rev.* 2007, 26 (1), 51-78
84. Zhang, X.; Quinn, K.; Cruickshank-Quinn, C.; Reisdorph, R.; Reisdorph N. *Curr. Opin. Chem. Biol.* 2018, 42, 60-66
85. Sinclair, E.; Hollywood, K. A.; Yan, C.; Blankley, R.; Rainer, B.; Barran P. *Analyst*, 2018, 19
86. Schrimpe-Rutledge, A. C.; Codreanu, S. G.; Sherrod, S. D.; McLean, J. A. *J. Am. Soc. Mass Spectrom.* 2016, 27 (12), 1897-1905
87. Wickramasekara, S.I.; Zandkarimi, F.; Morr e, J.; Kirkwood, J.; Legette, L.; Jiang, Y.; Gombart, A.F.; Stevens, J.F.; Maier, C.S *Metabolites*, 2013, 3, 701-717
88. Stow, M. S.; Causon, T. J.; Zheng, X.; Kurulugama, R. T.; Mairinger, T.; May, J. C.; Rennie, E. E.; Smith, R. D.; McLean, J. A.; Hann, S.; Fjeldsten, J. C. *Anal. Chem.* 2017, 89 (17), 9048-9055
89. Nichols, C. M.; Dodds, J. N.; Rose, B. S.; Picache, J. A.; Morris, C. B.; Codreanu, S. G.; May, J. C.; Sherrod, S. D.; McLean, J. A. *Anal. Chem.* 2018
90. Regueiro, J.; Negreira, N.; Berntssen, M. H. *Anal. Chem.* 2016, 88 (22), 11169-77.
91. Stephan, S.; Hippler, J.; K hler, T.; Deeb, A. A.; Schmidt, T. C.; Schmitz, O. J. *Anal. Bioanal. Chem.* 2016, 408, 24, 6545-55
92. Zheng, X.; Aly, N. A.; Zhou, Y.; Dupuis, K. T.; Bilbao, A.; Paurus, V. L.; Orton, D. J.; Wilson, R.; Payne, S. H.; Smith, R. D.; Baker, E. S. *Chem. Sci.* 2017, 8 (11), 7724-36
93. Hern andez-Mesa, M.; Le Bizec, B.; Monteau, F.; Garc a-Campa a, A. M.; Dervilly-Pinel, G. *Anal. Chem.* 2018, 90 (7), 4616-25
94. Picache, J. A.; Rose, B. S.; Balinski, A.; Leaptrot, K. L.; Sherrod, S. D.; May, J. C.; McLean, J. A. *Chem. Sci.* 2019, 10 (4), 983-993
95. Chen, T. C.; Ibrahim, Y. M.; Webb, I. K.; Garimella, S. V. B.; Zhang, X.; Hamid, A. M.; Deng, L. L.; Karnesky, W. E.; Prost, S. A.; Sandoval, J. A.; Norheim, R. V.; Anderson, G. A.; Tolmachev, A. V.; Baker, E. S.; Smith, R. D. *Anal. Chem.* 2016, 88 (3), 1728-1733.
96. Ibrahim, Y. M.; Hamid, A. M.; Deng, L. L.; Garimella, S. V. B.; Webb, I. K.; Baker, E. S.; Smith, R. D. *Analyst* 2017, 142 (7), 1010-1021.

97. Zhang, X. Y.; Garimella, S. V. B.; Prost, S. A.; Webb, I. K.; Chen, T. C.; Tang, K. Q.; Tolmachev, A. V.; Norheim, R. V.; Baker, E. S.; Anderson, G. A.; Ibrahim, Y. M.; Smith, R. D. *Anal. Chem.* 2015, 87 (12), 6010-6016.
98. Chouinard, C. D.; Nagy, G.; Webb, I. K.; Shi, T. J.; Baker, E. S.; Prost, S. A.; Liu, T.; Ibrahim, Y. M.; Smith, R. D. *Anal. Chem.* 2018, 90 (18), 10889-10896.
99. Garimella, S. V. B.; Ibrahim, Y. M.; Webb, I. K.; Tolmachev, A. V.; Zhang, X. Y.; Prost, S. A.; Anderson, G. A.; Smith, R. D. *J. Am. Soc. Mass Spectrom.* 2014, 25 (11), 1890-1896.
100. Webb, I. K.; Garimella, S. V. B.; Tolmachev, A. V.; Chen, T. C.; Zhang, X. Y.; Cox, J. T.; Norheim, R. V.; Prost, S. A.; LaMarche, B.; Anderson, G. A.; Ibrahim, Y. M.; Smith, R. D. *Anal. Chem.* 2014, 86 (19), 9632-9637.
101. Garimella, S. V. B.; Ibrahim, Y. M.; Webb, I. K.; Ipsen, A. B.; Chen, T. C.; Tolmachev, A. V.; Baker, E. S.; Anderson, G. A.; Smith, R. D. *Analyst* 2015, 14 (20), 6845-6852.
102. Deng, L. L.; Webb, I. K.; Garimella, S. V. B.; Hamid, A. M.; Zheng, X. Y.; Norheim, R. V.; Prost, S. A.; Anderson, G. A.; Sandoval, J. A.; Baker, E. S.; Ibrahim, Y. M.; Smith, R. D. *Anal. Chem.* 2017, 89 (8), 4628-4634.
103. Dodds, J. N.; May, J. C.; McLean, J. A. *Anal. Chem.* 2017, 89 (22), 12176-12184.
104. Fernandez-Lima, F. A.; Kaplan, D. A.; Suetering, J.; Park, M. A. *Int. J. Ion Mobil. Spectrom.* 2011, 14 (2-3), 93-98.
105. Adams, K. J.; Montero, D.; Aga, D.; Fernandez-Lima, F. *Int. J. Ion Mobil. Spectrom.* 2016, 19 (2-3), 69-76.
106. Michelmann, K.; Silveira, J. A.; Ridgeway, M. E.; Park, M. A. *J. Am. Soc. Mass Spectrom.* 2015, 26 (1), 14-24.
107. Hernandez, D. R.; DeBord, J. D.; Ridgeway, M. E.; Kaplan, D. A.; Park, M. A.; Fernandez-Lima, F. *Analyst* 2014, 139 (8), 1913-1921.
108. Silveira, J. A.; Danielson, W.; Ridgeway, M. E.; Park, M. A. *Int. J. Ion Mobil. Spectrom.* 2016, 19 (2-3), 87-94.
109. May, J. C.; Leaptrot, K. L.; Sundarapandian, S.; McLean, J. A. In *Theoretical Evaluation and Performance Characterization of an 8-Channel Spatially Multiplexed Ion Mobility-Mass Spectrometer*, 60th Annual ASMS Conference on Mass Spectrometry and Allied Topics, Vancouver, BC, May 2012; Vancouver, BC, 2012.
110. Asbury, G. R.; Hill, H. H. *Anal. Chem.* 2000, 72 (3), 580-584.
111. Matz, L. M.; Hill, H. H., Jr.; Beegle, L. W.; Kanik, I. J. *Am. Soc. Mass Spectrom.* 2002, 13 (4), 300-307.

112. Berant, Z.; Karpas, Z. *J. Am. Chem. Soc.* 1989, 111 (11), 3819-3824.
113. Howdle, M. D.; Eckers, C.; Laures, A. M. F.; Creaser, C. S. *Int. J. Mass Spectrom.* 2010, 298 (1-3), 72-77.
114. Purves, R. W.; Ozog, A. R.; Ambrose, S. J.; Prasad, S.; Belford, M.; Dunyach, J. J. *J. Am. Soc. Mass Spectrom.* 2014, 25 (7), 1274-1284.
115. Waraksa, E.; Perycz, U.; Namiesnik, J.; Sillanpaa, M.; Dymerski, T.; Wojtowicz, M.; Puton, J. *Trends Analyt. Chem.* 2016, 82, 237-249.
116. Schneider, B. B.; Covey, T. R.; Nazarov, E. G. *Int. J. Ion Mobil. Spectrom.* 2013, 16, 207-216.
117. Kafle, A.; Coy, S. L.; Wong, B. M.; Fornace, A. J.; Glick, J. J.; Vouros, P. J. *J. Am. Soc. Mass Spectrom.* 2014, 25 (7), 1098-1113.
118. Levin, D. S.; Vouros, P.; Miller, R. A.; Nazarov, E. G.; Morris, J. C. *Anal. Chem.* 2006, 78 (1), 96-106.
119. Porta, T.; Varesio, E.; Hopfgartner, G. *Anal. Chem.* 2013, 85 (24), 11771-11779.
120. Fernandez-Maestre, R.; Wu, C.; Hill, H. H. *Rapid Commun. Mass Spectrom.* 2012, 26 (19), 2211-2223.
121. Garabedian, A.; Leng, F. F.; Ridgeway, M. E.; Park, M. A.; Fernandez-Lima, F. *Int. J. Ion Mobil. Spectrom.* 2018, 21 (1-2), 43-48.
122. Beegle, L. W.; Kanik, I.; Matz, L.; Hill, H. H. *Anal. Chem.* 2001, 73 (13), 3028-3034.
123. Beegle, L. W.; Kanik, I.; Matz, L.; Hill, H. H. *Int. J. Mass Spectrom.* 2002, 216 (3), 257-268.
124. Chouinard, C. D.; Beekman, C. R.; Kemperman, R. H. J.; King, H. M.; Yost, R. A. *Int. J. Ion Mobil. Spectrom.* 2017, 20 (1-2), 31-39.
125. Fasciotti, M.; Lalli, P. M.; Klitzke, C. F.; Corilo, Y. E.; Pudenzi, M. A.; Pereira, R. C. L.; Bastos, W.; Daroda, R. J.; Eberlin, M. N. *Energy Fuels* 2013, 27 (12), 7277-7286.
126. Fasciotti, M.; Sanvido, G. B.; Santos, V. G.; Lalli, P. M.; McCullagh, M.; de Sá, G. F.; Daroda, R. J.; Peter, M. G.; Eberlin, M. N. *J. Mass Spectrom.* 2012, 47 (12), 1643-1647.
127. Bataglion, G. A.; Souza, G.; Heerdt, G.; Morgon, N. H.; Dutra, J. D. L.; Freire, R. O.; Eberlin, M. N.; Tata, A. J. *Mass Spectrom.* 2015, 50 (2), 336-343.
128. Ruotolo, B. T.; McLean, J. A.; Gillig, K. J.; Russell, D. H. *J. Mass Spectrom.* 2004, 39 (4), 361-367.

129. Jurieczko, E.; Kalapothakis, J.; Campuzano, I. D. G.; Morris, M.; Barran, P. E. *Anal. Chem.* 2012, 84 (20), 8524-8531.
130. Davidson, K. L.; Bush, M. F. *Anal. Chem.* 2017, 89 (3), 2017-2023.
131. Norris, J. L.; Farrow, M. A.; Gutierrez, D. B.; Palmer, L. D.; Muszynski, N.; Sherrod, S. D.; Pino, J. C.; Allen, J. L.; Spraggins, J. M.; Lubbock A. L. R.; Jordan, A.; Burns, W.; Poland, J. C.; Romer, C.; Manier, M. L.; Nei, Y.; Prentice, B. M.; Rose, K. L.; Hill, S.; Van de Plas, R.; Tsui, T.; Braman, N. M.; Keller, M. R.; Rutherford, S. A.; Lobdell, N.; Lopez, C. F.; Lacy, D. B.; McLean, J. A.; Wikswow, J. P.; Skaar, E. P.; Caprioli, R. M. J. *Proteome Res.* 2017, 16 (3), 1364-1375.
132. Paglia, G.; Stocchero, M.; Cacciato, S.; Lai, S.; Angel, P.; Alam, M. T.; Keller, M.; Ralsler, M.; Astarita, G. J. *Proteome Res.*, 2016, 15, 608-618.
133. Morgan, X. C.; Segata, N.; Huttenhower, C. *Trends Genet.* 2013, 29 (1), 51-58.
134. Weir, T. L.; Manter, D. K.; Brittany, B. A.; Heuberger, A. L.; Ryan, E. P. *PLoS One* 2013, 8, e70803.
135. Raman, M.; Ahmed, I.; Gillevet, P. M.; Probert, C. S.; Ratcliffe, N. M.; Smith, S.; Greenwood, R.; Sikaroodi, M.; Lam, V.; Crotty, P.; Bailey, J.; Meyes, R. P.; Rioux, K. P. *Clin. Gastroenterol. Hepatol.* 2013, 11, 7, 868-875.
136. Benson, D. A.; Cavanaugh, M.; Clark, K.; Karsch-Mizrachi, I.; Lipman, D. J.; Ostell, J.; Sayers, E. W. *Nucleic Acid Res.* 2013, 41, 36-42.
137. Bernstein, F. C.; Koetzle, T. F.; Williams, G. J. B.; Meyer Jr., E. F.; Brice, M. D.; Rodgers, J. R.; Kennard, O.; Shimanouchi, T.; Tasumi, M. J. *Mol. Biol.* 1977 112: 535-542.

CHAPTER 2

AN ION MOBILITY COLLISION CROSS SECTION COMPENDIUM

2.1 Introduction

In this review, we focus on an important aspect of ion mobility (IM) research, namely the reporting of quantitative ion mobility measurements in the form of the gas-phase collision cross section (CCS), which has provided a common basis for comparison across different instrument platforms and offers a unique form of structural information, namely size and shape preferences of analytes in the absence of bulk solvent. This review surveys the over 24,000 CCS values reported from IM methods spanning the era between 1975 to 2015, which provides both a historical and analytical context for the contributions made thus far, as well as insight into the future directions that quantitative ion mobility measurements will have in the analytical sciences. The analysis was conducted in 2016, so CCS values reported in that year are purposely omitted. In another few years, a review of this scope will be intractable, as the number of CCS values which will be reported in the next three to five years is expected to exceed the total amount currently published in the literature.

Quantitative ion mobility methods have seen a resurgence of recent and significant interest due to the fact that in the past three years, a number of new and updated ion mobility technologies combined with mass spectrometry (IM-MS) have emerged as commercially-available instrumentation for routine chemical analysis. These have included updates to traveling wave instrumentation (TWIMS), new uniform field drift tubes (DTIMS) operated at both elevated¹ and reduced pressures (less than 10 Torr),²⁻⁴ and a newly-developed ion trapping device operated in a

mobility-selective mode (trapped ion mobility spectrometry, TIMS) ⁵⁻⁷. Other ion mobility techniques including cyclic and extended path length traveling wave devices are currently in development.^{8,9} This recent and unprecedented commercial accessibility of IM-MS in combination with existing liquid chromatography and tandem MS functionality has provided powerful multidimensional separation capabilities to the greater research community,¹⁰⁻¹³ which in turn has broadened the scope of applications and fields in which IM-MS is now making a significant impact.¹⁴⁻¹⁹ Many of the contemporary challenges being addressed by IM-MS are grand challenges of our era of humanity.¹¹

Ion mobility is generally utilized in one of three ways by researchers (Table 2.1): (1) as an added dimension of separation for increasing the peak capacity and partitioning the chemical noise from analyte signals of interest, (2) as an additional measurement for analyte identification and characterization, and/or (3) as a structural measurement technique, where the ion mobility information is used to infer some details regarding the structure (either primary or higher-order) of the analyte. The latter two strategies, analyte identification and structural measurement, are achieved by converting the ion mobility measurement (typically drift time), to an ion-neutral collision cross section value, which represents a fundamental property of the analyte comparable across different laboratories. Analyte identification and correlation can also proceed using the standardized mobility value, as has been achieved in the field of stand-alone ion mobility spectrometers utilized for chemical detection and screening,^{20,21} although the fundamental meaning of the mobility measurement is more accessible when discussed in the context of the analyte CCS.

TABLE 2.1 – Three key analytical uses of ion mobility.

Analytical Use of Ion Mobility	Description	Additional Requirements	Example Application Areas
1. Chemical Separation	Partition signal from chemical noise and increase peak capacity of the analysis	None	Detection of Illicit compounds (<i>e.g.</i> , drugs and explosives) and screening of exogenous metabolites (<i>e.g.</i> , pesticides and industrial chemicals)
2. Analyte Identification and Characterization	Use CCS measurement to characterize unknowns by correlation	Reference values from databases and libraries incorporating normalized drift times, reduced mobilities, and/or CCS	Emerging omic and small molecule discovery initiatives
3. Structural Analysis	Utilize the experimental CCS to infer structural information	Computational methods to link theoretical structure(s) to the experimental CCS	Insights into protein complex arrangements and structure

Reprinted (adapted) with permission from Jody C. May, Caleb B. Morris, John A. McLean, "Ion Mobility Collision Cross Section Compendium," *Analytical Chemistry* 2017, 89 (2), 1032-1044. Copyright 2017 American Chemical Society.

2.2 The Collision Cross Section

One of the contemporary challenges with interpreting the meaning of the CCS lies in the fact that it is not a true molecular cross section, but rather represents an observational property that averages all geometric orientations and interaction types (head-on, “glancing”, and “orbiting” collisions, multiple collisions within cavities of the analyte, *etc.*) across the experimental measurement time.²²⁻²⁵ These effects include both contributions from the drift gas itself (momentum transfer and gas polarization effects) and contributions arising from the ion mobility experiment (temperature and magnitude of the electric field). Classically, the CCS determined from ion-gas collision measurements is referred to as the momentum transfer or diffusion CCS to specify the importance and dependence that the drift gas has on the resulting quantity being obtained.^{26,27}

As a result of these contributions, the empirical CCS is a macroscopic quantity which is specific to the identity of the drift gas as well as the temperature and electric field used during the measurement,^{28,29} and so by the strictest definition, CCS is not an intrinsic property of the analyte, although it is very closely linked to one (namely the microscopic cross section of the analyte). Mathematically, the CCS represents the area of a circle, and thus the structural information is “coarse-grained” in nature. While significant for small molecule studies, this level of granularity is less of an issue when probing coarse structural features such as domain-level information for protein assemblies.^{30,31}

The CCS is a quantity that is now routinely obtainable from a variety of ion mobility experiments, and, although less frequently discussed, the CCS can also be obtained from mass spectrometry experiments where gas collisions are present. Mass spectrometric methods utilized for measuring CCS have included pressure correlated ion loss studies in magnetic sector,³²⁻³⁴ triple

quadrupole,^{35,36} and time-of-flight instruments;³⁷ ion relaxation times in an ion trap;³⁸ and peak width analysis from ion cyclotron resonance measurements.^{39,40} Ion mobility methods currently provide the most precise measurements of the CCS, with precision being linked to the experimental certainty in all of the parameters which govern the IM separation, such as the gas temperature, electric field, gas number density (*via* pressure and temperature) and the geometric distances within the instrumentation. As such, uniform field drift tubes (DTIMS) and differential mobility analyzers (DMA) afford the highest CCS precision since experimental quantities in these techniques can be well-characterized. It should be noted here that precision and accuracy are important distinctions, as very reproducible CCS values can now be obtained (better than 2%),^{2,41} but their accuracy cannot be validated without comparing the ion mobility results to CCS measurements obtained from other techniques, which at this time are still in development.⁴²⁻⁴⁴ Despite these standing questions regarding the accuracy and meaning of the CCS, it is clear that there is immense value in reporting a standardized fundamental property of an analyte in the form of a CCS which is both highly-reproducible and now readily-accessible by a large number of researchers.

Recent publications have utilized an elegant nomenclature for CCS reporting whereby the measurement technique is denoted as a superscripted prefix, while the drift gas is specified as a subscripted suffix, for example, ^{DT}CCS_{N₂} to denote a nitrogen CCS value measured from a drift tube instrument.⁴⁵⁻⁴⁸ This nomenclature is summarized in Table 2.2 along with specific recommendations for the instrumentation shorthand. Given the oftentimes ambiguous nature of the experimental context in which CCS values are reported, the nomenclature formalized in Table 2.2 is recommended for future use in the field.

TABLE 2.2 – Formalized nomenclature for reporting CCS measurements in the context of the technique and drift gas utilized.

CCS Measurement Technique	Technique Shorthand ^a	Nomenclature for CCS Reporting ^b
Drift Tube Ion Mobility Spectrometry (DTIMS)	DT	^{DT} CCS _X
Traveling Wave Ion Mobility Spectrometry (TWIMS)	TW	^{TW} CCS _X
Trapped Ion Mobility Spectrometry (TIMS)	TIMS	^{TIMS} CCS _X
Differential Mobility Analyzer (DMA)	DMA	^{DMA} CCS _X
^a . Only the four major ion mobility techniques which report CCS are listed. ^b . X denotes the drift gas or drift gas equivalent for calibrated values (X = He, N ₂ , Ar, CO ₂ , <i>etc.</i>)		

Reprinted (adapted) with permission from Jody C. May, Caleb B. Morris, John A. McLean, “Ion Mobility Collision Cross Section Compendium,” *Analytical Chemistry* 2017, 89 (2), 1032-1044. Copyright 2017 American Chemical Society.

2.3 Significant CCS Contributions

The emerging importance of CCS to support contemporary analytical trends is evidenced by the fact that over half of the over 24,000 canonical CCS values reported between 1975 and 2015 has been published within the last five years (Figure 2.1(A)). Examining the histogram in Figure 2.1(A) indicates there was an initial surge of CCS values reported between 1995 and 1999 which was largely in response to the introduction of ESI and MALDI ionization techniques, followed by a decade of relatively few new CCS values being reported (2000-2009). Starting in 2010, the number of CCS values reported increased drastically, which is interpreted as being a direct response of the introduction of new ion mobility techniques, including commercial TWIMS technology in 2006,⁴⁹ confining RF DTIMS in 2010,⁵⁰ and DTIMS integrated with ion funnels, initially reported in 2005 and commercialized in 2014.^{2,51}

Major contributions from specific laboratories are noted in Figure 2.1(B) and include several large-scale studies from Clemmer and coworkers examining electrosprayed peptides and proteins in helium (*ca.* 4200 values),⁵²⁻⁵⁵ contributions from Bowers and coworkers on hydrocarbons and carbon clusters (*ca.* 400 values),⁵⁶⁻⁵⁹ studies from Jarrold and coworkers investigating carbon, silicon, and palladium clusters (*ca.* 550 values),⁶⁰⁻⁶³ contributions from Russell and coworkers reporting singly-charged CCS values of MALDI generated peptides and proteins (*ca.* 650 values);^{64,65} TWIMS and DTIMS studies from Pagel and coworkers investigating both helium and nitrogen CCS for carbohydrates (*ca.* 1300 values),^{45,66,67} work from McLean and coworkers which include a number of lipid, peptide, and carbohydrate CCS values in both helium and nitrogen (*ca.* 1000 values),^{2,68,69} and recent TWIMS work from Astarita and coworkers reporting nitrogen CCS values for both lipids and metabolites (*ca.* 450 values).^{70,71} The largest single quantitative ion mobility survey to date represents the *ca.* 8,700 nitrogen CCS values

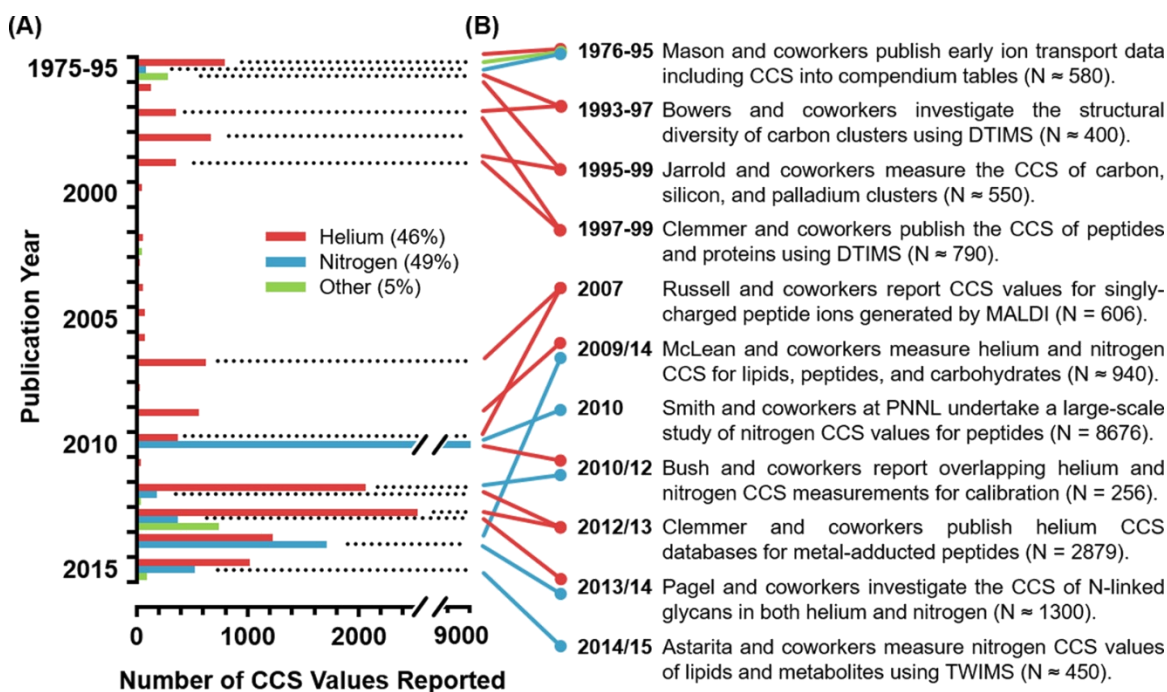


Figure 2.1 (A) The number of CCS values published over the 40-year span between 1975 and 2015. The drift gas used in the measurement or calibration is specified for each year bin. (B) The laboratories and studies which have made significant contributions in terms of number of values reported. Reprinted (adapted) with permission from Jody C. May, Caleb B. Morris, John A. McLean, "Ion Mobility Collision Cross Section Compendium," *Analytical Chemistry* 2017, 89 (2), 1032-1044. Copyright 2017 American Chemical Society.

published by Smith and coworkers for tryptic peptides in support of proteomics studies.⁷² While the early studies have focused on obtaining structural information through the measurement of the CCS, several of the recent contributions have been purposed as cross sectional databases in support of analyte characterization. The motivation for utilizing CCS as a molecular descriptor (*c.f.*, Table 2.1) is an emerging application area in the field of analytical chemistry. Additionally, the high quality CCS data from the Clemmer⁷³ and Bush laboratories^{41,50,74} are routinely used for calibrating ion mobility instrumentation.

While only major studies are highlighted here, the majority of contributions to the CCS canon (75%) have come from smaller studies which report 50 or fewer CCS values (Figure 2.2). In fact, there are only three individual studies which have reported over 1,000 CCS values and thus would be considered large-scale surveys,^{54,55,72} underscoring the fact that the reporting of quantitative ion mobility measurements is predominantly an interlaboratory initiative.

2.4 Drift Gases Represented

While measurements obtained in helium and nitrogen represent the vast majority of the CCS values reported (95%, *c.f.*, Figure 2.1), there have been a few quantitative studies conducted in alternative drift gases, most representing the classic atomic and small molecule studies compiled by Mason and coworkers during the early developments of analytical ion mobility,⁷⁵⁻⁷⁸ but also early work from Hill and coworkers exploring CCS differences of small peptides and drug molecules in helium, nitrogen, argon, and carbon dioxide.⁷⁹ Recent studies which explicitly report CCS values in alternative drift gases include measurements of ammonium in helium, nitrogen, argon and carbon dioxide from Viehland and coworkers,⁸⁰ the combined DTIMS and TWIMS study from Barran and coworkers investigating myoglobin in helium, nitrogen, argon, and neon,⁸¹

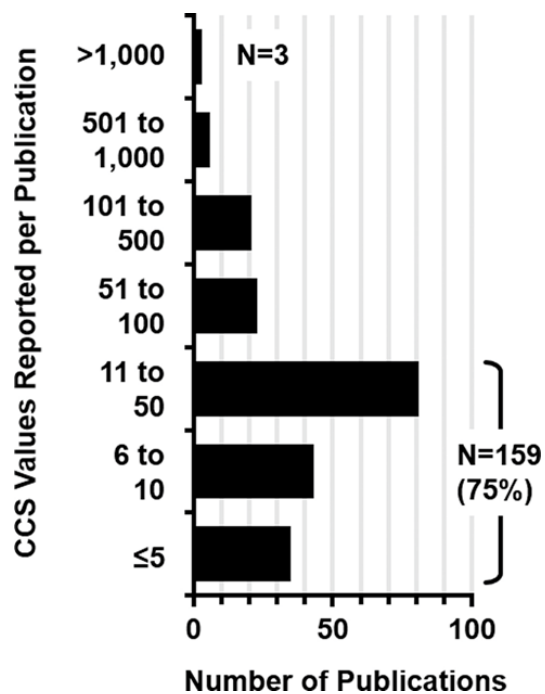


Figure 2.2 Histogram illustrating the number of CCS values which are reported per publication. The bracketed bins draw attention to the fact that most of the CCS measurements have come from smaller studies reporting 50 or fewer cross section values. Reprinted (adapted) with permission from Jody C. May, Caleb B. Morris, John A. McLean, "Ion Mobility Collision Cross Section Compendium," *Analytical Chemistry* 2017, 89 (2), 1032-1044. Copyright 2017 American Chemical Society.

DMA measurements of CCS in air from both de la Mora and coworkers⁸² and Hogan and coworkers,⁸³ and DTIMS work from Fjeldsted and coworkers exploring the CCS differences of pesticides in a variety of drift gases including helium, nitrogen, carbon dioxide, nitrous oxide, argon, and sulfur hexafluoride.⁸⁴

The sparse amount of CCS data reported for gases other than helium and nitrogen is largely a combined result of both technical challenges with operating under different drift gas conditions (instrument tuning, pressure gauge calibration issues, and uncertainty with calculating the CCS from measured drift times), as well as fundamental difficulties with interpreting the structural meaning of CCS values obtained using gases other than helium. The typically better correlation of helium CCS values to theoretical results is primarily a consequence of the lower contribution of ion-neutral polarization effects in atomic helium ($\alpha=0.21 \text{ \AA}^3$) as compared to diatomic nitrogen ($\alpha=1.74 \text{ \AA}^3$) and other neutral gases (*e.g.*, argon, $\alpha=1.64 \text{ \AA}^3$; carbon dioxide, $\alpha=2.91 \text{ \AA}^3$),^{79,85-87} although it should be noted that significant and recent efforts have been made in improving the fundamental theories used in predicting nitrogen-based CCS values from candidate structures.^{25,26,88,89} In addition to the better theoretical correlation of helium CCS, there is also some evidence that helium offers analytical benefits in reducing mass-mobility discrimination and improving ion transmission in dispersive (DTIMS and TWIMS) ion mobility instrumentation.^{90,91} The choice of nitrogen as a drift gas stems from practical considerations of cost and availability, fundamental considerations regarding nitrogen's resistance to electrical discharge (dielectric breakdown) and analytical improvements in resolving power due to the longer residence time of ions (*i.e.*, lower reduced mobility values) within the ion mobility experiment.⁹² While these attributes are shared by other drift gases such as argon and carbon dioxide, their use in quantitative IM research has not yet been significantly explored. It is anticipated that the meager quantitative

IM data currently available for alternative gases represents only a temporary deficiency as the instrumentation and CCS measurement capabilities to support different drift gases are now becoming widely available, and evidence is mounting in support of the analytical benefits of conducting IM separations in other drift gases such as argon and carbon dioxide.⁹³⁻⁹⁷

2.5 Composition of Measurements

An analysis of the composition the CCS values published from 1975 to 2015 is presented in Figure 2.3 for a few select categories. With regards to instrumentation (Figure 2.3(A)), most (87%) of the CCS values represent measurements conducted in DTIMS instruments, which include both elevated⁹⁸⁻¹⁰² and reduced pressure DTIMS instrumentation,¹⁰³⁻¹¹⁰ as well as instrumentation utilizing electric field-mediated ion focusing strategies such as periodic DC,^{111,112} confining RF,^{4,50} and electrodynamic ion funnels.^{2,51,113} A cursory comparison of the measurements themselves (not shown) indicates there is no significant differences between the CCS values obtained using these different modes of DTIMS operation, suggesting these focusing strategies do not perturb the resulting CCS. Because DTIMS still exhibits the highest precision when measuring the CCS and the direct relationship between drift time and cross section allows broad scale CCS determination of mixtures, it is no surprise that DTIMS has contributed to the majority of values published to date. TWIMS values obtained from calibration represent 9% of the CCS values,¹¹⁴⁻¹¹⁷ while the remaining values are from other IM techniques such as DMA^{82,83} and TIMS.¹¹⁸⁻¹²¹ Regarding the selection of drift gas (Figure 2.3(B)), there are slightly more CCS values being obtained in nitrogen (49%) as compared to helium (46%), with reporting of nitrogen-based CCS values being a recent analytical trend in the field (*c.f.*, Figure 2.1(A)). Measurements in ambient air comprise 3% of the CCS values, which are from elevated pressure DTIMS and DMA studies.

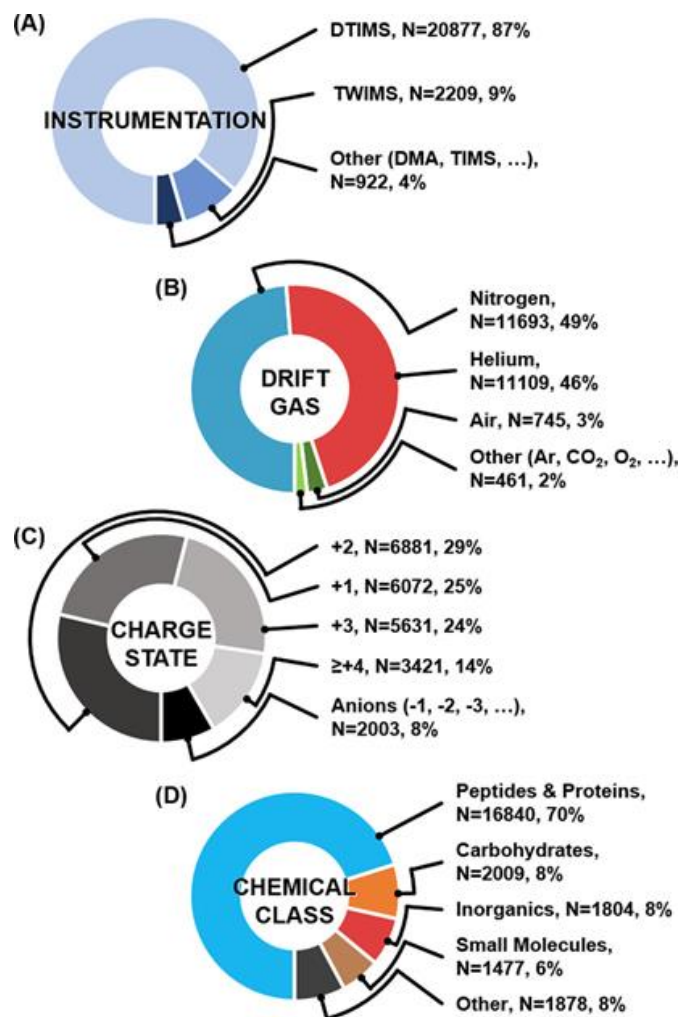


Figure 2.3 Composition of CCS values with respect to (A) the ion mobility instrumentation used, (B) the drift gas, (C) specific charge state reported, and (D) the chemical classes investigated. Reprinted (adapted) with permission from Jody C. May, Caleb B. Morris, John A. McLean, "Ion Mobility Collision Cross Section Compendium," *Analytical Chemistry* 2017, 89 (2), 1032-1044. Copyright 2017 American Chemical Society.

The remaining 2% of values are for measurements conducted in argon (0.5%), carbon dioxide (0.3%), oxygen (0.3%), neon (0.2%), nitrous oxide (0.2%), and others (0.5%). Specific motivations for drift gas selection are discussed in the previous section.

Figure 2.3(C) indicates that the majority of CCS values are for low charge-state cations (+1, +2, and +3 ions, collectively representing 78% of all values reported), and thus anion CCS values are currently underrepresented, comprising only 8% of the total body of work. This predominance of positive ion data is expected given that MS-based studies are preferentially conducted in positive ion mode. Most of the anions CCS values reported are from two recent carbohydrate studies, one on chemically-released glycans and corresponding ion fragments generated in source,⁶⁷ and another reporting negative ion CCS values on dextran and pullulan oligosaccharides.¹²² Remaining anion contributions represent the classic DTIMS studies on atomic and molecular clusters,^{57,63,123} and recent negative ion measurements for proteins,¹²⁴ lipids,^{1,71} and metabolites.^{70,125} The primary ionization method used in the quantitative measurement of the CCS is ESI (87%, not shown) which tends to produce primarily +2 ions for tryptic peptides.¹²⁶ As tryptic peptides represent the majority of CCS measurements reported in the literature (*vide infra*), it is no surprise that there are more +2 ions than any other charge state. Laser-based ionization (MALDI and LDI) which produce mainly +1 ions in positive ion mode comprise only 11% of the CCS values (not shown). Higher charge state cations (+4 or greater) comprise 14% of the CCS values reported, which is in line with the number of protein ion CCS values represented in the analysis (9% of the total, not shown).

Finally, in Figure 2.3(D), an analysis of the contributions made within specific chemical classes reveal the majority of CCS values reported in the literature are for peptides and proteins (70%), with carbohydrates (8%), inorganics (*e.g.*, clusters, nanomaterials, and salts; 8%), and other

small molecules (*e.g.*, hydrocarbons and metabolites; 6%) representing the remainder of values. The focus on peptide and protein work can be rationalized as being a result of continued efforts for adapting ion mobility technologies to proteomics workflows,¹²⁷⁻¹²⁹ but also a practical consequence of both the ease of generating large pools of peptides derived from enzymatic digestion¹³⁰ and the fact that the structural and charge-state heterogeneity of proteins necessitates the reporting of many CCS values for a single protein.¹³¹⁻¹³⁴ To summarize the observations in Figure 2.3, most quantitative ion mobility studies to date have used DTIMS for peptide and protein analysis, with an approximate equal number of measurements represented in both helium and nitrogen drift gases.

2.6 Chemical Space Represented by IM-MS Analysis

Figures 2.4 and 2.5 projects all of the canonical CCS values as a function of the ion mass, for helium and nitrogen-based ion mobility measurements, respectively. The scattering of measurements (lower panels) are noticeably different in both gases, underscoring the fact that different analytes and charge states are represented in each type of gas. For example, a larger percentage of helium CCS values are singly-charged (37%) compared to a smaller percentage of singly-charged values in nitrogen (13%). Nitrogen CCS values also contain a significant number of triply-charged measurements (34%), in contrast to helium CCS values, which are comprised of only 14% triply-charged CCS values. This is one reason for the more prominent clustering of higher charge-state measurements in nitrogen (Figure 2.5, lower panel). There are also a significant number of CCS values for atomic and molecular clusters (carbon, silicon, and inorganic salts) which are unique to the helium CCS measurements, resulting in the trends prominently observed at low CCS (Figure 2.4, lower panel). Nitrogen CCS values are larger in magnitude than helium

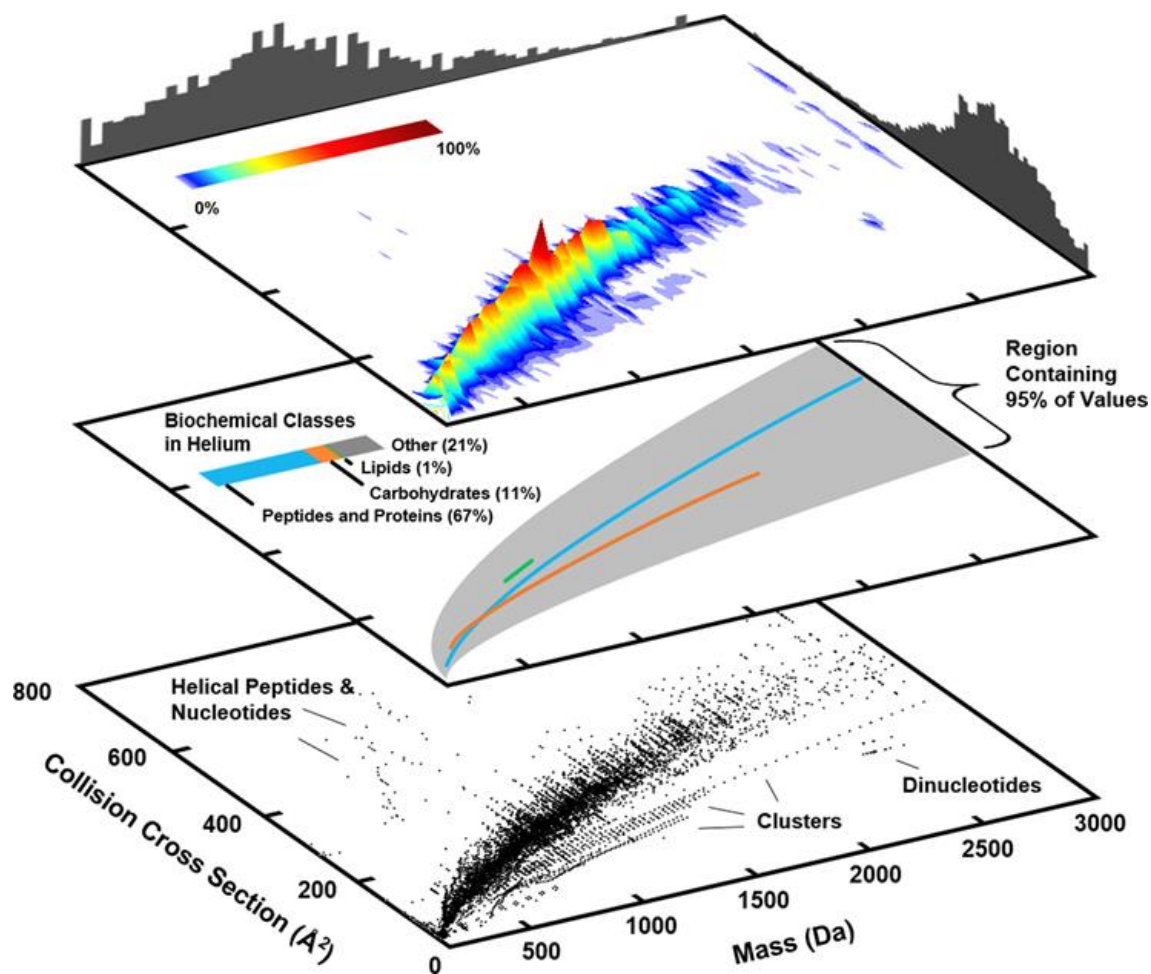


Figure 2.4 (lower panel) Helium-specific conformational space plot which projects helium-based CCS values as a function of the analyte mass. (middle panel) The composition and chemical space occupancy of specific biomolecules. (top panel) A 3-dimensional surface plot illustrating the regions of highest density in terms of the numbers of CCS values. Reprinted (adapted) with permission from Jody C. May, Caleb B. Morris, John A. McLean, "Ion Mobility Collision Cross Section Compendium," *Analytical Chemistry* 2017, 89 (2), 1032-1044. Copyright 2017 American Chemical Society.

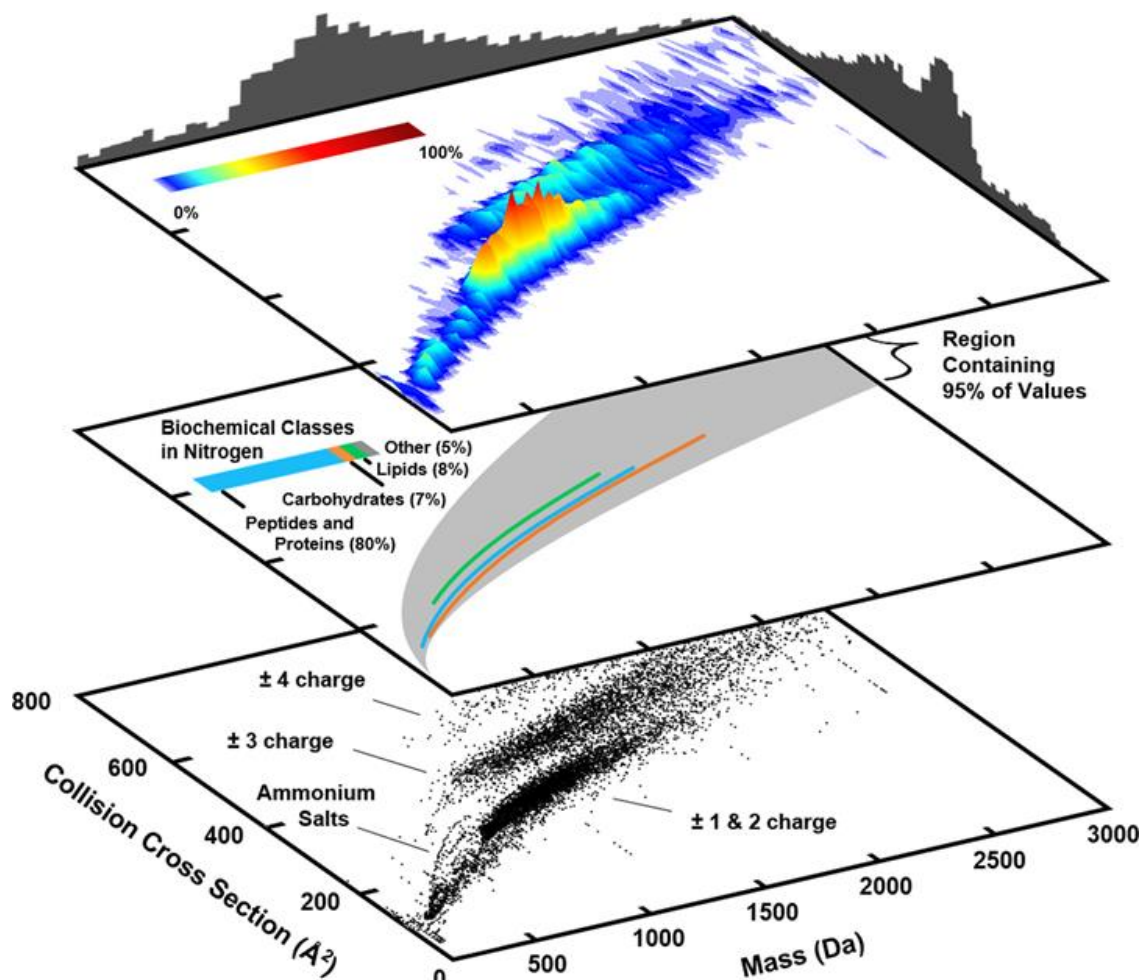


Figure 2.5 Nitrogen-specific conformational space plot which projects nitrogen-based CCS values as a function of the analyte mass, along with (middle panel) the biomolecular composition and occupancy and (top panel) the 3-dimensional surface density plot of CCS values reported. Reprinted (adapted) with permission from Jody C. May, Caleb B. Morris, John A. McLean, “Ion Mobility Collision Cross Section Compendium,” *Analytical Chemistry* 2017, 89 (2), 1032-1044. Copyright 2017 American Chemical Society.

values due to the higher momentum contribution of the nitrogen molecule as well as the stronger polarization which in turn leads to temporally-extended ion-neutral interactions in the IM experiment.

The central panels in both Figures 2.4 and 2.5 project the average mathematical fits to specific biochemical classes based on a power-law relationship.² Only the fits to singly-charged analyte is shown, and fits are not extrapolated beyond the range of measurements. The total chemical occupancy of all measurements is illustrated by a 95% data inclusion area (grey shaded region). The general conformational ordering of biomolecules observed here qualitatively correlates to the gas-phase structural trends noted from previously studies, that is, lipids adopt more extended structures in the gas-phase than peptides and carbohydrates.^{2,135,136} The quantitative differences observed between helium and nitrogen are a consequence of evaluating the CCS values corresponding to different analytes in each figure. This can be seen by examining the biochemical class compositions which are noted in the central panel of each figure, where for example, significantly more peptides and proteins are represented in nitrogen (80%) than helium (67%). The 3-dimensional surface plots and associated histograms projected on the top panels in Figures 2.4 and 2.5 illustrate the distribution of CCS values reported for both helium and nitrogen drift gas. Overall, the analytes surveyed from both gases fall within a similar mass window between 500 to 1500 Da with more values at lower mass reported for helium than nitrogen. As many of the helium measurements are from earlier work in the field and represent singly-charged analytes, it is no surprise that the overall coverage concerns lower mass analytes.

2.7 CCS Coverage over Time

Figure 2.6 compares the number of CCS values reported over the past 40 years as they correlate to mass. This analysis reveals that, as expected, the focus of quantitative ion mobility studies has shifted over time to higher mass due to improvements in technology and methods used to desorb, ionize, and stabilize large analytes such as biomolecules. Prior to the widespread use of soft ionization methods (*ca.* 1995), the average mass of ions for which CCS values were being reported was less than 100 Da,^{75-78,137-141} and in the decade following the adoption of MALDI and ESI (1996-2005) in research instrumentation, a broad range of ion masses up to *ca.* 2500 Da were investigated, though the majority of measurements were centered on low mass studies around 300 Da. In the past decade (2006-2015), the average ion mass was approximately 1000 Da and represents predominately peptide CCS values, however significant efforts were also made for reporting CCS values of lower mass ions centered around 400 Da, the latter representing analytical interests in short-chain carbohydrates,¹⁴²⁻¹⁴⁷ metabolites,^{70,125,148-151} and drug-like molecules.^{84,87,89,152} Figure 2.6(B) contains the distribution of CCS reporting with analyte masses extending up to the megaDalton range, which illustrates the recent analytical trend of utilizing quantitative ion mobility methods to study the structure of large protein assemblies,^{50,124,153-159} some of which are annotated in the figure. These studies specifically target IM-based measurements towards the interpretation of molecular structure. Note that the vertical scale in Figure 2.6 is the same in both panels, however, the bin size is increased in Figure 2.6(B) (from 50 Da to 10 kDa) to accommodate the broader mass range being projected. A final observation to make from Figure 2.6(A) is that the bimodal distribution observed over the past five years (2011-2015) closely mimics the analytical trend observed within the largest chemical database,

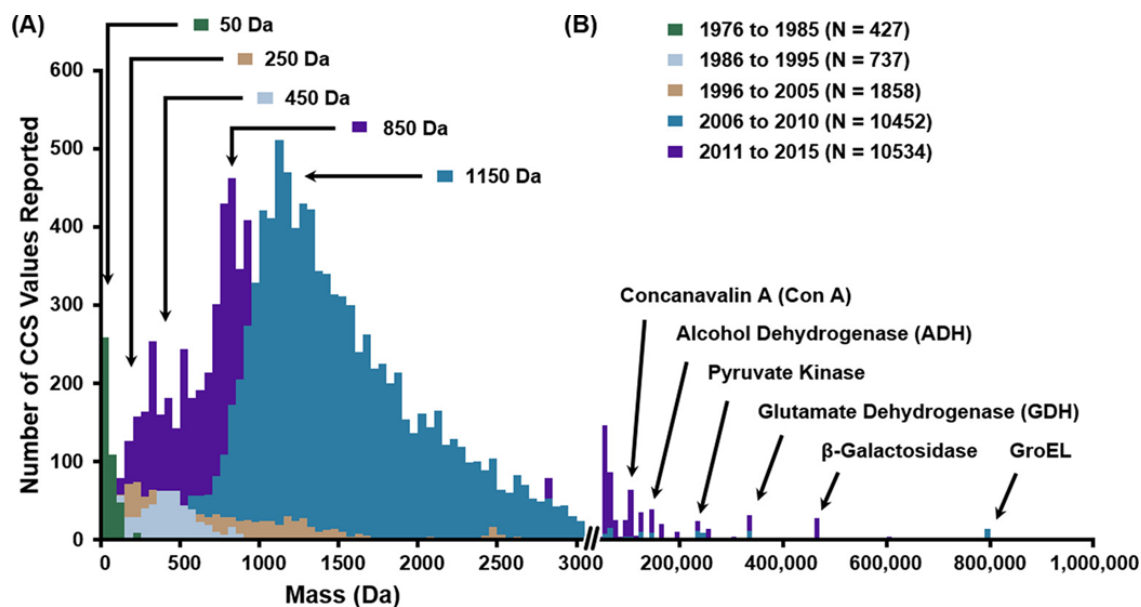


Figure 2.6 Histogram illustrating the number of CCS values reported as a function of mass with data sets delineated into specific timespans. Panel (A) contains the histogram for low mass analytes below 3000 Da, with arrows denoting the approximate mass where each distribution exhibits a maximum. Panel (B) contains the histogram for high mass analytes above 3000 Da, with labels calling out select protein assemblies which have been studied. Note that the vertical scales are the same in both panels; however, the bin size in panel B (10 kDa) is different than the bin sized used in panel A (50 Da). Reprinted (adapted) with permission from Jody C. May, Caleb B. Morris, John A. McLean, "Ion Mobility Collision Cross Section Compendium," *Analytical Chemistry* 2017, 89 (2), 1032-1044. Copyright 2017 American Chemical Society.

PubChem,^{160,161} where chemical entries have, over time, shifted to focusing on lower mass analytes while the total number of entries in PubChem currently exhibits a bimodal mass distribution.¹¹

The bubble plot projection in Figure 2.7 compares the number of CCS values reported over time with respect to specific analyte classes and types. In this projection, the bubble size correlates to the number of values reported for each corresponding year. Early quantitative IM studies focused on atomics and small molecules. A significant number of the small molecules CCS values consists of aromatic hydrocarbons.^{98,119,139,162-164} Starting in the 1990s, interest in inorganic compounds (metal salts, atomic and molecular clusters) began to emerge. Very few inorganic compound CCS values were reported between 2000 and 2010, with a resurgence of interest starting in 2013 which were primarily focused on gaining fundamental insights into the structures of inorganic salt and metal clusters.^{83,165-169} Protein CCS values were initially reported in the late 1990's by the Jarrold, Clemmer, and Bowers groups,¹⁷⁰⁻¹⁷³ with sparse numbers of measurements reported thereafter for several years. From the year 2000 onward, efforts in the field were largely concentrated on biological molecules. A significant number of peptide and protein CCS values started appearing again in the literature in 2007. The large blue bubble in Figure 2.7 corresponds to the 8676 peptide cross sections published by Smith and coworkers in 2010 in support of developing theoretical methods for predicting the IM drift time based upon the primary amino acid sequence.⁷² While most of the CCS values have been for tryptic peptides, there is recent and significant efforts being made in the quantitative IM analysis of structurally-interesting peptide and protein classes, including helical peptides,¹⁷⁴⁻¹⁷⁶ metalloproteins,¹⁷⁷⁻¹⁸⁰ intrinsically-disordered proteins,¹⁸¹⁻¹⁸⁴ metamorphic proteins,^{185,186} amyloids,¹⁸⁷⁻¹⁹⁴ and membrane-bound proteins and assemblies.^{117,195-198} The last three years has seen a balance of cross section reporting across most of the chemical classes, including lipids and carbohydrates. The exception is

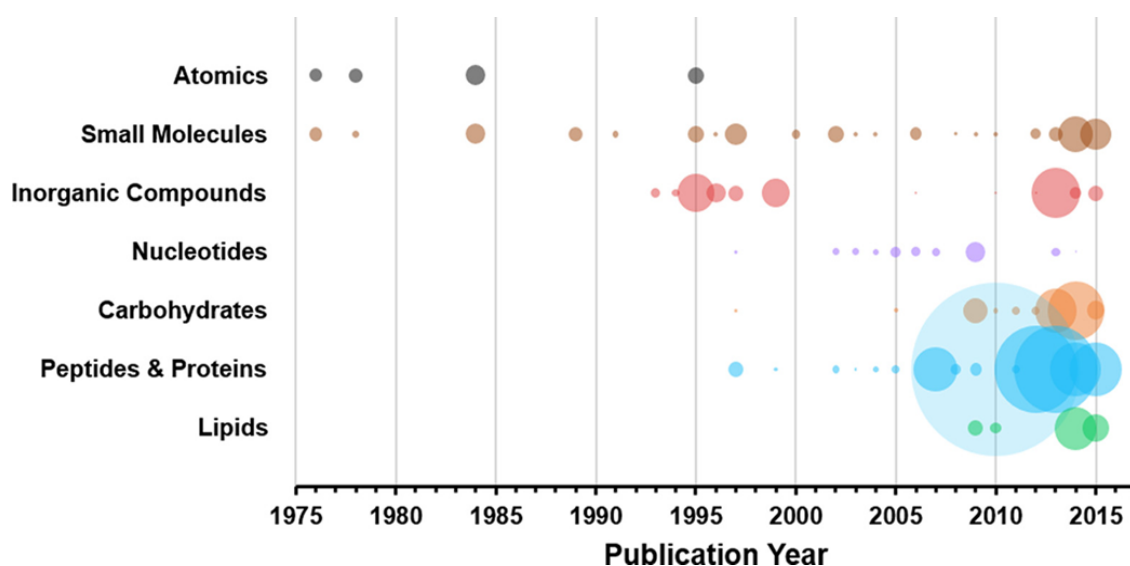


Figure 2.7 Bubble plot projecting the number of CCS values reported over time for the top 7 chemical classes represented. The size of each bubble encodes the relative number of CCS values for each respective year. Reprinted (adapted) with permission from Jody C. May, Caleb B. Morris, John A. McLean, "Ion Mobility Collision Cross Section Compendium," *Analytical Chemistry* 2017, 89 (2), 1032-1044. Copyright 2017 American Chemical Society.

nucleotide CCS values, which, aside for the 2009 study from McLean and coworkers,⁶⁸ have been published in small numbers spread across several studies and years, and currently comprise about 1% all CCS values reported.^{153,199-209} This observation is reflected in the fact that while many of these IM-based biomolecular studies have coincided strongly with developments in MS-based lipidomics, glycomics and metabolomics, the role of mass spectrometry related techniques in genomics research is, and has always been, relatively small.

Not shown in Figure 2.7 are the large number of studies which have focused on synthetic polymers,²¹⁰⁻²²⁰ which, like nucleotides, have seen a small but gradual number of CCS value reporting since the initial measurements by Bowers and coworkers in the late 1990s.²²¹⁻²²⁵ Several recent polymer studies have focused on reporting CCS values for dendrimers.²²⁶⁻²²⁸, and polymeric supermolecular assemblies utilized in molecular sensing, catalysis, and advanced materials applications.²²⁹⁻²³⁷ Overall, synthetic polymers comprise about 1% of the total number of CCS values reported to date, virtually all of which are measured in helium drift gas or are calibrated to helium-equivalent values. Also not reflected in the analysis presented in Figure 2.7 are the recent interests in characterizing natural products by IM-MS based CCS measurements.^{69,116,238-240} Many natural products contain complex and unusual scaffolds which motivates their study by a structurally-selective technique such as IM-MS, however, natural products are conventionally classified based on bioactivity rather than structure and as such molecules which can be considered natural products are represented in virtually all of the chemical classes delineated in this review. A similar issue is seen in metabolites (not shown) which is a classification that includes small peptides, carbohydrates and lipids. Finally, there are a number of CCS measurements which cannot easily be classified into a given chemical class category, such as compounds derived from

chemical synthesis.²⁴¹⁻²⁴⁵ It is anticipated that additional trends in the analysis of chemical classes not described in this review will become evident as the field of quantitative IM continues to grow.

2.8 Concluding Remarks

This current analysis of all collision cross section values published into the canonical literature from 1975 to 2015 reveals both important analytical trends in the field, such as the focus on biomolecules and drift tube studies, and also avenues where future efforts will make a significant impact. These future analytical prospects include, (1) the use of emerging ion mobility methods and mass-spectrometry based techniques for validating the accuracy of CCS measurements, (2) quantitative IM experiments exploring alternative drift gases such as carbon dioxide and argon, (3) overlapping analyte studies which explicitly compare fundamental differences across different gases, charge states, and polarities (4) anion studies to test whether or not conformational ordering observed for cations is retained in negative ion mode, (5) quantitative studies of underrepresented chemical classes such as nucleotides, lipids, and synthetic polymers, and (6) comprehensive CCS mapping of suites of analytes (*e.g.*, chemical classes, pharmacologically-active, or disease-implicated) in support of unknown identification and characterization by means of searching databases and libraries. In terms of the immediate analytical impact of this current work, the compilation of CCS measurements will provide a basis for correlating future measurements to the canonical literature, enable large-scale studies of the quantitative relationships within chemical classes and across different drift gases, and serve as a basis for developing predictive methods for CCS chemical space occupancy. Importantly, the compilation of these measurements will provide a foundation for supporting future efforts aimed at utilizing the CCS as an additional metric for analyte identification, with correspondence to other

analytical measurements such as exact mass, tandem MS data, and chromatographic retention time. Given the rapid growth now being seen in the field of quantitative ion mobility, many of the analytical prospects outlined in this review will likely be realized in the next few years.

2.9 Acknowledgements

This chapter contains the published research article: Jody C. May, Caleb B. Morris, John A. McLean, “Ion Mobility Collision Cross Section Compendium,” *Analytical Chemistry* **2017**, 89 (2), 1032-1044. Reprinted (adapted) with permission from Jody C. May, Caleb B. Morris, John A. McLean, “Ion Mobility Collision Cross Section Compendium,” *Analytical Chemistry* 2017, 89 (2), 1032-1044. Copyright 2017 American Chemical Society.

The authors thank Katrina Leaptrot and Stacy Sherrod for valuable suggestions during the preparation of this manuscript. This work was supported in part using the resources of the Center for Innovative Technology at Vanderbilt University. Financial support for this work was generously provided by the Vanderbilt Center for Quantitative Sciences under a CQS pilot project award, the National Institutes of Health (NIH R01GM092218), the U.S. Army Research Office and the Defense Advanced Research Projects Agency (DARPA) under Cooperative Agreement Number W911 NF-14-2-0022, and the U.S. Environmental Protection Agency (EPA) under Assistance Agreement No. 83573601. This work has not been formally reviewed by EPA and EPA does not endorse any products or commercial services mentioned in this publication. The views expressed in this document are solely those of the authors and should not be interpreted as representing the official policies, either expressed or implied, of the EPA, the Army Research Office, DARPA, or the U.S. Government. The U.S. Government is authorized to reproduce and distribute reprints for Government purposes notwithstanding any copyright notation herein.

2.10 References

1. Groessl, M.; Graf, S.; Knochenmuss, R. *Analyst* 2015, 140, 6904-6911.
2. May, J. C.; Goodwin, C. R.; Lareau, N. M.; Leaptrot, K. L.; Morris, C. B.; Kurulugama, R. T.; Mordehai, A.; Klein, C.; Barry, W.; Darland, E.; Overney, G.; Imatani, K.; Stafford, G. C.; Fjeldsted, J. C.; McLean, J. A. *Anal. Chem.* 2014, 86, 2107-2116.
3. Ibrahim, Y. M.; Baker, E. S.; Danielson III, W. F.; Norheim, R. V.; Prior, D. C.; Anderson, G. A.; Belov, M. E.; Smith, R. D. *Int. J. Mass Spectrom.* 2014, 377, 655-662.
4. Allen, S. J.; Giles, K.; Gilbert, T.; Bush, M. F. *Analyst* 2016, 141, 884-891.
5. Fernandez-Lima, F. A.; Kaplan, D. A.; Park, M. A. *Rev. Sci. Instrum.* 2011, 82, 126106.
6. Silveira, J. A.; Ridgeway, M. E.; Park, M. A. *Anal. Chem.* 2014, 86, 5624-5627.
7. Michelmann, K.; Silveira, J. A.; Ridgeway, M. E.; Park, M. A. *J. Am. Soc. Mass Spectrom.* 2015, 26, 14-24.
8. Deng, L.; Ibrahim, Y. M.; Baker, E. S.; Aly, N. A.; Hamid, A. M.; Zhang, X.; Zheng, X.; Garimella, S. V.; Webb, I. K.; Prost, S. A. *ChemistrySelect* 2016, 1, 2396-2399.
9. Hamid, A. M.; Garimella, S. V. B.; Ibrahim, Y. M.; Deng, L.; Zheng, X.; Webb, I. K.; Anderson, G. A.; Prost, S. A.; Norheim, R. V.; Tolmachev, A. V.; Baker, E. S.; Smith, R. D. *Anal. Chem.* 2016, 88, 8949-8956.
10. Sherrod, S. D.; McLean, J. A. *Clinical Chemistry* 2016, 62, 77-83.
11. May, J. C.; McLean, J. A. *Ann. Rev. Anal. Chem.* 2016, 9.
12. Ortmayr, K.; Causon, T. J.; Hann, S.; Koellensperger, G. *TrAC, Trends Anal. Chem.* 2016, 82, 358-366.
13. Stephan, S.; Jakob, C.; Hippler, J.; Schmitz, O. *J. Anal. Bioanal. Chem.* 2016, 408, 3751-3759.
14. Chouinard, C. D.; Wei, M. S.; Beekman, C. R.; Kemperman, R. H. J.; Yost, R. A. *Clinical Chemistry* 2016, 62, 124-133.
15. Lanucara, F.; Holman, S. W.; Gray, C. J.; Evers, C. E. *Nat Chem* 2014, 6, 281-294.
16. Zhong, Y.; Hyung, S.-J.; Ruotolo, B. T. *Expert Rev Proteomic* 2012, 9, 47-58.
17. Kliman, M.; May, J. C.; McLean, J. A. *Biochimica et Biophysica Acta (BBA) - Molecular and Cell Biology of Lipids* 2011, 1811, 935-945.

18. Gray, C. J.; Thomas, B.; Upton, R.; Migas, L. G.; Eyers, C. E.; Barran, P. E.; Flitsch, S. L. *Biochimica et Biophysica Acta (BBA) - General Subjects* 2016, 1860, 1688-1709.
19. May, J. C.; Goodwin, C. R.; McLean, J. A. In *Encyclopedia of Drug Metabolism and Interactions*, Lyubimov, A. V., Ed.; John Wiley & Sons, Inc., 2011.
20. Kaur-Atwal, G.; O'Connor, G.; Aksenov, A. A.; Bocos-Bintintan, V.; Paul Thomas, C. L.; Creaser, C. S. *International Journal for Ion Mobility Spectrometry* 2009, 12, 1-14.
21. Crawford, C. L.; Hauck, B. C.; Tufariello, J. A.; Harden, C. S.; McHugh, V.; Siems, W. F.; Hill Jr, H. H. *Talanta* 2012, 101, 161-170.
22. Mesleh, M. F.; Hunter, J. M.; Shvartsburg, A. A.; Schatz, G. C.; Jarrold, M. F. J. *Phys. Chem.* 1996, 100, 16082-16086.
23. Shvartsburg, A. A.; Jarrold, M. F. *Chem. Phys. Lett.* 1996, 261, 86-91.
24. Wytttenbach, T.; Bleiholder, C.; Bowers, M. T. *Anal. Chem.* 2013, 85, 2191-2199.
25. Larriba, C.; Hogan, C. J. *Journal of Computational Physics* 2013, 251, 344-363.
26. Bleiholder, C.; Johnson, N. R.; Contreras, S.; Wytttenbach, T.; Bowers, M. T. *Anal. Chem.* 2015, 87, 7196-7203.
27. Mason, E. A.; McDaniel, E. W. *Transport Properties of Ions in Gases*; John Wiley & Sons: New York, 1988, p 560.
28. Siems, W. F.; Viehland, L. A.; Hill, H. H. *Anal. Chem.* 2012, 84, 9782-9791.
29. McDaniel, E. W. *Collision Phenomena in Ionized Gases*; Wiley: New York, 1964.
30. Marklund, Erik G.; Degiacomi, Matteo T.; Robinson, Carol V.; Baldwin, Andrew J.; Benesch, Justin L. P. *Structure* 2015, 23, 791-799.
31. Benesch, J. L.; Ruotolo, B. T. *Curr. Opin. Struct. Biol.* 2011, 21, 641-649.
32. Yoon, B. U.; Kim, M. S. *Org. Mass Spectrom.* 1990, 25, 397-403.
33. van Houte, J. J.; de Koster, C. G.; van Thuijl, J. *Int. J. Mass Spectrom. Ion Processes* 1992, 115, 173-183.
34. Roussis, S. G. *J. Am. Soc. Mass Spectrom.* 1995, 6, 803-811.
35. Covey, T.; Douglas, D. J. *J. Am. Soc. Mass Spectrom.* 1993, 4, 616-623.
36. Javahery, G.; Thomson, B. A. *J. Am. Soc. Mass Spectrom.* 1997, 8, 697-702.
37. Ring, S.; Naaman, R.; Rudich, Y. *Anal. Chem.* 1999, 71, 648-651.

38. Plass, W. R.; Gill, L. A.; Bui, H. A.; Cooks, R. G. *J Phys. Chem. A* 2000, 104, 5059-5065.
39. Wobschall, D.; Graham, J. R.; Malone, D. P. *Phys. Rev.* 1963, 131, 1565-1571.
40. Wobschall, D. C.; Fluegge, R. A.; Graham, J. R. *J. Appl. Phys.* 1967, 38, 3761-3767.
41. Salbo, R.; Bush, M. F.; Naver, H.; Campuzano, I.; Robinson, C. V.; Pettersson, I.; Jorgensen, T. J.; Haselmann, K. F. *Rapid communications in mass spectrometry : RCM 2012*, 26, 1181-93.
42. Yang, F.; Voelkel, J. E.; Dearden, D. V. *Anal. Chem.* 2012, 84, 4851-4857.
43. Mao, L.; Chen, Y.; Xin, Y.; Chen, Y.; Zheng, L.; Kaiser, N. K.; Marshall, A. G.; Xu, W. *Anal. Chem.* 2015, 87, 4072-4075.
44. Jiang, T.; Chen, Y.; Mao, L.; Marshall, A. G.; Xu, W. *Physical Chemistry Chemical Physics* 2016, 18, 713-717.
45. Hofmann, J.; Hahm, H. S.; Seeberger, P. H.; Pagel, K. *Nature* 2015, 526, 241-+.
46. Benigni, P.; Bravo, C.; Quirke, J. M. E.; DeBord, J. D.; Mebel, A. M.; Fernandez-Lima, F. *Energy & Fuels* 2016.
47. Reading, E.; Munoz-Muriedas, J.; Roberts, A. D.; Dear, G. J.; Robinson, C. V.; Beaumont, C. *Anal. Chem.* 2016, 88, 2273-2280.
48. Pacholarz, K. J.; Barran, P. E. *Anal. Chem.* 2015, 87, 6271-6279.
49. Pringle, S. D.; Giles, K.; Wildgoose, J. L.; Williams, J. P.; Slade, S. E.; Thalassinos, K.; Bateman, R. H.; Bowers, M. T.; Scrivens, J. H. *Int. J. Mass Spectrom.* 2007, 261, 1-12.
50. Bush, M. F.; Hall, Z.; Giles, K.; Hoyes, J.; Robinson, C. V.; Ruotolo, B. T. *Anal. Chem.* 2010, 82, 9557-9565.
51. Tang, K.; Shvartsburg, A. A.; Lee, H. N.; Prior, D. C.; Buschbach, M. A.; Li, F.; Tolmachev, A. V.; Anderson, G. A.; Smith, R. D. *Anal. Chem.* 2005, 77, 3330-3339.
52. Valentine, S. J.; Counterman, A. E.; Clemmer, D. E. *J. Am. Soc. Mass Spectrom.* 1999, 10, 1188-1211.
53. Valentine, S. J.; Counterman, A. E.; Hoaglund-Hyzer, C. S.; Clemmer, D. E. *J Phys. Chem. B* 1999, 103, 1203-1207.
54. Dilger, J. M.; Valentine, S. J.; Glover, M. S.; Ewing, M. A.; Clemmer, D. E. *Int. J. Mass Spectrom.* 2012, 330-332, 35-45.
55. Dilger, J. M.; Valentine, S. J.; Glover, M. S.; Clemmer, D. E. *J. Am. Soc. Mass Spectrom.* 2013, 24, 768-779.

56. von Helden, G.; Hsu, M.; Gotts, N.; Kemper, P.; Bowers, M. *Chem. Phys. Lett.* 1993, 204, 15-22.
57. Gotts, N. G.; von Helden, G.; Bowers, M. T. *Int. J. Mass Spectrom. Ion Processes* 1995, 149, 217-229.
58. Lee, S.; Gotts, N.; von Helden, G.; Bowers, M. T. *J Phys. Chem. A* 1997, 101, 2096-2102.
59. von Helden, G.; Porter, E.; Gotts, N. G.; Bowers, M. T. *J Phys. Chem.* 1995, 99, 7707-7714.
60. Clemmer, D. E.; Jarrold, M. F. *J. Am. Chem. Soc.* 1995, 117, 8841-8850.
61. Shelimov, K. B.; Jarrold, M. F. *J Phys. Chem.* 1995, 99, 17677-17679.
62. Shelimov, K. B.; Jarrold, M. F. *J. Am. Chem. Soc.* 1996, 118, 1139-1147.
63. Hudgins, R. R.; Imai, M.; Jarrold, M. F.; Dugourd, P. J. *Chem. Phys.* 1999, 111, 7865-7870.
64. Tao, L.; McLean, J. R.; McLean, J. A.; Russell, D. H. *J. Am. Soc. Mass Spectrom.* 2007, 18, 1727-1728.
65. Fernandez-Lima, F. A.; Blase, R. C.; Russell, D. H. *International Journal for Mass Spectrometry* 2010, 298, 111-118.
66. Pagel, K.; Harvey, D. J. *Anal. Chem.* 2013, 85, 5138-5145.
67. Hofmann, J.; Struwe, W. B.; Scarff, C. A.; Scrivens, J. H.; Harvey, D. J.; Pagel, K. *Anal. Chem.* 2014, 86, 10789-10795.
68. Fenn, L. S.; Kliman, M.; Mahsut, A.; Zhao, S. R.; McLean, J. A. *Anal. Bioanal. Chem.* 2009, 394, 235-244.
69. Goodwin, C. R.; Fenn, L. S.; Derewacz, D. K.; Bachmann, B. O.; McLean, J. A. *Journal of Natural Products* 2012, 75, 48-53.
70. Paglia, G.; Williams, J. P.; Menikarachchi, L.; Thompson, J. W.; Tyldesley-Worster, R.; Halldórsson, S.; Rolfsson, O.; Moseley, A.; Grant, D.; Langridge, J.; Palsson, B. O.; Astarita, G. *Anal. Chem.* 2014, 86, 3985-3993.
71. Paglia, G.; Angel, P.; Williams, J. P.; Richardson, K.; Olivos, H. J.; Thompson, J. W.; Menikarachchi, L.; Lai, S.; Walsh, C.; Moseley, A.; Plumb, R. S.; Grant, D. F.; Palsson, B. O.; Langridge, J.; Geromanos, S.; Astarita, G. *Anal. Chem.* 2015, 87, 1137-1144.
72. Shah, A. R.; Agarwal, K.; Baker, E. S.; Singhal, M.; Mayampurath, A. M.; Ibrahim, Y. M.; Kangas, L. J.; Monroe, M. E.; Zhao, R.; Belov, M. E.; Anderson, G. A.; Smith, R. D. *Bioinformatics* 2010, 26, 1601-1607.

73. Clemmer, D. E.:
http://www.indiana.edu/~clemmer/Research/Cross%20Section%20Database/cs_database.php.
74. Bush, M. F.: <http://depts.washington.edu/bushlab/ccsdatabase/>.
75. Ellis, H. W.; Pai, R. Y.; McDaniel, E. W.; Mason, E. A.; Viehland, L. A. *At. Data Nucl. Data Tables* 1976, 17, 177-210.
76. Ellis, H. W.; McDaniel, E. W.; Albritton, D. L.; Viehland, L. A.; Lin, S. L.; Mason, E. A. *At. Data Nucl. Data Tables* 1978, 22, 179-217.
77. Ellis, H. W.; Thackston, M. G.; McDaniel, E. W.; Mason, E. A. *At. Data Nucl. Data Tables* 1984, 31, 113-151.
78. Viehland, L. A.; Mason, E. A. *At. Data Nucl. Data Tables* 1995, 60, 37-95.
79. Matz, L. M.; Hill, H. H., Jr.; Beegle, L. W.; Kanik, I. J. *Am. Soc. Mass Spectrom.* 2002, 13, 300-307.
80. Abedi, A.; Sattar, L.; Gharibi, M.; Viehland, L. A. *Int. J. Mass Spectrom.* 2014, 370, 101-106.
81. Jurneczko, E.; Kalapothakis, J.; Campuzano, I. D. G.; Morris, M.; Barran, P. E. *Anal. Chem.* 2012, 84, 8524-8531.
82. Fernandez-Garcia, J.; de la Mora, J. F. J. *Am. Soc. Mass Spectrom.* 2013, 24, 1872-1889.
83. Ouyang, H.; Larriba-Andaluz, C.; Oberreit, D. R.; Hogan, C. J. J. *Am. Soc. Mass Spectrom.* 2013, 24, 1833-1847.
84. Kurulugama, R. T.; Darland, E.; Kuhlmann, F.; Stafford, G.; Fjeldsted, J. *Analyst* 2015, 14, 6834-6844.
85. Bush, M. F.; Campuzano, I. D. G.; Robinson, C. V. *Anal. Chem.* 2012, 84, 7124-7130.
86. Chudinov, A. V.; Martynovich, Y. G.; Sulimenkov, I. V.; Brusov, V. S.; Filatov, V. V.; Pikhtev, A. R.; Kozlovskiy, V. I. *Journal of Analytical Chemistry* 2015, 70, 1647-1653.
87. Laphorn, C.; Pullen, F. S.; Chowdhry, B. Z.; Wright, P.; Perkins, G. L.; Heredia, Y. *Analyst* 2015, 140, 6814-6823.
88. Larriba-Andaluz, C.; Hogan, C. J. J. *Chem. Phys.* 2014, 141, 194107.
89. Campuzano, I.; Bush, M. F.; Robinson, C. V.; Beaumont, C.; Richardson, K.; Kim, H.; Kim, H. I. *Anal. Chem.* 2011, 84, 1026-1033.

90. Giles, K.; Williams, J. P.; Campuzano, I. *Rapid Commun. Mass Spectrom.* 2011, 25, 1559-1566.
91. Ibrahim, Y. M.; Garimella, S. V.; Tolmachev, A. V.; Baker, E. S.; Smith, R. D. *Anal. Chem.* 2014, 86, 5295-5299.
92. May, J. C.; Dodds, J. N.; Kurulugama, R. T.; Stafford, G. C.; Fjeldsted, J. C.; McLean, J. A. *Analyst* 2015, 140, 6824-6833.
93. Lalli, P. M.; Corilo, Y. E.; Fasciotti, M.; Riccio, M. F.; de Sa, G. F.; Daroda, R. J.; Souza, G. H. M. F.; McCullagh, M.; Bartberger, M. D.; Eberlin, M. N.; Campuzano, I. D. G. *J. Mass Spectrom.* 2013, 48, 989-997.
94. Reid Asbury, G.; Hill, H. H., Jr. *Anal. Chem.* 2000, 72, 580-584.
95. Fasciotti, M.; Sanvido, G. B.; Santos, V. G.; Lalli, P. M.; McCullagh, M.; de Sá, G. F.; Daroda, R. J.; Peter, M. G.; Eberlin, M. N. *J. Mass Spectrom.* 2012, 47, 1643-1647.
96. Fasciotti, M.; Lalli, P. M.; Klitzke, C. c. F.; Corilo, Y. E.; Pudenzi, M. A.; Pereira, R. C.; Bastos, W.; Daroda, R. J.; Eberlin, M. N. *Energy & Fuels* 2013, 27, 7277-7286.
97. Howdle, M. D.; Eckers, C.; Laures, A. M. F.; Creaser, C. S. *Int. J. Mass Spectrom.* 2010, 298, 72-77.
98. Beitz, T.; Laudien, R.; LÃ¶hmannsrÃ¶ben, H.-G.; Kallies, B. *J Phys. Chem. A* 2006, 110, 3514-3520.
99. Bonakdarzadeh, P.; Topic, F.; Kalenius, E.; Bhowrnik, S.; Sato, S.; Groessler, M.; Knochenmuss, R.; Rissanen, K. *Inorg. Chem.* 2015, 54, 6055-6061.
100. Wu, C.; Siems, W. F.; Reid Asbury, G.; Hill, H. H., Jr. *Anal. Chem.* 1998, 70, 4929-4938.
101. Steiner, W. E.; Clowers, B. H.; Fuhrer, K.; Gonin, M.; Matz, L. M.; Siems, W. F.; Schultz, J. A.; Hill, H. H., Jr. *Rapid Commun. Mass Spectrom.* 2001, 15, 2221-2226.
102. Sysoev, A.; Adamov, A.; Viidanoja, J.; Ketola, R. A.; Kostianen, R.; Kotiaho, T. *Rapid Commun. Mass Spectrom.* 2004, 18, 3131-3139.
103. Jarrold, M. F. *J Phys. Chem.* 1995, 99, 11-21.
104. Dugourd, P.; Hudgins, R. R.; Clemmer, D. E.; Jarrold, M. F. *Rev. Sci. Instrum.* 1997, 68, 1122-1129.
105. Kemper, P. R.; Bowers, M. T. *J. Am. Soc. Mass Spectrom.* 1990, 1, 197-207.
106. Hoaglund, C. S.; Valentine, S. J.; Clemmer, D. E. *Anal. Chem.* 1997, 69, 4156-4161.
107. Hoaglund, C. S.; Valentine, S. J.; Sporleder, C. R.; Reilly, J. P.; Clemmer, D. E. *Anal. Chem.* 1998, 70, 2236-2242.

108. Gillig, K. J.; Ruotolo, B. T.; Stone, E. G.; Russell, D. H.; Fuhrer, K.; Gonin, M.; Schultz, J. A. *Anal. Chem.* 2000, 72, 3965-3971.
109. Sundarapandian, S.; May, J. C.; McLean, J. A. *Anal. Chem.* 2010, 82, 3247-3254.
110. McCullough, B. J.; Kalapothakis, J.; Eastwood, H.; Kemper, P.; MacMillan, D.; Taylor, K.; Dorin, J.; Barran, P. E. *Anal. Chem.* 2008, 80, 6336-6344.
111. Gillig, K. J.; Ruotolo, B. T.; Stone, E. G.; Russell, D. H. *Int. J. Mass Spectrom.* 2004, 239, 43-49.
112. Blase, R. C.; Silveira, J. A.; Gillig, K. J.; Gamage, C. M.; Russell, D. H. *Int. J. Mass Spectrom.* 2011, 301, 166-173.
113. Koeniger, S. L.; Merenbloom, S. I.; Valentine, S. J.; Jarrold, M. F.; Udseth, H. R.; Smith, R. D.; Clemmer, D. E. *Anal. Chem.* 2006, 78, 4161-4174.
114. Ridenour, W. B.; Kliman, M.; McLean, J. A.; Caprioli, R. M. *Anal. Chem.* 2010, 82, 1881-1889.
115. Hilton, G. R.; Thalassinou, K.; Grabenauer, M.; Sanghera, N.; Slade, S. E.; Wyttenbach, T.; Robinson, P. J.; Pinheiro, T. J.; Bowers, M. T.; Scrivens, J. H. *J. Am. Soc. Mass Spectrom.* 2010, 21, 845-854.
116. Fouque, K. J. D.; Afonso, C.; Zirah, S.; Hegemann, J. D.; Zimmermann, M.; Marahiel, M. A.; Rebuffat, S.; Lavanant, H. *Anal. Chem.* 2015, 87, 1166-1172.
117. Watkinson, T. G.; Calabrese, A. N.; Giusti, F.; Zoonens, M.; Radford, S. E.; Ashcroft, A. E. *Int. J. Mass Spectrom.* 2015, 391, 54-61.
118. Schenk, E. R.; Almeida, R.; Miksovská, J.; Ridgeway, M. E.; Park, M. A.; Fernandez-Lima, F. *J. Am. Soc. Mass Spectrom.* 2015, 26, 555-563.
119. Castellanos, A.; Benigni, P.; Hernandez, D. R.; DeBord, J. D.; Ridgeway, M. E.; Park, M. A.; Fernandez-Lima, F. *Analytical Methods* 2014, 6, 9328-9332.
120. Molano-Arevalo, J. C.; Hernandez, D. R.; Gonzalez, W. G.; Miksovská, J.; Ridgeway, M. E.; Park, M. A.; Fernandez-Lima, F. *Anal. Chem.* 2014, 86, 10223-10230.
121. Benigni, P.; Thompson, C. J.; Ridgeway, M. E.; Park, M. A.; Fernandez-Lima, F. *Anal. Chem.* 2015, 87, 4321-4325.
122. Rashid, A. M.; Saalbach, G.; Bornemann, S. *Rapid Commun. Mass Spectrom.* 2014, 28, 191-199.
123. Dugourd, P.; Hudgins, R. R.; Jarrold, M. F. *Chem. Phys. Lett.* 1997, 267, 186-192.
124. Allen, S. J.; Schwartz, A. M.; Bush, M. F. *Anal. Chem.* 2013, 85, 12055-12061.
125. Zhang, L. W.; Vertes, A. *Anal. Chem.* 2015, 87, 10397-10405.

126. Liu, H.; Zhang, J.; Sun, H.; Xu, C.; Zhu, Y.; Xie, H. *Procedia Environmental Sciences* 2011, 8, 483-491.
127. Baker, E. S.; Livesay, E. A.; Orton, D. J.; Moore, R. J.; Danielson, W. F.; Prior, D. C.; Ibrahim, Y. M.; LaMarche, B. L.; Mayampurath, A. M.; Schepmoes, A. A.; Hopkins, D. F.; Tang, K.; Smith, R. D.; Belov, M. E. *J. Proteome Res.* 2010, 9, 997-1006.
128. McLean, J. A.; Ruotolo, B. T.; Gillig, K. J.; Russell, D. H. *Int. J. Mass Spectrom.* 2005, 240, 301-315.
129. Shliaha, P. V.; Bond, N. J.; Gatto, L.; Lilley, K. S. *J. Proteome Res.* 2013, 12, 2323-2339.
130. Lietz, C. B.; Yu, Q.; Li, L. *J. Am. Soc. Mass Spectrom.* 2014, 25, 2009-2019.
131. Knapman, T. W.; Valette, N. M.; Warriner, S. L.; Ashcroft, A. E. *Current Analytical Chemistry* 2013, 9, 181-191.
132. Vahidi, S.; Stocks, B. B.; Konermann, L. *Anal. Chem.* 2013, 85, 10471-10478.
133. May, J. C.; McLean, J. A. *Proteomics* 2015, 15, 2862-2871.
134. Phillips, A. S.; Gomes, A. F.; Kalapothakis, J. M. D.; Gillam, J. E.; Gasparavicius, J.; Gozzo, F. C.; Kunath, T.; MacPhee, C.; Barran, P. E. *Analyst* 2015, 140, 3070-3081.
135. McLean, J. A. *J. Am. Soc. Mass Spectrom.* 2009, 20, 1775-1781.
136. Wilkins, C. L.; Trimpin, S.; May, J. C.; McLean, J. A. In *Ion Mobility Spectrometry-Mass Spectrometry: Theory and Applications*; CRC Press, 2010, pp 327-343.
137. Karpas, Z.; Berant, Z.; Shahal, O. *J. Am. Chem. Soc.* 1989, 111, 6015 - 6018.
138. Berant, Z.; Karpas, Z. *J. Am. Chem. Soc.* 1989, 111, 3819-3824.
139. Krishnamurthy, M.; de Gouw, J. A.; Bierbaum, V. M.; Leone, S. R. *J Phys. Chem.* 1996, 100, 14908-14913.
140. de Gouw, J. A.; Krishnamurthy, M.; Bierbaum, V. M.; Leone, S. R. *Int. J. Mass Spectrom. Ion Processes* 1997, 167, 281-289.
141. Karpas, Z.; Tironi, C. *Structural Chemistry* 1991, 2, 655-659.
142. Li, H.; Giles, K.; Bendiak, B.; Kaplan, K.; Siems, W. F.; Hill Jr, H. H. *Anal. Chem.* 2012, 84, 3231-3239.
143. Fenn, L. S.; McLean, J. A. *Phys. Chem. Chem. Phys.* 2011, 13, 2196-2205.
144. Gelb, A. S.; Jarratt, R. E.; Huang, Y. T.; Dodds, E. D. *Anal. Chem.* 2014, 86, 11396-11402.
145. Huang, Y. T.; Dodds, E. D. *Anal. Chem.* 2015, 87, 5664-5668.

146. Gaye, M. M.; Kurulugama, R.; Clemmer, D. E. *Analyst* 2015, 140, 6922-6932.
147. Williams, J. P.; Grabenauer, M.; Holland, R. J.; Carpenter, C. J.; Wormald, M. R.; Giles, K.; Harvey, D. J.; Bateman, R. H.; Scrivens, J. H.; Bowers, M. T. *Int. J. Mass Spectrom.* 2010, 298, 119-127.
148. Zhang, F.; Guo, S.; Zhang, M.; Zhang, Z.; Guo, Y. *J. Mass Spectrom.* 2015, 50, 906-913.
149. Pacini, T.; Fu, W. Q.; Gudmundsson, S.; Chiaravalle, A. E.; Brynjolfson, S.; Palsson, B. O.; Astarita, G.; Paglia, G. *Anal. Chem.* 2015, 87, 2593-2599.
150. Aqai, P.; Blesa, N. G.; Major, H.; Pedotti, M.; Varani, L.; Ferrero, V. E.; Haasnoot, W.; Nielen, M. W. *Anal. Bioanal. Chem.* 2013, 405, 9427-9436.
151. Shimizu, A.; Chiba, M. *Drug Metabolism and Disposition* 2013, 41, 1295-1299.
152. Warnke, S.; Seo, J.; Boschmans, J.; Sobott, F.; Scrivens, J. H.; Bleiholder, C.; Bowers, M. T.; Gewinner, S.; Schollkopf, W.; Pagel, K.; von Helden, G. *J. Am. Chem. Soc.* 2015, 137, 4236-4242.
153. Ma, X.; Shah, S.; Zhou, M.; Park, C. K.; Wysocki, V. H.; Horton, N. C. *Biochemistry* 2013, 52, 4373-4381.
154. Politis, A.; Park, A. Y.; Hall, Z.; Ruotolo, B. T.; Robinson, C. V. *Journal of Molecular Biology* 2013, 425, 4790-4801.
155. Ma, X.; Zhou, M. W.; Wysocki, V. H. *J. Am. Soc. Mass Spectrom.* 2014, 25, 368-379.
156. Zhang, Y.; Ju, Y.; Huang, C. S.; Wysocki, V. H. *Anal. Chem.* 2014, 86, 1342-1346.
157. Pacholarz, K. J.; Porrini, M.; Garlish, R. A.; Burnley, R. J.; Taylor, R. J.; Henry, A. J.; Barran, P. E. *Angew. Chem. Int. Ed.* 2014, 53, 7765-7769.
158. Beveridge, R.; Covill, S.; Pacholarz, K. J.; Kalapothakis, J. M.; MacPhee, C. E.; Barran, P. E. *Anal. Chem.* 2014, 86, 10979-10991.
159. Quintyn, R. S.; Zhou, M. W.; Yan, J.; Wysocki, V. H. *Anal. Chem.* 2015, 87, 11879-11886.
160. Bolton, E. E.; Wang, Y.; Thiessen, P. A.; Bryant, S. H. In *Annual Reports in Computational Chemistry*, Ralph, A. W.; David, C. S., Eds.; Elsevier, 2008, pp 217-241.
161. Kim, S.; Thiessen, P. A.; Bolton, E. E.; Chen, J.; Fu, G.; Gindulyte, A.; Han, L.; He, J.; He, S.; Shoemaker, B. A. *Nucleic Acids Res* 2015, gkv951.
162. Creaser, C. S.; Benyazzar, M.; Griffiths, J. R.; Stygall, J. W. *Anal. Chem.* 2000, 72, 2724-2729.

163. Momoh, P. O.; Attah, I. K.; El-Shall, M. S.; Kanters, R. P. F.; Pinski, J. M.; Abrash, S. A. *J. Phys. Chem. A* 2014, 118, 8251-8263.
164. Rusyniak, M.; Ibrahim, Y. M.; Alsharaeh, E.; Meot-Ner, M.; El-Shall, M. S. *J. Phys. Chem. A* 2003, 107, 7656-7666.
165. Ota, K.; Koyasu, K.; Ohshimo, K.; Misaizu, F. *Chem. Phys. Lett.* 2013, 588, 63-67.
166. Ohshimo, K.; Komukai, T.; Moriyama, R.; Misaizu, F. *J. Phys. Chem. A* 2014, 118, 3899-3905.
167. Ohshimo, K.; Takahashi, T.; Moriyama, R.; Misaizu, F. *J. Phys. Chem. A* 2014, 118, 9970-9975.
168. Ohshimo, K.; Norimasa, N.; Moriyama, R.; Misaizu, F. *Journal of Chemical Physics* 2016, 144, 8.
169. Wu, J. W. J.; Moriyama, R.; Tahara, H.; Ohshimo, K.; Misaizu, F. *J. Phys. Chem. A* 2016, 120, 3788-3796.
170. Shelimov, K. B.; Clemmer, D. E.; Hudgins, R. R.; Jarrold, M. F. *J. Am. Chem. Soc.* 1997, 119, 2240-2248.
171. Valentine, S. J.; Anderson, J. G.; Ellington, A. D.; Clemmer, D. E. *J. Phys. Chem. B* 1997, 101, 3891-3900.
172. Valentine, S. J.; Counterman, A. E.; Clemmer, D. E. *J. Am. Soc. Mass Spectrom.* 1997, 8, 954-961.
173. Wyttenbach, T.; Batka, J. J.; Gidden, J.; Bowers, M. T. *Int. J. Mass Spectrom.* 1999, 193, 143-152.
174. Morrison, L. J.; Wysocki, V. H. *J. Am. Chem. Soc.* 2014, 136, 14173-14183.
175. Xiao, C. Y.; Perez, L. M.; Russell, D. H. *Analyst* 2015, 140, 6933-6944.
176. Tao, L.; Dahl, D. B.; Pérez, L. M.; Russell, D. H. *J. Am. Soc. Mass Spectrom.* 2009, 20, 1593-1602.
177. Wyttenbach, T.; Grabenauer, M.; Thalassinou, K.; Scrivens, J. H.; Bowers, M. T. *J. Phys. Chem. B* 2009, 114, 437-447.
178. Chen, S. H.; Chen, L. X.; Russell, D. H. *J. Am. Chem. Soc.* 2014, 136, 9499-9508.
179. Calabrese, A. N.; Bowie, J. H.; Pukala, T. L. *Biochemistry* 2015, 54, 567-576.
180. Berezovskaya, Y.; Porrini, M.; Nortcliffe, C.; Barran, P. E. *Analyst* 2015, 140, 2847-2856.
181. D'Urzo, A.; Konijnenberg, A.; Rossetti, G.; Habchi, J.; Li, J. Y.; Carloni, P.; Sobott, F.; Longhi, S.; Grandori, R. *J. Am. Soc. Mass Spectrom.* 2015, 26, 472-481.

182. Dickinson, E. R.; Jurneczko, E.; Pacholarz, K. J.; Clarke, D. J.; Reeves, M.; Ball, K. L.; Hupp, T.; Campopiano, D.; Nikolova, P. V.; Barran, P. E. *Anal. Chem.* 2015, 87, 3231-3238.
183. Beveridge, R.; Phillips, A. S.; Denbigh, L.; Saleem, H. M.; MacPhee, C. E.; Barran, P. E. *Proteomics* 2015, 15, 2872-2883.
184. Saikusa, K.; Kuwabara, N.; Kokabu, Y.; Inoue, Y.; Sato, M.; Iwasaki, H.; Shimizu, T.; Ikeguchi, M.; Akashi, S. *Analyst* 2013, 138, 1441-1449.
185. Harvey, S. R.; Porrini, M.; Konijnenberg, A.; Clarke, D. J.; Tyler, R. C.; Langridge-Smith, P. R. R.; MacPhee, C. E.; Volkman, B. F.; Barran, P. E. *Journal of Physical Chemistry B* 2014, 118, 12348-12359.
186. Harvey, S. R.; Porrini, M.; Tyler, R. C.; MacPhee, C. E.; Volkman, B. F.; Barran, P. E. *Physical Chemistry Chemical Physics* 2015, 17, 10538-10550.
187. Scarff, C. A.; Sicorello, A.; Tome, R. J. L.; Macedo-Ribeiro, S.; Ashcroft, A. E.; Radford, S. E. *Int. J. Mass Spectrom.* 2013, 345, 63-70.
188. Cole, H.; Porrini, M.; Morris, R.; Smith, T.; Kalapothakis, J.; Weidt, S.; Mackay, C. L.; MacPhee, C. E.; Barran, P. E. *Analyst* 2015, 140, 7000-7011.
189. Young, L. M.; Cao, P.; Raleigh, D. P.; Ashcroft, A. E.; Radford, S. E. *J. Am. Chem. Soc.* 2014, 136, 660-670.
190. Bernstein, S. L.; Wyttenbach, T.; Baumketner, A.; Shea, J.-E.; Bitan, G.; Teplow, D. B.; Bowers, M. T. *J. Am. Chem. Soc.* 2005, 127, 2075-2084.
191. Dupuis, N. F.; Wu, C.; Shea, J.-E.; Bowers, M. T. *J. Am. Chem. Soc.* 2009, 131, 18283-18292.
192. Murray, M. M.; Krone, M. G.; Bernstein, S. L.; Baumketner, A.; Condrón, M. M.; Lazo, N. D.; Teplow, D. B.; Wyttenbach, T.; Shea, J.-E.; Bowers, M. T. *J. Phys. Chem. B* 2009, 113, 6041-6046.
193. Daly, S.; Kulesza, A.; Poussiguet, F.; Simon, A. L.; Choi, C. M.; Knight, G.; Chirot, F.; MacAleese, L.; Antoine, R.; Dugourd, P. *Chemical Science* 2015, 6, 5040-5047.
194. Bernstein, S. L.; Dupuis, N. F.; Lazo, N. D.; Wyttenbach, T.; Condrón, M. M.; Bitan, G.; Teplow, D. B.; Shea, J.-E.; Ruotolo, B. T.; Robinson, C. V.; Bowers, M. T. *Nat. Chem.* 2009, 1, 326-331.
195. Calabrese, A. N.; Watkinson, T. G.; Henderson, P. J. F.; Radford, S. E.; Ashcroft, A. E. *Anal. Chem.* 2015, 87, 1118-1126.
196. Konijnenberg, A.; Yilmaz, D.; Ingolfsson, H. I.; Dimitrova, A.; Marrink, S. J.; Li, Z. L.; Venien-Bryan, C.; Sobott, F.; Kocer, A. *Proc. Nat. Acad. Sci. U.S.A.* 2014, 111, 17170-17175.

197. Laganowsky, A.; Reading, E.; Allison, T. M.; Ulmschneider, M. B.; Degiacomi, M. T.; Baldwin, A. J.; Robinson, C. V. *Nature* 2014, 510, 172-+.
198. Kelker, M. S.; Berry, C.; Evans, S. L.; Pai, R.; McCaskill, D. G.; Wang, N. X.; Russell, J. C.; Baker, M. D.; Yang, C.; Pflugrath, J. W.; Wade, M.; Wess, T. J.; Narva, K. E. *Plos One* 2014, 9, 15.
199. Hoaglund, C. S.; Liu, Y.; Ellington, A. D.; Pagel, M.; Clemmer, D. E. *J. Am. Chem. Soc.* 1997, 119, 9051-9052.
200. Gidden, J.; Bowers, M. *The European Physical Journal D-Atomic, Molecular, Optical and Plasma Physics* 2002, 20, 409-419.
201. Gidden, J.; Bowers, M. T. *J Phys. Chem. B* 2003, 107, 12829-12837.
202. Gidden, J.; Bowers, M. T. *J. Am. Soc. Mass Spectrom.* 2003, 14, 161-170.
203. Gidden, J.; Ferzoco, A.; Baker, E. S.; Bowers, M. T. *J. Am. Chem. Soc.* 2004, 126, 15132-15140.
204. Baker, E. S.; Bernstein, S. L.; Bowers, M. T. *J. Am. Soc. Mass Spectrom.* 2005, 16, 989-997.
205. Baker, E. S.; Manard, M. J.; Gidden, J.; Bowers, M. T. *J Phys. Chem. B* 2005, 109, 4808-4810.
206. Baker, E. S.; Hong, J. W.; Gaylord, B. S.; Bazan, G. C.; Bowers, M. T. *J. Am. Chem. Soc.* 2006, 128, 8484-8492.
207. Baker, E. S.; Bowers, M. T. *J. Am. Soc. Mass Spectrom.* 2007, 18, 1188-1195.
208. Baker, E. S.; Dupuis, N. F.; Bowers, M. T. *J Phys. Chem. B* 2009, 113, 1722-1727.
209. Burmistrova, A.; Gabelica, V.; Duwez, A. S.; De Pauw, E. J. *Am. Soc. Mass Spectrom.* 2013, 24, 1777-1786.
210. Gidden, J.; Bowers, M. T.; Jackson, A. T.; Scrivens, J. H. *J. Am. Soc. Mass Spectrom.* 2002, 13, 499-505.
211. Baker, E. S.; Gidden, J.; Simonsick, W. J.; Grady, M. C.; Bowers, M. T. *Int. J. Mass Spectrom.* 2004, 238, 279-286.
212. Jackson, A. T.; Scrivens, J. H.; Williams, J. P.; Baker, E. S.; Gidden, J.; Bowers, M. T. *Int. J. Mass Spectrom.* 2004, 238, 287-297.
213. Forsythe, J. G.; Stow, S. M.; Nefzger, H.; Kwiecien, N. W.; May, J. C.; McLean, J. A.; Hercules, D. M. *Anal. Chem.* 2014, 86, 4362-4370.
214. Stow, S. M.; Onifer, T. M.; Forsythe, J. G.; Nefzger, H.; Kwiecien, N. W.; May, J. C.; McLean, J. A.; Hercules, D. M. *Anal. Chem.* 2015, 87, 6288-6296.

215. Kim, K.; Lee, J. W.; Chang, T.; Kim, H. I. *J. Am. Soc. Mass Spectrom.* 2014, 25, 1771-1779.
216. Guo, K.; Guo, Z. H.; Ludlow, J. M.; Xie, T. Z.; Liao, S. Y.; Newkome, G. R.; Wesdemiotis, C. *Macromolecular Rapid Communications* 2015, 36, 1539-1552.
217. Alalwiat, A.; Grieshaber, S. E.; Paik, B. A.; Kiick, K. L.; Jia, X. Q.; Wesdemiotis, C. *Analyst* 2015, 140, 7550-7564.
218. Katzenmeyer, B. C.; Cool, L. R.; Williams, J. P.; Craven, K.; Brown, J. M.; Wesdemiotis, C. *Int. J. Mass Spectrom.* 2015, 378, 303-311.
219. Liu, X. M.; Cool, L. R.; Lin, K.; Kasko, A. M.; Wesdemiotis, C. *Analyst* 2015, 140, 1182-1191.
220. Alsharaeh, E. H.; El-Shall, M. S. *Polymer* 2011, 52, 5551-5559.
221. Wyttenbach, T.; von Helden, G.; Bowers, M. T. *Int. J. Mass Spectrom. Ion Processes* 1997, 165, 377-390.
222. Gidden, J.; Wyttenbach, T.; Batka, J. J.; Weis, P.; Bowers, M. T.; Jackson, A. T.; Scrivens, J. H. *J. Am. Soc. Mass Spectrom.* 1999, 10, 883-895.
223. Gidden, J.; Wyttenbach, T.; Jackson, A. T.; Scrivens, J. H.; Bowers, M. T. *J. Am. Chem. Soc.* 2000, 122, 4692-4699.
224. Gidden, J.; Jackson, A. T.; Scrivens, J. H.; Bowers, M. T. *Int. J. Mass Spectrom.* 1999, 188, 121-130.
225. von Helden, G.; Wyttenbach, T.; Bowers, M. T. *Int. J. Mass Spectrom. Ion Processes* 1995, 146-147, 349-364.
226. Maire, F.; Coadou, G.; Cravello, L.; Lange, C. M. *J. Am. Soc. Mass Spectrom.* 2013, 24, 238-248.
227. Tintaru, A.; Pricl, S.; Denbigh, L.; Liu, X. X.; Peng, L.; Charles, L. *Int. J. Mass Spectrom.* 2013, 354, 235-241.
228. Leriche, E. D.; Afonso, C.; Lange, C. M.; Grossel, M. C.; Truong, L.; Coadou, G.; Oulyadi, H.; Loutelier-Bourhis, C. *Rsc Advances* 2014, 4, 1744-1753.
229. Baker, E. S.; Gidden, J.; Fee, D. P.; Kemper, P. R.; Anderson, S. E.; Bowers, M. T. *Int. J. Mass Spectrom.* 2003, 227, 205-216.
230. Anderson, S. E.; Baker, E. S.; Mitchell, C.; Haddad, T. S.; Bowers, M. T. *Chemistry of Materials* 2005, 17, 2537-2545.
231. Anderson, S. E.; Mitchell, C.; Haddad, T. S.; Vij, A.; Schwab, J. J.; Bowers, M. T. *Chemistry of Materials* 2006, 18, 1490-1497.

232. Brocker, E. R.; Anderson, S. E.; Northrop, B. H.; Stang, P. J.; Bowers, M. T. J. *Am. Chem. Soc.* 2010, 132, 13486-13494.
233. Liang, Y. P.; He, Y. J.; Lee, Y. H.; Chan, Y. T. *Dalton Transactions* 2015, 44, 5139-5145.
234. Lee, J. W.; Shin, M. H.; Mobley, W.; Urbach, A. R.; Kim, H. I. *J. Am. Chem. Soc.* 2015, 137, 15322-15329.
235. Xie, T. Z.; Guo, K.; Guo, Z. H.; Gao, W. Y.; Wojtas, L.; Ning, G. H.; Huang, M. J.; Lu, X. C.; Li, J. Y.; Liao, S. Y.; Chen, Y. S.; Moorefield, C. N.; Saunders, M. J.; Cheng, S. Z. D.; Wesdemiotis, C.; Newkome, G. R. *Angewandte Chemie-International Edition* 2015, 54, 9224-9229.
236. Zhang, H.; Grabenauer, M.; Bowers, M. T.; Dearden, D. V. *J Phys. Chem. A* 2009, 113, 1508-1517.
237. Chan, Y.-T.; Li, X.; Yu, J.; Carri, G. A.; Moorefield, C. N.; Newkome, G. R.; Wesdemiotis, C. *J. Am. Chem. Soc.* 2011, 133, 11967-11976.
238. Poyer, S.; Loutelier-Bourhis, C.; Coadou, G.; Mondeguer, F.; Enche, J.; Bossee, A.; Hess, P.; Afonso, C. *J. Mass Spectrom.* 2015, 50, 175-181.
239. Baker, E. S.; Dupuis, N. F.; Bowers, M. T. *Int. J. Mass Spectrom.* 2009, 283, 105-111.
240. Poyer, S.; Loutelier-Bourhis, C.; Tognetti, V.; Joubert, L.; Enche, J.; Bossée, A.; Mondeguer, F.; Hess, P.; Afonso, C. *Int. J. Mass Spectrom.* 2016, 402, 20-28.
241. Nortcliffe, C.; Migas, L. G.; Liu, X. J.; Ngo, H. T.; Jolliffe, K. A.; Barran, P. E. *Int. J. Mass Spectrom.* 2015, 391, 62-70.
242. Domalain, V.; Tognetti, V.; Hubert-Roux, M.; Lange, C. M.; Joubert, L.; Baudoux, J.; Rouden, J.; Afonso, C. *J. Am. Soc. Mass Spectrom.* 2013, 24, 1437-1445.
243. Stojko, J.; Fieulaine, S.; Petiot-Becard, S.; Van Dorsselaer, A.; Meinnel, T.; Giglione, C.; Cianferani, S. *Analyst* 2015, 140, 7234-7245.
244. Coughlan, N. J. A.; Catani, K. J.; Adamson, B. D.; Wille, U.; Bieske, E. J. *Journal of Chemical Physics* 2014, 140, 10.
245. Baker, E. S.; Bushnell, J. E.; Wecksler, S. R.; Lim, M. D.; Manard, M. J.; Dupuis, N. F.; Ford, P. C.; Bowers, M. T. *J. Am. Chem. Soc.* 2005, 127, 18222-18228.

CHAPTER 3

UNTARGETED MOLECULAR DISCOVERY IN PRIMARY METABOLISM: COLLISION CROSS SECTION AS A MOLECULAR DESCRIPTOR IN ION MOBILITY-MASS SPECTROMETRY

3.1 Introduction

From the central dogma of molecular biology, studies of genomics, transcriptomics, and proteomics provide higher order information about gene and protein expression to better understand implicated phenotypes.^{1,2} However, these approaches provide limited information about real-time production of chemical species related to cellular metabolism as a function of external stimuli or phenotype of interest. To address the need for rapid characterization of cellular metabolism, metabolomics seeks to uncover molecular information on a per-molecule basis by examining expressed cellular products that can be correlated with a specific phenotype, stimuli, or other experimental conditions.³

While several analytical approaches have been utilized to study metabolism and related cellular processes (*e.g.* NMR, electrochemistry, etc.),^{4,5} mass spectrometry (MS) is gaining widespread adoption as a result of its high throughput, low limits of detection, and molecular specificity. Mass spectrometers can collect chemical information on the microsecond (μs) time scale,⁶ and with the rise of high-resolution, accurate mass techniques such as time of flight (TOF), Orbitrap, and ion cyclotron instruments, a unique chemical formula can often be generated based solely on mass measurement for a specific analyte signal.^{7,8} While identifying a specific chemical formula is advantageous, many metabolic pathways include isomeric molecules covering a range of

biological classes, such as carbohydrates (*e.g.* glucose/galactose),⁹ nucleosides (*e.g.* adenosine/deoxyguanosine), and lipids (7-dehydrocholesterol/desmosterol).¹⁰ As biological function follows molecular structure, characterization of isomeric species is imperative for complete molecular identification and accurate pathway analysis. In many MS experiments, fragmentation techniques such as collision induced dissociation (CID) or electron transfer dissociation (ETD) are utilized to provide structural information about a specific analyte measured in the study.^{11,12} However, as many metabolite isomers are less than 300 Dalton, these compounds often possess identical fragmentation spectra at similar energy thresholds and hence molecular fingerprinting by MS/MS and high resolution precursor mass is often not specific enough to identify a unique molecular structure.¹³ Furthermore, as quadrupoles isolate on nominal mass, molecules with different molecular formulas but similar exact mass (*i.e.* nominal mass isobars) cannot be isolated, thereby complicating MS/MS analysis.¹⁴ To address these challenges, pre-separation techniques such as gas and liquid chromatography,^{15,16} and more recently ion mobility spectrometry,¹⁷ have been interfaced prior to mass analysis to provide enhanced structural recognition and increased analyte coverage. For untargeted analysis, metabolomic databases (*e.g.* METLIN, HMDB, etc)¹⁸ include multiple descriptors of analyte information (*e.g.* accurate mass, ion adduct form, fragmentation pattern, and retention time) to increase confidence in molecular identification.¹⁹ With the advent of commercially-available ion mobility-mass spectrometers in 2006,²⁰ collision cross section (CCS) has become an additional molecular descriptor for untargeted experiments. CCS measurements are being standardized across instrumental platforms using rigid experimental protocols, and as such provide a molecular descriptor independent of system settings which are transferable between laboratories.^{17,21-23} These collected CCS measurements provide the capability to distinguish isomeric species in complex mixtures, provided enough resolution is

accessible in the IM dimension.²⁴ In order to provide additional confidence in molecular identification for untargeted metabolomic analysis, significant efforts are being made in the IM community to establish reliable CCS databases for analyzing unknown features across a range of biochemical classes, including lipids, metabolites, and xenobiotics.^{21,22,25,26} In this work, we use uniform field IM-MS to develop a library of CCS values focused on primary metabolites established with analytical standards to facilitate chemical identification in untargeted metabolomic workflows. Furthermore, we demonstrate the utility of these measurements by analyzing a commercially available extract of human serum (NIST 1950) which has been characterized previously in traditional GC and LC-MS experiments.^{27,28}

3.2 Experimental Methods

3.2.1 MSMLS Sample Preparation

The Mass Spectrometry Metabolite Library of Standards (MSMLS, IROA technologies) is supplied as dried standards distributed across seven 96-well plates (Sigma-Aldrich; St. Louis, MO) and each well contains 5 μg of analytical standard. All solvents used to reconstitute the analytes prior to analysis, including water (H_2O), methanol (MeOH), acetonitrile (ACN), isopropanol (IPA), and chloroform (CHCl_3) were Optima LC-MS grade purchased from Fisher Scientific (Fair Lawn, NJ). Stock solutions of the hydrophilic standards were prepared by adding 100 μL 1:9 (MeOH: H_2O) to each well prior to mixing on a waving rotator for 5 minutes. The stocks were then distributed in 20 μL aliquots throughout five 96-well plates (Waters part no. 186005837). Stock plates that were not immediately analyzed were capped and transferred to $-80\text{ }^\circ\text{C}$ for storage. Working solutions of the hydrophilic standards were prepared by adding 80 μL of water with 0.1%

formic acid to the 20 μL stock solutions, sealed with plate covers (Waters part no. 186006332), and subsequently mixed on a waving rotator for 5 minutes. The hydrophobic analyte set was prepared similarly, where stock solutions were prepared with 100 μL 2:1:1:0.3 (MeOH: CHCl_3 : IPA: H_2O), and distributed in 20 μL aliquots throughout five 96-well plates. Working solutions were prepared by adding 80 μL of 1:1 (MeOH: IPA). The concentration of the working solutions used for IM-MS analysis was 10 $\mu\text{g}/\text{mL}$.

3.2.2 Collision Cross Section Measurements

CCS measurements for the MSMLS were obtained on a commercially available drift tube ion mobility-mass spectrometer (DTIMS, Agilent 6560) operated with nitrogen gas (3.95 Torr) at room temperature (~ 25 $^\circ\text{C}$) and using both single-field and stepped-field approaches previously established in an inter-laboratory study.²¹ The single-field CCS values reported here were measured in triplicate, while the stepped-field values were collected in a single acquisition. Stepped-field measurements were acquired using an automated flow injection analysis (FIA) stepped-field approach described previously.²⁹ Briefly, the FIA method was performed with a liquid chromatography system (Agilent 1290) modified with a 100 μL sample loop (Agilent part no. G4226-87303) coupled to an IM-MS (6560, Agilent). 20 μL of the working solution was injected from the 96-well plate with 1:1 (water: isopropanol) as the carrier solvent. For traditional stepped-field CCS determination by FIA, following a 0.5 s delay, an entrance potential was stepped every 0.5 min. in increments of 100 V from 1074 V to 1674 V; the first step from 1074 to 1174 occurred at 1.0 minute rather than 0.5 min. For stepped-field measurements, the fundamental low field ion mobility equation is used to determine CCS values. For single-field CCS determination using FIA, 4 μL of sample was injected into the carrier solvent at a flow of 800 $\mu\text{L}/\text{min}$. Data was

collected for 0.5 min, followed by a 0.4 min postrun flushing cycle. A drift tube entrance voltage of 1574 V was used with an exit voltage of 224 V, which corresponds to a drift field of 17.3 V/cm. DTIMS exhibits a linear relationship between drift time and CCS,⁶ and single-field CCS values are determined by first measuring the drift time of reference standards (ESI Low Concentration Tuning Mix, Agilent) with a known CCS. The reference ions were infused for 0.5 minutes while IM-MS spectra are collected; calibration experiments were performed intermittently to ensure instrument stability. IM-MS Browser (Agilent, B.08) was used to plot the linear regression of the calibration ions for single field experiments, and the instrumental coefficients β and T_{fix} , were extracted and used to convert raw ion drift times to CCS.²¹ The resulting single- and stepped-field CCS library can be found in Appendix A.

3.2.3 IM-MS Source and Drift Cell Conditions

To obtain high coverage of analytes within the MSMLS, both electrospray (Agilent Jet Stream, AJS) and chemical ionization (APCI) sources were used. The majority of the samples collected with the AJS source in both ion modes were measured using the following conditions: gas temperature, 250 °C; drying gas flow rate, 8 L/min; nebulizer gas, 60 psig; sheath gas temperature, 300 °C; sheath gas flow rate, 11 L/min; capillary voltage (V_{Cap}), 3500 V; nozzle voltage, 800 V; fragmentor, 340 V; octopole 1 RF, 750 V_{pp}. All metabolites were first investigated using the AJS source; those which were not observed in either ion polarity were subsequently investigated using the APCI source under the following conditions: gas temperature, 250 °C; vaporizer, 200 °C; drying gas flow rate, 7 L/min; nebulizer gas, 30 psig; V_{Cap}, 3800 V; corona needle current, 5 μ A; fragmentor, 350 V; octopole 1 RF, 750 V_{pp}. Some of the low m/z ions (typically ≤ 200 Da) exhibited metastable ion dissociation in the DTIMS which resulted in

uncorrelated mobilities (Figure B.1). In these cases, we increased the fragmentor potential to > 350 V and decreased the Trap Funnel RF to ≤ 80 V_{pp} to correlate the ion signal into a single IM distribution. The IM-MS settings for the CCS values reported herein are as follows: 0.9 frames/s; 18 IM transients/frame; 60 ms max drift time; 600 TOF transients/IM transient; 20000 μ s trap fill time; 180 μ s trap release time; drift tube exit voltage, 224 V; rear funnel entrance voltage, 217.5 V; rear funnel exit voltage, 45 V.

3.2.4 Nonlinear Regression Analysis

Iterative nonlinear regression modeling for the super classes was performed using GraphPad Prism 7, and 99% confidence intervals were generated for each biomolecular super class. Three fits were tested for each super class: power fit (PF), 4-parameter sigmoidal (4P), and 5-parameter sigmoidal (5P). The most parsimonious fit was chosen by a probabilistic comparison of the corrected Akaike information criterion (AICc) values.

3.2.5 Human Serum Preparation

Protein precipitation was performed by adding 800 μ L of ice cold MeOH to 100 μ L NIST 1950 serum and stored at -80 °C for one hour. The sample was centrifuged at 14,000 rpm for 5 minutes before collecting the supernatant. Next, 2.4 mL ice cold methyl tert-butyl ether and 800 μ L ice cold water were added. The sample was vortexed then centrifuged at 10,000 rpm at 4 °C for 10 minutes. The polar and nonpolar fractions were separated and dried separately *in vacuo*. Samples were stored at -20 °C until analysis. Dried fractions were resuspended in 200 μ L of the initial mobile phase solvent and analyzed via LC-IM-MS.

3.2.6 Liquid Chromatography

LC-IM-MS was performed on the prepared NIST 1950 serum using HILIC chromatography for the hydrophilic layer of the liquid-liquid extraction. For this method, 4 μL of sample was injected onto a column heated to 40 $^{\circ}\text{C}$. The Millipore SeQuant Zic-HILIC (2.1 x 100 mm, 3.5 μm) column was used with mobile phase A and B being 9:1 and 1:9 (water: acetonitrile, buffered with 5 mM ammonium formate), respectively. The mobile phase flow rate was 200 $\mu\text{L}/\text{min}$. The gradient was initially held at 98 %B from 0 to 1 minutes, decreased to 45 %B from 1 to 20 minutes, held at 45 % B from 20 to 22 minutes, increased to 98 %B from 22 to 40 minutes, and subsequently held at 98 %B from 40 to 45 minutes prior to the next injection.

3.3 Results and Discussion

3.3.1 MSMLS Plate Coverage

In total, the MSMLS plates analyzed in this work contained 554 unique compounds across a large breadth of biological classes found in canonical metabolite pathways (See Figure 3.1(A)). Of these 554 analytes, one or more CCS values were measured for 417, resulting in *ca.* 75% coverage. Of these 554 analytes, one or more CCS values were measured for 417, resulting in *ca.* 75% coverage. Many of the remaining analytes were detected by MS but were unable to produce a measurable CCS. Of these compounds, many were not well ionized by ESI and, therefore, were of insufficient abundance to generate the signal required to result in a confident mobility distribution. Other species were subject to metastable transitions in the drift tube, leading to uncorrelated mobility (See Figure B.1). Collectively, these 417 analytes produced 1246 CCS measurements using both positive (701 measurements) and negative ion polarities (545

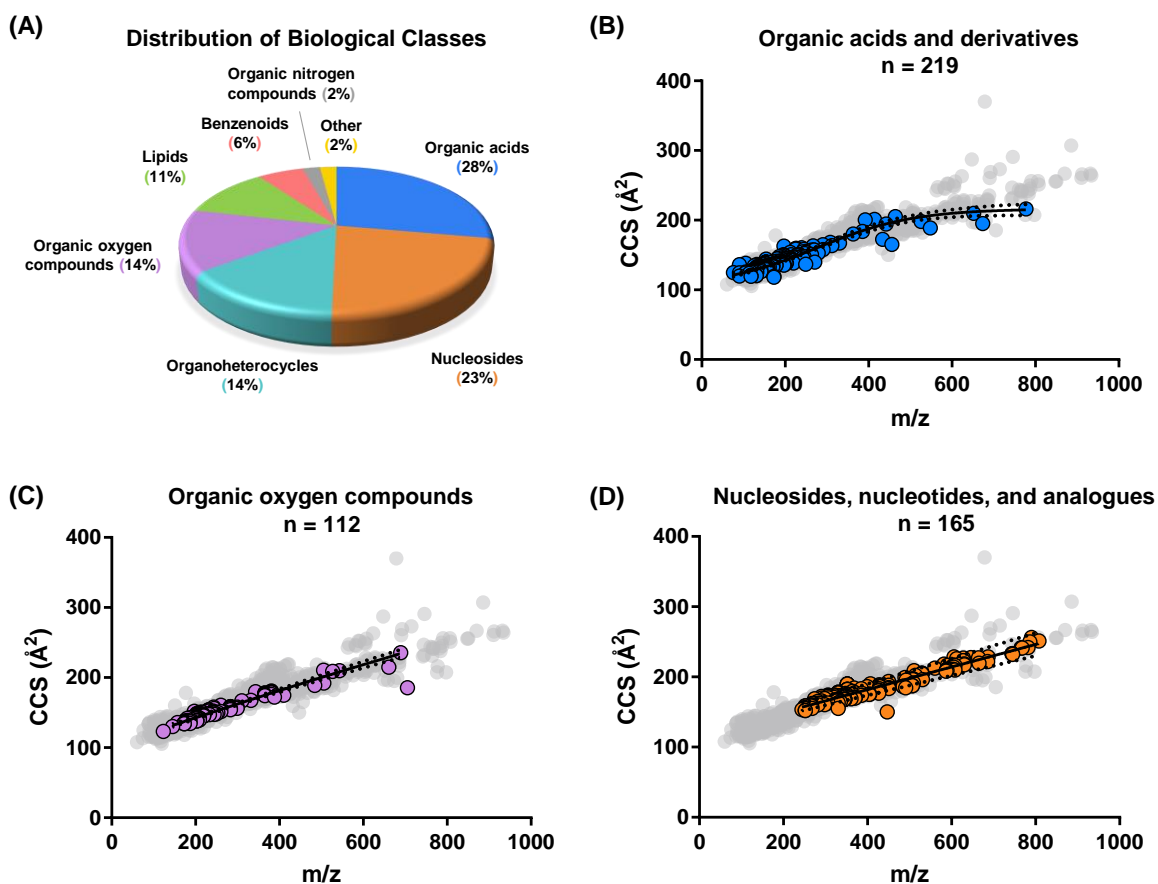


Figure 3.1 (A) Distribution of biological categories associated with the primary metabolites examined in the MSMLS plate library. (B, C, and D) Conformational space plots of three singly charged molecular super classes contained in the MSMLS library. Representative nonlinear regression fits (solid black lines) along with 99 % confidence intervals (black dotted lines) are shown for each. Gray dots denote all molecules CCS values obtained in the library. All CCS error bars are smaller than their respective symbols. (B) “Organic acids and derivatives” with a 4-parameter sigmoidal fit. (C) “Organic oxygen compounds” with a power fit and (D) “Nucleosides, nucleotides, and analogues” with a power fit. Reprinted (adapted) with permission from Charles M. Nichols, James N. Dodds, Bailey S. Rose, Jaqueline A. Picache, Caleb B. Morris, Simona G. Codreanu, Jody C. May, Stacy D. Sherrod, John A. McLean, “Untargeted Molecular Discovery in Primary Metabolism: Collision Cross Section as a Molecular Descriptor in Ion Mobility-Mass Spectrometry,” *Analytical Chemistry* 2018, 90 (24), 14484-14492. Copyright 2018 American Chemical Society.

measurements) across several adduct types (*e.g.* $[M+Na]^+$, $[M-H]^-$, *etc.*, see Figure B.2). Analyte identification and relevant descriptors (chemical name, formula, KEGG ID, Metlin ID, adduct type, measured mass, CCS, and other information) have been uploaded to Metabolomics Workbench.³⁰

3.3.2 Mass-Mobility Correlation Analysis

In these data, we observed several distinct relationships between m/z and CCS for individual structural super classes represented in the MSMLS library similar to previous IM-MS literature.^{31–35} Mass-mobility relationships have been shown to have utility as an additional rapid identifier of biomolecular class for uncharacterized biological samples,³⁶ making the mathematical description of these relationships by nonlinear regression modeling particularly useful. Unlike the canonical biochemical classes (nucleotides, proteins, carbohydrates, and lipids), metabolites exhibit less distinguished structural differences between chemical classes, and so several mathematical fits were investigated in order to find mass-mobility correlations which exhibit high class specificity. Fits and confidence intervals for representative super classes are shown in Figure 3.1 (B, C, and D), and detailed mathematical expressions are provided in Appendix B (Equations B.1-B.6).

3.3.3 Metabolic Pathway Coverage

As the MSMLS was designed to provide analytical standards of primary metabolism, we also evaluated metabolite coverage using pathway analysis by inputting KEGG IDs for all of the analytes measured in our CCS database in MetaboAnalyst 4.0.³⁷ In total, 64 pathways were covered with a wide range of biological activity including key metabolic processes such as the

citric acid cycle, amino acid metabolism, and glycolysis (Figure 3.2(A) and Table B.1). Pathway coverage presented in this work is solely based on analyte coverage from the standards, and therefore provides qualitative reflection on the number of analytes in each specific pathway which are accounted for in the CCS library. MetaboAnalyst 4.0 also provides detailed information for specific pathways of interest, wherein molecular coverage can be evaluated on a per-analyte basis. For example, 10 pivotal metabolites in the citric acid cycle (see Figure 3.2(B)) are represented within the standards, and out of 20 total, 8 of these molecules exhibited a measurable CCS (green), while only 2 (orange) were observable in the mass spectrum but did not result in a collected CCS due to low ion intensity. Of note, many other compounds described in the KEGG pathways which are not components in the standard set (10 compounds, light blue) are protein enzymes or oxidized derivatives, and only 3 of these 10 are available for purchase as analytical standards. Hence it is unlikely that 100% coverage of canonical pathways is obtainable with chemical standards. As an analogy, it is not necessary to have 100% peptide coverage for a specific protein in proteomic analysis for confident identification.

3.3.4 Isomers in Metabolomics

Of the more than 500 compounds in the MSMLS library, almost one-third (31%) have a chemical formula in common with another compound, forming an isomeric pair, Figure B.3. Isomeric compounds are ubiquitous in metabolomic processes across a wide range of biological classes, for example the carbohydrate rearrangements for glucose 6-phosphate isomerization to fructose 6-phosphate in glycolysis. Figure 3.2(B) highlights two key metabolic intermediates of the citric acid cycle, citrate and isocitrate, which are constitutional rearrangements of a single hydroxyl group along the central carbon chain. As these compounds have the same chemical

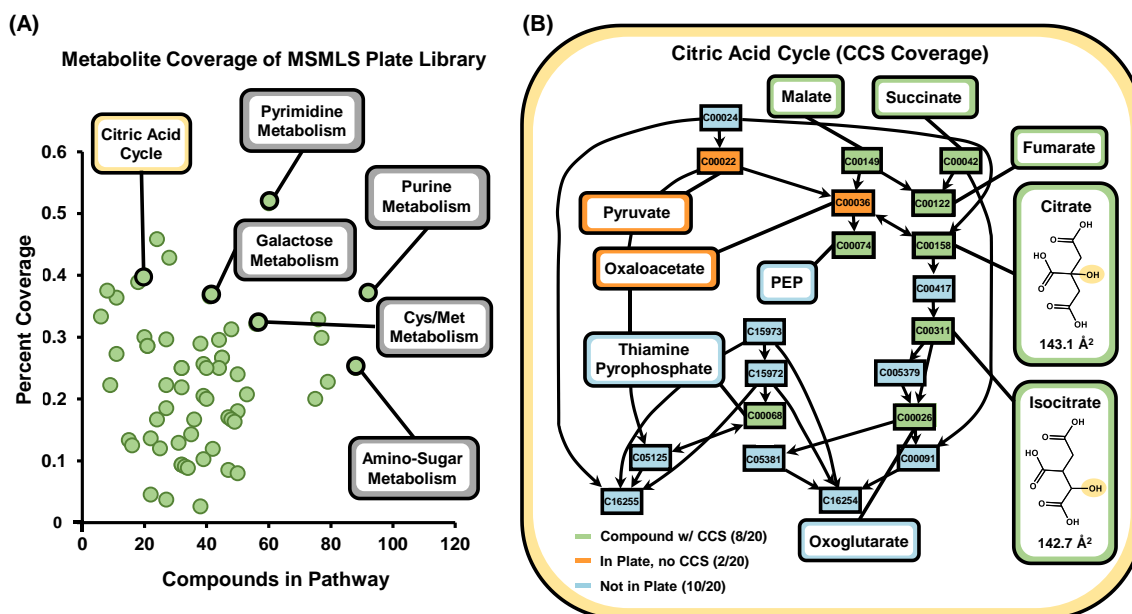


Figure 3.2 (A) KEGG pathway coverage of metabolites with measured CCS evaluated in this study. A total of 64 pathways are covered by metabolites in our CCS library based on the MSMLS. After a specific pathway is selected **(B)**, metabolite-specific coverage can be evaluated. In many pathways, isomerization is a key intermediate in primary metabolism, noted by the callouts for citrate and isocitrate in the citric acid cycle. Reprinted (adapted) with permission from Charles M. Nichols, James N. Dodds, Bailey S. Rose, Jaqueline A. Picache, Caleb B. Morris, Simona G. Codreanu, Jody C. May, Stacy D. Sherrod, John A. McLean, "Untargeted Molecular Discovery in Primary Metabolism: Collision Cross Section as a Molecular Descriptor in Ion Mobility-Mass Spectrometry," *Analytical Chemistry* 2018, 90 (24), 14484-14492. Copyright 2018 American Chemical Society.

formula, they will also possess identical masses, requiring additional separation in the chromatographic dimension for increased identification confidence in pathway analysis.^{17, 38} In the example depicted in Figure 3.2(B), ion mobility allows for differentiation of these two isomeric metabolites (CCS = 143.1 Å² vs. CCS = 142.7 Å², for citrate and isocitrate, respectively), which are indistinguishable by mass alone. Adding the ion mobility dimension to existing untargeted workflows allows for additional separation and characterization of isomeric metabolites that interfaces within the timescale of traditional chromatographic techniques.⁶

As a specific example, adenosine 5-diphosphate, adenosine 3,5-diphosphate, and 2'-deoxyguanosine-5'-diphosphate are nucleoside isomers which are key metabolites in purine metabolism and are depicted in Figure 3.3(A). Note that the only structural difference between A-5-DP (blue) and A-3,5-DP (green) is the location of a phosphate group from the central ribose unit. These two isomers are in turn differentiated structurally from 2'-deoxyguanosine-5'-diphosphate (DGDP, orange) by molecular substitutions on the purine ring, where a hydroxyl group has been relocated from the ribose sugar to the guanine ring, as well as an amine rearrangement in the same region. Structurally, these three nucleoside compounds are also constitutional isomers, a subcategory of isomeric compounds which have been heavily characterized in previous ion mobility literature.³⁹⁻⁴¹ Also noted in Figure 3.3(A), adduct formation has a substantial effect on the overall selectivity of the IM separation. Specifically, each nucleoside isomer has a distinct cross sectional distribution which are distinguishable in the protonated [M+H]⁺ and sodium adducted [M+Na]⁺ species, however the rearrangement of the phosphate group between A-5-DP and A-3,5-DP provides no resolution for the deprotonated form observed in negative ion mode [M-H]⁻. Other metabolite separations in this study were more readily separated in negative ion mode such as the isomers L-glutamic acid and N-methyl-D-aspartic acid (see Figure B.4). The

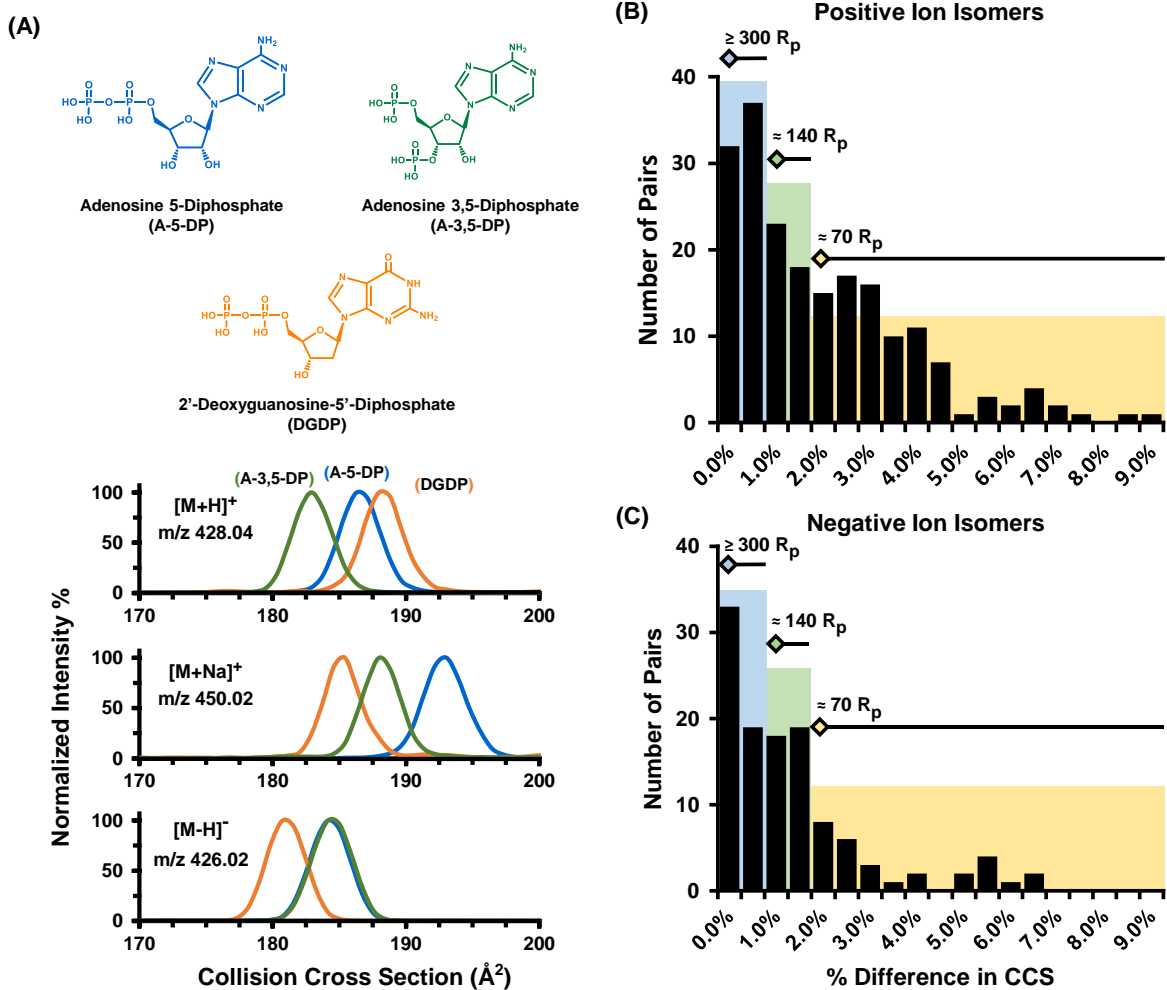


Figure 3.3 (A) IM separation of nucleoside isomers (chemical structures illustrated at the top of the panel) for $[M+H]^+$, $[M+Na]^+$, and $[M-H]^-$ ion forms, respectively. For these particular isomers, enhanced separation is noted for the sodium adducts, while the negative mode A-5-DP $[M-H]^-$ and A-3,5-DP CCS distributions are indistinguishable. After sorting all observed isomer sets in the MSMLS dataset, pairwise matches were created and evaluated based on their percent difference in CCS. The resulting difficulty in separations is noted in panels (B) for positive and (C) negative ion forms. Reprinted (adapted) with permission from Charles M. Nichols, James N. Dodds, Bailey S. Rose, Jaqueline A. Picache, Caleb B. Morris, Simona G. Codreanu, Jody C. May, Stacy D. Sherrod, John A. McLean, "Untargeted Molecular Discovery in Primary Metabolism: Collision Cross Section as a Molecular Descriptor in Ion Mobility-Mass Spectrometry," *Analytical Chemistry* 2018, 90 (24), 14484-14492. Copyright 2018 American Chemical Society.

broad range of chemical diversity present in small molecules presents unique advantages in the range of ion types that can be utilized. Collectively, these results demonstrate the advantage of utilizing both ion polarities in untargeted analyses in which various charge adducts formed during the ionization process can be exploited to substantially enhance the selectivity in IM-MS analysis by increasing the absolute CCS difference between isomers. This allows a significant improvement in separation without instrumental upgrades that would otherwise be necessary to achieve improved separation *via* increased resolving power. This enhanced separation, in turn, provides additional confidence in identification through CCS library matches and enhanced ion mobility resolution. A potential future direction in the field will utilize molecular modeling and machine learning approaches for prediction of adduct specific CCS values and optimal separation conditions.

3.3.5 IM-MS Separation in Primary Metabolites

In addition to enhanced separation through charged adduct formation, recent advances in ion mobility resolving power (R_p) have provided increased separation coverage of isomeric species.^{42,43} In order to determine the resolving power in the IM dimension needed for untargeted metabolomic experiments, we analyzed pairwise matches of all isomers which provided a usable CCS and binned the resulting pairs by percent difference in cross section ($\% \Delta \text{CCS}$). In brief, analytes with identical chemical formulas were grouped into isomeric sets and were subsequently matched in a pairwise comparison. Each pairwise match was generated using an enumeration strategy wherein a percent difference in CCS was calculated for each possible combination of isomers. Most isomeric sets consist of 2-3 compounds, whereas the largest isomeric set was comprised of 9 unique analytes (see Figure B.3). In one example, there are 5 sugar compounds

which share the same chemical formula ($C_6H_{13}O_9PNa^+$, exact m/z 283.0195), which results in a total of 10 pairwise isomer matches in this analysis. The percent difference in CCS for all isomer matches were calculated, and the compiled results for all isomer pairings are displayed in Figure 3.3(B) (positive ion mode) and Figure 3.3(C) (negative ion mode). Approximately half of the isomer pairs generated are $\geq 2.0\%$ different in CCS and require *ca.* 70 resolving power (CCS/ Δ CCS) to separate at half height.^{43,44} In order to separate additional isomers, more resolving power would be required (*ca.* 140 for ~ 1.0 - 2.0% difference in CCS, and *ca.* >300 for $\sim 0.5\%$ CCS difference). Currently, only two commercially available IM-MS platforms provide this level of resolving power (*i.e.* atmospheric pressure DTIMS and trapped IMS),^{39,44} although several research instrument prototypes have been developed which are capable of accessing resolving powers in excess of 300 (CCS/ Δ CCS).^{6,45}

While IM instruments are continually increasing in resolving power capabilities, current untargeted metabolomic workflows identification is based first on primary mass measurement and subsequently supported with retention time, isotope ratios, and fragmentation matching. From this viewpoint, it is also imperative to describe how much resolving power in the mass dimension is necessary for metabolomic studies. By sorting the entire MSMLS library based on primary mass alone, our analysis shows that most analytes (64%) are resolvable based only on the mass dimension utilizing 40,000 mass resolving power (*e.g.* high resolution TOF, see Figure 3.4). Increasing levels of mass resolving power (300,000 for Orbitrap and up to 40,000,000 for FT-ICR, respectively)^{46,47} provides minimal increases in resolution of these metabolites (*ca.* 3% more). As *ca.* 30% of the compounds in the MSMLS library are isomers, essentially no level of increased mass spectrometry efficiency (short of excited state isomer resolution with MS resolving power of *ca.* 10 billion as theorized by Marshall and coworkers.⁴⁸) will be able to resolve these compounds,

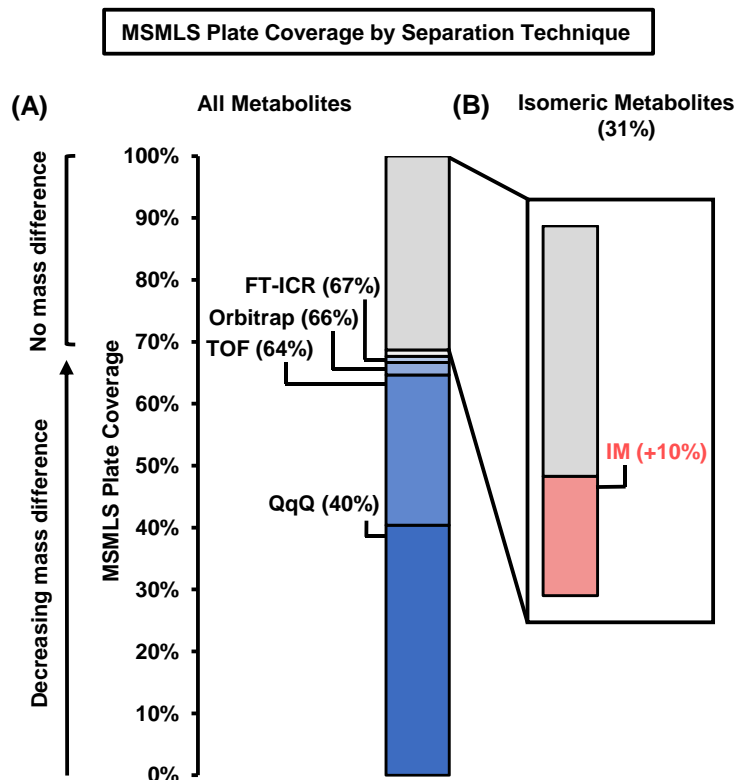


Figure 3.4 MSMLS plate coverage using different separation strategies. **(A)** Many analytes contained in the library can be resolved in the mass dimension at modest resolving power (TOF $R_p = 40,000$), with only incremental increases in coverage resulting from the use of an instrument with significantly higher resolving power (FT-ICR $R_p = 40,000,000$). **(B)** The addition of IM prior to mass analysis allows for isomeric separation and thus increases plate coverage by 10%. Reprinted (adapted) with permission from Charles M. Nichols, James N. Dodds, Bailey S. Rose, Jaqueline A. Picache, Caleb B. Morris, Simona G. Codreanu, Jody C. May, Stacy D. Sherrod, John A. McLean, "Untargeted Molecular Discovery in Primary Metabolism: Collision Cross Section as a Molecular Descriptor in Ion Mobility-Mass Spectrometry," *Analytical Chemistry* 2018, 90 (24), 14484-14492. Copyright 2018 American Chemical Society.

and hence orthogonal separation techniques are still required (*i.e.* GC, LC, or IM). Modest resolving power for commercially available IM instrumentation (*ca.* 70 CCS/ Δ CCS) resolves an additional 10% of compounds in the library, which outweighs the benefits of additional mass resolving power beyond 40,000 (*e.g.* TOF MS). We note, however, that this analysis does not consider mass measurement accuracy, which is typically higher for FTMS instruments (Orbitrap and FT-ICR). Nevertheless, in order to obtain the widest scope of molecular coverage in untargeted workflows, possessing sequential separation dimensions based on chemical affinity, gas-phase area, and m/z (LC-IM-MS) would strengthen analyte identification strategies.

3.3.6 LC-IM-MS Characterization of NIST 1950 Serum

The NIST 1950 human serum standard has been previously characterized in the literature,^{27,28,49} and is analyzed in this work to underscore the importance of isomeric characterization in untargeted experiments. Separation and characterization of isomeric species in biological extracts often requires multiple steps of chemical separation in order to gain increased confidence in assigning molecular structure. For example, the base peak chromatogram in Figure 3.5(A) shows the molecular complexity of the NIST 1950 human serum and the extracted ion chromatogram (lower trace) details a specific molecular feature at m/z 203.0528 that elutes into an unresolved broad peak over a *ca.* 2 minute chromatographic window. This broad distribution in the elution profile indicates the potential presence of multiple isomeric forms with similar, yet not identical, retention times. Although TOF MS has high resolving power (*ca.* 40,000), potentially two chemical formulas are within 10 ppm of the measured m/z ($C_6H_{12}O_6Na$ and $C_7H_8N_4O_2Na$, at 1.7 ppm and 8.3 ppm respectively; see Figure 3.5(C)). While assignment of this feature to chemical formula $C_6H_{12}O_6Na$ is more probable due to lower observed mass error, isotope ratios were used

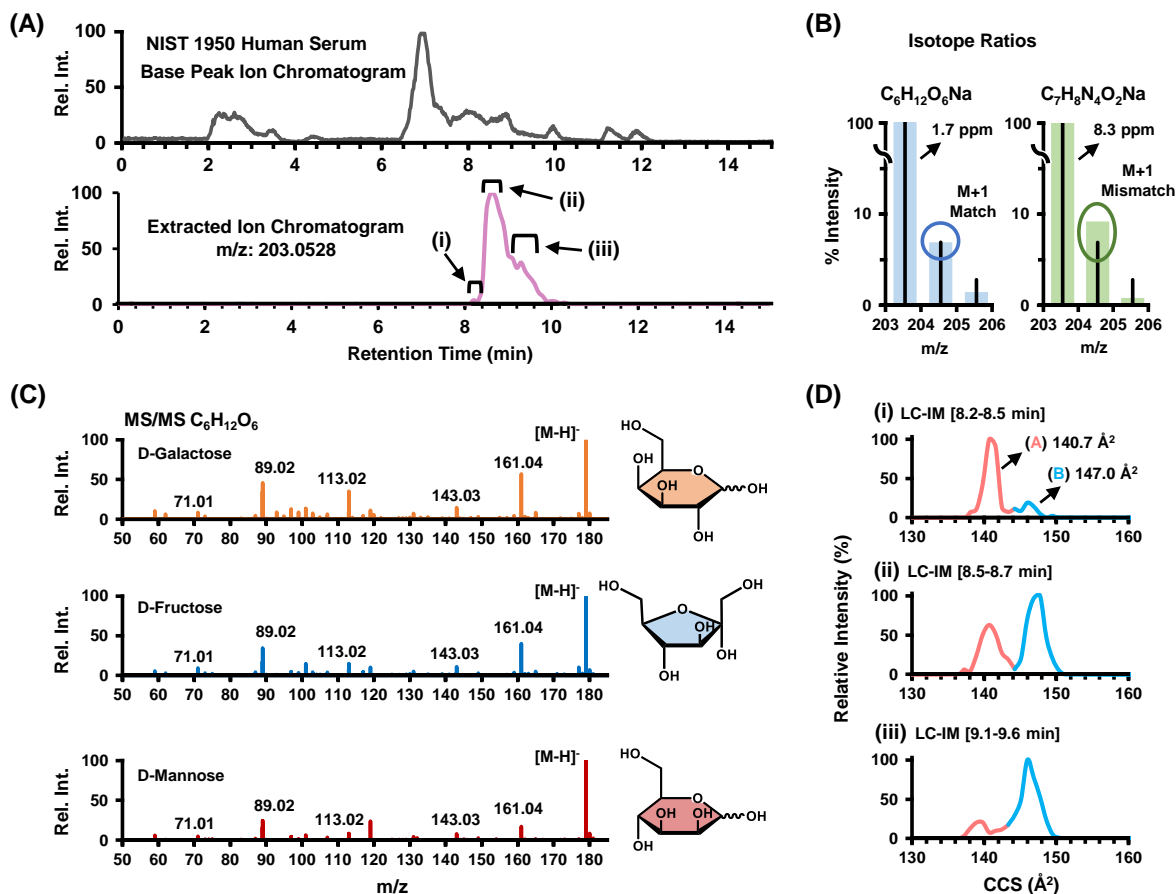


Figure 3.5 (A) HILIC base peak chromatogram for NIST 1950 human serum sample and (lower trace) the extracted ion chromatogram of m/z 203.0528, which consists of two distributions of interest that were further examined by isotope ratio pattern and ion mobility for structural characterization. (B) Expected and measured isotope ratio abundances for two possible chemical formulas corresponding to m/z 203 within 10 ppm. The chemical formula $C_6H_{12}O_6$ $[M+Na]^+$ more closely aligns with experimental measurements from the NIST serum both on basis of mass accuracy (2 ppm) and isotope ratio pattern (M+1). (C) Fragmentation spectra for isomers with the shared chemical formula $C_6H_{12}O_6$ $[M-H]^-$. (D) Selected ion mobility distributions for m/z 203 extracted over three time points in the chromatographic dimension. Reprinted (adapted) with permission from Charles M. Nichols, James N. Dodds, Bailey S. Rose, Jaqueline A. Picache, Caleb B. Morris, Simona G. Codreanu, Jody C. May, Stacy D. Sherrod, John A. McLean, "Untargeted Molecular Discovery in Primary Metabolism: Collision Cross Section as a Molecular Descriptor in Ion Mobility-Mass Spectrometry," *Analytical Chemistry* 2018, 90 (24), 14484-14492. Copyright 2018 American Chemical Society.

to confirm this molecular formula assignment, wherein the relative abundance of the M+1 peak in the serum more closely aligns with the isotope model for C₆H₁₂O₆Na as opposed to C₇H₈N₄O₂Na (Figure 3.5(B)). However, even after a specific molecular formula is determined, 9 potential isomers (including both constitutional rearrangements and stereochemistry for this chemical formula) exist within the MSMLS standards, all of which are carbohydrates. These isomers possess almost identical fragmentation profiles (see [M-H]⁻ ion, Figure 3.5(C)), and sophisticated algorithms for identification by MS/MS are needed, an observation which has been previously noted in other carbohydrate studies.⁵⁰ Note that Figure 3.5(C) utilizes the deprotonated ion of C₆H₁₂O₆, as the [M+Na]⁺ species noted in the other panels provides no fragmentation spectra due to preferential loss of the sodium charge carrier during collisional activation. Although previous energy-correlated MS/MS studies utilized relative abundance ratios of fragment ions to determine molecular structure, these techniques are time intensive and currently is not readily amended to rapid structural determination in untargeted workflows.⁵⁰ Similar to the chromatographic profile, ion mobility distributions obtained at three separate time points in the chromatogram (lower case Roman numerals) also indicate two separate chemical species present in the serum (Figure 3.5(D)). The collision cross sections measured for these two distributions helps narrow potential chemical structures from 9 potential isomeric forms down to 4 tentative identifications based on a CCS match within 1%. The smaller distribution at 140.7 Å² (light red, A) closely aligns with 3 isomers of C₆H₁₂O₆ in the standards (fructose, galactose and mannose at *ca.* 141.5 Å²). The larger distribution at 147.0 Å² (light blue, B) closely aligns with α-D-glucose, which is noted at 146.3 Å² in the database. Although in this example ion mobility does not provide definitive identification of the compounds observed in the NIST serum, it does significantly reduce the possible candidates, from the 9 potential structures noted in the database down to 3. Whereas the 1% CCS threshold

match used in this example effectively reduced the number of possible isomers by two-thirds, using a less conservative threshold could further reduce the ambiguity in assigning these molecular features with structural identities. By using collision cross section as additional metric for tentative identification, higher confidence in identifying molecular signatures can be gained in untargeted metabolomics.

3.4 Conclusions

In this work we have developed a CCS library based on primary metabolites obtained from the MSMLS library of analyte standards. As many key intermediates across metabolic pathways are formed through isomerization processes, utilizing orthogonal dimensions of separation in addition to mass analysis is imperative to fully characterize metabolic pathways. The intrinsic mass-mobility relationships for metabolites noted in this work, and others, illustrates a reproducible method of characterization for biochemical classes which interfaces seamlessly into the timescale of traditional LC/GC-MS workflows. Furthermore, we demonstrated that while additional resolving power in the m/z dimension is always advantageous, the diminishing returns of these efforts may not offset the additional costs associated with these instruments and the longer analysis times required for ultra-high resolution mass acquisition (*i.e.* FT processes). However, orthogonal separation techniques such as LC and IM can often resolve many isomeric forms, facilitating their identification for a more comprehensive understanding of the biochemical implications of experimental samples. Finally, we have demonstrated the advantages of adding CCS as a molecular descriptor in untargeted metabolomic analyses through characterization of a well-studied human serum extract (NIST 1950) by LC-IM-MS.

3.5 Acknowledgements

This chapter contains the published research article: Charles M. Nichols, James N. Dodds, Bailey S. Rose, Jaqueline A. Picache, Caleb B. Morris, Simona G. Codreanu, Jody C. May, Stacy D. Sherrod, John A. McLean, “Untargeted Molecular Discovery in Primary Metabolism: Collision Cross Section as a Molecular Descriptor in Ion Mobility-Mass Spectrometry,” *Analytical Chemistry* **2018**, *90* (24), 14484-14492. Reprinted (adapted) with permission from Charles M. Nichols, James N. Dodds, Bailey S. Rose, Jaqueline A. Picache, Caleb B. Morris, Simona G. Codreanu, Jody C. May, Stacy D. Sherrod, John A. McLean, “Untargeted Molecular Discovery in Primary Metabolism: Collision Cross Section as a Molecular Descriptor in Ion Mobility-Mass Spectrometry,” *Analytical Chemistry* 2018, *90* (24), 14484-14492. Copyright 2018 American Chemical Society.

Financial support for aspects of this research was provided by The National Institutes of Health (NIH NIGMS R01GM092218 and NCI R03CA222-452-01), the U. S. Environmental Protection Agency under Assistance Agreement No. 83573601, and the U.S. Army Research Office and the Defense Advanced Research Projects Agency (DARPA) under Cooperative Agreement no. W911 NF-14-2-0022. This work has not been formally reviewed by EPA. The views expressed in this document are solely those of the authors and do not necessarily reflect those of the funding agencies and organizations. EPA, DARPA, or the U.S. Government does not endorse any products or commercial services mentioned in this publication.

3.6 References

1. Crick, F. *Nature* 1970, 227 (5258), 561–563.
2. Joyce, A. R.; Palsson, B. Ø. *Nat. Rev. Mol. Cell Biol.* 2006, 7 (3), 198–210.
3. Goodacre, R.; Broadhurst, D.; Smilde, A. K.; Kristal, B. S.; Baker, J. D.; Beger, R.; Bessant, C.; Connor, S.; Capuani, G.; Craig, A.; Ebbels, T.; Kell, D. B.; Manetti, C.; Newton, J.; Paternostro, G.; Somorjai, R.; Sjöström, M.; Trygg, J.; Wulfert, F. *Metabolomics* 2007, 3 (3), 231–241.
4. Sumner, S.; Snyder, R.; Burgess, J.; Myers, C.; Tyl, R.; Sloan, C.; Fennell, T. J. *Appl. Toxicol.* 2009, 29 (8), 703–714.
5. Kimmel, D. W.; Dole, W. P.; Cliffler, D. E. *J. Lipids* 2017, 2017, 1–9.
6. May, J. C.; McLean, J. A. *Analytical Chemistry*. 2015, pp 1422–1436.
7. Kind, T.; Tsugawa, H.; Cajka, T.; Ma, Y.; Lai, Z.; Mehta, S. S.; Wohlgemuth, G.; Kumar, D.; Showalter, M. R.; Arita, M.; Fiehn, O. 2018, No. March 2017, 513–532.
8. Kim, S.; Rodgers, R. P.; Marshall, A. G. *Int. J. Mass Spectrom.* 2006, 251 (2–3), 260–265.
9. Hofmann, J.; Hahm, H. S.; Seeberger, P. H.; Pagel, K. *Nature* 2015, 526 (7572), 241–244.
10. Kyle, J. E.; Zhang, X.; Weitz, K. K.; Monroe, M. E.; Ibrahim, Y. M.; Moore, R. J.; Cha, J.; Sun, X.; Lovelace, E. S.; Wagoner, J.; Polyak, S. J.; Metz, T. O.; Dey, S. K.; Smith, R. D.; Burnum-Johnson, K. E.; Baker, E. S. *Analyst* 2016, 141 (5), 1649–1659.
11. Yost, R. A.; Enke, C. G.; McGilvery, D. C.; Smith, D.; Morrison, J. D. *Int. J. Mass Spectrom. Ion Phys.* 1979, 30 (2), 127–136.
12. Lareau, N. M.; May, J. C.; McLean, J. A. *Analyst* 2015, 140 (10), 3335–3338.
13. Dodds, J. N.; May, J. C.; McLean, J. A. *Anal. Chem.* 2017, 89 (1), 952–959.
14. Ekroos, K.; Chernushevich, I. V.; Simons, K.; Shevchenko, A. *Anal. Chem.* 2002, 74 (5), 941–949.
15. Kanani, H.; Chrysanthopoulos, P. K.; Klapa, M. I. *J. Chromatogr. B Anal. Technol. Biomed. Life Sci.* 2008, 871 (2), 191–201.
16. Lu, W.; Bennett, B. D.; Rabinowitz, J. D. *J. Chromatogr. B Anal. Technol. Biomed. Life Sci.* 2008, 871 (2), 236–242.
17. Mairinger, T.; Causon, T. J.; Hann, S. *Curr. Opin. Chem. Biol.* 2018, 42, 9–15.
18. Smith, C. a; O’Maille, G.; Want, E. J.; Qin, C.; Trauger, S. A.; Brandon, T. R.; Custodio, D. E.; Abagyan, R.; Siuzdak, G. *Ther. Drug Monit.* 2005, 27 (6), 747–751.

19. Schrimpe-Rutledge, A. C.; Codreanu, S. G.; Sherrod, S. D.; McLean, J. A. *J. Am. Soc. Mass Spectrom.* 2016, 27 (12), 1897–1905.
20. Pringle, S. D.; Giles, K.; Wildgoose, J. L.; Williams, J. P.; Slade, S. E.; Thalassinou, K.; Bateman, R. H.; Bowers, M. T.; Scrivens, J. H. *Int. J. Mass Spectrom.* 2007, 261 (1), 1–12.
21. Stow, S. M.; Causon, T. J.; Zheng, X.; Kurulugama, R. T.; Mairinger, T.; May, J. C.; Rennie, E. E.; Baker, E. S.; Smith, R. D.; McLean, J. A.; Hann, S.; Fjeldsted, J. C. *Anal. Chem.* 2017, 89 (17), 9048–9055.
22. Paglia, G.; Williams, J. P.; Menikarachchi, L.; Thompson, J. W.; Tyldesley-Worster, R.; Halldórsson, S.; Rolfsson, O.; Moseley, A.; Grant, D.; Langridge, J.; Palsson, B. O.; Astarita, G. *Anal. Chem.* 2014, 86 (8), 3985–3993.
23. Paglia, G.; Astarita, G. *Nat. Protoc.* 2017, 12 (4), 797–813.
24. Pu, Y.; Ridgeway, M. E.; Glaskin, R. S.; Park, M. A.; Costello, C. E.; Lin, C. *Anal. Chem.* 2016, 88 (7), 3440–3443.
25. Paglia, G.; Angel, P.; Williams, J. P.; Richardson, K.; Olivos, H. J.; Thompson, J. W.; Menikarachchi, L.; Lai, S.; Walsh, C.; Moseley, A.; Plumb, R. S.; Grant, D. F.; Palsson, B. O.; Langridge, J.; Geromanos, S.; Astarita, G. *Anal. Chem.* 2015, 87 (2), 1137–1144.
26. Zheng, X.; Aly, N. A.; Zhou, Y.; Dupuis, K. T.; Bilbao, A.; Paurus, V. L.; Orton, D. J.; Wilson, R.; Payne, S. H.; Smith, R. D.; Baker, E. S. *Chem. Sci.* 2017, 8, 7724–7736.
27. Simón-Manso, Y.; Lowenthal, M. S.; Kilpatrick, L. E.; Sampson, M. L.; Telu, K. H.; Rudnick, P. A.; Mallard, W. G.; Bearden, D. W.; Schock, T. B.; Tchekhovskoi, D. V.; Blonder, N.; Yan, X.; Liang, Y.; Zheng, Y.; Wallace, W. E.; Neta, P.; Phinney, K. W.; Remaley, A. T.; Stein, S. E. *Anal. Chem.* 2013, 85 (24), 11725–11731.
28. Telu, K. H.; Yan, X.; Wallace, W. E.; Stein, S. E.; Simón-Manso, Y. *Rapid Commun. Mass Spectrom.* 2016, 30 (5), 581–593.
29. Nichols, C. M.; May, J. C.; Sherrod, S. D.; McLean, J. A. *Analyst* 2018, 143 (7), 1556–1559.
30. Sud, M.; Fahy, E.; Cotter, D.; Azam, K.; Vadivelu, I.; Burant, C.; Edison, A.; Fiehn, O.; Higashi, R.; Nair, K. S.; Sumner, S.; Subramaniam, S. *Nucleic Acids Res.* 2016, 44 (D1), D463–D470.
31. May, J. C.; Goodwin, C. R.; Lareau, N. M.; Leaptrot, K. L.; Morris, C. B.; Kurulugama, R. T.; Mordehai, A.; Klein, C.; Barry, W.; Darland, E.; Overney, G.; Imatani, K.; Stafford, G. C.; Fjeldsted, J. C.; McLean, J. A. *Anal. Chem.* 2014, 86 (4), 2107–2116.
32. Hines, K. M.; Ashfaq, S.; Davidson, J. M.; Opalenik, S. R.; Wikswo, J. P.; McLean, J. A. *Anal. Chem.* 2013, 85 (7), 3651–3659.
33. Hines, K. M.; Ross, D. H.; Davidson, K. L.; Bush, M. F.; Xu, L. *Anal. Chem.* 2017, 89 (17), 9023–9030.

34. Dwivedi, P.; Wu, P.; Klopsch, S. J.; Puzon, G. J.; Xun, L.; Hill, H. H. *Metabolomics* 2008, 4 (1), 63–80.
35. McLean, J. A. *J. Am. Soc. Mass Spectrom.* 2009, 20 (10), 1775–1781.
36. Goodwin, C. R.; Fenn, L. S.; Derewacz, D. K.; Bachmann, B. O.; McLean, J. A. *J. Nat. Prod.* 2012, 75 (1), 48–53.
37. Chong, J.; Soufan, O.; Li, C.; Caraus, I.; Li, S.; Bourque, G.; Wishart, D. S.; Xia, J. *Nucleic Acids Res.* 2018, 46 (W1), W486–W494.
38. May, J. C.; McLean, J. A. *Annu. Rev. Anal. Chem.* 2016, 9 (1), 387–409.
39. Groessl, M.; Graf, S.; Knochenmuss, R. *Analyst* 2015, 140 (20), 6904–6911.
40. Li, H.; Giles, K.; Bendiak, B.; Kaplan, K.; Siems, W. F.; Hill, H. H. *Anal. Chem.* 2012, 84 (7), 3231–3239.
41. Giles, K.; Williams, J. P.; Campuzano, I. *Rapid Commun. Mass Spectrom.* 2011, 25 (11), 1559–1566.
42. D’Atri, V.; Causon, T.; Hernandez-Alba, O.; Mutabazi, A.; Veuthey, J. L.; Cianferani, S.; Guillarme, D. *J. Sep. Sci.* 2018, 41 (1), 20–67.
43. Dodds, J. N.; May, J. C.; McLean, J. A. *Anal. Chem.* 2017, 89 (22), 12176–12184.
44. Fernandez-Lima, F. A.; Kaplan, D. A.; Park, M. A. *Rev. Sci. Instrum.* 2011, 82 (12).
45. Deng, L.; Ibrahim, Y. M.; Baker, E. S.; Aly, N. A.; Hamid, A. M.; Zhang, X.; Zheng, X.; Garimella, S. V. B.; Webb, I. K.; Prost, S. A.; Sandoval, J. A.; Norheim, R. V.; Anderson, G. A.; Tolmachev, A. V.; Smith, R. D. *ChemistrySelect* 2016, 1 (10), 2396–2399.
46. N. Nikolaev, E.; N. Vladimirov, G.; Jertz, R.; Baykut, G. *Mass Spectrom.* 2013, 2, S0010–S0010.
47. Zubarev, R. A.; Makarov, A. *Anal. Chem.* 2013, 85 (11), 5288–5296.
48. Marshall, A. G.; Hendrickson, C. L.; Shi, S. D.-H. *Anal. Chem.* 2002, 74 (9), 252 A–259 A.
49. Bowden, J. A.; Heckert, A.; Ulmer, C. Z.; Jones, C. M.; Koelmel, J. P.; Abdullah, L.; Ahonen, L.; Alnouti, Y.; Armando, A. M.; Asara, J. M.; Bamba, T.; Barr, J. R.; Bergquist, J.; Borchers, C. H.; Brandsma, J.; Breitkopf, S. B.; Cajka, T.; Cazenave-Gassiot, A.; Checa, A.; Cinel, M. A.; Colas, R. A.; Cremers, S.; Dennis, E. A.; Evans, J. E.; Fauland, A.; Fiehn, O.; Gardner, M. S.; Garrett, T. J.; Gotlinger, K. H.; Han, J.; Huang, Y.; Neo, A. H.; Hyötyläinen, T.; Izumi, Y.; Jiang, H.; Jiang, H.; Jiang, J.; Kachman, M.; Kiyonami, R.; Klavins, K.; Klose, C.; Köfeler, H. C.; Kolmert, J.; Koal, T.; Koster, G.; Kuklennyik, Z.; Kurland, I. J.; Leadley, M.; Lin, K.; Maddipati, K. R.; McDougall, D.; Meikle, P. J.; Mellett, N. A.; Monnin, C.; Moseley, M. A.; Nandakumar, R.; Oresic, M.; Patterson, R.; Peake, D.; Pierce, J. S.; Post, M.; Postle, A. D.; Pugh, R.; Qiu, Y.; Quehenberger, O.; Ramrup, P.; Rees, J.; Rembiesa, B.; Reynaud, D.; Roth, M. R.; Sales, S.; Schuhmann, K.; Schwartzman, M. L.; Serhan, C.

- N.; Shevchenko, A.; Somerville, S. E.; St. John-Williams, L.; Surma, M. A.; Takeda, H.; Thakare, R.; Thompson, J. W.; Torta, F.; Triebl, A.; Trötz Müller, M.; Ubhayasekera, S. J. K.; Vuckovic, D.; Weir, J. M.; Welti, R.; Wenk, M. R.; Wheelock, C. E.; Yao, L.; Yuan, M.; Zhao, X. H.; Zhou, S. J. *Lipid Res.* 2017, 58 (12), 2275–2288.
50. Fang, T. T.; Bendiak, B. J. *Am. Chem. Soc.* 2007, 129 (31), 9721–9736.

CHAPTER 4

CONFORMATIONAL ORDERING OF BIOMOLECULES IN THE GAS PHASE: NITROGEN COLLISION CROSS-SECTIONS MEASURED ON A PROTOTYPE HIGH RESOLUTION DRIFT TUBE ION MOBILITY-MASS SPECTROMETER

4.1 Introduction

With the rising demand for high-throughput analyses of increasingly complex samples, ion mobility-mass spectrometry (IM-MS) has found broad application in the analysis of biological systems, as this rapid 2D separation (ms and μ s, respectively) provides comprehensive molecular information regarding analyte size, mass, and relative abundance. In ion mobility, separation is achieved by low-energy interactions of charged analytes with an inert buffer gas (conventionally helium or nitrogen), where analyte size-to-charge ratio is measured as a function of the time required to traverse the mobility region.¹ As a means of comparison with other laboratory measurements, drift time values are either normalized to standard temperature and pressure as a reduced mobility (K_0) or converted to a collision cross-section (CCS) value, the latter of which is a size parameter related to the averaged momentum transfer impact area of the molecule.² Structural information in the form of CCS values assists in the characterization of analytes by biomolecular class, as these classes are known to separate in IM-MS space and adopt conformational correlations due to prevailing class-specific structural folding in the gas-phase.^{3,4} These class-specific mobility-mass correlations can be used as a predictor for molecule class, demonstrating the potential value of IM-MS structural separations for life sciences research which seek systems biology level information. Expanding upon this concept, CCS-based molecular

prediction has previously been explored for peptides, utilizing intrinsic size parameter calculations^{5,6} and machine learning algorithms⁷ for sequence prediction, but no detailed study of other biochemical classes has yet been undertaken.

The separation and characterization of biological samples by IM-MS has been achieved using both commercial and laboratory built instrumentation. Virtually all contemporary commercial IM-MS instruments utilize nitrogen as the buffer gas for IM separations, motivated by practical considerations of cost, availability, and technical considerations for pumping requirements and electrical discharge. The most common commercial IM-MS platform utilizes an electrodynamic field (*i.e.*, a traveling wave potential) for mobility separation,⁸ and drift time measurements must be calibrated against electrostatic drift tube data in order to convert these measurements to CCS values.^{9,10} Conversely, many independently constructed instruments incorporate uniform electrostatic field mobility regions utilizing helium as the buffer gas. Uniform field measurements serve as the benchmark for electrodynamic CCS value determination, as the CCS obtained from a uniform field drift tube can be determined empirically through kinetic theory.

11,12

One common practice among researchers utilizing IM-MS is calibration of nitrogen-based traveling wave ion mobility measurements against helium-based CCS values reported in the literature.^{13,14} The use of helium-based CCS values to calibrate nitrogen-based drift time measurements results in calibrated “helium-equivalent” CCS values, which can be useful for comparing with literature values and correlating measurements to theory.^{15,16} There is, however, concern that this practice introduces added experimental error, as nitrogen vs. helium mobility measurements differ substantially in magnitude, and the success of calibration strategies relies heavily on careful selection of calibrants that accurately describe the sample conditions, charge

state, mass range and chemical class of the system of interest.^{9,14,17} Differences in CCS values in helium versus nitrogen arise due to several factors including intrinsic size differences between the buffer gases, mass effects which factor into the momentum transfer cross-section (the experimental CCS), and the over 8 fold difference in gas polarizability between helium and nitrogen (0.21×10^{-24} and $1.74 \times 10^{-24} \text{ cm}^3$, respectively).^{12,18}

Recently, a prototype IM-MS instrument utilizing nitrogen drift gas was developed (Agilent Technologies, Santa Clara, CA). This instrument incorporates a uniform electrostatic field ion mobility separator bracketed by electrodynamic focusing devices (ion funnels), which allows for high sensitivity and direct measurements of CCS values in nitrogen.^{7,19} Presented in this report is an extensive and diverse database of empirically-derived nitrogen CCS measurements (594 values), which comprises four molecular classes and expands upon several previous databases for the structural characterization of biological molecules.^{5,7,9,20-23} This affords the opportunity to explore the fundamental considerations of buffer gas composition and the subsequent effects on ion mobility parameters (reduced mobility and CCS) across different molecular classes.

4.2 Experimental Methods

4.2.1 Preparation of Standards

4.2.1.1 Lipids All solvents and buffers were purchased as HPLC grade from Sigma-Aldrich (St. Louis, MO, USA). Dry lipid extracts were purchased from Avanti Lipids (Birmingham, AL, USA) and constituted in chloroform prior to analysis. Lipid extracts include sphingomyelins (SM, porcine brain), glycosphingolipids (GlcCer, porcine brain), phosphatidylcholines (PC, chicken egg), phosphatidylserines (PS, porcine brain), and

phosphatidylethanolamines (PE, chicken egg). For analysis, lipid standards were diluted in 90% chloroform/10% methanol (v/v) with 10 mM sodium acetate to a final concentration of 10 µg/mL. Putative identification of lipids was performed using the exact mass measurement through the Lipid Metabolites and Pathways Strategy (LIPID MAPS) Structural Database (LMSD).²⁴ A full list of identified lipids can be found in Appendix C.

4.2.1.2 Carbohydrates Carbohydrate dextrans (linear and cyclic) and sugar alcohol standards were purchased from Sigma-Aldrich. Lacto-N-difucohexaose I and II and lacto-N-fucopentaose I and II were purchased from Dextra Laboratories (Reading, UK). All carbohydrate standards were prepared as received and reconstituted in water with 10 mM ammonium acetate to final concentrations of 10 µg/mL. For cationization, 10 mM NaCl, 10 mM LiCl, 10 mM CsCl, 10 mM KCl, and 10 mM RbCl solutions were prepared in water to a final concentration of *ca.* 10 µM. A full list of identified carbohydrates can be found in Appendix C.

4.2.1.3 Peptides Predigested peptide standards (MassPREP) were purchased from Waters (Milford, MA, USA). Peptide standards (SDGRG and GRGDS) were purchased from Sigma-Aldrich. All peptide standards were received as a lyophilized powder and reconstituted in 10 mM ammonium acetate in water to a final concentration of 10 µg/mL. The MassPREP digestion standard mix contained approximately equimolar concentrations of four tryptically digested proteins: Alcohol Dehydrogenase (ADH, yeast), Serum Albumin (BSA, bovine), Phosphorylase B (PHOSPH, Rabbit) and Enolase (ENOLASE, yeast). Peptide identifications were assigned based on exact mass of all possible tryptic peptides (no missed cleavages) produced by the Expert Protein Analysis System (ExPASy) PeptideMass proteomics tool²⁵ (Swiss Institute of Bioinformatics, Lausanne, Switzerland) using the SWISS-PROT database entry number for each intact protein

(P00330, P02769, P00924 and P00489, respectively). A full list of identified peptides can be found in Appendix C.

4.2.1.4 Quaternary Ammonium Salts Tetraalkylammonium (TAA) salts with alkyl chain lengths between 1 and 18 carbons (TAA1 to TAA18) were purchased from the following sources: TAA2, TAA4, TAA6, TAA7, TAA10, TAA12, and TAA16 from Sigma-Aldrich; TAA1, TAA3, TAA5, and TAA8 from Acros Organics; and TAA18 from Alfa Aesar. All TAA salts were supplied with a stated purity of greater than 98% and were prepared as received. TAA1 to TAA8 were prepared in 50% methanol/50% water, while TAA10, TAA12, TAA16 and TAA18 were prepared in 50% methanol/50% isopropanol. Final concentrations were *ca.* 1 µg/mL. A full list of primary TAA salt standards and concomitant ions identified in the samples can be found in Appendix C.

4.2.2 Instrumentation

A schematic of the instrumentation used to obtain the cross-section measurements is shown in Figure 4.1. The instrument used in this work is a commercial prototype IM-MS which incorporates a drift tube coupled to a quadrupole time-of-flight mass spectrometer (IM-Q-TOFMS, Agilent Technologies, Santa Clara, CA). For this work, an orthogonal electrospray ionization (ESI) source (Agilent Jet Stream) was utilized which incorporates a heated sheath gas nebulizer to aerodynamically focus and desolvate ions prior to introduction into the vacuum system. Ions from the ESI are introduced to a single-bore glass capillary tube which is resistively coated across its length, allowing the nebulizer to be maintained at ground potential, while the exit end of the capillary can be biased to around 2100 V.²⁶ Ions exiting the capillary are introduced into a tandem ion funnel interface consisting of a high-pressure transmission ion funnel in the first stage,²⁷

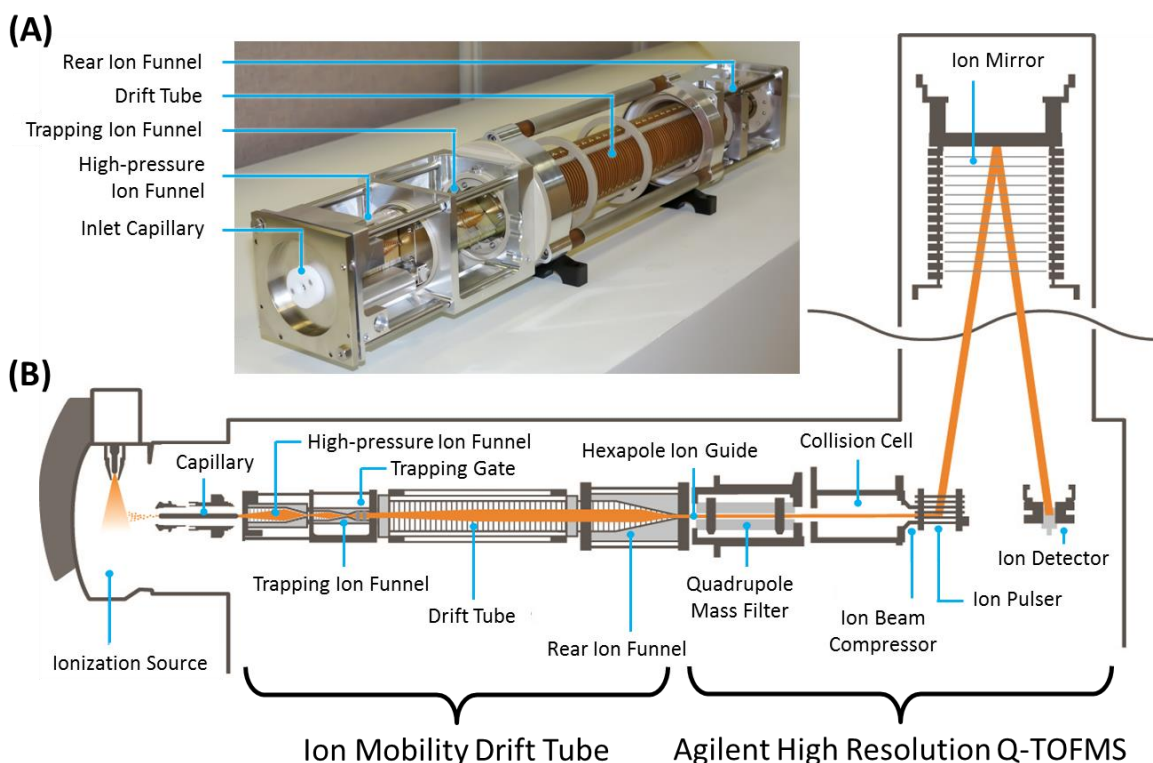


Figure 4.1 Details of the prototype IM-MS instrumentation used in this study. **(A)** A picture of the ion optical elements of the ion mobility component. **(B)** A representative schematic of the instrumentation used with significant components annotated. Adapted from Jody C. May, Cody R. Goodwin, Nichole M. Lareau, Katrina L. Leaprot, Caleb B. Morris, Ruwan T. Kurulugama, A. Mordehai, C. Klein, W. Barry, E. Darland, G. Overney, K. Imatani, George C. Stafford, John C. Fjeldsted, John A. McLean, "Conformational Ordering of Biomolecules in the Gas Phase: Nitrogen Collision Cross Sections Measured on a Prototype High Resolution Drift Tube Ion Mobility-Mass Spectrometer," *Analytical Chemistry* 2014, 86 (4), 2107-2116. (<https://pubs.acs.org/doi/10.1021/ac4038448>) Note that further permissions related to the material excerpted should be directed to the ACS.

followed by a second stage trapping ion funnel which incorporates a dual-grid ion gate.²⁸ The second stage ion funnel trap operates as an ion focusing and accumulation region whereby temporally narrow (typically 100 to 150 μs) ion pulses are gated into the IM spectrometer. Mobility separation occurs in a 78 cm uniform field drift tube comprised of a series (*ca.* 150) of 50 mm internal diameter gold-plated ring electrodes. The buffer gas is high purity nitrogen. Ions traverse the drift tube under the influence of a weak electric field (10 to 20 $\text{V}\cdot\text{cm}^{-1}$) and consequently drift under low-field conditions. The combination of extended drift length, precision electronics, and high drift voltages enables high resolution ion mobility separations in excess of 60 resolving power ($t/\Delta t$, observed for a +1 ion, m/z 294). Ions exiting the drift region are refocused axially using an ion funnel and traverse a differential pressure interface region by means of a resistively-coated hexapole ion guide. Following the hexapole, ions are introduced into a modified Q-TOFMS (Agilent 6550), which incorporates a quadrupole mass filter and collision cell to enable mass-selective ion fragmentation experiments. The TOFMS is capable of greater than 40,000 mass resolving power and can acquire MS spectra at a rate of up to 8.3 kHz (120 μs transients at m/z 1700). Additional instrumentation details are provided in Figure 4.1.

4.2.3 Experimental Parameters

All 2D IM-MS spectra were acquired via direct infusion using positive mode electrospray ionization (Agilent Jet Stream Source) with a flow rate of *ca.* 10 $\mu\text{L}/\text{min}$. The Jet Stream source was operated with a nitrogen sheath gas temperature between 400 and 600 K (solvent dependent) at a flow rate of 12 L/min. Nitrogen drying gas applied at the source entrance was heated to *ca.* 570 K at a flow rate of 10 L/min. The source was operated in positive mode with the following voltages: ground potential emitter, -4.5 kV capillary entrance, and -1.8 kV nozzle. The three ion

funnels were operated as follows: high-pressure funnel RF 100 Vpp (peak-to-peak) at 1.5MHz, 150 V DC; trapping funnel RF 100 Vpp at 1.2 MHz, 180 V DC; rear funnel RF 100 Vpp at 1.2 MHz, 200 V DC. The IM drift gas pressure (nitrogen) was maintained at *ca.* 4 Torr and *ca.* 300 K, while the drift potential varied from 750 V to 1450 V, which represents an E/N ratio of 7 to 15 Td. In this E/N range, the mobility operates under low field conditions as all analytes investigated exhibited a linear change in drift times with respect to the electric field. Data was acquired with a modified version of the MassHunter software (Agilent Technologies). The mass measurement was calibrated externally using a series of homogeneously-substituted fluorinated triazatriphosphorines (Agilent tuning mixture, *ca.* 100 to 3000 m/z), which are characterized as being amphoteric and nonreactive. Additionally, a mixture of tetraalkylammonium salts (TAA1 to TAA18) was added to all samples as an internal mass and mobility calibration standard for positive mode analysis.

4.2.4 Collision Cross-Section Calculations

Uncorrected drift times are extracted as centroid values using a beta version of the IM-MS Browser (Agilent Technologies). This uncorrected drift time represents the total transit time of the ions, including the mobility drift time and the flight time through the interfacing IM-MS ion optics and MS. Because the non-mobility flight time component (the transit time of ions outside the drift region) is independent of the drift voltage, this value can be determined from a plot of the measured drift time versus the inverse drift voltage,²⁹ where a linear fit to the data will indicate the non-mobility time component (y-intercept) in the limit of infinite electric field ($1/V$ of zero). Time measurements are obtained from a minimum of six different drift voltages, ranging from 750 V to 1450 V. The determined non-mobility time is subtracted from the uncorrected drift times in order to obtain the corrected ion mobility drift time. Corrected drift times are used to determine the gas-

phase momentum transfer collision cross-section (CCS) using the Mason-Schamp relationship,³⁰ incorporating the scaling terms for standard temperature and pressure. Based on a propagation-of-error analysis incorporating the limits of precision for individual experimental parameters, we estimate the accuracy of all CCS values to be better than 2% (see Appendix C).

4.3 Results and Discussion

4.3.1 Database Description and General Cross-Section Trends in Nitrogen

A total of 594 nitrogen collision cross-section values were measured empirically in this study, representing three biomolecular classes (lipids, carbohydrates, and peptides), and TAA salts. This includes 92 peptides, 125 carbohydrates, 314 lipids, and 63 TAA salts and TAA salt derivatives. The range of CCS values measured spans from 140-460 Å², covering a mass range of 130-2150 Da. Summary statistics regarding the CCS database are provided in Table 4.1. The average RSD of all database values was 0.3% ($\pm 0.1\%$), with each CCS value representing an average of 11 (± 4) measurements. A complete list of all analytes and respective CCS measurements is provided as supplemental material in Appendix C.

TAA salts ranging from tetraethylammonium (TAA2) to tetraoctadecylammonium (TAA18) were analyzed and their subsequent CCS values were compared with literature values in order to estimate the CCS measurement accuracy.¹⁶ Results of this comparison are summarized in Table 4.2. Where CCS literature values existed for nitrogen, the absolute differences were found to be less than 2% and, in most cases, less than 1% deviation was observed. All TAA salts investigated exhibited excellent CCS measurement reproducibility (less than 0.5% RSD). TAA2

Table 4.1 A summary of statistics related to the CCS database.

	Collision Cross-Section Statistics					Fits to Empirical Data		
	Number of CCS Values	Mass Range [Da]	CCS Range [Å ²]	Average CCS Precision ¹	Average N for Each Value	Fit Equation Coefficients (y = Ax ^B)	Coefficient of Determination ²	Amount of Data Included Within ±5% of Fit ³
Peptides	92	430 – 1760	200 – 450	0.2% (±0.1%)	7 (±2)	A= 6.8440 B= 0.5547	R ² = 0.975	91%
Carbohydrates	125	190 – 2150	140 – 410	0.3% (±0.1%)	12 (±3)	A= 11.553 B= 0.4656	R ² = 0.983	89%
Lipids	314	500 – 1600	220 – 460	0.2% (±0.1%)	10 (±2)	A= 5.2469 B= 0.6000	R ² = 0.949	96%
Tetraalkylammonium Salts	63	130 – 1030	140 – 400	0.4% (±0.1%)	18 (±8)	A= 8.2631 B= 0.5561	R ² = 0.991	98%
<p>1. The precision reported here represents the reproducibility across replicate measurements. The total precision due to propagation of uncertainty in experimental parameters is estimated to be less than 2%.</p> <p>2. The observed R² value for the nonlinear power fit.</p> <p>3. The data inclusion band chosen is based on the smallest sized band which incorporates the most amount of data (refer to Figure 4.2(B), inset).</p>								

Adapted from Jody C. May, Cody R. Goodwin, Nichole M. Lareau, Katrina L. Leaprot, Caleb B. Morris, Ruwan T. Kurulugama, A. Mordehai, C. Klein, W. Barry, E. Darland, G. Overney, K. Imatani, George C. Stafford, John C. Fjeldsted, John A. McLean, "Conformational Ordering of Biomolecules in the Gas Phase: Nitrogen Collision Cross Sections Measured on a Prototype High Resolution Drift Tube Ion Mobility-Mass Spectrometer," *Analytical Chemistry* 2014, 86 (4), 2107-2116. (<https://pubs.acs.org/doi/10.1021/ac4038448>) Note that further permissions related to the material excerpted should be directed to the ACS.

Table 4.2 Measured CCS values for the TAA salts compared with literature values.

Name		Exact Mass [Da]	CCS (This Work) ¹ [Å ²]	CCS (Literature) ² [Å ²]	Abs. Percent Difference ³ [%]
Tetramethylammonium	TAA1	74.14	-	107.40	-
Tetraethylammonium	TAA2	130.25	-	122.20	-
Tetrapropylammonium	TAA3	186.36	144.1 ± 0.7 (23)	143.80	0.22%
Tetrabutylammonium	TAA4	242.46	166.6 ± 0.9 (16)	166.00	0.36%
Tetrapentylammonium	TAA5	298.57	190.1 ± 1.0 (28)	190.10	0.02%
Tetrahexylammonium	TAA6	354.68	213.5 ± 1.0 (31)	214.00	0.23%
Tetraheptylammonium	TAA7	410.78	236.4 ± 0.4 (31)	236.80	0.17%
Tetraoctylammonium	TAA8	466.54	256.6 ± 0.7 (31)	258.30	0.64%
Tetradecylammonium	TAA10	579.11	293.5 ± 0.7 (24)	-	-
Tetradodecylammonium	TAA12	691.32	319.0 ± 0.9 (24)	-	-
Tetrahexadecylammonium	TAA16	915.04	361.5 ± 0.9 (24)	-	-
Tetraoctadecylammonium	TAA18	1027.16	379.0 ± 1.7 (21)	-	-

1. Number of measurements are reported in parenthesis. The error due to experimental uncertainty is reported next to each value and is less than 0.5% for all measurements. The total error based on propagating the limits of precision in experimental parameters is estimated to be less than 2%.

2. Literature values from: Campuzano *et al.* Analytical Chemistry 2011, 84, 1026-1033.

3. The absolute percent difference is the difference in CCS compared to the average of both values.

Adapted from Jody C. May, Cody R. Goodwin, Nichole M. Lareau, Katrina L. Leaptrot, Caleb B. Morris, Ruwan T. Kurulugama, A. Mordehai, C. Klein, W. Barry, E. Darland, G. Overney, K. Imatani, George C. Stafford, John C. Fjeldsted, John A. McLean, "Conformational Ordering of Biomolecules in the Gas Phase: Nitrogen Collision Cross Sections Measured on a Prototype High Resolution Drift Tube Ion Mobility-Mass Spectrometer," Analytical Chemistry 2014, 86 (4), 2107-2116. (<https://pubs.acs.org/doi/10.1021/ac4038448>) Note that further permissions related to the material excerpted should be directed to the ACS.

was included in the sample, but ultimately did not appear in significant abundance in the IM-MS spectra.

A scatter plot of CCS versus m/z for all database values is presented in Figure 4.2(A), separated into chemical classes. We refer to this type of 2D IM-MS projection as conformational space analysis,^{4,31} as the differential scaling of mass (m/z) and size (CCS) between molecular classes is indicative of differences in gas-phase packing efficiency.²⁰

4.3.2 Description of the Fits to the Empirical Data

Several different equation functional forms were evaluated in order to determine which expression best described molecular class correlations between CCS and m/z values, and, it was found that the datasets were adequately described by a power-law relationship ($y=Ax^B$), based upon the coefficient of determination (R^2). Conceptually, power-law equations are descriptors for several phenomena related to mass-size scaling, including allometric scaling laws in biology,³² stellar velocity dispersion relative to black hole mass (M-sigma relation),³³ and the well-known square-cube law, first described by Galileo,³⁴ which universally relates any shape's increase in volume relative to its surface area. Additionally, power-law relationships are scale-invariant such that different power-law functions can be related by a simple scaling factor, which has implications for describing universal relationships independent of the specific details of the measurement.

The resulting power-law fits to the empirical data are presented in Figure 4.2(B). Coefficients and associated R^2 values are summarized in Table 4.1. The data inclusion bands projected in Figure 4.2(B) representing $\pm 5\%$ deviation from the line of best fit. Other inclusion band sizes are summarized in Figure 4.2(B), inset, averaged across the four datasets. For all datasets, a $\pm 5\%$ inclusion band incorporated an average of 94% ($\pm 4\%$) of data. Decreasing the

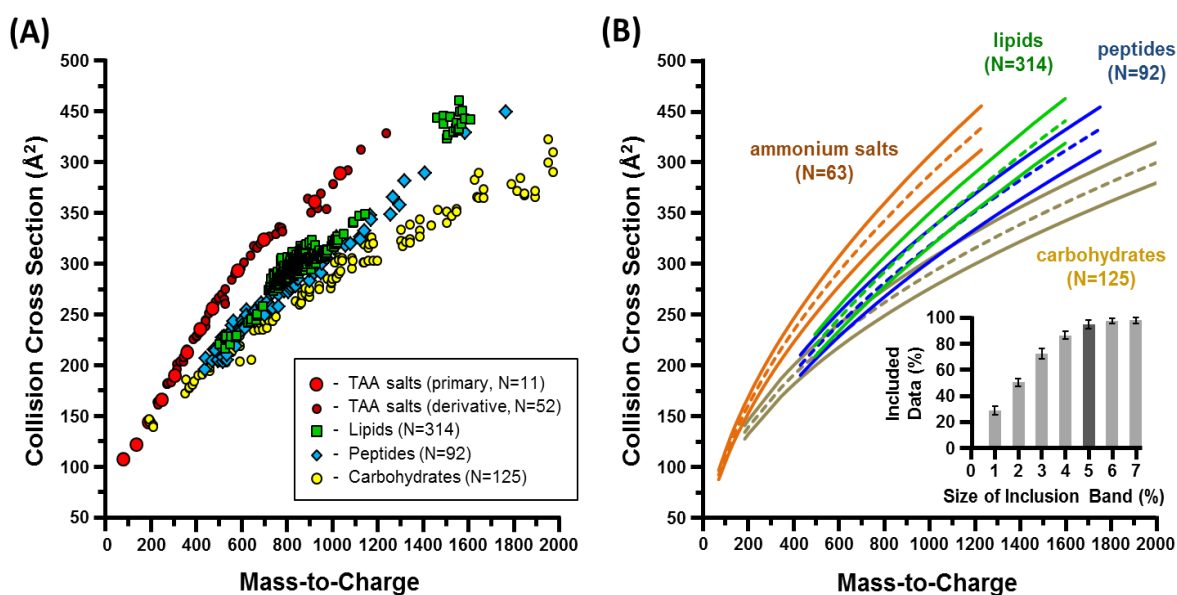


Figure 4.2 (A) A scatter plot of the CCS values measured in this study, separated by chemical class. **(B)** Best fit lines of the data, separated into class and fit to a power-law function. Also shown are data inclusion bands representing $\pm 5\%$ deviation from the best fit line. The inset bar graph represents the amount of data included within different sized inclusion bands. Fit equations and their corresponding coefficients of determination (R^2) can be found in Table 4.1. Adapted from Jody C. May, Cody R. Goodwin, Nichole M. Lareau, Katrina L. Leaptrot, Caleb B. Morris, Ruwan T. Kurulugama, A. Mordehai, C. Klein, W. Barry, E. Darland, G. Overney, K. Imatani, George C. Stafford, John C. Fjeldsted, John A. McLean, "Conformational Ordering of Biomolecules in the Gas Phase: Nitrogen Collision Cross Sections Measured on a Prototype High Resolution Drift Tube Ion Mobility-Mass Spectrometer," *Analytical Chemistry* 2014, 86 (4), 2107-2116. (<https://pubs.acs.org/doi/10.1021/ac4038448>) Note that further permissions related to the material excerpted should be directed to the ACS.

band to $\pm 4\%$ results in an average of 86% ($\pm 3\%$) of data being included (a decrease of *ca.* 8% data inclusion), whereas increasing the band to $\pm 6\%$ only incorporated an additional 3% ($\pm 2\%$) of data on average. Thus, the $\pm 5\%$ data inclusion band represents an optimal balance between specificity and data incorporation. Interestingly, the $\pm 5\%$ band describes all datasets similarly, regardless of chemical class.

Several observations can be made from the data contained in Figure 4.2. The TAA salts were found to exhibit the highest CCS values relative to m/z , and were located in a region of 2D IM-MS space which was disparate from the biomolecules. Previously, TAA salts were recommended as an ion mobility calibrant due to their low propensity for forming clusters, which otherwise complicates the interpretation of mobility data.³⁵ Here, it is found that in addition to the lack of clustering, the TAA salts are useful mobility-mass calibrants as the complete series (1 to 18 carbons) span a wide range of CCS values (107 to 400 \AA^2), m/z values (75 to 1027 Da), and occupy a region of 2D IM-MS space where biomolecules are not predicted to occur. Carbohydrates were observed to have the lowest CCS values relative to their mass, while peptides and lipids occupy similar regions of conformational space. In general, all of the biochemical classes surveyed were readily separated above a mass of *ca.* 1200 Da, indicating that differences in relative gas-phase packing scale with molecular size and mass.

4.3.3 Extraction of Sub-Trend Information from the Data

From a cursory analysis of the CCS database described in this report, it is evident that the general chemical class information is retained through the specific mobility-mass correlation trends in the 2D IM-MS projection. Such trends hold promise for conducting comprehensive omics experiments whereby unknown analytes originating from a complex sample (*e.g.*, blood, tissue,

whole cell lysate) can be prioritized based upon their likely chemical class. This biomolecular filtering would allow for the sorting of unknown analytes into distinct identification workflows, as lipid, peptide, metabolite, and glycan identification methods often warrant searching of specific databases. In order to determine the detail of class-specific information obtained from the conformational space analysis, select coarse biomolecular classes were further categorized into finer specific sub-classes. Figure 4.3 contains a detailed analysis of carbohydrates, which were further delineated into glycans (human milk oligosaccharides), cyclic dextrans (cyclodextrins), and linear dextrans (maltose polysaccharides). Figure 4.3(A and B) illustrates the relative location of each carbohydrate sub-class in conformational space, while Figure 4.3(C) describes the data as a histogram relative to the best fit line. In general, there is no strong correlation between the carbohydrate sub-classes, with all signals distributed in relatively the same locations with respect to the power-law fit. This suggests that the carbohydrates surveyed do not adopt strong structural differences which can be easily differentiated in the 2D analysis. On the other hand, the sub-classes chosen here represent broad descriptors for carbohydrate structure, and as such are not structurally-descriptive sub-classifications. For example, glycans can represent both linear and branched oligosaccharides and thus occupy a broad region of the total carbohydrate conformational trend. Interestingly, the cyclization of sugars (cyclodextrins) does not seem to enhance gas-phase packing efficiency as compared with their linear analogues. A more comprehensive carbohydrate dataset may engender sub-class differentiation, or differences may bear out for more limited situations such as positional and structural isomers or various metal-coordinated species.³⁶

Application of a similar sub-class analysis to the lipid dataset is illustrated in Figure 4.4. In this case, the lipid dataset is substantially larger than the carbohydrate dataset (N=314 vs. N=125, respectively), and measurements were obtained from five distinct lipid structural classes.

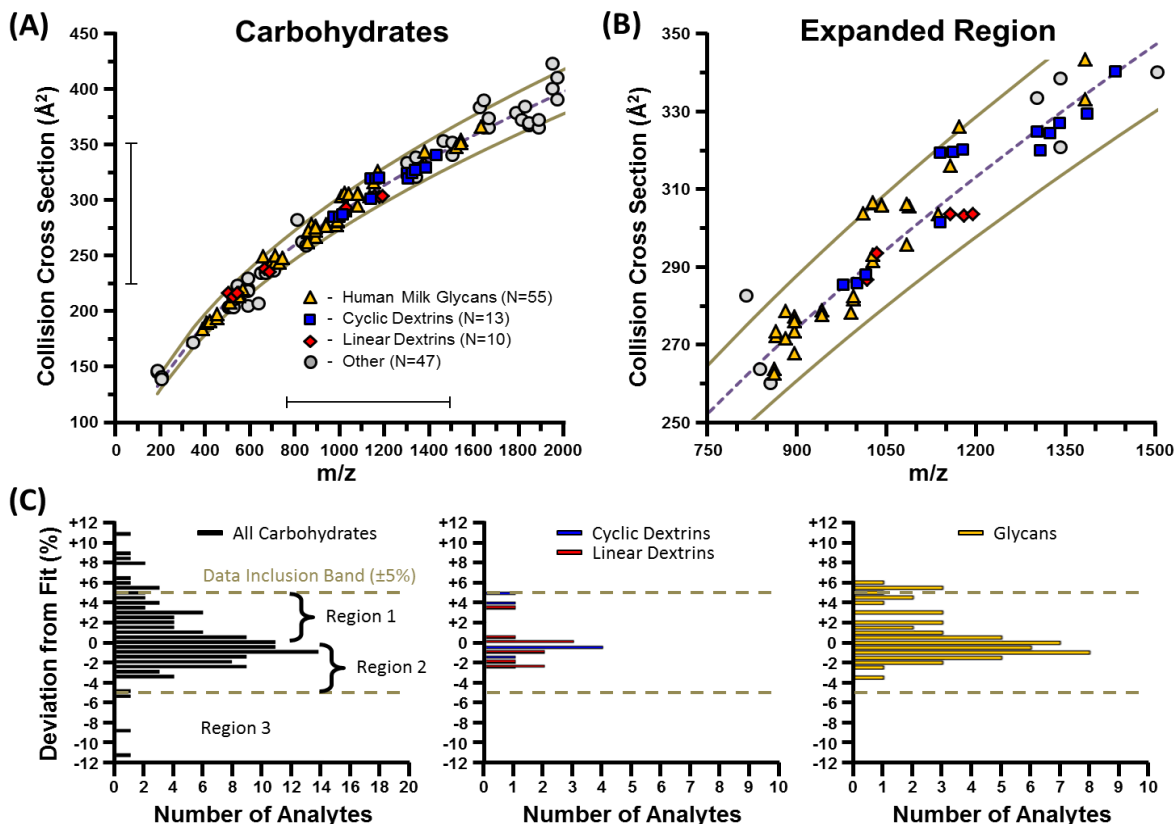


Figure 4.3 A sub-class analysis of carbohydrates, with sub-classes comprised of human milk derived glycans, cyclic, and linear dextrins. **(A)** A scatter plot of the relative location of carbohydrate sub-classes in 2D IM-MS conformational space. **(B)** An expanded region of the scatter plot where all three sub-classes of carbohydrates are observed. **(C)** A histogram analysis of carbohydrate sub-class deviation in 2D IM-MS space relative to the best fit line. In general, the carbohydrate sub-classes do not differentiate into distinct regions of conformational space. Adapted from Jody C. May, Cody R. Goodwin, Nichole M. Lareau, Katrina L. Leaptrot, Caleb B. Morris, Ruwan T. Kurulugama, A. Mordehai, C. Klein, W. Barry, E. Darland, G. Overney, K. Imatani, George C. Stafford, John C. Fjeldsted, John A. McLean, "Conformational Ordering of Biomolecules in the Gas Phase: Nitrogen Collision Cross Sections Measured on a Prototype High Resolution Drift Tube Ion Mobility-Mass Spectrometer," *Analytical Chemistry* 2014, 86 (4), 2107-2116. (<https://pubs.acs.org/doi/10.1021/ac4038448>) Note that further permissions related to the material excerpted should be directed to the ACS.

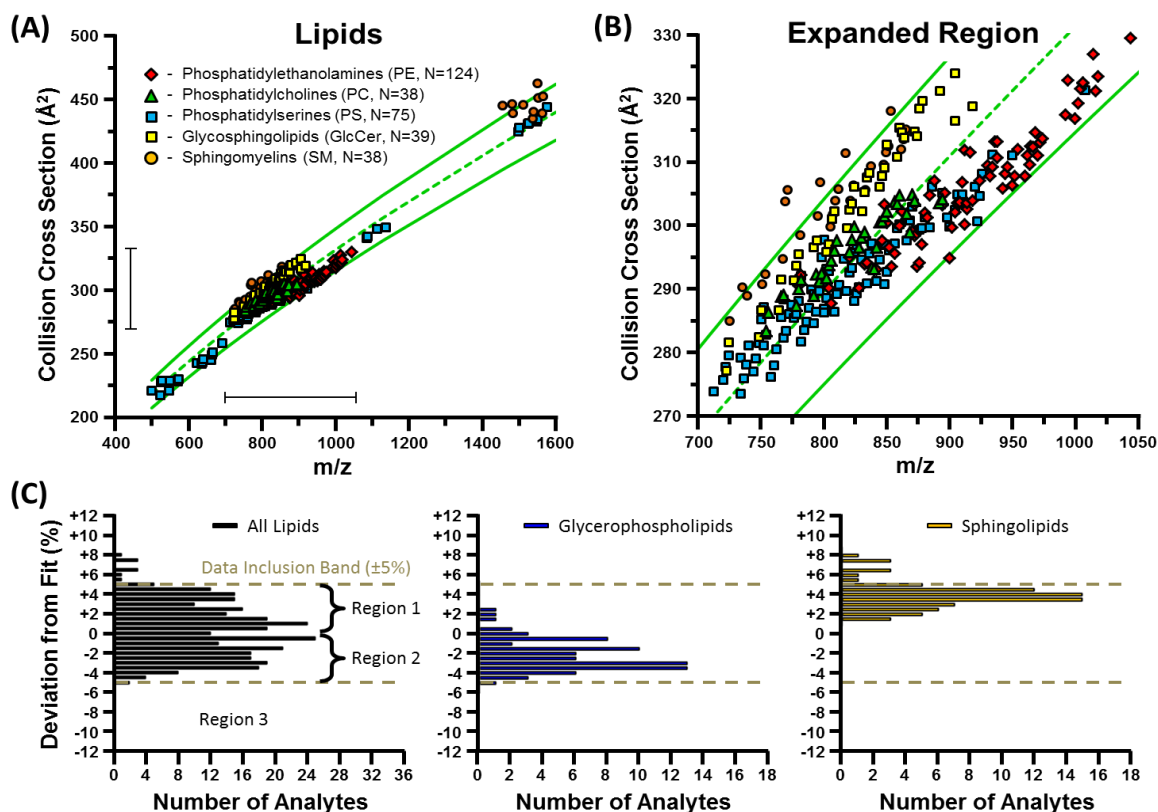


Figure 4.4 A sub-class analysis of lipids comprised of PE, PC, PS, GlcCer, and SM lipids. These lipids are further categorized into two general structural groups: glycerophospholipids (PE, PC, PS) and sphingolipids (GlcCer, SM). **(A)** A scatter plot of the conformational ordering of each sub-class of lipid. **(B)** An expanded region of the scatter plot detailing a preferential ordering of the different lipid sub-classes in conformational space. **(C)** A histogram analysis and locations of general lipid structural groups relative to the best fit line. Unlike carbohydrates, individual lipid sub-classes partition into distinct regions of 2D IM-MS space, allowing for finer structural information to be extracted from the conformational space analysis. Adapted from Jody C. May, Cody R. Goodwin, Nichole M. Lareau, Katrina L. Leaptrot, Caleb B. Morris, Ruwan T. Kurulugama, A. Mordehai, C. Klein, W. Barry, E. Darland, G. Overney, K. Imatani, George C. Stafford, John C. Fjeldsted, John A. McLean, "Conformational Ordering of Biomolecules in the Gas Phase: Nitrogen Collision Cross Sections Measured on a Prototype High Resolution Drift Tube Ion Mobility-Mass Spectrometer," *Analytical Chemistry* 2014, 86 (4), 2107-2116. (<https://pubs.acs.org/doi/10.1021/ac4038448>) Note that further permissions related to the material excerpted should be directed to the ACS.

These lipid sub-classes can be broadly categorized into two structural classes as sphingolipids (SM, GlcCer) and glycerophospholipids (PE, PC, PS). It is qualitatively evident in Figure 4.4(A and B) that each class of lipid exists in a distinct region of conformational space. The histogram distribution analysis in Figure 4.4(C) (right panel) indicates that sphingolipids fall predominantly above the best fit line (97% in region 1), whereas glycerophospholipids (Figure 4.4(C), middle panel) are more broadly dispersed around the mobility-mass correlation (33% in region 1, 65% in region 2), and adopt denser gas phase conformations than sphingolipids. These results suggest that, with proper structural sub-class descriptors, conformational space analysis is capable of differentiating finer structural detail beyond general biomolecular class.

4.3.4 Comparisons between Helium and Nitrogen CCS Values

The diverse compilation of CCS values described in this report allows for direct comparisons against helium-derived CCS values reported in the literature. Of the over 3000 singly-charged helium CCS values surveyed from the literature, overlapping measurements exist for 121 nitrogen CCS values in the current database (8 TAA salts, 49 lipids, 40 peptides, and 24 carbohydrates; refer to Appendix C). Differences between helium and nitrogen-derived CCS measurements have been previously noted for atomic species,³⁷ small molecules and peptides,³⁸ and, more recently, proteins and large protein complexes.^{9,23} Here, we add the differences observed for TAA salts, lipids, and carbohydrates, in addition to corroborating previous peptide observations.

A scatter plot of the overlapping helium and nitrogen CCS values is provided in Figure 4.5(A). Vertical error bars representing $\pm 2\%$ are also included, although this error is sufficiently small such that most of the error bars are obscured within the scale of individual data points. Figure

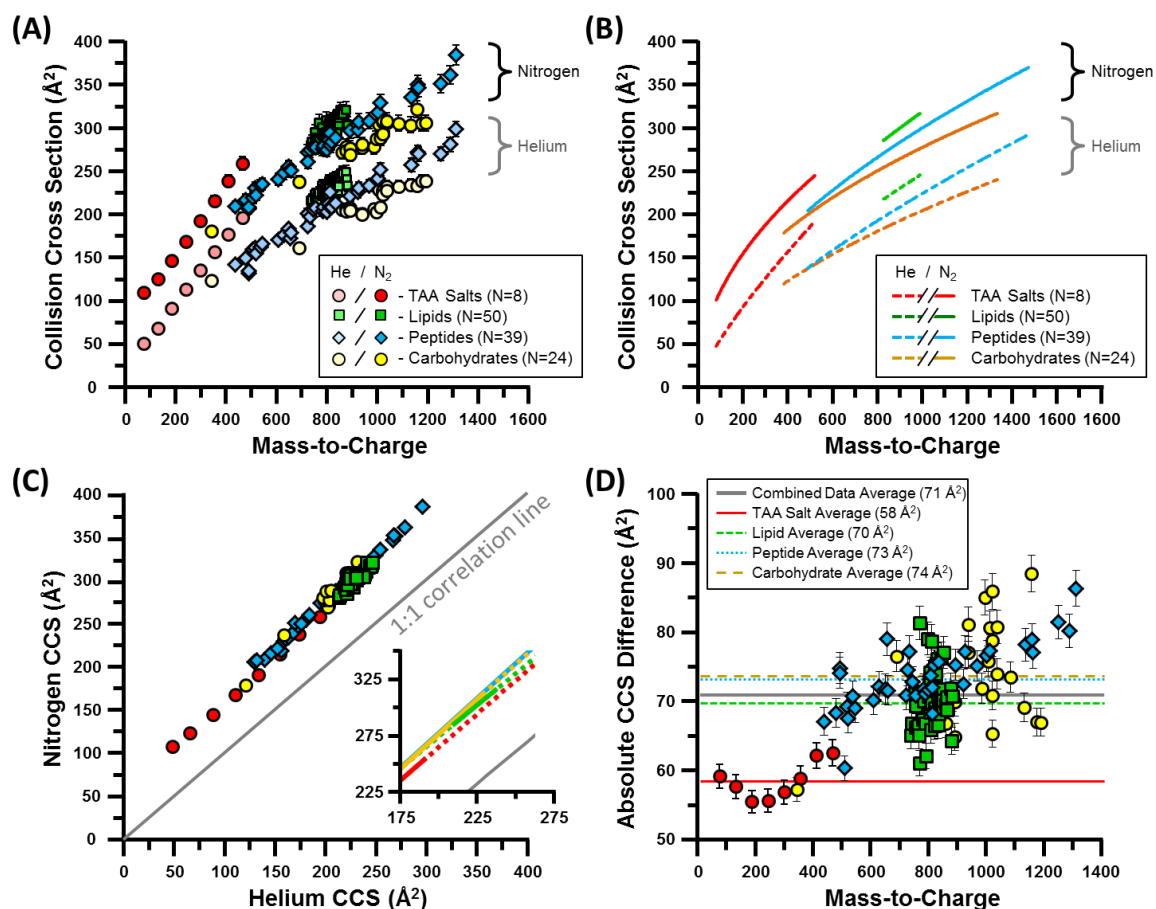


Figure 4.5 Comparisons between helium and nitrogen-derived CCS values. **(A)** A scatter plot of class-specific subsets of CCS data measured in both helium and nitrogen. **(B)** Power fits to the data projected in panel A. **(C)** Correlation plot of helium vs. nitrogen CCS values. **(D)** Absolute differences in CCS between helium and nitrogen measurements, plotted as a function of mass-to-charge. In general, nitrogen CCS values are significantly larger than helium, with subtle differences being observed between different chemical classes. Adapted from Jody C. May, Cody R. Goodwin, Nichole M. Lareau, Katrina L. Leaprot, Caleb B. Morris, Ruwan T. Kurulugama, A. Mordehai, C. Klein, W. Barry, E. Darland, G. Overney, K. Imatani, George C. Stafford, John C. Fjeldsted, John A. McLean, "Conformational Ordering of Biomolecules in the Gas Phase: Nitrogen Collision Cross Sections Measured on a Prototype High Resolution Drift Tube Ion Mobility-Mass Spectrometer," *Analytical Chemistry* 2014, 86 (4), 2107-2116. (<https://pubs.acs.org/doi/10.1021/ac4038448>) Note that further permissions related to the material excerpted should be directed to the ACS.

4.5(B) contains the power fits to the data, which are useful in visualizing differences between datasets. In general, gross separation trends between chemical classes are retained within the helium and nitrogen-based datasets, with qualitatively similar conformational space ordering being exhibited regardless of the drift gas (*i.e.* carbohydrate density > peptide density > lipid density > TAA salt density). However, subtle differences exist with respect to the amount of average separation observed between class-specific fits. For example, the lipids and peptides exhibit slightly better average separation as a group in helium than in nitrogen, whereas the peptides and carbohydrate are better separated in nitrogen than in helium. These trends can also be observed in Figure 4.5(C), which contains the same overlap data as projected on a plot of nitrogen versus helium CCS values. In Figure 4.5(C), all of the class-specific data reside within the same region of the projection, indicating that overall differences between helium and nitrogen CCS are systematic within this range, and thus can be accounted for to allow conversion of one dataset to another, with some loss in precision associated with error propagation. This possibility of generating effective helium-based CCS values from nitrogen measurements was previously noted by Bush *et al.* for peptides and proteins.^{9,22} Recently, Pagel and Harvey noted good correlation (less than 1.5% error) between helium and nitrogen CCS measurements for singly-charged carbohydrates, though significant error was introduced when multiply-charged values were incorporated into the calibration.¹⁷ Here we confirm a strong correlation between singly-charged helium and nitrogen CCS values for lipids, peptides, carbohydrates and TAA salts. It should be cautioned, however, that the relationship between helium and nitrogen-based CCS values are both charge-state and mass-dependent,³⁹ and it is expected that any correlation between the two measurements would deviate at the extremes of low and high mass. In fact, Bush *et al.* previously noted that cross-calibration error from nitrogen to helium CCS is higher at lower masses (up to

15% error) where the magnitude of the CCS value is small, while at higher masses, the error can be reduced to as low as 2.2% for predicting helium CCS from nitrogen measurements.⁹ It was also noted in this study and elsewhere that calibration across different chemical classes (*e.g.*, using literature peptide values to calibrate lipids¹⁴) introduces additional and significant error (*ca.* 7%), further underscoring the importance of compiling a chemically diverse set of empirical drift tube CCS values. Figure 4.5(C), inset contains the linear best fits to the data, with the axes rescaled to a region where data exists for all four chemical classes. Linear fits are extrapolated (dotted lines) for visualization purposes. Here, the small but notable differences between chemical classes can be observed as offset correlation lines, which corroborate with the absolute CCS differences between helium and nitrogen noted previously for each chemical class. Specifically, peptides, carbohydrates, and lipids fall along a similar helium-nitrogen CCS correlation trend, while the TAA salts exhibit a slightly lower correlation. Interestingly, all class correlations exhibit similar slopes (*ca.* 1), suggesting that the factors which give rise to the cross-sectional differences between helium and nitrogen (buffer gas size, mass and polarizability) affect different chemical classes in a similar manner across a broad range of both size and mass.

Absolute CCS differences between the helium and nitrogen datasets are plotted as a function of mass in Figure 4.5(D), with error bars representing $\pm 2\%$ CCS uncertainty. Average absolute CCS differences are projected as a horizontal line through each class distribution, with the following values: TAA salts, $58 (\pm 3) \text{ \AA}^2$; lipids, $70 (\pm 4) \text{ \AA}^2$; carbohydrates, $74 (\pm 8) \text{ \AA}^2$; and peptides, $73 (\pm 5) \text{ \AA}^2$. Cross-sectional differences are lowest for the TAA salts, while lipids, carbohydrates and peptides differ by approximately the same amount. Overall, there is a small but notable increase in the helium-nitrogen CCS difference with increasing mass for all classes except lipids where a limited mass range is surveyed. This suggests that the nitrogen and helium CCS are

not increasing at the same rate relative to the mass of the analyte, with the greater CCS increase occurring in nitrogen. Wyttchenbach *et al.* recently noted that ion systems up to *ca.* 760 Da (sodiated PEG₁₇) still exhibit strong contributions from the ion-neutral interaction potential in their measured CCS.⁴⁰ From their atomic superposition argument, it would be expected that with nitrogen buffer gas, the combined effect of each atomic potential for large polyatomic systems would give rise to a steeper increase in CCS than with helium buffer gas, since the atom-nitrogen interaction potential is stronger than the atom-helium interaction potential. In other words, the stronger interaction potential of nitrogen would be expected to scale with the number of atoms in the ionic system being measured, at least to a first approximation. Ion systems with different heteroatom compositions (*e.g.*, lipids *vs.* peptides) would also be expected to exhibit different scaling of mass to CCS between helium and nitrogen; this effect cannot be definitively observed in the relatively narrow mass range surveyed in this work, though cursory effects of gas polarization seem to be present in the enhanced high-mass separation of lipids and peptides in nitrogen *vs.* helium. Such class-specific CCS differences may bear out as more overlapping measurements are obtained in future studies.

4.4 Conclusions

The large database of nitrogen-derived CCS values presented here offers a glimpse at the intrinsic intermolecular packing forces of four chemically-different molecular classes across a relatively wide range of both size (*ca.* 150 to 450 Å²) and mass (*ca.* 150 to 2200 Da). Four molecular classes were investigated in this study, with relative gas-phase densities observed as follows, from least to most efficient packing: TAA salts, lipids, peptides and carbohydrates. The biopolymers (carbohydrates and peptides) demonstrated the highest efficiency for gas-phase

packing, and among these, carbohydrates tend to adopt the most compact gas-phase CCS values. This observation is somewhat intuitive in that carbohydrates have considerable degrees of freedom and can adopt both linear and branched primary structures. In contrast, lipids exhibit the largest CCS values among the biomolecules investigated, and this observation appears to be intrinsic to the inability of lipids for forming compact, self-solvated structures in the gas-phase. Noteworthy among these findings is that despite the significant differences between helium and nitrogen in terms of mass, degrees-of-freedom (atomic *vs.* diatomic) and polarization, the biomolecular class trends observed here for the nitrogen-based ion mobility are qualitatively the same as those previously observed in helium.^{3,20} We do observe evidence that these qualitative trends between the two drift gases are not retained at low mass, and a more detailed investigation of helium and nitrogen-based ion mobility studies for low mass analytes (less than 200 Da) will be the subject of future studies.

We emphasize that these studies are only possible by the remarkable advances made over the past decade in the development of biological IM-MS instrumentation. The IM-MS described in this report can achieve high resolving powers with high sensitivity, making it possible to observe and characterize low abundance isomeric species in highly complex samples with unprecedented scale and throughput. While we have purposely chosen to report only the highest abundant species, we note that the observation of multiple ion mobility peak features (mass isomers) is routine with this instrumentation, requiring that a new paradigm be accepted whereby it is no longer a question of if a particular isomer exists, but rather how much if it is present and in what context.

4.5 Acknowledgements

This chapter contains the published research article (<https://pubs.acs.org/doi/10.1021/ac4038448>): Jody C. May, Cody R. Goodwin, Nichole M. Lareau, Katrina L. Leaptrot, Caleb B. Morris, Ruwan T. Kurulugama, A. Mordehai, C. Klein, W. Barry, E. Darland, G. Overney, K. Imatani, George C. Stafford, John C. Fjeldsted, John A. McLean, “Conformational Ordering of Biomolecules in the Gas Phase: Nitrogen Collision Cross Sections Measured on a Prototype High Resolution Drift Tube Ion Mobility-Mass Spectrometer,” *Analytical Chemistry* **2014**, *86* (4), 2107-2116. Note that further permissions related to the material excerpted should be directed to the ACS.

Financial support was provided by the NIH National Center for Advancing Translational Sciences (UH2TR000491); the Defense Threat Reduction Agency (HDTRA1-09-1-00-13 and DTRA100271 A-5196); the Defense Advanced Research Projects Agency (W911NF-12-2-0036); the Vanderbilt Institute of Chemical Biology; and the Vanderbilt Institute for Integrative Biosystems Research and Education. NML acknowledges a Vanderbilt Chemical Biology Interface training grant (T32GM065086).

4.6 References

1. McDaniel, E. W. Collision phenomena in ionized gases; Wiley: New York, 1964; Vol. 1.
2. McDaniel, E. W.; Mason, E. A. Mobility and diffusion of ions in gases; John Wiley and Sons, Inc., New York, 1973.
3. Fenn, L.; McLean, J. Analytical and Bioanalytical Chemistry 2008, 391, 905-909.
4. McLean, J. A. J. Am. Soc. Mass Spectrom. 2009, 20, 1775-1781.
5. Valentine, S. J.; Counterman, A. E.; Clemmer, D. E. J. Am. Soc. Mass Spectrom. 1999, 10, 1188-1211; Valentine, S. J.; Counterman, A. E.; Hoaglund-Hyzer, C. S.; Clemmer, D. E. J Phys. Chem. B 1999, 103, 1203-1207.
6. Shvartsburg, A. A.; Siu, K. W. M.; Clemmer, D. E. J. Am. Soc. Mass Spectrom. 2001, 12, 885-888.
7. Shah, A. R.; Agarwal, K.; Baker, E. S.; Singhal, M.; Mayampurath, A. M.; Ibrahim, Y. M.; Kangas, L. J.; Monroe, M. E.; Zhao, R.; Belov, M. E.; Anderson, G. A.; Smith, R. D. Bioinformatics 2010, 26, 1601-1607.
8. Giles, K.; Pringle, S. D.; Worthington, K. R.; Little, D.; Wildgoose, J. L.; Bateman, R. H. Rapid Communications in Mass Spectrometry 2004, 18, 2401-2414; Pringle, S. D.; Giles, K.; Wildgoose, J. L.; Williams, J. P.; Slade, S. E.; Thalassinios, K.; Bateman, R. H.; Bowers, M. T.; Scrivens, J. H. Int. J. Mass Spectrom. 2007, 261, 1-12.
9. Bush, M. F.; Hall, Z.; Giles, K.; Hoyes, J.; Robinson, C. V.; Ruotolo, B. T. Anal. Chem. 2010, 82, 9557-9565.
10. Williams, J. P.; Grabenauer, M.; Holland, R. J.; Carpenter, C. J.; Wormald, M. R.; Giles, K.; Harvey, D. J.; Bateman, R. H.; Scrivens, J. H.; Bowers, M. T. International Journal of Mass Spectrometry 2010, 298, 119-127.
11. Revercomb, H. E.; Mason, E. A. Anal. Chem. 1975, 47, 970-983.
12. Mason, E. A.; McDaniel, E. W. Transport Properties of Ions in Gases; John Wiley & Sons: New York, 1988, p 560.
13. Ruotolo, B. T.; Giles, K.; Campuzano, I.; Sandercock, A. M.; Bateman, R. H.; Robinson, C. V. Science 2005, 310, 1658-1661; Ruotolo, B. T.; Benesch, J. L. P.; Sandercock, A. M.; Hyung, S.-J.; Robinson, C. V. Nat. Protocols 2008, 3, 1139-1152; Knapman, T. W.; Berryman, J. T.; Campuzano, I.; Harris, S. A.; Ashcroft, A. E. Int. J. Mass Spectrom. 2010, 298, 17-23.
14. Ridenour, W. B.; Kliman, M.; McLean, J. A.; Caprioli, R. M. Analytical Chemistry 2010, 82, 1881-1889.
15. Shvartsburg, A. A.; Mashkevich, S. V.; Siu, K. W. M. J Phys. Chem. A 2000, 104, 9448-9453; Shvartsburg, A. A.; Hudgins, R. R.; Dugourd, P.; Jarrold, M. F. Chem. Soc. Rev. 2001, 30, 26-35; Larriba, C.; Hogan, C. J. J Phys. Chem. A 2013, 117, 3887-3901.

16. Campuzano, I.; Bush, M. F.; Robinson, C. V.; Beaumont, C.; Richardson, K.; Kim, H.; Kim, H. I. *Anal. Chem.* 2011, 84, 1026-1033.
17. Pagel, K.; Harvey, D. J. *Anal. Chem.* 2013, 85, 5138-5145.
18. Haynes, W. M.; Lide, D. R.; Bruno, T. J. *CRC Handbook of Chemistry and Physics* 2012-2013, 93 ed.; CRC press, 2012.
19. Baker, E. S.; Clowers, B. H.; Li, F.; Tang, K.; Tolmachev, A. V.; Prior, D. C.; Belov, M. E.; Smith, R. D. *Journal of the American Society for Mass Spectrometry* 2007, 18, 1176-1187.
20. Fenn, L.; Kliman, M.; Mahsut, A.; Zhao, S.; McLean, J. *Anal. Bioanal. Chem.* 2009, 394, 235-244.
21. Tao, L.; McLean, J. R.; McLean, J. A.; Russell, D. H. *Journal of the American Society for Mass Spectrometry* 2007, 18, 1232-1238.
22. Bush, M. F.; Campuzano, I. D. G.; Robinson, C. V. *Analytical Chemistry* 2012, 84, 7124-7130.
23. Salbo, R.; Bush, M. F.; Naver, H.; Campuzano, I.; Robinson, C. V.; Pettersson, I.; Jørgensen, T. J. D.; Haselmann, K. F. *Rapid Communications in Mass Spectrometry* 2012, 26, 1181-1193.
24. Sud, M.; Fahy, E.; Cotter, D.; Brown, A.; Dennis, E. A.; Glass, C. K.; Merrill, A. H.; Murphy, R. C.; Raetz, C. R. H.; Russell, D. W.; Subramaniam, S. *Nucleic Acids Res* 2007, 35, D527-D532.
25. Wilkins, M. R.; Lindskog, I.; Gasteiger, E.; Bairoch, A.; Sanchez, J.-C.; Hochstrasser, D. F.; Appel, R. D. *Electrophoresis* 1997, 18, 403-408.
26. Fenn, J.; Mann, M.; Meng, C.; Wong, S.; Whitehouse, C. *Science* 1989, 246, 64-71.
27. Ibrahim, Y.; Tang, K.; Tolmachev, A. V.; Shvartsburg, A. A.; Smith, R. D. *J. Am. Soc. Mass Spectrom.* 2006, 17, 1299-1305.
28. Ibrahim, Y.; Belov, M. E.; Tolmachev, A. V.; Prior, D. C.; Smith, R. D. *Anal. Chem.* 2007, 79, 7845-7852.
29. Kemper, P. R.; Bowers, M. T. *J. Am. Soc. Mass Spectrom.* 1990, 1, 197-207; von Helden, G.; Hsu, M.-T.; Kemper, P. R.; Bowers, M. T. *J. Chem. Phys.* 1991, 95, 3835-3837.
30. Mason, E. A.; Schamp, H. W. *Annals of Physics* 1958, 4, 233-270.
31. McLean, J. A.; Ruotolo, B. T.; Gillig, K. J.; Russell, D. H. *Int. J. Mass Spectrom.* 2005, 240, 301-315.
32. West, G. B.; Brown, J. H.; Enquist, B. J. *Science* 1997, 276, 122-126.
33. Shen, Y.; Greene, J. E.; Strauss, M. A.; Richards, G. T.; Schneider, D. P. *The Astrophysical Journal* 2008, 680, 169.

34. Galilei, G. Leiden (1638) 1638.
35. Viidanoja, J.; Sysoev, A.; Adamov, A.; Kotiaho, T. *Rapid Commun. Mass Spectrom.* 2005, 19, 3051-3055.
36. Fenn, L. S.; McLean, J. A. *Phys. Chem. Chem. Phys.* 2011, 13, 2196-2205.
37. Ellis, H. W.; Pai, R. Y.; McDaniel, E. W.; Mason, E. A.; Viehland, L. A. *At. Data Nucl. Data Tables* 1976, 17, 177-210; Ellis, H. W.; McDaniel, E. W.; Albritton, D. L.; Viehland, L. A.; Lin, S. L.; Mason, E. A. *At. Data Nucl. Data Tables* 1978, 22, 179-217; Ellis, H. W.; Thackston, M. G.; McDaniel, E. W.; Mason, E. A. *At. Data Nucl. Data Tables* 1984, 31, 113-151; Viehland, L. A.; Mason, E. A. *At. Data Nucl. Data Tables* 1995, 60, 37-95.
38. Matz, L. M.; Hill Jr, H. H.; Beegle, L. W.; Kanik, I. *Journal of the American Society for Mass Spectrometry* 2002, 13, 300-307.
39. Berant, Z.; Karpas, Z. *J. Am. Chem. Soc.* 1989, 111, 3819-3824.
40. Wyttenbach, T.; Bleiholder, C.; Bowers, M. T. *Anal. Chem.* 2013, 85, 2191-2199; von Helden, G.; Wyttenbach, T.; Bowers, M. T. *Int. J. Mass Spectrom. Ion Processes* 1995, 146-147, 349-364.

CHAPTER 5

EVALUATING SEPARATION SELECTIVITY AND COLLISION CROSS SECTION MEASUREMENT REPRODUCIBILITY IN HELIUM, NITROGEN, ARGON, AND CARBON DIOXIDE DRIFT GASES FOR DRIFT TUBE ION MOBILITY-MASS SPECTROMETRY

5.1 Introduction

Ion mobility spectrometry (IM) is an important analytical technique for the rapid separation and identification of a wide variety of chemical compounds¹⁻⁶. In a conventional drift tube, the separation of chemical species results from numerous, near-thermal collision between analyte ions and a chemically-inert drift gas. Total IM separation times occur on the order of milliseconds, and thus are both high throughput and sufficiently fast to allow for integration with other analytical separation techniques⁷⁻⁸. Whereas in conventional gas and liquid phase chromatography, it is well-established that the chemical selectivity of the separation can be enhanced by choosing different stationary phases, IM is more appropriately described as a gas-phase electrophoretic technique, and as such does not incorporate a stationary phase. Instead, varying the drift gas composition has been demonstrated to affect separation efficiency in a similar manner as changing solvent conditions in capillary electrophoresis to tune separation selectivity. Most notably in high-field IM techniques such as high-field asymmetric waveform ion mobility spectrometry (FAIMS) and differential mobility spectrometry (DMS), the carrier gas composition is commonly altered to increase the resolution for closely spaced analytes⁹⁻¹⁵. For conventional low field IM techniques such as drift tube (DTIMS) and traveling wave (TWIMS), this practice is less common, although several notable cases exist¹⁶⁻¹⁸. For example, seminal work from Hill and coworkers demonstrated enhanced

analyte selectivity on an ambient pressure drift tube when varying the drift gas from low to high polarizability (helium, nitrogen, argon, and carbon dioxide) ¹⁹⁻²². Eberlin and coworkers reported improved separation of isomeric haloanilines, carbohydrates, and petroleum constituents when operating a traveling wave instrument in CO₂ as opposed to conventional N₂ gas ²³⁻²⁶. Recently, Yost and coworkers demonstrated increased resolving power for several isobaric steroids, analyzed in a reduced-pressure drift tube instrument, using CO₂ as the drift gas ²⁷. In many cases, however, the more polarizable drift gases (e.g., Ar, CO₂, and N₂O) are not reported to dramatically improve the overall IM peak capacity and resolution for chemically-similar analytes, including peptides, amino acids, structural isomers, and protein conformers, in comparison to He or N₂ drift gases ²⁸⁻³¹. A large survey of various drift gases (He, N₂, Ar, CO₂, N₂O, SF₆) recently conducted on a commercial drift tube instrument by Fjeldsted and coworkers investigated the separation of isomeric carbohydrates, fluoroalkyl phosphazenes, and various small molecule pesticides. Higher resolution was generally observed for drift gases with access to the highest resolving powers in the instrumentation, namely conventional He and N₂. Some enhanced selectivity and resolution was observed for the more polarizable drift gases (CO₂, N₂O, and SF₆), although results were specific to the analyte pairs being investigated ³². The literature examining the roles various drift gases play on IM separation capabilities are complicated and must be taken case-by-case. Given the potential analytical power that the drift gas composition can play in enhancing the IM resolution, there is a need for exploring IM separations in alternate drift gases across a broader range of analytes, and reporting quantitatively-comparable metrics of separation capabilities obtained from various laboratories. To accomplish this, a common framework for acquiring and comparing ion mobility data obtained in different drift gases needs to be established.

In addition to providing analyte structural information, collision cross section (CCS) values are useful for comparing IM measurements obtained using different IM instrumentation and techniques^{1, 33-35} and recently have been used as an additional molecular description combined with accurate mass and retention time information for high confidence identification of unknowns arising from complex samples^{34, 36-40}. While some fundamental work has been done using matrix-assisted laser desorption ionization (MALDI)⁴¹⁻⁴², the majority of CCS measurements has been conducted using electrospray ionization (ESI), including the work here. For alternate drift gas work, separations conducted across different instrument platforms, such as drift tube and traveling wave, cannot be directly compared without utilizing a normalized measurement such as CCS³³. Comparisons of IM separation performance are hindered by the fact that the majority (95%) of CCS measurements have been reported only in conventional He and N₂ drift gas¹. In addition to the general lack of reporting CCS measurements in alternate drift gas work, a large-scale study of the effects of drift gas on a wide mass range, multiple biological classes, and varying charge states has yet to be accomplished. In this work, we investigate four of the most commonly used drift gases, helium (He), nitrogen (N₂), argon (Ar), and carbon dioxide (CO₂), and establish instrument conditions necessary to achieve high reproducibility and enhanced separation efficiency for diverse sets of structurally-homogeneous analytes representing various charge states and chemical classes. We assess the separation efficiency in each gas using a combination of single-peak resolving power, two-peak resolution, and peak capacity, and provide detailed reporting of the CCS measured in each drift gas for low field DTIMS.

5.2 Methods

5.2.1 Instrumentation

A commercial drift tube ion mobility-mass spectrometer (6560, Agilent Technologies) equipped with a thermally-assisted electrospray ionization source (Jet Stream, Agilent) was used for all measurements described herein⁴³. The drift gases used were high purity N₂, He, Ar, and CO₂ (Air Liquide). N₂, He, and Ar were UHP grade supplied at 99.999% purity, whereas CO₂ was Coleman grade, at 99.99% purity. The high-pressure funnel (HPF), trap funnel (TF), and drift tube (DT) regions of the instrument, shown in the schematic in Figure 5.1, were supplied with either He, N₂, Ar, or CO₂ using a commercially-upgraded drift gas manifold (Alternate Gas Kit, Agilent). Briefly, the gas kit consists of a precision closed-loop pressure controller (640B, MKS Instruments) which makes real-time adjustments to the pressures based on readings from a capacitance manometer (CDG-500, Agilent) mounted on the DT chamber. Prior to being directed into the instrument, each drift gas was passed through a passive purifier specific for He, Ar (RMSH-4, Agilent), N₂ (RMSN-4, Agilent), or CO₂ (P600-2, VICI Metronics). Instrument tuning utilized the vendor autotune function in standard mass range (m/z 3200 mode). For He, tuning was performed in N₂ before switching to He to mitigate issues related to gas breakdown at high voltage, manifesting as uncorrelated low m/z noise in the 2D ion mobility-mass spectrometry (IM-MS) spectrum. For N₂, Ar, and CO₂, tuning was performed in the chosen drift gas. During gas switching, the DT was allowed to equilibrate for at least 60 minutes, after which, pressures were confirmed to be stable and minor adjustments made as necessary. The HPF was operated at 4.80 Torr for N₂ and Ar, 4.35 Torr for He, and 4.30 Torr for CO₂. The TF was operated at 3.80 Torr for N₂, 3.74 Torr for Ar, and 3.72 Torr for both CO₂ and He. CCS measurements utilize a stepped-field procedure in

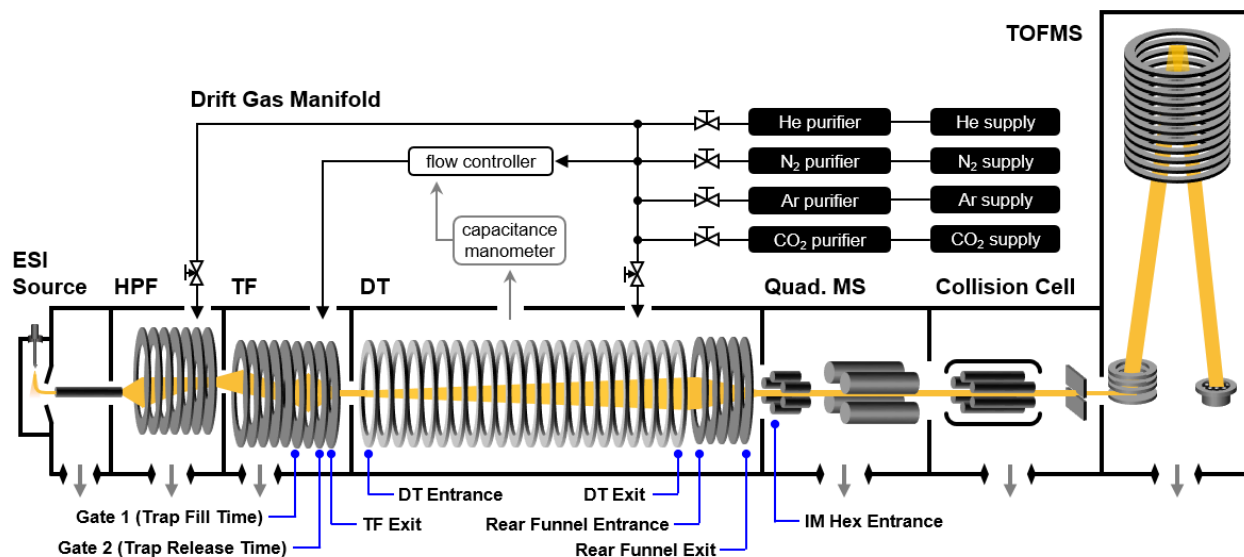


Figure 5.1 A conceptual schematic of the commercial drift tube ion mobility-mass spectrometer (6560, Agilent) used in this work. The selected drift gas is supplied to the high-pressure funnel (HPF), trap funnel (TF), and drift tube (DT) regions. The flow controller adjusts the gas flow into TF region based on the DT pressure readback, maintaining a constant pressure in the DT. The DT is isolated from the vacuum system, and gas evacuation from DT is thus facilitated via the entrance and exit apertures of the chamber. Adapted from Caleb B. Morris, Jody C. May, Katrina L. Leaptrot, and John A. McLean, "Evaluating Separation Selectivity and Collision Cross Section Measurement Reproducibility in Helium, Nitrogen, Argon, and Carbon Dioxide Drift Gases for Drift Tube Ion Mobility-Mass Spectrometry," *Journal of the American Society for Mass Spectrometry* 2019 (in press).

which several drift fields are surveyed in order to determine the ion transit time within the mobility drift region. For N₂, Ar, and CO₂ the specific voltages used for the DT and associated ion transfer optics (TF exit, rear ion funnel, and post-IM hexapole) are identical to settings used in a standardized CCS method described in a recent interlaboratory study ³⁴. Specifically, this standardized, stepped-field method incorporates seven electric field strengths (E/N , where E is electric field and N is the molecular number density) between 8 and 15 Td with a static pressure of 3.95 Torr in the DT. For He, the same DT pressure (3.95 Torr) is utilized, however, a different range of electric fields are surveyed between 6 and 13 Td to optimize resolving power across a broad mass range while mitigating electrical breakdown of the gas. Detailed experimental settings for each drift gas are provided in Table D.1. The trap release time (referred to as ion gating time in other IM instrumentation) was set to 100 μ s for all experiments to maximize instrument resolving power ⁴⁴, and the TF exit voltage (defining the ion “injection” voltage into the DT) was kept at 10 V, minimizing end effects which otherwise shift drift times to lower values ⁴⁵. Ion source conditions were as follows: 325°C gas temperature, 13 L/min drying gas flow rate, 275°C and 12 L/min sheath gas temperature and flow rate, and nebulizer pressure at 20 psig. Additional experimental conditions for each drift gas are summarized in Table D.1. The vendor-supplied software (LC/MS Data Acquisition B.07.00, Agilent) was used for all data acquisition.

5.2.2 Variable Pressure Experiments

In prior work with He drift gas, it was found that the operational pressures of the HPF and TF had an effect on the measured CCS, presumably due to changes in gas purity within the DT ³⁵, ⁴⁶. In order to better characterize these pressure dependencies, the gas pressures were varied in increments of 0.10 Torr and 0.02 Torr for the HPF and TF regions, respectively, while keeping the

DT at 3.95 Torr. This allowed CCS measurements to be obtained at multiple pressure combinations for both regions. The upper pressure limits surveyed for N₂, Ar, and CO₂ were based upon pressures utilized for normal N₂ operation (i.e., 4.80 Torr in the HPF and 3.80 Torr in the TF)³². Operational limits of the flow controller (calibrated for N₂) restricted helium experiments to a maximum of 4.63 Torr in the HPF with 3.80 Torr in the TF. To obtain CCS values comparable to those reported in the literature, measurements were taken above the minimum operational pressure bounds of the HPF and TF; however, despite the proximity to operational pressure limits, CCS measurements were reproducible and subsequently represent the values reported in this work.

5.2.3 Effective Length

All CCS values observed in all drift gases are listed in Table D.2, with CCS values not observed in all drift gases listed in Table D.3, and calculated using a drift tube effective length of 78.06 cm. The effective length differs slightly from the geometric length of the instrument (ca. 78.12 cm), and is determined using a previously-reported protocol whereby CCS values for the MS tuning mixture (hexakis(fluoroalkoxy)phosphazenes, HFAP, *m/z* 322-*m/z* 2722) are scaled to reference measurements obtained using a gridded DT instrument^{34, 47}. The effective length determined from this procedure is instrument-specific and was used to calculate CCS values for all drift gases.

5.2.4 Chemical Standards

Isopropanol, acetonitrile, water, and formic acid (Optima LC-MS grade) were obtained from Fisher Scientific. The chemical standards were purchased from several vendors, summarized in Table D.4. Tetraalkylammonium salts (TAA) were received as dry powder and reconstituted in

isopropanol. All chemical standards except the HFAP tuning mixture were prepared at 10 $\mu\text{g/mL}$ and directly infused into the ESI source at a flow rate of 10 $\mu\text{L/min}$. Poly-DL-alanine and maltose standards were prepared in methanol:water (50:50% v:v) with 0.1% formic acid. The MS tuning mixture containing HFAP (ESI-L Low Concentration Tuning Mixture, Agilent) is supplied from the vendor as a mixture of components dissolved in acetonitrile:water (95:5% v:v), and was prepared as per the vendor instructions by diluting the solution by a factor of ten using acetonitrile:water (98:2% v:v).

5.3 Results and Discussion

5.3.1 Analyte Selection

The analytes chosen for this study were selected as belonging to sets of structurally-homogeneous molecules spanning a wide mass coverage (Figure 5.2(a)). Specifically, HFAP increases by symmetric additions of fluoroalkyl (CF_2) subunits to the six terminal ethers, while TAA cations increase symmetrically by alkyl (CH_2) subunits, and the carbohydrates represent oligosaccharides with repeating α -D-glucose units linked by an $\alpha(1\rightarrow4)$ glycosidic bond. Although the MS tuning mixture also contains m/z 118 (betaine), this molecule is not a HFAP, and thus was not included in this study. Poly-DL-alanine has been used in previous IM studies for CCS calibration⁴⁸⁻⁴⁹ and, in addition to possessing repeating alanine subunits, forms multiple charge states from ESI, allowing for the investigation of charge state effects in different drift gases.

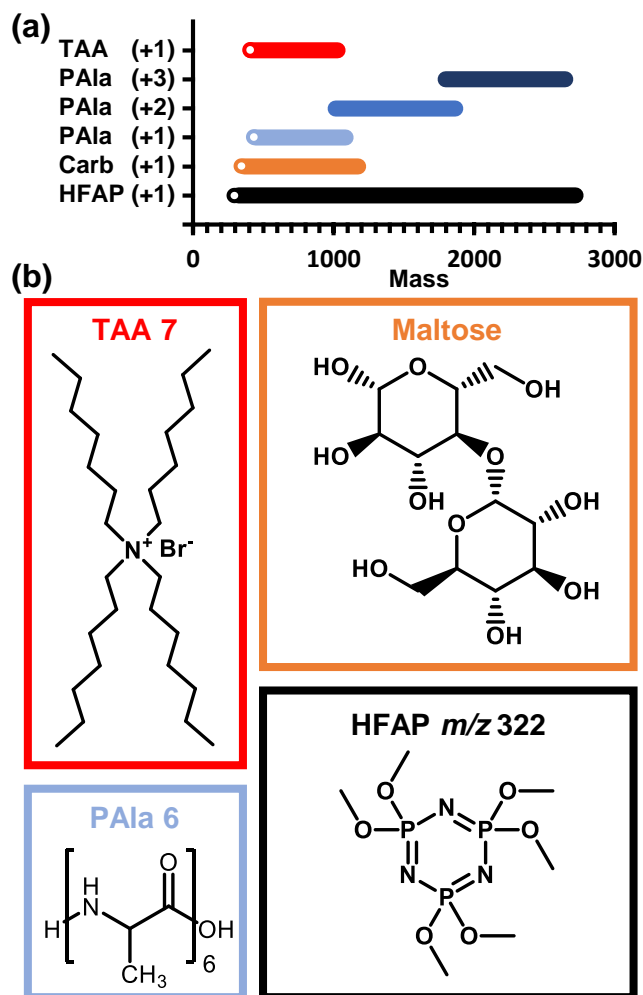


Figure 5.2 (a) Mass coverage of each class of molecules investigated. (b) Representative structures for each of the four classes of molecules investigated in this study, with their respective masses indicated by the white dots in panel a. Adapted from Caleb B. Morris, Jody C. May, Katrina L. Leaptrot, and John A. McLean, "Evaluating Separation Selectivity and Collision Cross Section Measurement Reproducibility in Helium, Nitrogen, Argon, and Carbon Dioxide Drift Gases for Drift Tube Ion Mobility-Mass Spectrometry," *Journal of the American Society for Mass Spectrometry* 2019 (in press).

5.3.2 Pressure Effects

Pressure conditions in the ion transfer funnels prior to the drift tube were systematically investigated for each drift gas to determine the effect on the measured CCS. The cesium cation (Cs^+) was used for quantitative comparisons of the CCS measurement due to ease of ionization, lack of multiple conformations, and CCS measurements have been previously documented in the literature for the drift gases investigated in this present study. The Cs^+ CCS results for select combinations of pressure conditions are presented in Figure 5.3, representing the upper (red boxes) and lower limits of pressures (blue boxes) surveyed for each funnel region. In all cases, the drift tube pressure was maintained at 3.95 Torr. The CCS value and corresponding variance reported in the literature for Cs^+ is also shown at the bottom of each panel (unfilled bars), as reported for He, N_2 , Ar, and CO_2 ⁵⁰. While there was no significant change in the N_2 CCS ($^{\text{DT}}\text{CCS}_{\text{N}_2}$) values for Cs^+ (0.08% difference or less), CCS measurements in the other drift gases were sensitive to HPF and TF pressure changes, most notably with changes to the TF pressure, where as high as 47.96%, 7.99%, 0.81% differences in CCS were observed for He, CO_2 , and Ar respectively. Previously, it has been suggested that for this particular instrument configuration, the pressure difference between the TF and the DT affects the gas purity within the IM region, and our results support this idea, with lower pressure differences shifting the Cs^+ $^{\text{DT}}\text{CCS}_{\text{He}}$ to higher values, and lower CCS values for the other gases, implicating contamination of the drift tube with gas from the ion source, the latter of which is N_2 sourced from the boil-off of a cryogenic tank ^{32, 46}. Though not reported previously, it was found in this study that lower pressures in the upstream HPF could also improve gas purity in the DT, and this effect is shown in Figure 5.3 for He, Ar, and CO_2 . As with the TF pressure, lowering the HPF pressure affected the Cs^+ CCS measurement by shifting it to lower values for He, and higher values for Ar and CO_2 . In He, the CCS continues to decrease as the HPF

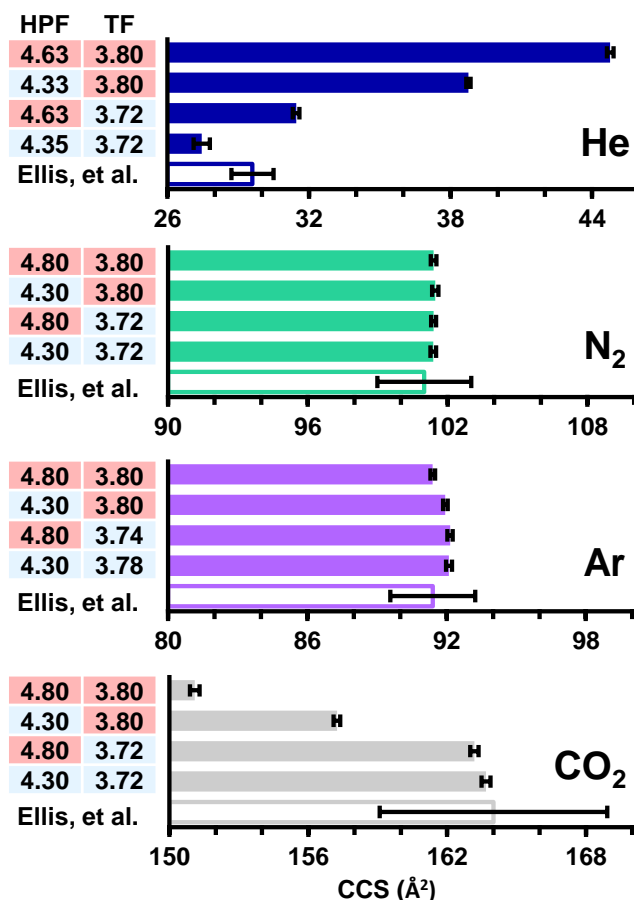


Figure 5.3 A comparison of the CCS values obtained for Cs⁺ (132.91 Da) in multiple drift gases (filled bars) and at various HPF and TF operational pressures (vertical axes labels, in Torr) along with the CCS and corresponding error (outlined bars) reported by Ellis et al. (Ellis, HW; McDaniel, EW; Albritton, DL; Viehland, LA; Lin, SL; Mason, EA; Atomic Data and Nuclear Data Tables 22, 179-217, 1978). Error bars for data obtained in this study correspond to 7 repeat measurements. Red and blue shading in the vertical axes labels indicates high or low relative pressure conditions for HPF and TF. Adapted from Caleb B. Morris, Jody C. May, Katrina L. Leaptrot, and John A. McLean, "Evaluating Separation Selectivity and Collision Cross Section Measurement Reproducibility in Helium, Nitrogen, Argon, and Carbon Dioxide Drift Gases for Drift Tube Ion Mobility-Mass Spectrometry," *Journal of the American Society for Mass Spectrometry* 2019 (in press).

and TF pressures are reduced, with the lowest pressures surveyed exhibiting the closest CCS correlation to the literature. The CCS response to HPF and TF pressures indicate improved drift gas purity at lower HPF and TF pressures for drift gases other than nitrogen. At some pressures, the CCS response is minimal as the pressure is further lowered. Since the interpretation is that lower HPF and TF pressures show increased gas purity, as evidenced by better CCS agreement with literature values, the lowest pressures that could be achieved in He, Ar, and CO₂, without signal degradation of the reported analytes, are recommended. This CCS shift exhibits some mass-dependence, as evidenced by comparing the CCS of the HFAP tuning mixture ions across various pressure conditions (cf., Figure D.1). Specifically, the lower mass HFAP ions (m/z 322 and m/z 622) experience a greater shift in CCS in response to changes in HPF and TF operational pressures, which we interpret as due to a greater magnitude of the so-called “end effect” documented for DTIMS, where ions subject to either higher fields or less collisional dampening (i.e., He) at the entrance to the IM region experience deeper penetration into the drift region^{45, 51}. This delayed thermalization of ions results in a shorter effective drift length, and thus a shift in the apparent measured CCS to lower values as the TF operational pressure is decreased. For the lower limits of pressure, operating the TF and HPF regions at pressures below those recommended here was found to significantly degrade ion transmission in He, Ar, and CO₂. Additionally for Ar, lower pressures resulted in non-linear behavior in the drift times obtained across multiple drift fields, while in He, gas discharge occurs, which manifests as uncorrelated spectral noise in the lower m/z range. The lower pressure limits for N₂ were chosen to overlap with the limits observed for the other drift gases. The high pressure limits for operating the TF and HPF regions for each drift gas were determined based on the recommended values previously established for N₂³². Recommended pressure settings for all drift gases evaluated are summarized in Table D.1.

5.3.3 Ion Source Temperature Effects

CCS changes were also observed when adjusting the ion source gas temperatures (i.e., nebulizer sheath gas and source entrance drying gas). Specifically, when varying ion source gas temperatures, as much as a 2.7% change in the $^{DT}CCS_{He}$ was observed, while the $^{DT}CCS_{N_2}$ shifted by a more modest amount, 0.3% or less. This result is interpreted as being due to changes in the gas flow dynamics between the ion source and the DT, which results in gas impurities being introduced into the drift region despite efforts to maintain constant operational pressures in the HPF, TF, and DT regions. Thus, the CCS results presented in this study are obtained under constant ion source temperature conditions which were selected in order to achieve close correlation of Cs^+ CCS values to those described in the literature.

5.3.4 Ion Injection Potential

The TF exit voltage establishes the potential bias between the TF and the DT. This potential affects the ion “injection” into the DT and plays a role in ion transmission, resolving power, ion internal energy, and the measured drift time.^{45, 52-53} In order to quantitatively evaluate these effects, the potential difference between the TF exit and DT was varied from 0 to 45V (35V in He) using the HFAP tuning mixture ions as a test system. Ion transmission, CCS, and resolving power were measured for each injection voltage (Figures D.2-D.4). It was found that in all drift gases, ion injection voltages between 5 and 15V yielded the highest ion transmissions based on peak area analysis (Figure D.2), whereas resolving powers were found to be the highest for 10 and 15V. In this range, no strong correlation was observed for any particular HFAP ion, suggesting that between 10 and 15V the mass and mobility-dependent effects were minimal. Importantly, the ion injection voltage was found to shift the measured CCS for all gases surveyed, most dramatically

for the low (0 and 5V) and high (≥ 15 V) potential settings. For example, $^{DT}CCS_{N_2}$ differences relative to 10V for m/z 1522 was found to be between 2.13% and 1.24%, respectively. Specifically, low ion introduction voltages (≤ 5 V) yielded high CCS values, whereas the high ion introduction voltages (≥ 15 V) resulted in low CCS values regardless of the identity of the drift gas. These results can be interpreted as a consequence of different ion injection energies, specifically, for low voltages, ions spend more time at the DT entrance prior to being entrained in the drift field, whereas for high voltages, ions penetrate deeper into the drift region before reaching a steady-state drift velocity. It is somewhat surprising that, without an ion introduction potential (0V), ions still transfer against a pressure gradient into the DT, although this observation is not investigated further in this work. Also of note is that, despite what is typically observed for drift tube instruments, the higher ion injection potentials in this DTIMS configuration did not yield more ion signal, but rather decreased ion transmission and resolving power. The default setting for the injection potential (designated as the TF exit voltages in the software) is 10V, which yielded good results in terms of high ion transmission and high resolving power for all gases and HFAP ions evaluated. As such, the TF exit voltage used for all subsequent experiments was 10V.

5.3.5 CCS Measurements

The CCS measurement reproducibility (precision) was found to depend on the drift gas. For example, 95% of the $^{DT}CCS_{He}$ values exhibit an RSD of less than 1.4%, whereas in Ar, CO₂, and N₂, the precision was found to be much better, with the majority (95%) of CCS values exhibiting less than 0.6%, 0.5%, and 0.3% RSD, respectively (c.f., Figure D.5). The cause of the lower precision in He is likely due to pressure fluctuations during CCS measurements as a result of the pressure controller valve orifice used in this work being optimized for N₂, although it should be

noted here that the vendor offers high flow valve configurations which should improve the pressure control when operating in He drift gas. In order to keep the recommended parameters in this work accessible to a wider network of researchers, an alternate pressure controller optimized for He was not used. Instead, the pressure controller shipped with the alternate gas kit was used for all four drift gases. As noted previously, both the HPF and TF pressures affect the CCS and operating the instrument at the lower HPF and TF pressures yield measurements which are closely aligned with canonical CCS values. Note that Cs^+ in He never matched with the literature value, even accounting for error. As only a single literature source could be found which reported $^{\text{DT}}\text{CCS}_{\text{He}}$ values for the cesium cation, this observation could not be further evaluated. While HFAP ion CCS values have not been previously published for gases other than N_2 , HFAP ions were subsequently compared to previously published $^{\text{DT}}\text{CCS}_{\text{N}_2}$ values (Figure D.6) ^{34, 54}, demonstrating excellent agreements of 0.56% or less, with a relative standard deviation of measurements taken for this study of 0.31% or less. For poly-DL-alanine, CCS values obtained in this work showed less agreement with the literature, with a maximum bias of 1.7% observed for N_2 and a 4.8% bias for He (Figure D.7). This agreement is still seen as reasonable, given these measurements were from disparate instrument designs and the error reported for the literature values was estimated at 3% ^{34, 54}. Previously published He and N_2 values for TAA cations ^{34, 54} were also compared to the current measurements (Figure D.8), and it was found that, in general, the literature values were typically higher, with differences ranging from -2.96% to 3.67% observed among the different reports. Overall, the settings recommended in this study (Table D.1) provide good CCS measurement reproducibility while corresponding reasonably well to prior measurements. Ongoing international efforts are aimed at further improvements in CCS measurement precision and accuracy.

5.3.6 Chemical Class Behavior

The gas-specific conformational space plots for all analytes investigated is shown in Figure 5.4. The low mass region is highlighted in each of the insets and depicts a region of IM-MS space where multiple chemical classes reside in close proximity. In general, all of the class-specific mobility-mass trends are qualitatively the same with the higher charge state ions exhibiting larger CCS values than the lower charge state ions, while for singly-charged ions, the CCS increases in the following order: HFAP < carbohydrates < peptides < TAA cations. As discussed in a number of previous reports, this conformational ordering is indicative of the relative gas-phase packing efficiency of each chemical class, with ions exhibiting less-restrictive degrees of freedom (peptides and carbohydrates) are able to arrange themselves into more compact gas-phase structures⁵⁵⁻⁵⁶. For singly-charged ions, the relative CCS values in N₂ and Ar are similar, whereas ^{DT}CCS_{Ar} values are all slightly lower than those measured in N₂. Note that for multiply charged species, the CCS differences are greater between the various gases than singly charged species. This is apparent in Figure 5.4 when comparing the relative spacing between the poly-DL-alanine +2 and +3 ion trends (dark blue triangles) to the +1 trend (light blue triangles), as well as plotting CCS as a function of gas polarizability (Figure D.9), where linear fits to the higher charge states exhibit larger slopes. In addition to charge state effects, the carbohydrates as a whole are strongly affected by the identity of the drift gas compared to the other classes investigated. This effect is shown in Figure 5.5, where the carbohydrates shift in drift time to a greater extent than other classes, resulting in an inversion in the IM elution orders. For example, in CO₂, polyalanine 13-mer (blue dashed trace, *m/z* 942.5008) exhibits a lower measured drift time than the carbohydrate, maltohexaose (orange dashed trace, *m/z* 1013.3173). In all other drift gases, however, this relative elution order is reversed. This effect has been noted previously for small molecules with masses below 500 Da^{19, 57}

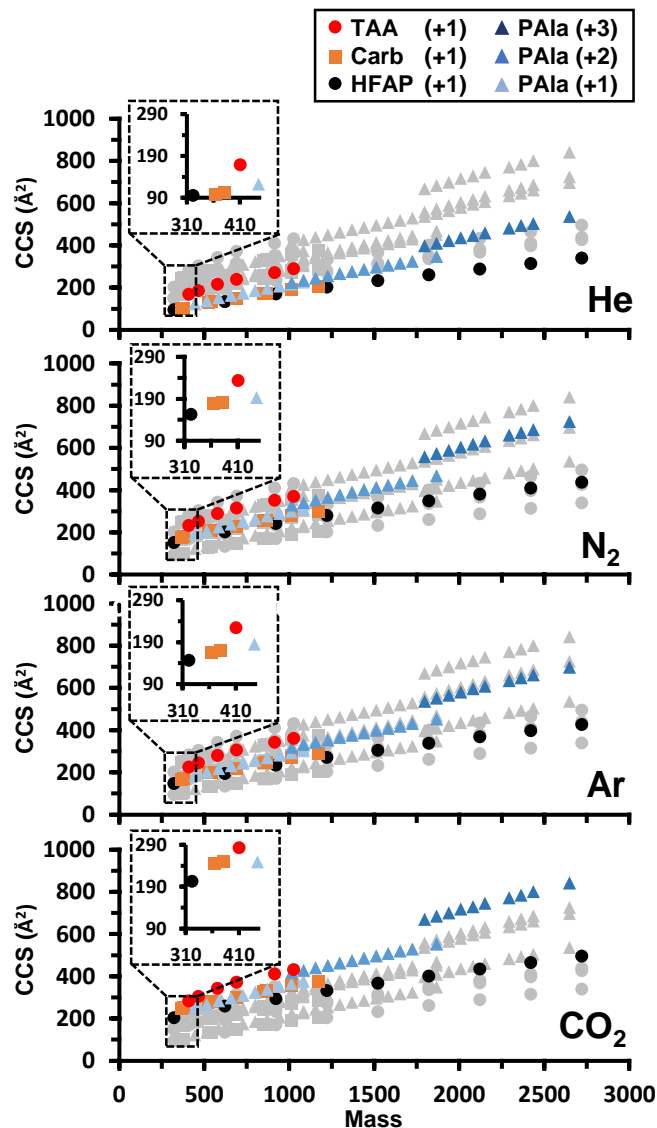


Figure 5.4 Mass versus CCS plots for each drift gas investigated. The location of all measurements are designated with grey symbols for comparison. The inset in each panel shows an expanded region at low m/z which contains various compound classes. Note that the CCS of carbohydrates (orange squares) relative to the other compounds exhibits a strong dependency on the identity of the drift gas utilized. Adapted from Caleb B. Morris, Jody C. May, Katrina L. Leap-trot, and John A. McLean, "Evaluating Separation Selectivity and Collision Cross Section Measurement Reproducibility in Helium, Nitrogen, Argon, and Carbon Dioxide Drift Gases for Drift Tube Ion Mobility-Mass Spectrometry," *Journal of the American Society for Mass Spectrometry* 2019 (in press).

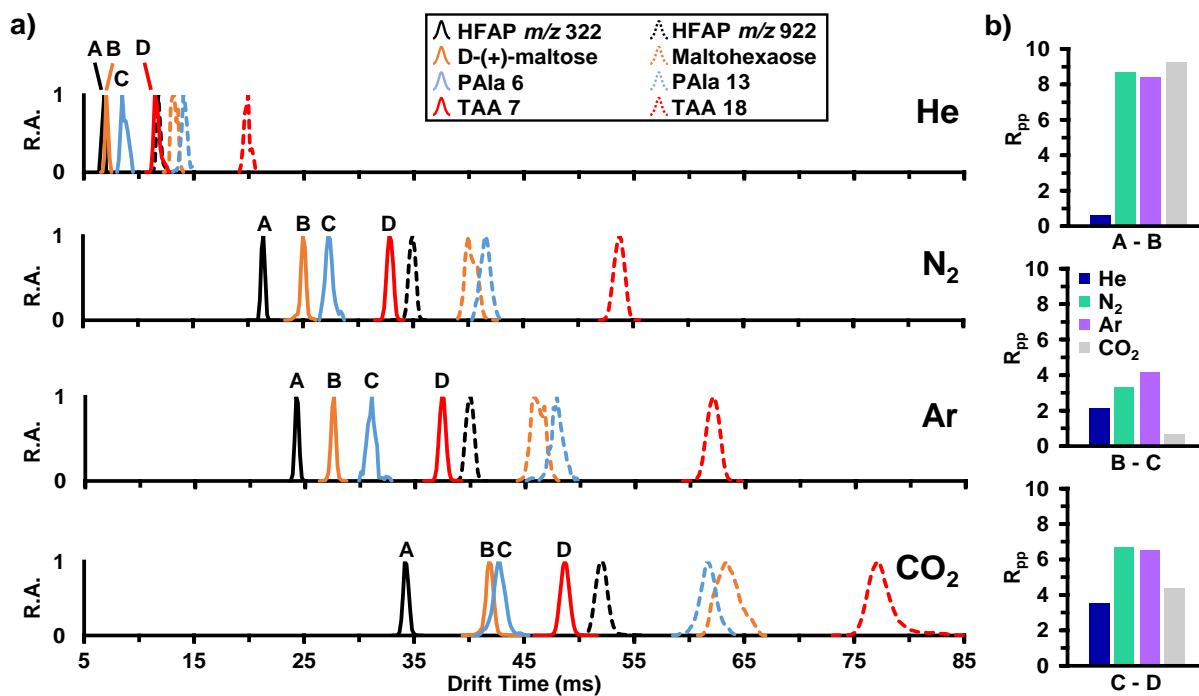


Figure 5.5 Relative abundance (R.A.) vs drift time for two ions from each class are shown for the four drift gases at the same field strength. Solid lines show four ions of similar mass, with one ion from each of the four classes (structures are depicted in Figure 5.2(b)); dashed lines show four ions of higher mass, with one ion from each class. (b) Two peak resolution (R_{pp}) is shown as histogram plots for each closest-mass ion pair of the lower mass group, those depicted with solid lines in the IM spectra. Note the drift time inversion for the high mass carbohydrate (dashed orange) and polyaniline (dashed blue) in CO₂ compared to the other three drift gases. Adapted from Caleb B. Morris, Jody C. May, Katrina L. Leaptrot, and John A. McLean, "Evaluating Separation Selectivity and Collision Cross Section Measurement Reproducibility in Helium, Nitrogen, Argon, and Carbon Dioxide Drift Gases for Drift Tube Ion Mobility-Mass Spectrometry," *Journal of the American Society for Mass Spectrometry* 2019 (in press).

and this present work demonstrates that CCS inversion can occur at higher masses as well. This drift gas selectivity can be useful depending upon the ion species being separated. For instance, in the peak-to-peak resolution (R_{pp}) example shown in Figure 5.5, utilizing N_2 or Ar would be ideal for separation of the lower mass ions shown, however, the best resolution for certain ion pairs is observed in CO_2 specifically between HFAP m/z 322 and maltose (labeled as analytes A and B). It is interesting to note that, with respect to the relative elution orders and resolutions observed, IM separations in Ar (39.96 Da, 1.64 \AA^3) are most similar to those observed in N_2 (28.01 Da, 1.74 \AA^3), rather than CO_2 (43.99 Da, 2.91 \AA^3),⁵⁸ indicating CCS is more dependent on the polarizability of the drift gas than the neutral drift gas mass for the species measured here. While the experimental CCS is a function of both ion and drift gas size, the relative size of the drift gas as experienced by the ion is dominated by its polarizability, and thus plots of CCS versus polarization exhibit near linear trends²². This is shown in Figure 5.6(a), with the select ions investigated plotted as a function of the drift gas polarizability. Of note is that, despite the relative differences in CCS observed across the different drift gases surveyed, ions of similar chemical class exhibit similar slopes in the CCS vs. polarizability plot.

5.3.7 Drift Gas Selection Criteria

In choosing the appropriate drift gas, analytical figures-of-merit such as single-peak resolving power (R_p), two-peak resolution (R_{pp}), and peak capacity are important considerations. Equations associated with these analytical figures-of-merit can be found in Appendix D. Peak capacity, a measure of the number of peaks that can occupy a given analytical separation space at half height, was found to be the highest in Ar, followed by N_2 at the lower mass range (Figure 5.6(b), top panel), whereas N_2 outperformed all of the other gases for higher mass analytes due to

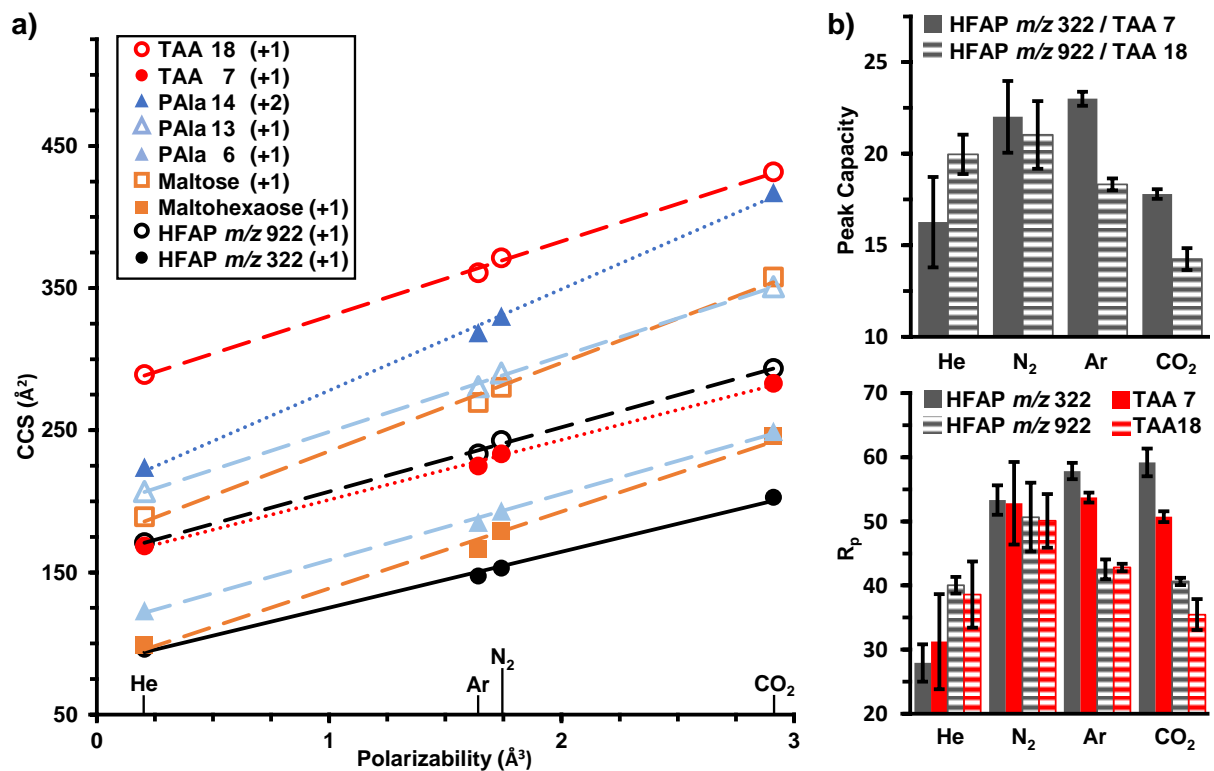


Figure 5.6 (a) The CCS for select ions plotted against the polarizability of the drift gas as given in the CRC Handbook of Chemistry and Physics.⁴⁵ All ions are singly charged except polyalanine 14-mer (PALa 14) which is doubly charged. Increasing the polarizability of the drift gas is correlated with an increase in CCS. However, the relative change in CCS with the drift gas polarizability is both class and charge-state specific, as indicated by the different slopes. The slope, intercept, and regression coefficient values are given in Table D.5. Error bars are within the marker size. (b) Resolving power (R_p) and peak capacity bar graphs for each drift gas. Maximum R_p values are shown, requiring a different drift field for He (8.3 V/cm) versus the other drift gases (16.0 V/cm). Peak capacity was calculated between HFAP and TAA cations of similar mass. Error bars were based on five measurements conducted on different days. Adapted from Caleb B. Morris, Jody C. May, Katrina L. Leaptrot, and John A. McLean, "Evaluating Separation Selectivity and Collision Cross Section Measurement Reproducibility in Helium, Nitrogen, Argon, and Carbon Dioxide Drift Gases for Drift Tube Ion Mobility-Mass Spectrometry," *Journal of the American Society for Mass Spectrometry* 2019 (in press).

the ability for N₂ to access higher resolving powers in this mass range (Figure 5.6(b), bottom panel). CO₂ exhibited the lowest peak capacities for the two mass ranges investigated, but certain systems may benefit from the increased analytical selectivity as previously described. Overall, N₂ would be recommended in most cases due to low %RSD, excellent peak capacity, and a consistently high resolving power over a wide mass range. Helium may be chosen when comparison to computational or literature values is needed. Argon performed similarly to nitrogen but may be chosen over nitrogen if a slight increase in resolving power is needed for lower mass analytes. CO₂ may be chosen to improve separation for specific analyte pairs.

5.4 Conclusion

This work evaluates detailed experimental conditions necessary for operating a commercial drift tube instrument (Agilent 6560) with a variety of drift gases that include He, N₂, Ar, and CO₂. Criteria used to evaluate the optimal instrument settings needed for each gas include those parameters which provided the highest measurement repeatability of the CCS and the closest correspondence of CCS (e.g., cesium, tuning mixture ions, and poly-DL-alanines) to previously published values. Using these optimal operational settings, a large and highly-consistent set of CCS measurements (N=280, 56 unique ions with 5 replicates each) for a variety of structurally-heterogeneous compounds (TAA cations, poly-DL-alanines, fluoroalkyl phosphazenes, and $\alpha(1\rightarrow4)$ -linked glucose oligosaccharides) are subsequently compiled, which are suitable as reference values for future studies. Comparison between the CCS response of the various classes, charge states, and masses surveyed in each drift gas is provided to aid future investigators in selecting the appropriate drift gas for their particular applications. The specific CCS trends observed were found to correlate strongly with the drift gas polarizability, thus providing a basis for predicting relative elution orders

for gases not yet investigated. Overall, it was found that N₂ exhibited the highest resolving powers and peak capacities across a broad range of masses with a correspondingly high CCS reproducibility (less than 0.40% RSD). CO₂ exhibited relatively low peak capacities, but demonstrated high chemical class and charge state specific selectivity, and in some cases, resulted in inverted analyte elution times as compared to the other drift gases. In general, the reference CCS values and recommended experimental parameters outlined in this manuscript are expected to aid IM researchers in selecting the drift gas appropriate for their analytical problem, as well as providing guidance for incorporating alternative drift gases in future work. Finally, the highly-consistent CCS values measured in this study can be used as a basis for improving fundamental IM theory and developing algorithms which consider the identity of the drift gas in predicting IM elution behavior.

5.5 Acknowledgements

This chapter contains the published research article: Caleb B. Morris, Jody C. May, Katrina L. Leaptrot, and John A. McLean, “Evaluating Separation Selectivity and Collision Cross Section Measurement Reproducibility in Helium, Nitrogen, Argon, and Carbon Dioxide Drift Gases for Drift Tube Ion Mobility-Mass Spectrometry,” *Journal of the American Society for Mass Spectrometry* **2019** (in press).

The authors gratefully acknowledge Ruwan Kurulugama and John Fjeldsted at Agilent Technologies and Robin Kemperman and Richard Yost at the University of Florida for insightful discussions regarding the use of alternative drift gases on the instrument platform used in this study. This work was supported in part using the resources of the Center for Innovative Technology at Vanderbilt University. Financial support for this work was provided by the National Institutes of Health (NIH NIGMS R01GM092218 and NCI R03CA222-452-01), the U.S. Environmental

Protection Agency under Assistance Agreement No. 83573601, and the U.S. Army Research Office and the Defense Advanced Research Projects Agency (DARPA) under Cooperative Agreement no. W911 NF-14-2-0022. This work has not been formally reviewed by EPA. The views expressed in this document are solely those of the authors and do not necessarily reflect those of the funding agencies and organizations. EPA, DARPA, or the U.S. Government do not endorse any products or commercial services mentioned in this publication.

5.6 References

1. May, J. C.; Morris, C. B.; McLean, J. A. *Anal. Chem.* 2017, 89 (2), 1032-1044.
2. Metz, T. O.; Baker, E. S.; Schymanski, E. L.; Renslow, R. S.; Thomas, D. G.; Causon, T. J.; Webb, I. K.; Hann, S.; Smith, R. D.; Teeguarden, J. G. *Bioanalysis* 2017, 9 (1), 81-98.
3. Sans, M.; Feider, C. L.; Eberlin, L. S. *Curr. Opin. Chem. Biol.* 2018, 42, 138-146.
4. Schrimpe-Rutledge, A. C.; Sherrod, S. D.; McLean, J. A. *Curr. Opin. Chem. Biol.* 2018, 42, 160-166.
5. Morrison, K. A.; Clowers, B. H. *Curr. Opin. Chem. Biol.* 2018, 42, 119-129.
6. May, J. C.; Gant-Branum, R. L.; McLean, J. A. *Curr. Opin. Biotech.* 2016, 39, 192-197.
7. May, J. C.; McLean, J. A. *Anal. Chem.* 2015, 87 (3), 1422-1436.
8. May, J. C.; McLean, J. A. *Annu. Rev. Anal. Chem.* 2016, 9 (1), 387-409.
9. Purves, R. W.; Ozog, A. R.; Ambrose, S. J.; Prasad, S.; Belford, M.; Dunyach, J. J. *J. Am. Soc. Mass Spectr.* 2014, 25 (7), 1274-1284.
10. Waraksa, E.; Perycz, U.; Namiesnik, J.; Sillanpää, M.; Dymerski, T.; Wojtowicz, M.; Puton, J. *Trends Anal. Chem.* 2016, 82, 237-249.
11. Schneider, B. B.; Covey, T. R.; Nazarov, E. G. *Int. J. Ion. Mobil. Spectrom.* 2013, 16 (3), 207-216.
12. Kafle, A.; Coy, S. L.; Wong, B. M.; Fornace, A. J.; Glick, J. J.; Vouros, P., J. *Am. Soc. Mass Spectr.* 2014, 25 (7), 1098-1113.
13. Levin, D. S.; Vouros, P.; Miller, R. A.; Nazarov, E. G.; Morris, J. C. *Anal. Chem.* 2006, 78 (1), 96-106.
14. Porta, T.; Varesio, E.; Hopfgartner, G., *Anal. Chem.* 2013, 85 (24), 11771-11779.
15. Waraksa, E.; Perycz, U.; Namieśnik, J.; Sillanpää, M.; Dymerski, T.; Wójtowicz, M.; Puton, J., *Trends Anal. Chem.* 2016, 82, 237-249.
16. Fernández-Maestre, R.; Wu, C.; Hill Jr., H. H. *Rapid Commun. Mass Spectrom.* 2012, 26 (19), 2211-2223.
17. Butcher, D.; Miksovská, J.; Ridgeway, M. E.; Park, M. A.; Fernandez-Lima, F. *Rapid Commun. Mass Spectrom.* 2018, 0 (ja).
18. Garabedian, A.; Leng, F.; Ridgeway, M. E.; Park, M. A.; Fernandez-Lima, F. *Int. J. Ion. Mobil. Spectrom.* 2018, 21 (1), 43-48.

19. Asbury, G. R.; Hill, H. H. *Anal. Chem.* 2000, 72 (3), 580-584.
20. Beegle, L. W.; Kanik, I.; Matz, L.; Hill, H. H. *Anal. Chem.* 2001, 73 (13), 3028-3034.
21. Beegle, L. W.; Kanik, I.; Matz, L.; Hill, H. H. *Int. J. Mass Spectrom.* 2002, 216 (3), 257-268.
22. Matz, L. M.; Hill, H. H., Jr.; Beegle, L. W.; Kanik, I. J. *Am. Soc. Mass Spectr.* 2002, 13 (4), 300-307.
23. Fasciotti, M.; Sanvido, G. B.; Santos, V. G.; Lalli, P. M.; McCullagh, M.; de Sa, G. F.; Daroda, R. J.; Peter, M. G.; Eberlin, M. N. *J. Mass Spectrom.* 2012, 47 (12), 1643-1647.
24. Fasciotti, M.; Lalli, P. M.; Klitzke, C. F.; Corilo, Y. E.; Pudenzi, M. A.; Pereira, R. C. L.; Bastos, W.; Daroda, R. J.; Eberlin, M. N. *Energy & Fuels* 2013, 27 (12), 7277-7286.
25. Lalli, P. M.; Corilo, Y. E.; Fasciotti, M.; Riccio, M. F.; de Sa, G. F.; Daroda, R. J.; Souza, G.; McCullagh, M.; Bartberger, M. D.; Eberlin, M. N.; Campuzano, I. D. G. *J. Mass Spectrom.* 2013, 48 (9), 989-997.
26. Bataglione, G. A.; Souza, G. H.; Heerdt, G.; Morgon, N. H.; Dutra, J. D.; Freire, R. O.; Eberlin, M. N.; Tata, A. J. *Mass Spectrom.* 2015, 50 (2), 336-43.
27. Chouinard, C. D.; Beekman, C. R.; Kemperman, R. H. J.; King, H. M.; Yost, R. A. *Int. J. Ion Mobil. Spectrom.* 2017, 20 (1), 31-39.
28. Ruotolo, B. T.; McLean, J. A.; Gillig, K. J.; Russell, D. H. *J. Mass Spectrom.* 2004, 39 (4), 361-367.
29. Howdle, M. D.; Eckers, C.; Laures, A. M. F.; Creaser, C. S. *Int. J. Mass Spectrom.* 2010, 298 (1-3), 72-77.
30. Jurneczko, E.; Kalapothakis, J.; Campuzano, I. D. G.; Morris, M.; Barran, P. E. *Anal. Chem.* 2012, 84 (20), 8524-8531.
31. Davidson, K. L.; Bush, M. F. *Anal. Chem.* 2017, 89 (3), 2017-2023.
32. Kurulugama, R. T.; Darland, E.; Kuhlmann, F.; Stafford, G.; Fjeldsted, J. *Analyst* 2015, 14 (20), 6834-6844.
33. Dodds, J. N.; May, J. C.; McLean, J. A. *Anal. Chem.* 2017, 89 (22), 12176-12184.
34. Stow, S. M.; Causon, T. J.; Zheng, X. Y.; Kurulugama, R. T.; Mairinger, T.; May, J. C.; Rennie, E. E.; Baker, E. S.; Smith, R. D.; McLean, J. A.; Hann, S.; Fjeldsted, J. C. *Anal. Chem.* 2017, 89 (17), 9048-9055.
35. May, J. C.; Jurneczko, E.; Stow, S. M.; Kratochvil, I.; Kalkhof, S.; McLean, J. A. *Int. J. Mass Spectrom.* 2018, 427, 79-90.

36. Paglia, G.; Williams, J. P.; Menikarachchi, L.; Thompson, J. W.; Tyldesley-Worster, R.; Halldórsson, S.; Rolfsson, O.; Moseley, A.; Grant, D.; Langridge, J.; Palsson, B. O.; Astarita, G. *Anal. Chem.* 2014, 86 (8), 3985-3993.
37. Paglia, G.; Angel, P.; Williams, J. P.; Richardson, K.; Olivos, H. J.; Thompson, J. W.; Menikarachchi, L.; Lai, S.; Walsh, C.; Moseley, A.; Plumb, R. S.; Grant, D. F.; Palsson, B. O.; Langridge, J.; Geromanos, S.; Astarita, G. *Anal. Chem.* 2015, 87 (2), 1137-1144.
38. Regueiro, J.; Negreira, N.; Berntssen, M. H. G. *Anal. Chem.* 2016, 88 (22), 11169-11177.
39. D'Atri, V.; Causon, T.; Hernandez-Alba, O.; Mutabazi, A.; Veuthey, J. L.; Cianferani, S.; Guillarme, D. *J. Sep. Sci.* 2018, 41 (1), 20-67.
40. Nichols, C. M.; Dodds, J. N.; Rose, B. S.; Picache, J. A.; Morris, C. B.; Codreanu, S. G.; May, J. C.; Sherrod, S. D.; McLean, J. A. *Anal. Chem.* 2018.
41. Tao, L.; McLean, J. R.; McLean, J. A.; Russell, D. H. *J. Am. Soc. Mass Spectr.* 2007, 18 (7), 1232-1238.
42. Fernandez-Lima, F. A.; Blase, R. C.; Russell, D. H. *Int. J. Mass Spectrom.* 2010, 298 (1), 111-118.
43. May, J. C.; Goodwin, C. R.; Lareau, N. M.; Leaptrot, K. L.; Morris, C. B.; Kurulugama, R. T.; Mordehai, A.; Klein, C.; Barry, W.; Darland, E.; Overney, G.; Imatani, K.; Stafford, G. C.; Fjeldsted, J. C.; McLean, J. A. *Anal. Chem.* 2014, 86 (4), 2107-2116.
44. May, J. C.; Dodds, J. N.; Kurulugama, R. T.; Stafford, G. C.; Fjeldsted, J. C.; McLean, J. A. *Analyst* 2015, 140 (20), 6824-6833.
45. Kemper, P. R.; Bowers, M. T. *J. Am. Soc. Mass Spectr.* 1990, 1 (3), 197-207.
46. May, J. C.; McLean, J. A. *Proteomics* 2015, 15 (16), 2862-2871.
47. Picache, J. A.; Rose, B. S.; Balinski, A.; Leaptrot, K. L.; Sherrod, S. D.; May, J. C.; McLean, J. A. *Chem. Sci.* 2019.
48. Campuzano, I.; Bush, M. F.; Robinson, C. V.; Beaumont, C.; Richardson, K.; Kim, H.; Kim, H. I. *Anal. Chem.* 2012, 84 (2), 1026-1033.
49. Bush, M. F.; Hall, Z.; Giles, K.; Hoyes, J.; Robinson, C. V.; Ruotolo, B. T. *Anal. Chem.* 2010, 82 (22), 9557-9565.
50. Ellis, H. W.; McDaniel, E. W.; Albritton, D. L.; Viehland, L. A.; Lin, S. L.; Mason, E. A. *Atom. Data Nucl. Data* 1978, 22 (3), 179-217.
51. May, J. C.; Russell, D. H. *J. Am. Soc. Mass Spectr.* 2011, 22 (7), 1134-1145.
52. Clemmer, D. E.; Jarrold, M. F. *J. Mass Spectrom.* 1997, 32 (6), 577-592.

53. Henderson, S. C.; Valentine, S. J.; Counterman, A. E.; Clemmer, D. E. *Anal. Chem.* 1999, 71 (2), 291-301.
54. Hines, K. M.; May, J. C.; McLean, J. A.; Xu, L. *Anal. Chem.* 2016, 88 (14), 7329-7336.
55. Fenn, L. S.; McLean, J. A. *Mol. Biosyst.* 2009, 5 (11), 1298-1302.
56. McLean, J. A. *J. Am. Soc. Mass Spectr.* 2009, 20 (10), 1775-1781.
57. Lalli, P. M.; Corilo, Y. E.; Fasciotti, M.; Riccio, M. F.; de Sa, G. F.; Daroda, R. J.; Souza, G. H. M. F.; McCullagh, M.; Bartberger, M. D.; Eberlin, M. N.; Campuzano, I. D. G. *J. Mass Spectrom.* 2013, 48 (9), 989-997.
58. Rumble, J. R., *CRC Handbook of Chemistry and Physics*. 99th ed.; CRC Press/Taylor & Francis: Boca Raton, FL, 2018.

CHAPTER 6

CONCLUSION AND FUTURE DIRECTIONS

6.1 Conclusion

Ion mobility-mass spectrometry (IM-MS) has been established as a valuable technique by adding a reproducible molecular descriptor that allows for enhanced identification of unknowns beyond using mass spectrometry alone. In addition, IM improves peak capacity and allows inference of structural information based on the experimental CCS. For improvement of unknown identification, databases have been created. Databases with multiple descriptors including collision cross section (CCS) have great utility in untargeted workflows or large-scale analyses with complex biological samples to which IM-MS is well suited. Databases also enable development of predictive methods for CCS to further assist unknown identification. This work has encompassed a large collection of canonical literature CCS values, identifying important analytical trends in IM and underrepresented areas of study where a significant impact can be made. This CCS compilation provides the basis for predicting CCS chemical space occupancy and enables large-scale studies of chemical class relationships. It also provides a foundation for utilizing CCS as a molecular descriptor in future work. Furthermore, utilizing a commercially available drift tube IM-MS, a CCS database was created of metabolite standards. This descriptor adds information that can allow identification of isomers without the need for costly ultra-high resolution mass spectrometers with long analysis times, hindering high throughput methods. This study shows the benefits in using an orthogonal separation such as IM to improve isomer separation. Further improvement on separation is still needed. Alternate drift gases show potential in this area but have

not been well studied. An initial study of multiple classes was conducted in nitrogen and compared to helium literature values. Class filtering was shown in both drift gases, creating disparate trend lines for each class based on gas-phase packing efficiency. It was noted that TAA salts were the least efficient in packing followed by lipids, peptides, and carbohydrates. Differences at low mass could be seen between helium and nitrogen trend lines, indicating that drift gas can affect separation. Instrument operating parameters had to be developed for further investigation of CCS under a variety of conditions such as alternate drift gases. After development of such methodology, the effect of drift gas on CCS was investigated and further instrument parameters defined for operation under different drift gases to include He, N₂, Ar, and CO₂. A large set of various classes spanning a wide range of mobilities, masses, and charge states were investigated in these four drift gases. Recommendations were made for the selection and use of each drift gas based on this investigation. It was found that CCS trends correlated strongly with drift gas polarizability, allowing for prediction of relative elution orders in drift gases not yet investigated. This work presents a significant study of drift gases spanning a broad range of classes, mobilities, masses, and charge states to aid future work with alternate drift gases. The recommendations made here give future investigators the tools for selection of alternate drift gases. This work also can be used to improve fundamental IM theory as well as aid in generating algorithms that predict mobility elution order based on drift gas parameters. Based on this work, there are several avenues for future investigations.

6.2 Future Directions

6.2.1 Mathematical Descriptors in Databases

As databases become increasingly populated with high quality CCS data, it becomes imperative to describe this data in a meaningful way for analysis of trends and enabling predictive capabilities. Mathematical descriptors can be used as a predictive tool where unknowns are classified based on proximity to various trends. This prediction can be used as an enhancement to other descriptors such as mass, charge state, ion adduct, and LC retention time to improve unknown identification. Mathematical descriptors have already been discussed in this work but relied on the relatively simple power fit. This is an appropriate descriptor until inclusion of low mass (<200 Da) data. With this inclusion, more complex descriptors such as sigmoidal fits become necessary. These equations can predict the minimum cross section achievable in a drift gas. This value has been calculated with the mobility of polarization where the minimum mobility in a drift gas is based off the drift gas polarizability.¹ However, with these equations, such drift gas values can be empirically derived from large datasets in multiple drift gases in the future. Such mathematical descriptors need further development. Complex mathematical formulas may not be utilized by many investigators as quickly as more simple power law descriptors. However, with online databases being developed, such complexity can be programmed into an online interface to facilitate ease of use. For example, a user should need to only input the unknown's CCS, mass, and other relative information into the interface and the mathematical descriptor should be applied immediately to generate predictions on class. Simultaneously, using this generated class prediction and the information entered by the user, the unknown should be compared to the entire database, generating a series of possible matches scored based on how well each possible match aligns with

the unknown. With current IM-MS technology able to generate highly reproducible CCS values in a wide range of drift gases, databases will continue to grow and with it, the need for mathematical descriptors.

6.2.2 CCS Prediction

There is a need for rapid prediction of CCS in a variety of drift gases. Algorithms based on first principles are both complex and computationally expensive.² Here, a possible way of predicting CCS is presented using an empirical method to achieve CCS prediction. This method would be simpler than current computational methods, which can take hours or days for a predicted CCS, and could be implemented using an online interface. A user would enter an unknown's mass, CCS, charge state, and the drift gas used to generate the CCS, and this method would generate a list of CCS values in other drift gases in seconds. The method starts with the understanding that CCS is a rotationally averaged collision cross section. As such, CCS can be described as a circle

$$CCS = \pi(r_{molecule} + r_{gas})^2 \quad (6.1)$$

where the radius is made up of the sum of the molecular and drift gas radii. From this, an equation can be derived describing the relationship between the CCS of an analyte in one drift gas to the CCS of that analyte in another drift gas. The derivation is shown in Figure 6.1 with the final relationship shown as

$$CCS_{gas_1} = CCS_{gas_2} + C_1\sqrt{CCS_{gas_2}} + C_2 \quad (6.2)$$

where C_1 and C_2 are constants defined in Figure 6.1. The equation solely accounts for hard sphere interactions. If a helium CCS is attempted to be converted into a nitrogen CCS, this equation will underestimate the nitrogen CCS as it does not account for all interactions. To account for long range interaction potentials, the radius definition for each drift gas in the equation must be

$r_{molecule}$ = radius of the molecule r_{gas1} = radius of gas 1 r_{gas2} = radius of gas 2

CCS_{gas1} = collision cross section of the molecule in gas 1

CCS_{gas2} = collision cross section of the molecule in gas 2

$$CCS_{gas1} = \pi(r_{molecule} + r_{gas1})^2$$

$$CCS_{gas2} = \pi(r_{molecule} + r_{gas2})^2$$

$$\pi r_{molecule}^2 + 2\pi r_{gas1} r_{molecule} + \pi r_{gas1}^2 - CCS_{gas1} = 0$$

$$\pi r_{molecule}^2 + 2\pi r_{gas2} r_{molecule} + \pi r_{gas2}^2 - CCS_{gas2} = 0$$

$$r_{molecule} = \frac{-b \pm \sqrt{b^2 - 4ac}}{2a}$$

$$\frac{-2\pi r_{gas1} \pm \sqrt{(2\pi r_{gas1})^2 - 4\pi(\pi r_{gas1}^2 - CCS_{gas1})}}{2\pi} = \frac{-2\pi r_{gas2} \pm \sqrt{(2\pi r_{gas2})^2 - 4\pi(\pi r_{gas2}^2 - CCS_{gas2})}}{2\pi}$$

$$-2\pi r_{gas1} \pm \sqrt{4\pi^2 r_{gas1}^2 - 4\pi^2 r_{gas1}^2 + 4\pi CCS_{gas1}} = -2\pi r_{gas2} \pm \sqrt{4\pi^2 r_{gas2}^2 - 4\pi^2 r_{gas2}^2 + 4\pi CCS_{gas2}}$$

$$-2\pi r_{gas1} \pm \sqrt{4\pi CCS_{gas1}} = -2\pi r_{gas2} \pm \sqrt{4\pi CCS_{gas2}}$$

$$r_{molecule} > 0$$

$$-2\pi r_{gas1} + \sqrt{4\pi CCS_{gas1}} = -2\pi r_{gas2} + \sqrt{4\pi CCS_{gas2}}$$

$$2\sqrt{\pi} \sqrt{CCS_{gas1}} - 2\sqrt{\pi} \sqrt{CCS_{gas2}} = 2\pi(r_{gas1} - r_{gas2})$$

$$\sqrt{CCS_{gas1}} = \sqrt{CCS_{gas2}} + \sqrt{\pi}(r_{gas1} - r_{gas2})$$

$$CCS_{gas1} = CCS_{gas2} + 2\sqrt{\pi}(r_{gas1} - r_{gas2})\sqrt{CCS_{gas2}} + \pi(r_{gas1} - r_{gas2})^2$$

$$C_1 = 2\sqrt{\pi}(r_{gas1} - r_{gas2})$$

$$C_2 = \pi(r_{gas1} - r_{gas2})^2$$

$$CCS_{gas1} = CCS_{gas2} + C_1\sqrt{CCS_{gas2}} + C_2$$

Figure 6.1 Derivation of a mathematical relationship between CCS in gas 1 to CCS in gas 2 based solely on hard sphere interactions.

modified. It has been noted that to describe empirical mobility data, the drift gas radius should vary based on the analyte mass,³ where a given gas radius is defined as⁴

$$r_{gas} = (r_{0gas} + z_{gas} * mass_{molecule}) * \left(1 + \left(\frac{mass_{molecule}}{mass_{gas}} \right)^{\frac{1}{3}} \right) \quad (6.3)$$

where r_{0gas} is the hard sphere radius of the gas, z_{gas} is a correction factor and a constant, $mass_{molecule}$ is the analyte mass, and $mass_{gas}$ is the drift gas mass. Note that when the analyte mass reaches zero, the radius of the drift gas is equivalent to its hard sphere radius. Substituting Equation 6.3 for radius in the definitions for C_1 and C_2 in Equation 6.2 results in a complex equation where the constants z and r_0 must be defined for each drift gas through numerical analysis for a given class and charge state. A table of constants could be generated this way. Though these initial calculations would be computationally expensive, the advantage over current methods is that once completed, the equation can be paired with previously generated constants to quickly predict the CCS value for an analyte based on its previous drift gas CCS value, its charge state, and class. This last calculation could easily be completed through an online interface where users would enter the relevant data and the equation would be ran with the necessary constants pulled from the previously generated table. To generate reliable constants, these numerical analyses will require a large set of analytes across multiple drift gases. With the parameters established in this work to achieve reproducible CCS in multiple drift gases, such a large set can now be obtained across a wide range of drift gases for further development of this CCS prediction method.

6.2.3 Drift Gas Selection

Drift gases have been shown in this work to exhibit selectivity for certain classes. It has been shown here and elsewhere⁵⁻⁶ that polarizability correlates strongly with CCS, with certain classes and charge states exhibiting greater CCS increase as drift gas polarizability increases. This

trend hints at the potential use of drift gas polarizability for prediction of relative IM elution orders if class and charge state are known. Additionally, this effect has the potential to allow classification of unknowns based on behavior in multiple drift gases. Where an unknown in one drift gas may not easily be classified based on proximity to known class trends in said drift gas, analysis of this unknown in multiple alternate drift gases may allow a mobility profile to be developed. This mobility profile would track the unknown's mobility as a function of drift gas polarizability and be compared to profiles of known classes. In this way, a more definitive classification may be made. Further analysis of this trend as well as developing a large database of values in multiple drift gases will require careful selection of alternate drift gases. Drift gas selection in future studies should consider the mass and polarizability of the drift gas. The magnitude of the effect of drift gas mass and drift gas polarizability across multiple classes, mobilities, analyte masses, and charge states is still unclear. Certain drift gases chosen in this work allowed for comparison of results from drift gases that either have similar polarizability or similar mass. Argon has similar polarizability to nitrogen but similar mass to carbon dioxide. CCS values in argon were closer to that of nitrogen than carbon dioxide, indicating that polarizability may have a greater effect on CCS than drift gas mass. If such an observation were to be further described along with investigation of this effect in other drift gases selected in the same fashion, this would greatly improve fundamental IM understanding and prediction of drift gas effect. Other drift gases to investigate beyond nitrogen, argon and carbon dioxide include but are not limited to krypton, carbon tetrafluoride, xenon, and sulfur hexafluoride. From this list, several groups of three can be made wherein two of the three have similar polarizability and another two of the three have similar mass. This is graphically represented in Figure 6.2. Such analysis would build upon the methods

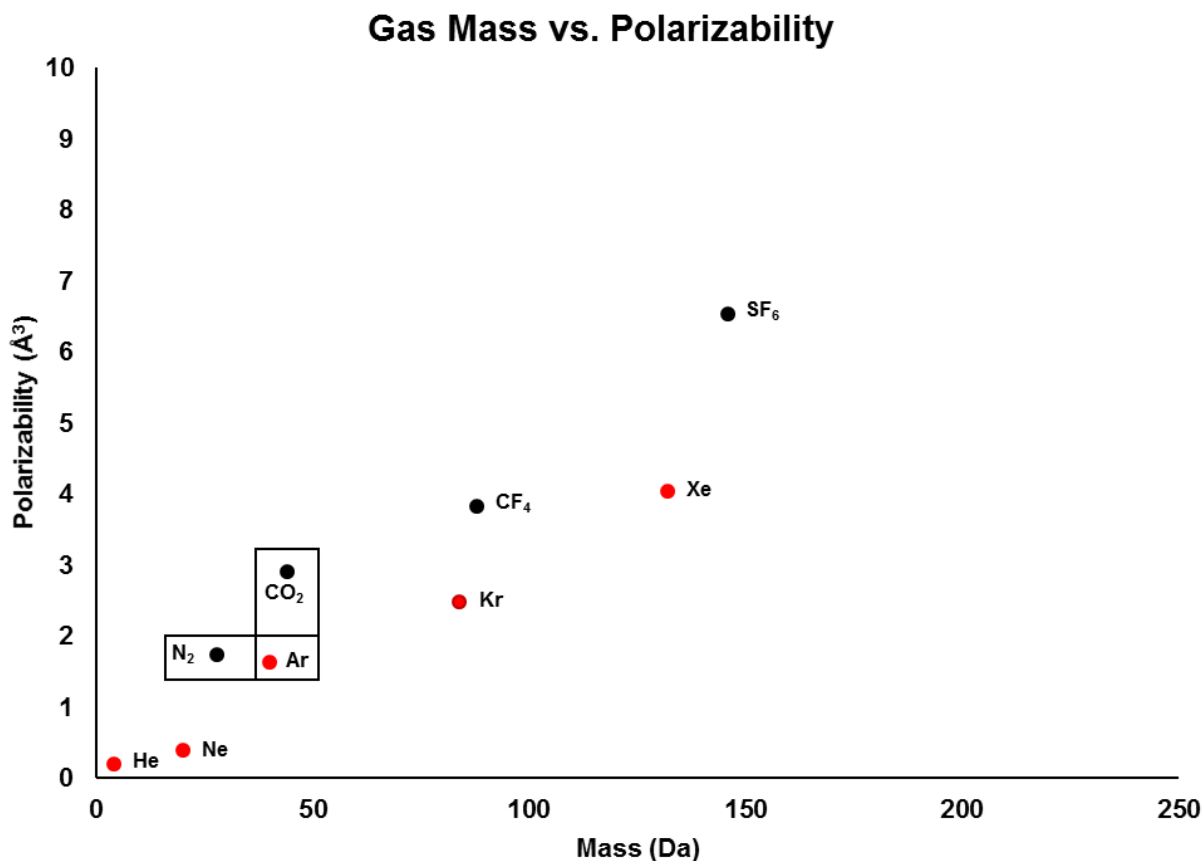


Figure 6.2 A list of possible drift gases for use in future drift gas studies. A method for selecting a group comprised of three drift gases is shown. Such a selection results in two of the three drift gases (nitrogen and argon) having similar polarizability and two of the three drift gases (argon and carbon dioxide) having similar mass. In future work, groups of three drift gases can be chosen to achieve a similar result, such as a group comprised of krypton, carbon tetrafluoride, and xenon.

and instrumental parameters demonstrated in this work and enable further description of the drift gas effect in terms of drift gas polarizability and mass.

6.3 References

1. Mason, E. A.; McDaniel, E. W. Wiley: New York, 1973; p 372.
2. Mason, E. A.; McDaniel, E. W. John Wiley & Sons: New York, 1988; p 560.
3. Karpas, Z.; Berant, Z. J. Phys. Chem. 1989, 93 (8), 3021-3025.
4. Berant, Z.; Karpas, Z. J. Amer. Chem. Soc. 1989, 111 (11), 3819-3824.
5. Matz, L. M.; Hill, H. H., Jr.; Beegle, L. W.; Kanik, I. J. Am. Soc. Mass Spectrom. 2002, 13 (4), 300-307.
6. Asbury, G. R.; Hill, H. H. Anal. Chem. 2000, 72 (3), 580-584.

APPENDIX A

REFERENCES FOR ADAPTATION OF CHAPTERS

- Chapter 1. **Caleb B. Morris**, James C. Poland, Jody C. May, John A. McLean, “Fundamentals of Ion Mobility Mass Spectrometry for the Analysis of Biomolecules,” Invited chapter for inclusion in “Ion Mobility Mass Spectrometry – Methods and Protocols,” Guiseppe Astarita and Guiseppe Paglia, Eds., Springer Nature (to be published in 2019)
- Chapter 2. Jody C. May, **Caleb B. Morris**, John A. McLean, “Ion Mobility Collision Cross Section Compendium,” *Analytical Chemistry* **2017**, *89* (2), 1032-1044.
- Chapter 3. Charles M. Nichols, James N. Dodds, Bailey S. Rose, Jaqueline A. Picache, **Caleb B. Morris**, Simona G. Codreanu, Jody C. May, Stacy D. Sherrod, John A. McLean, “Untargeted Molecular Discovery in Primary Metabolism: Collision Cross Section as a Molecular Descriptor in Ion Mobility-Mass Spectrometry,” *Analytical Chemistry* **2018**, *90* (24), 14484-14492.
- Chapter 4. Jody C. May, Cody R. Goodwin, Nichole M. Lareau, Katrina L. Leaptrot, **Caleb B. Morris**, Ruwan T. Kurulugama, A. Mordehai, C. Klein, W. Barry, E. Darland, G. Overney, K. Imatani, George C. Stafford, John C. Fjeldsted, John A. McLean, “Conformational Ordering of Biomolecules in the Gas Phase: Nitrogen Collision Cross Sections Measured on a Prototype High Resolution Drift Tube Ion Mobility-Mass Spectrometer,” *Analytical Chemistry* **2014**, *86* (4), 2107-2116.
- Chapter 5. **Caleb B. Morris**, Jody C. May, Katrina L. Leaptrot, and John A. McLean, “Evaluating Separation Selectivity and Collision Cross Section Measurement Reproducibility in Helium, Nitrogen, Argon, and Carbon Dioxide Drift Gases for Drift Tube Ion Mobility-Mass Spectrometry,” *Journal of the American Society for Mass Spectrometry* **2019** (in press)

APPENDIX B

SUPPLEMENTAL INFORMATION FOR CHAPTER 3

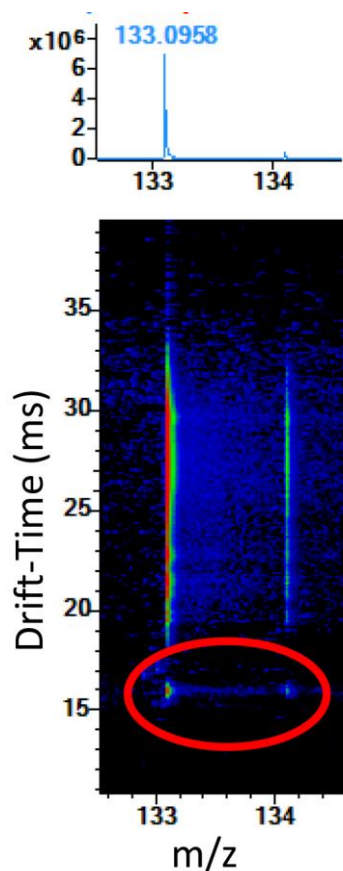


Figure B.1. IM-MS spectra for D-Ornathine. The standard is subject to metastable ion dissociation in the DTIMS, resulting in uncorrelated mobility. The true reported conformer is circled in red. Reprinted (adapted) with permission from Charles M. Nichols, James N. Dodds, Bailey S. Rose, Jaqueline A. Picache, Caleb B. Morris, Simona G. Codreanu, Jody C. May, Stacy D. Sherrod, John A. McLean, "Untargeted Molecular Discovery in Primary Metabolism: Collision Cross Section as a Molecular Descriptor in Ion Mobility-Mass Spectrometry," *Analytical Chemistry* 2018, 90 (24), 14484-14492. Copyright 2018 American Chemical Society.

Mass/Mobility Fitting Equations: Power fits for biomolecular superclasses selected in the manuscript (See Figure 3.2).

Power Association (General)

$$y = y_0 + (\text{plateau} - y_0) * (1 - e^{-Kx}) \quad (\text{B.1})$$

4P sigmoidal (General)

$$y = y_0 + \frac{y_{max} - y_0}{1 + 10^{(\log y_{50} - x) \cdot H}} \quad (\text{B.2})$$

Lipids and lipid-like molecules- Power association

$$y = 75.41 + (516.9 - 75.41) * (1 - e^{-0.000851x}) \quad (\text{B.3})$$

Organic oxygen compounds- Power association

$$y = 101.9 + (935.0 - 101.9) * (1 - e^{-0.000251x}) \quad (\text{B.4})$$

Nucleosides, nucleotides, and analogues- Power association

$$y = 117.6 + (1.52 \times 10^7 - 117.6) * (1 - e^{-1.06 \times 10^{-8}x}) \quad (\text{B.5})$$

Organic acids and derivatives – 4P sigmoidal

$$y = 104.8 + \frac{216.3 - 104.8}{1 + 10^{(277.4 - x) \cdot 0.00376}} \quad (\text{B.6})$$

Table B.1. Metabolic pathways covered by compounds with at least one measured CCS the MSMLS plate study. (See Figure 3.3) Reprinted (adapted) with permission from Charles M. Nichols, James N. Dodds, Bailey S. Rose, Jaqueline A. Picache, Caleb B. Morris, Simona G. Codreanu, Jody C. May, Stacy D. Sherrod, John A. McLean, “Untargeted Molecular Discovery in Primary Metabolism: Collision Cross Section as a Molecular Descriptor in Ion Mobility-Mass Spectrometry,” *Analytical Chemistry* 2018, 90 (24), 14484-14492. Copyright 2018 American Chemical Society.

Pathway	Total	Expected	Hits	Raw p	#NAME ?	Holm adjust	FDR	Impact	% of Hits
Pyrimidine metabolism	60	10.2	31	5E-10	21.4	4E-08	4E-08	0.7	52
Purine metabolism	92	15.7	34	2E-06	13.0	2E-04	9E-05	0.5	37
Tyrosine metabolism	76	12.9	25	5E-04	7.7	4E-02	1E-02	0.5	33
Alanine, aspartate and glutamate metabolism	24	4.1	11	9E-04	7.0	7E-02	2E-02	0.6	46
beta-Alanine metabolism	28	4.8	12	1E-03	6.8	9E-02	2E-02	0.4	43
Galactose metabolism	41	7.0	15	2E-03	6.2	1E-01	3E-02	0.3	37
Arginine and proline metabolism	77	13.1	23	3E-03	5.7	2E-01	4E-02	0.5	30
Cysteine and methionine metabolism	56	9.5	18	4E-03	5.6	3E-01	4E-02	0.8	32
Glycine, serine and threonine metabolism	48	8.2	15	1E-02	4.5	8E-01	9E-02	0.4	31
Citrate cycle (TCA cycle)	20	3.4	8	1E-02	4.4	9E-01	1E-01	0.3	40
Sulfur metabolism	18	3.1	7	2E-02	3.8	1	2E-01	0.3	39
Nicotinate and nicotinamide metabolism	44	7.5	13	3E-02	3.6	1	2E-01	0.4	30
Amino sugar and nucleotide sugar metabolism	88	15.0	22	3E-02	3.4	1	2E-01	0.5	25
Glutathione metabolism	38	6.5	11	5E-02	3.1	1	3E-01	0.4	29
Phenylalanine metabolism	45	7.7	12	7E-02	2.7	1	3E-01	0.1	27
Ascorbate and aldarate metabolism	45	7.7	12	7E-02	2.7	1	3E-01	0.4	27
Pantothenate and CoA biosynthesis	27	4.6	8	7E-02	2.6	1	3E-01	0.3	30
Biotin metabolism	11	1.9	4	1E-01	2.3	1	4E-01	0.4	36
Taurine and hypotaurine metabolism	20	3.4	6	1E-01	2.2	1	4E-01	0.5	30
Tryptophan metabolism	79	13.5	18	1E-01	2.2	1	4E-01	0.5	23
Nitrogen metabolism	39	6.6	10	1E-01	2.2	1	4E-01	0.0	26
Histidine metabolism	44	7.5	11	1E-01	2.2	1	4E-01	0.4	25
Butanoate metabolism	40	6.8	10	1E-01	2.0	1	4E-01	0.1	25
Starch and sucrose metabolism	50	8.5	12	1E-01	2.0	1	4E-01	0.5	24
Riboflavin metabolism	21	3.6	6	1E-01	2.0	1	4E-01	0.1	29
Caffeine metabolism	21	3.6	6	1E-01	2.0	1	4E-01	0.5	29
D-Arginine and D-ornithine metabolism	8	1.4	3	1E-01	2.0	1	4E-01	0.5	38
Pentose phosphate pathway	32	5.5	8	2E-01	1.8	1	5E-01	0.4	25
Vitamin B6 metabolism	32	5.5	8	2E-01	1.8	1	5E-01	0.4	25
Synthesis and degradation of ketone bodies	6	1.0	2	3E-01	1.3	1	7E-01	0.9	33
Pentose and glucuronate interconversions	53	9.0	11	3E-01	1.3	1	7E-01	0.2	21
D-Glutamine and D-glutamate metabolism	11	1.9	3	3E-01	1.3	1	7E-01	0.1	27
Aminoacyl-tRNA biosynthesis	75	12.8	15	3E-01	1.2	1	7E-01	0.2	20
Lysine biosynthesis	32	5.5	7	3E-01	1.2	1	7E-01	0.3	22
Phenylalanine, tyrosine and tryptophan biosynthesis	27	4.6	6	3E-01	1.2	1	7E-01	0.3	22
Glycerophospholipid metabolism	39	6.6	8	3E-01	1.1	1	8E-01	0.3	21
Valine, leucine and isoleucine degradation	40	6.8	8	4E-01	1.0	1	8E-01	0.2	20
One carbon pool by folate	9	1.5	2	5E-01	0.8	1	1E+00	0.2	22
Glyoxylate and dicarboxylate metabolism	50	8.5	9	5E-01	0.7	1	1E+00	0.1	18
Valine, leucine and isoleucine biosynthesis	27	4.6	5	5E-01	0.7	1	1E+00	0.1	19
Lysine degradation	47	8.0	8	6E-01	0.6	1	1E+00	0.3	17
Fructose and mannose metabolism	48	8.2	8	6E-01	0.5	1	1E+00	0.2	17
Ubiquinone and other terpenoid-quinone biosynthesis	36	6.1	6	6E-01	0.5	1	1E+00	0.2	17
Thiamine metabolism	24	4.1	4	6E-01	0.5	1	1E+00	0.3	17
Fatty acid biosynthesis	49	8.3	8	6E-01	0.5	1	1E+00	0.0	16

Propanoate metabolism	35	6.0	5	7E-01	0.3	1	1E+00	0.1	14
Selenoamino acid metabolism	22	3.7	3	8E-01	0.3	1	1E+00	0.1	14
Linoleic acid metabolism	15	2.6	2	8E-01	0.3	1	1E+00	0.7	13
Cyanoamino acid metabolism	16	2.7	2	8E-01	0.2	1	1E+00	0.0	13
Glycolysis or Gluconeogenesis	31	5.3	4	8E-01	0.2	1	1E+00	0.1	13
Sphingolipid metabolism	25	4.3	3	8E-01	0.2	1	1E+00	0.2	12
Folate biosynthesis	42	7.2	5	9E-01	0.1	1	1E+00	0.1	12
Inositol phosphate metabolism	39	6.6	4	9E-01	0.1	1	1E+00	0.2	10
Pyruvate metabolism	32	5.5	3	9E-01	0.1	1	1E+00	0.0	9
Glycerolipid metabolism	32	5.5	3	9E-01	0.1	1	1E+00	0.0	9
Terpenoid backbone biosynthesis	33	5.6	3	9E-01	0.1	1	1E+00	0.1	9
Methane metabolism	34	5.8	3	9E-01	0.1	1	1E+00	0.0	9
Primary bile acid biosynthesis	47	8.0	4	1E+00	0.0	1	1E+00	0.0	9
Fatty acid metabolism	50	8.5	4	1E+00	0.0	1	1E+00	0.1	8
Retinol metabolism	22	3.7	1	1E+00	0.0	1	1E+00	0.2	5
Fatty acid elongation in mitochondria	27	4.6	1	1E+00	0.0	1	1E+00	0.0	4
N-Glycan biosynthesis	38	6.5	1	1E+00	0.0	1	1E+00	0.0	3
Steroid hormone biosynthesis	99	16.9	6	1E+00	0.0	1	1E+00	0.1	6
Porphyrin and chlorophyll metabolism	104	17.7	6	1E+00	0.0	1	1E+00	0.1	6

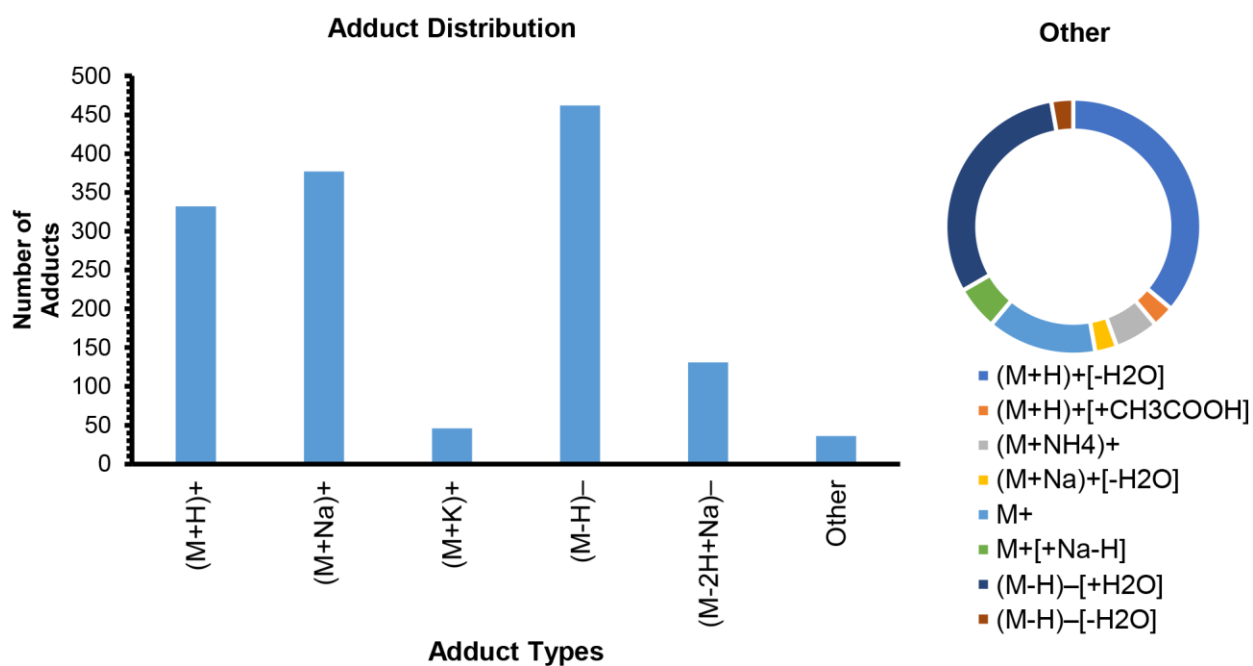


Figure B.2. A distribution of the adduct types observed from the MSMLS study. Reprinted (adapted) with permission from Charles M. Nichols, James N. Dodds, Bailey S. Rose, Jaqueline A. Picache, Caleb B. Morris, Simona G. Codreanu, Jody C. May, Stacy D. Sherrod, John A. McLean, "Untargeted Molecular Discovery in Primary Metabolism: Collision Cross Section as a Molecular Descriptor in Ion Mobility-Mass Spectrometry," *Analytical Chemistry* 2018, 90 (24), 14484-14492. Copyright 2018 American Chemical Society.

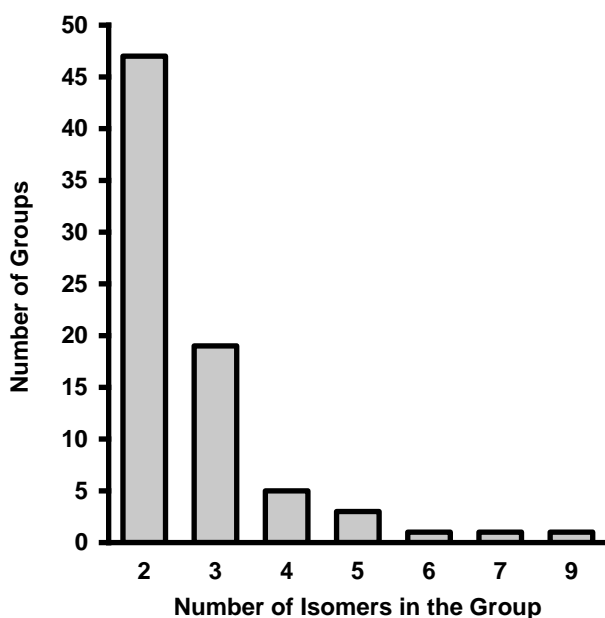


Figure B.3. The distribution of isomeric families within the MSMLS. Most isomeric sets contain 2 or 3 isomers per group, and the largest set contained 9 isomers. Reprinted (adapted) with permission from Charles M. Nichols, James N. Dodds, Bailey S. Rose, Jaqueline A. Picache, Caleb B. Morris, Simona G. Codreanu, Jody C. May, Stacy D. Sherrod, John A. McLean, “Untargeted Molecular Discovery in Primary Metabolism: Collision Cross Section as a Molecular Descriptor in Ion Mobility-Mass Spectrometry,” *Analytical Chemistry* 2018, 90 (24), 14484-14492. Copyright 2018 American Chemical Society.

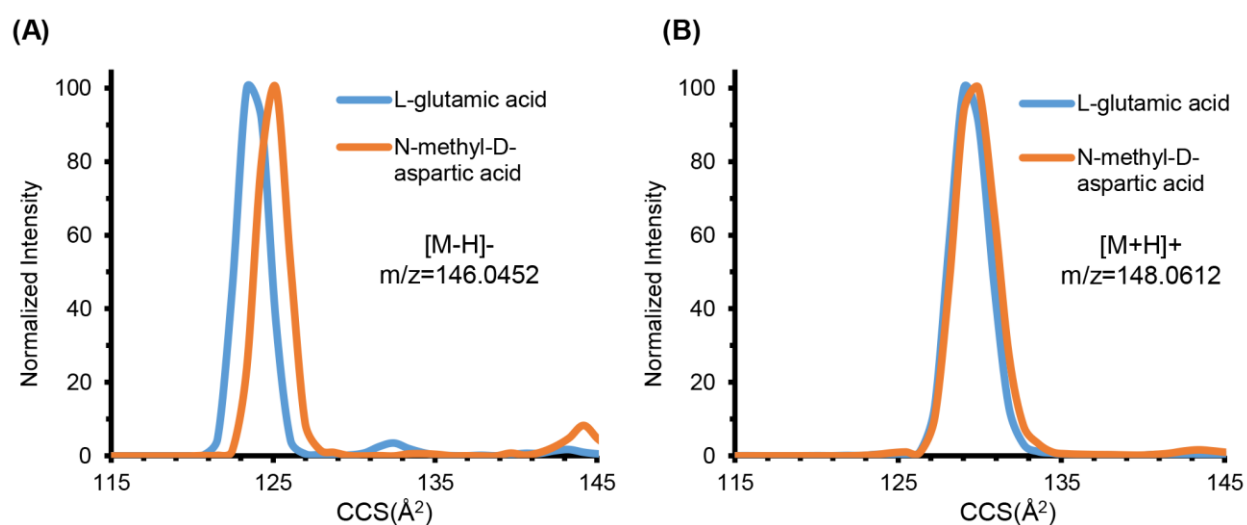


Figure B.4. IM separation of the deprotonated **(A)** and protonated **(B)** isomers of neutral mass 147.0532 (L-glutamic acid and N-methyl-D-aspartic acid). Reprinted (adapted) with permission from Charles M. Nichols, James N. Dodds, Bailey S. Rose, Jaqueline A. Picache, Caleb B. Morris, Simona G. Codreanu, Jody C. May, Stacy D. Sherrod, John A. McLean, “Untargeted Molecular Discovery in Primary Metabolism: Collision Cross Section as a Molecular Descriptor in Ion Mobility-Mass Spectrometry,” *Analytical Chemistry* 2018, 90 (24), 14484-14492. Copyright 2018 American Chemical Society.

APPENDIX C

SUPPLEMENTAL INFORMATION FOR CHAPTER 4

C.1 Comments Regarding Limits of Precision for the CCS Measurements

The experimental uncertainty is determined from technical replicates representing a minimum of six measurements of CCS, obtained during separate instrument acquisitions. We consider a parsimonious approach essential when compiling a database, and thus individual CCS measurements which contributed to a percent relative standard deviation (RSD) beyond 0.5% were generally found to be indicative of a poor centroid fit (*i.e.*, multiple peak features or low ion counting statistics) and ultimately were not included in the datasets reported in this manuscript. While all CCS values reported are better than 0.5% in experimental uncertainty, the accuracy associated with the result is a sum of this experimental reproducibility and the uncertainty associated with measuring each experimental parameter. The CCS uncertainty for significant experimental parameters is estimated as follows for the lowest CCS value measured in this work (TAA3, 144 Å²): Pressure ±0.05 Torr (±1.3%), temperature ±1 K (±0.3%), drift voltage ±2.5 V (±0.2%), and time centroid extraction ±0.1 ms (±0.6%), resulting in a total uncertainty of ±1.5%, as propagated through the Mason-Schamp equation. There is good reason to believe that the measurement precision is better than what is estimated in the above example. Thus, the accuracy of all values within the database is estimated to be better than 2%.

C.2 Notes on Supplemental Tables

In many cases, lower abundance concomitant species were present in the analytical standards, denoted as *derivative signal* in the tables. Analyte identities for the derivative signals are putative and based on the mass measurement. No special considerations were made to optimize for accurate mass data, and so the measured mass and associated accuracies reported in the tables are as obtained from the production prototype instrumentation using an offline calibration. CCS and K_0 measurement precision representing experimental reproducibility error (σ) is reported along with the number of measurements (N). The total accuracy of all transport property values (CCS and K_0) is estimated to be better than 2% (refer to the above discussion).

C.3 Symbol Key, Definitions, and Associated Equations:

Mass Accuracy – Mass accuracy (in ppm) is calculated from the following expression:

$$\text{Mass Accuracy} = \frac{\text{Exact Mass} - \text{Measured Mass}}{\text{Exact Mass}} \cdot 10^6 \quad (\text{C.1})$$

K_0 – Reduced mobility (the mobility scaled to standard temperature and pressure), as calculated from the following equation:

$$K_0 = \frac{L^2}{V \cdot t_d} \left(\frac{273.15}{T} \right) \left(\frac{P}{760} \right) \quad (\text{C.2})$$

Here, L is the drift length (cm), V is the drift voltage (V), t_d is the corrected drift times (s), T is the drift gas temperature (K), and P is the drift gas pressure (Torr). This gives the units of K_0 in $\text{cm}^2 \cdot \text{V}^{-1} \cdot \text{s}^{-1}$. Reduced mobility values are classically reported for small mass ions, and provided in the following tables for convenience.

CCS – The first approximation solution of the momentum transfer collision cross-section, as calculated from the following equation (the expanded Mason-Schamp relationship, Mason & Schamp 1958):

$$CCS = \left(\frac{3 \cdot Z \cdot e_c}{16 \cdot N} \right) \cdot \left(\frac{2\pi}{k_B \cdot T} \right)^{\frac{1}{2}} \cdot \left(\frac{m_{ion} + m_{gas}}{m_{ion} \cdot m_{gas}} \right)^{\frac{1}{2}} \cdot \left(\frac{V \cdot t_d}{L^2} \cdot \frac{273.15}{T} \cdot \frac{P}{760} \right) \quad (C.3)$$

Here, Z is the integer charge state of the ion (unitless), e_c is the constant for elementary charge ($1.60217657 \times 10^{-19}$ C), N is the gas number density (determined from the ideal gas law, in units of molecules/m³), k_B is the Boltzmann constant ($1.3806488 \times 10^{-23}$ J·K⁻¹), m_{ion} is the ion mass (Da), and m_{gas} is the neutral drift gas masses (N₂ in this work, Da), respectively. Other terms are as described previously.

Note that here and by convention, the CCS is reported in units of Å² (square angstroms). In order to obtain square angstroms directly from the above calculation, it is necessary to multiply the expression (in m²) by 10⁻²⁰, with consideration given for converting the above terms to the proper units: e_c (C), N (molecules/m³), k_B (J·K⁻¹), T (K), m_{ion} and m_{gas} (kg), V (V), t_d (s), L (m), and P (Torr).

The CCS expression above is considered a first approximation due to the actual dependency on the cross section on the effective ion temperature (two-temperature theory, Mason & McDaniel 1988, Chapter 6-2-C), which is the gas temperature plus the field-induced ion temperature. In the Agilent IM-MS instrument described in this manuscript, for the smallest ion investigated (TAA3, m/z 186) at the highest drift field utilized (20 V·cm⁻¹ at 4 Torr, or *ca.* 15 Td) the field-induced ion temperature is *ca.* 3 K greater than the gas temperature (Wannier 1953). This affects the magnitude of the CCS by less than 0.5% for the ions investigated in this work and so only the drift gas temperature is used for all CCS calculations. For low mass ions where the CCS values are small, incorporating a higher-order (two- or three-temperature) scaling may be significant.

RSD – Relative standard deviation represents the measurement precision (reported as a unitless percentage) and is calculated as follows:

$$RSD = \frac{\sigma}{average} \cdot 100 \quad (C.4)$$

Here, σ is the standard deviation from multiple measurements.

Analyte Source – Can be either from a known *analytical standard*, or as a *derivative signal* which represents a concomitant ion signal that appears in the samples, often at lower abundances than the standard. For example, the TAA salts were analyzed as received with a reported purity of 98%. The instrument sensitivity was high enough to observe additional ions representing differences of CH_2 (m/z 14), which is suggestive of low abundance impurities possessing various alkyl chain lengths. Note that for the lipid samples, the analyte sources were biological extracts purified into specific lipid classes, thus analyte identifications are putatively based on the mass measurement and the expected mobility-mass correlation trends.

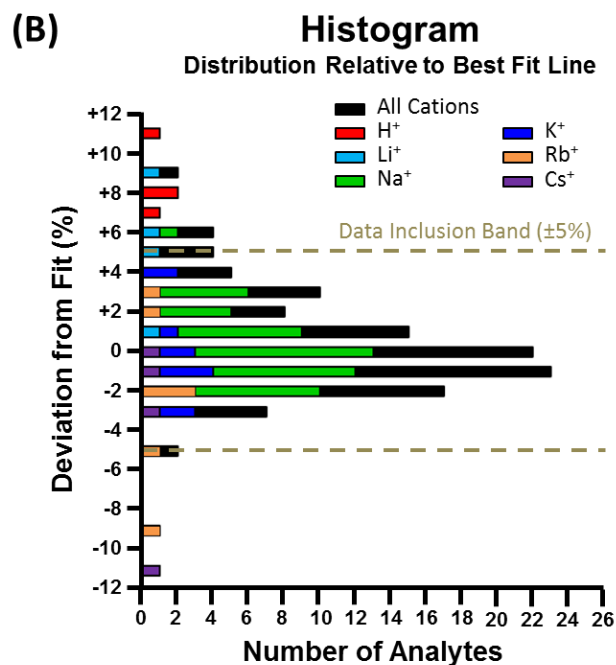
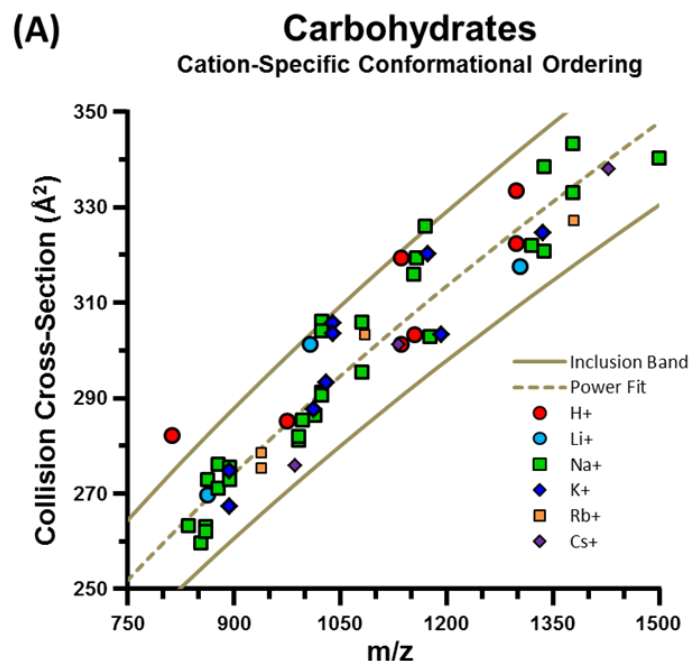


Figure C.1 Cation-Specific Conformational Space Analysis of Carbohydrates. Adapted from Jody C. May, Cody R. Goodwin, Nichole M. Lareau, Katrina L. Leaptrot, Caleb B. Morris, Ruwan T. Kurulugama, A. Mordehai, C. Klein, W. Barry, E. Darland, G. Overney, K. Imatani, George C. Stafford, John C. Fjeldsted, John A. McLean, “Conformational Ordering of Biomolecules in the Gas Phase: Nitrogen Collision Cross Sections Measured on a Prototype High Resolution Drift Tube Ion Mobility-Mass Spectrometer,” *Analytical Chemistry* 2014, 86 (4), 2107-2116. (<https://pubs.acs.org/doi/10.1021/ac4038448>) Note that further permissions related to the material excerpted should be directed to the ACS.

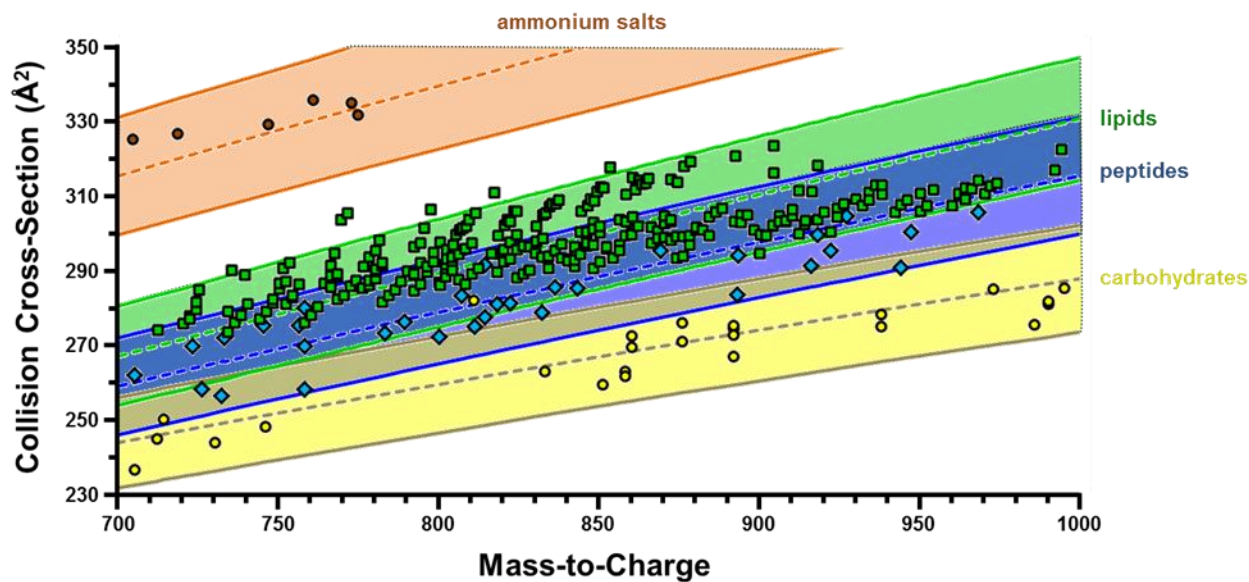


Figure C.2 Class-Specific Mobility-Mass Correlations at Intermediate Mass-to-Charge. Adapted from Jody C. May, Cody R. Goodwin, Nichole M. Lareau, Katrina L. Leaptrot, Caleb B. Morris, Ruwan T. Kurulugama, A. Mordehai, C. Klein, W. Barry, E. Darland, G. Overney, K. Imatani, George C. Stafford, John C. Fjeldsted, John A. McLean, “Conformational Ordering of Biomolecules in the Gas Phase: Nitrogen Collision Cross Sections Measured on a Prototype High Resolution Drift Tube Ion Mobility-Mass Spectrometer,” *Analytical Chemistry* 2014, 86 (4), 2107-2116. (<https://pubs.acs.org/doi/10.1021/ac4038448>) Note that further permissions related to the material excerpted should be directed to the ACS.

Table C.1 Collision Cross-Section Database of Tetraalkylammonium Salt Cations. Adapted from Jody C. May, Cody R. Goodwin, Nichole M. Lareau, Katrina L. Leaptrot, Caleb B. Morris, Ruwan T. Kurulugama, A. Mordehai, C. Klein, W. Barry, E. Darland, G. Overney, K. Imatani, George C. Stafford, John C. Fjeldsted, John A. McLean, "Conformational Ordering of Biomolecules in the Gas Phase: Nitrogen Collision Cross Sections Measured on a Prototype High Resolution Drift Tube Ion Mobility-Mass Spectrometer," *Analytical Chemistry* 2014, 86 (4), 2107-2116. (<https://pubs.acs.org/doi/10.1021/ac4038448>) Note that further permissions related to the material excerpted should be directed to the ACS.

Analyte	z	Exact m/z	Measured m/z	K_0	$K_0 \sigma$	CCS	CCS σ	RSD (%)	N	Analyte Source	Vendor Source
TAA3 - 2H	+	184.21	184.21	1.517	0.007	142.8	0.7	0.5%	14	Derivative Signal	
TAA3	+	186.22	186.22	1.506	0.010	144.0	0.7	0.5%	23	Analytical Standard	Acros Organics
TAA4 - CH4	+	226.25	226.25	1.306	0.005	163.9	0.6	0.3%	16	Derivative Signal	
TAA4 - (CH2) (peak 1)	+	228.27	228.27	1.313	0.005	162.9	0.7	0.4%	15	Derivative Signal	
TAA4 - (CH2) (peak 2)	+	228.27	228.27	1.326	0.006	161.3	0.7	0.5%	7	Derivative Signal	
TAA4	+	242.28	242.28	1.280	0.007	166.6	0.9	0.5%	16	Analytical Standard	Sigma-Aldrich
TAA5 - (CH2)2 - 2H	+	268.30	268.30	1.166	0.004	181.9	0.6	0.3%	8	Derivative Signal	
TAA5 - (CH2)2	+	270.32	270.32	1.163	0.005	182.3	0.7	0.4%	16	Derivative Signal	
TAA5 - (CH2)	+	284.33	284.33	1.155	0.006	183.2	0.9	0.5%	15	Derivative Signal	
TAA5	+	298.35	298.35	1.116	0.003	190.1	1.0	0.5%	28	Analytical Standard	Acros Organics
TAA6 - (CH2)3 - 2H	+	310.34	310.35	1.046	0.003	201.5	0.7	0.3%	16	Derivative Signal	
TAA6 - (CH2)3	+	312.36	312.36	1.074	0.004	196.3	0.7	0.4%	16	Derivative Signal	
TAA6 - (CH2)2	+	326.38	326.38	1.032	0.004	203.7	0.7	0.4%	16	Derivative Signal	
TAA6 - (CH2) - 2H	+	338.37	338.38	1.031	0.004	203.8	0.7	0.4%	15	Derivative Signal	
TAA6 - (CH2)	+	340.39	340.40	1.008	0.002	208.4	0.4	0.2%	16	Derivative Signal	
TAA6 - 2H	+	352.39	352.39	0.971	0.002	215.4	0.9	0.4%	31	Derivative Signal	
TAA6	+	354.41	354.41	0.986	0.003	213.5	1.0	0.5%	31	Analytical Standard	Sigma-Aldrich
TAA7 - (CH2)2	+	382.44	382.44	0.926	0.003	225.8	0.8	0.4%	16	Derivative Signal	
TAA7 - (CH2) (peak 1)	+	396.46	396.45	0.913	0.004	228.7	1.1	0.5%	15	Derivative Signal	
TAA7 - (CH2) (peak 2)	+	396.46	396.45	0.910	0.003	229.4	0.9	0.4%	13	Derivative Signal	
TAA7 - 2H	+	408.46	408.46	0.898	0.004	232.3	0.8	0.3%	28	Derivative Signal	
TAA7	+	410.47	410.47	0.883	0.001	236.4	0.4	0.2%	31	Analytical Standard	Sigma-Aldrich
TAA8 - (CH2)2 - 2H	+	436.49	436.49	0.852	0.002	244.4	0.6	0.3%	31	Derivative Signal	
TAA8 - (CH2)2 (peak 1)	+	438.50	438.50	0.874	0.002	238.3	0.5	0.2%	16	Derivative Signal	
TAA8 - (CH2)2 (peak 2)	+	438.50	438.50	0.855	0.002	243.6	0.7	0.3%	16	Derivative Signal	
TAA8 - (CH2)	+	452.52	452.52	0.827	0.004	251.6	1.2	0.5%	16	Derivative Signal	
TAA8 - 2H	+	464.52	464.52	0.818	0.003	254.3	0.9	0.4%	16	Derivative Signal	
TAA8	+	466.54	466.54	0.808	0.001	256.6	0.7	0.3%	31	Analytical Standard	Acros Organics
TAA10 - (CH2)7	+	480.55	480.55	0.791	0.003	262.5	1.1	0.4%	16	Derivative Signal	
TAA10 - (CH2)6	+	494.57	494.57	0.779	0.002	266.6	0.6	0.2%	31	Derivative Signal	
TAA10 - (CH2)5	+	508.58	508.58	0.769	0.002	269.9	0.7	0.3%	31	Derivative Signal	
TAA10 - (CH2)4 - 2H	+	520.58	520.58	0.781	0.003	265.4	0.9	0.3%	16	Derivative Signal	

TAA10 - (CH2)4 (peak 1)	+	522.60	522.60	0.793	0.003	260.7	1.2	0.5%	31	Derivative Signal	
TAA10 - (CH2)4 (peak 2)	+	522.60	522.60	0.754	0.003	275.5	1.0	0.4%	31	Derivative Signal	
TAA10 - (CH2)2	+	550.63	550.63	0.729	0.002	284.7	0.9	0.3%	28	Derivative Signal	
TAA10 - (CH2)	+	564.64	564.64	0.711	0.002	290.8	0.6	0.2%	28	Derivative Signal	
TAA10	+	578.66	578.66	0.702	0.001	293.5	0.7	0.2%	28	Analytical Standard	Sigma-Aldrich
TAA12 - (CH2)7	+	592.68	592.66	0.697	0.002	296.0	0.8	0.3%	27	Derivative Signal	
TAA12 - (CH2)6	+	606.69	606.68	0.686	0.003	301.5	1.3	0.4%	28	Derivative Signal	
TAA12 - (CH2)4	+	634.72	634.72	0.668	0.003	308.6	1.3	0.4%	14	Derivative Signal	
TAA12 - (CH2)3	+	648.74	648.74	0.649	0.002	317.6	1.2	0.4%	9	Derivative Signal	
TAA12 - (CH2)2	+	662.75	662.75	0.655	0.002	316.3	1.6	0.5%	22	Derivative Signal	
TAA12 - (CH2)	+	676.77	676.77	0.641	0.002	320.1	1.5	0.5%	21	Derivative Signal	
TAA12	+	690.79	690.79	0.644	0.002	319.0	0.9	0.2%	24	Analytical Standard	Sigma-Aldrich
TAA16 - (CH2)15	+	704.80	704.80	0.627	0.000	325.5	1.6	0.5%	18	Derivative Signal	
TAA16 - (CH2)14	+	718.82	718.82	0.625	0.002	327.2	1.6	0.5%	22	Derivative Signal	
TAA16 - (CH2)12	+	746.85	746.85	0.624	0.002	329.6	1.0	0.3%	12	Derivative Signal	
TAA16 - (CH2)11	+	760.86	760.86	0.611	0.003	336.3	1.6	0.5%	9	Derivative Signal	
TAA16 - (CH2)10 - 2H	+	772.86	772.87	0.613	0.002	335.3	1.0	0.3%	11	Derivative Signal	
TAA16 - (CH2)10	+	774.88	774.88	0.619	0.001	332.1	0.4	0.1%	12	Derivative Signal	
TAA16 - (CH2)2	+	887.00	887.01	0.562	0.002	364.6	1.3	0.4%	9	Derivative Signal	
TAA16 - (CH2)	+	901.02	901.03	0.584	0.002	350.9	1.3	0.4%	8	Derivative Signal	
TAA16	+	915.04	915.04	0.569	0.004	360.3	0.9	0.2%	25	Analytical Standard	Sigma-Aldrich
TAA18 - (CH2)7	+	929.05	929.04	0.577	0.003	355.1	1.8	0.5%	10	Derivative Signal	
TAA18 - (CH2)6	+	943.07	943.07	0.554	0.002	369.7	1.4	0.4%	10	Derivative Signal	
TAA18 - (CH2)4	+	971.10	971.09	0.578	0.002	354.5	1.4	0.4%	6	Derivative Signal	
TAA18 - (CH2)2	+	999.13	999.12	0.540	0.002	379.2	1.2	0.3%	6	Derivative Signal	
TAA18	+	1027.16	1027.16	0.538	0.002	379.0	1.7	0.3%	6	Analytical Standard	Alfa Aesar
TAA (1064)	+	1064.17	1064.15	0.521	0.002	392.7	1.3	0.3%	8	Derivative Signal	
TAA (1120)	+	1120.23	1120.22	0.495	0.002	412.8	1.9	0.5%	6	Derivative Signal	
TAA (1232)	+	1232.36	1232.34	0.476	0.002	428.6	1.9	0.4%	6	Derivative Signal	

Table C.2 Collision Cross-Section Database of Carbohydrates. Adapted from Jody C. May, Cody R. Goodwin, Nichole M. Lareau, Katrina L. Leaptrot, Caleb B. Morris, Ruwan T. Kurulugama, A. Mordehai, C. Klein, W. Barry, E. Darland, G. Overney, K. Imatani, George C. Stafford, John C. Fjeldsted, John A. McLean, "Conformational Ordering of Biomolecules in the Gas Phase: Nitrogen Collision Cross Sections Measured on a Prototype High Resolution Drift Tube Ion Mobility-Mass Spectrometer," *Analytical Chemistry* 2014, 86 (4), 2107-2116. (<https://pubs.acs.org/doi/10.1021/ac4038448>) Note that further permissions related to the material excerpted should be directed to the ACS.

Analyte	z	Exact m/z	Measured m/z	K_0	$K_0 \sigma$	CCS	$\frac{CCS}{\sigma}$	RSD (%)	N	Analyte Source	Vendor Source
Mannitol	+Li	189.10	189.10	1.497	0.001	144.5	0.1	0.1%	14	Analytical Standard	Sigma-Aldrich
Sorbitol	+H	189.10	189.09	1.470	0.004	147.2	0.4	0.3%	8	Analytical Standard	Sigma-Aldrich
Mannitol	+Na	205.07	205.07	1.531	0.006	140.6	0.5	0.4%	14	Analytical Standard	Sigma-Aldrich
Sorbitol (peak 1)	+Na	205.07	205.07	1.544	0.004	139.4	0.3	0.2%	8	Analytical Standard	Sigma-Aldrich
(Hex) ₂ - H ₂ O	+Na	347.10	347.09	1.220	0.006	172.0	0.8	0.5%	14	Derivative Signal	
Lactose	+Li	349.13	349.13	1.126	0.003	186.3	0.5	0.3%	7	Analytical Standard	Sigma-Aldrich
Lactose/Mannose Mixture	+Na	365.11	365.11	1.178	0.005	177.8	0.8	0.4%	15	Analytical Standard	Sigma-Aldrich
Lactose	+Na	365.11	365.10	1.176	0.002	178.1	0.3	0.1%	8	Analytical Standard	Sigma-Aldrich
Lactose/Mannose Mixture	+K	381.08	381.08	1.155	0.005	181.1	0.8	0.5%	16	Analytical Standard	Sigma-Aldrich
HexNAc-Hex - H ₂ O	+Na	388.12	388.12	1.134	0.004	184.3	0.6	0.3%	16	Derivative Signal	
HexNAc-Hex	+Na	406.13	406.14	1.097	0.003	190.2	0.5	0.3%	16	Derivative Signal	
HexNAc-Hex	+K	422.11	422.11	1.091	0.003	191.1	0.6	0.3%	16	Derivative Signal	
Hex-(Fuc) ₂ - H ₂ O (peak 1)	+H	455.18	455.18	1.071	0.005	194.2	0.9	0.5%	13	Derivative Signal	
Hex-(Fuc) ₂ - H ₂ O (peak 2)	+H	455.18	455.18	1.053	0.004	197.6	0.8	0.4%	9	Derivative Signal	
Maltotriose	+H	505.18	505.18	0.959	0.005	216.3	1.0	0.5%	14	Analytical Standard	Sigma-Aldrich
Melezitose	+H	505.18	505.18	1.023	0.005	202.6	1.0	0.5%	10	Analytical Standard	Sigma-Aldrich
(Hex) ₃ - H ₂ O	+Na	509.15	509.15	1.012	0.003	204.9	0.7	0.3%	16	Derivative Signal	
Melezitose	+Li	511.19	511.18	1.022	0.001	202.9	0.3	0.1%	14	Analytical Standard	Sigma-Aldrich
HexNAc-Fuc-Hex - H ₂ O	+H	512.20	512.20	0.996	0.003	208.2	0.5	0.3%	16	Derivative Signal	
Melezitose	+Na	527.16	527.16	0.974	0.004	212.8	0.8	0.4%	16	Analytical Standard	Sigma-Aldrich
Maltotriose	+Na	527.16	527.16	1.022	0.001	202.7	0.2	0.1%	14	Analytical Standard	Sigma-Aldrich
Raffinose	+Na	527.16	527.15	0.983	0.001	210.7	0.2	0.1%	8	Analytical Standard	Sigma-Aldrich
HexNAc-Fuc-Hex - H ₂ O	+Na	534.18	534.17	0.969	0.005	213.7	1.1	0.5%	16	Derivative Signal	
Maltotriose	+K	543.13	543.13	0.955	0.003	216.8	0.7	0.3%	16	Analytical Standard	Sigma-Aldrich
melezitose	+K	543.13	543.13	0.933	0.004	221.9	0.9	0.4%	14	Analytical Standard	Sigma-Aldrich
Raffinose	+K	543.13	543.13	0.973	0.002	212.7	0.3	0.2%	8	Analytical Standard	Sigma-Aldrich
HexNAc-(Hex) ₂ - H ₂ O	+Na	550.17	550.17	0.957	0.005	216.3	1.0	0.5%	15	Derivative Signal	
HexNAc-Fuc-Hex	+Na	552.19	552.18	0.969	0.005	213.6	1.1	0.5%	13	Derivative Signal	
HexNAc-(Hex) ₂	+Na	568.19	568.18	0.940	0.004	220.0	1.0	0.5%	16	Derivative Signal	
Melezitose (peak 1)	+Rb	589.08	589.08	1.012	0.001	204.1	0.2	0.1%	13	Analytical Standard	Sigma-Aldrich

Melezitose (peak 2)	+Rb	589.08	589.08	0.943	0.004	219.2	0.9	0.4%	13	Analytical Standard	Sigma-Aldrich
Raffinose (peak 1)	+Rb	589.08	589.09	0.945	0.004	218.7	0.9	0.4%	7	Analytical Standard	Sigma-Aldrich
Raffinose (peak 2)	+Rb	589.08	589.09	0.900	0.003	229.7	0.9	0.4%	7	Analytical Standard	Sigma-Aldrich
Melezitose	+Cs	637.07	637.07	1.002	0.001	205.8	0.2	0.1%	14	Analytical Standard	Sigma-Aldrich
(Hex) ₄ - H ₂ O	+H	649.22	649.21	0.878	0.004	234.7	1.2	0.5%	15	Derivative Signal	
HexNAc-(Fuc) ₂ -Hex - H ₂ O	+H	658.26	658.25	0.827	0.004	249.3	1.1	0.4%	14	Derivative Signal	
Maltotetraose	+H	667.23	667.23	0.865	0.004	238.3	1.2	0.5%	14	Analytical Standard	Sigma-Aldrich
(Hex) ₄ - H ₂ O	+Na	671.20	671.20	0.877	0.003	234.8	0.8	0.3%	16	Derivative Signal	
HexNAc-(Fuc) ₂ -Hex - H ₂ O	+Na	680.24	680.23	0.858	0.004	240.2	1.1	0.5%	16	Derivative Signal	
Maltotetraose	+Na	689.21	689.21	0.875	0.002	235.3	0.5	0.2%	16	Analytical Standard	Sigma-Aldrich
HexNAc-Fuc-(Hex) ₂ - H ₂ O	+Na	696.23	696.23	0.845	0.004	243.8	1.2	0.5%	16	Derivative Signal	
(Hex) ₄	+K	705.19	705.18	0.870	0.003	236.6	0.8	0.3%	16	Derivative Signal	
HexNAc-(Hex) ₃ - H ₂ O	+Na	712.23	712.22	0.840	0.003	244.9	1.0	0.4%	16	Derivative Signal	
HexNAc-Fuc-(Hex) ₂	+Na	714.24	714.24	0.822	0.004	250.3	1.2	0.5%	16	Derivative Signal	
HexNAc-(Hex) ₃	+Na	730.24	730.23	0.843	0.002	244.0	0.4	0.2%	16	Derivative Signal	
HexNAc-(Hex) ₃	+K	746.21	746.20	0.829	0.004	248.2	1.1	0.5%	16	Derivative Signal	
(Hex) ₅ - H ₂ O	+H	811.27	811.27	0.727	0.002	282.3	0.7	0.3%	14	Derivative Signal	
(Hex) ₅ - H ₂ O	+Na	833.25	833.25	0.780	0.002	263.1	0.8	0.3%	16	Derivative Signal	
(Hex) ₅	+Na	851.26	851.26	0.791	0.003	259.5	0.8	0.3%	16	Derivative Signal	
HexNAc-Fuc-(Hex) ₃ - H ₂ O (peak 1)	+Na	858.29	858.28	0.780	0.004	263.1	1.3	0.5%	14	Derivative Signal	
HexNAc-Fuc-(Hex) ₃ - H ₂ O (peak 2)	+Na	858.29	858.28	0.783	0.003	262.0	0.9	0.3%	7	Derivative Signal	
HexNAc-(Fuc) ₂ -(Hex) ₂	+Na	860.30	860.30	0.752	0.004	272.8	1.4	0.5%	16	Derivative Signal	
Lacto-N-Fucopentaose I	+Li	860.32	860.32	0.761	0.002	269.6	0.6	0.2%	14	Analytical Standard	Dextra Laboratories
Lacto-N-Fucopentaose II	+Na	876.30	876.29	0.756	0.001	271.1	0.3	0.1%	8	Analytical Standard	Dextra Laboratories
Lacto-N-Fucopentaose I	+Na	876.30	876.29	0.743	0.001	276.1	0.4	0.1%	13	Analytical Standard	Dextra Laboratories
Lacto-N-Fucopentaose II	+K	892.27	892.26	0.767	0.002	267.2	0.7	0.3%	8	Analytical Standard	Dextra Laboratories
Lacto-N-Fucopentaose I	+K	892.27	892.27	0.746	0.001	274.7	0.5	0.2%	14	Analytical Standard	Dextra Laboratories
HexNAc-(Hex) ₄ (peak 1)	+Na	892.29	892.27	0.751	0.004	272.9	1.3	0.5%	16	Derivative Signal	
HexNAc-(Hex) ₄ (peak 2)	+Na	892.29	892.27	0.744	0.002	275.5	0.9	0.3%	16	Derivative Signal	
Lacto-N-Fucopentaose II	+Rb	938.22	938.21	0.736	0.003	278.4	1.0	0.4%	7	Analytical Standard	Dextra Laboratories
Lacto-N-Fucopentaose I	+Rb	938.22	938.21	0.744	0.002	275.2	0.8	0.3%	13	Analytical Standard	Dextra Laboratories
Alpha-Cyclodextrin	+H	973.32	973.32	0.718	0.002	285.2	0.8	0.3%	14	Analytical Standard	Sigma-Aldrich
Lacto-N-Fucopentaose I	+Cs	986.21	986.21	0.743	0.003	275.6	0.9	0.3%	14	Analytical Standard	Dextra Laboratories
HexNAc-(Fuc) ₄ -Hex (peak 1)	+Na	990.36	990.35	0.728	0.002	281.2	0.7	0.2%	14	Derivative Signal	
HexNAc-(Fuc) ₄ -Hex (peak 2)	+Na	990.36	990.35	0.726	0.001	282.1	0.5	0.2%	6	Derivative Signal	
Alpha-Cyclodextrin	+Na	995.31	995.31	0.717	0.001	285.5	0.4	0.1%	14	Analytical Standard	Sigma-Aldrich
Lacto-N-Difucohexaose I	+Li	1006.38	1006.38	0.679	0.001	301.4	0.3	0.1%	14	Analytical Standard	Dextra Laboratories
Alpha-Cyclodextrin	+K	1011.28	1011.28	0.711	0.001	287.7	0.6	0.2%	14	Analytical Standard	Sigma-Aldrich
Maltohexaose	+Na	1013.32	1013.31	0.714	0.002	286.4	0.7	0.2%	14	Analytical Standard	Sigma-Aldrich

Lacto-N-Difucohexaose II (peak 1)	+Na	1022.35	1022.34	0.703	0.003	291.2	1.4	0.5%	8	Analytical Standard	Dextra Laboratories
Lacto-N-Difucohexaose II (peak 2)	+Na	1022.35	1022.34	0.668	0.001	306.3	0.6	0.2%	8	Analytical Standard	Dextra Laboratories
Lacto-N-Difucohexaose I (peak 1)	+Na	1022.35	1022.35	0.704	0.003	290.6	1.3	0.5%	14	Analytical Standard	Dextra Laboratories
Lacto-N-Difucohexaose I (peak 2)	+Na	1022.35	1022.35	0.673	0.001	304.2	0.5	0.2%	14	Analytical Standard	Dextra Laboratories
Maltohexaose	+K	1029.29	1029.29	0.698	0.002	293.3	0.6	0.2%	14	Analytical Standard	Sigma-Aldrich
Lacto-N-Difucohexaose II	+K	1038.33	1038.31	0.669	0.002	305.8	0.8	0.3%	8	Analytical Standard	Dextra Laboratories
Lacto-N-Difucohexaose I	+K	1038.33	1038.33	0.674	0.001	303.5	0.4	0.1%	14	Analytical Standard	Dextra Laboratories
(HexNAc) ₂ -(Hex) ₃ -Fuc (peak 2)	+Na	1079.38	1079.37	0.692	0.003	295.5	1.4	0.5%	12	Derivative Signal	
(HexNAc) ₂ -(Hex) ₃ -Fuc (peak 1)	+Na	1079.38	1079.37	0.668	0.003	306.0	1.5	0.5%	10	Derivative Signal	
Lacto-N-Difucohexaose I	+Rb	1084.28	1084.27	0.674	0.002	303.2	0.7	0.2%	14	Analytical Standard	Dextra Laboratories
Lacto-N-Difucohexaose I	+Cs	1132.27	1132.27	0.679	0.002	301.2	0.7	0.2%	14	Analytical Standard	Dextra Laboratories
Beta-Cyclodextrin (peak 1)	+H	1135.38	1135.37	0.678	0.002	301.3	0.9	0.3%	14	Analytical Standard	Sigma-Aldrich
Beta-Cyclodextrin (peak 2)	+H	1135.38	1135.37	0.639	0.002	319.6	1.2	0.4%	12	Analytical Standard	Sigma-Aldrich
HexNAc-(Fuc) ₄ -(Hex) ₂	+Na	1152.42	1152.40	0.646	0.002	316.1	0.9	0.3%	12	Derivative Signal	
Maltoheptaose	+H	1153.39	1153.39	0.674	0.002	303.3	0.7	0.2%	14	Analytical Standard	Sigma-Aldrich
Beta-Cyclodextrin	+Na	1157.36	1157.36	0.639	0.000	319.7	0.7	0.2%	11	Analytical Standard	Sigma-Aldrich
HexNAc-(Fuc) ₃ -(Hex) ₃	+Na	1168.41	1168.41	0.626	0.003	326.3	1.5	0.4%	11	Derivative Signal	
Beta-Cyclodextrin	+K	1173.33	1173.33	0.638	0.001	320.3	0.5	0.2%	12	Analytical Standard	Sigma-Aldrich
Maltoheptaose	+Na	1175.37	1175.37	0.674	0.001	303.1	0.5	0.2%	14	Analytical Standard	Sigma-Aldrich
Maltoheptaose	+K	1191.34	1191.34	0.673	0.001	303.4	0.5	0.2%	14	Analytical Standard	Sigma-Aldrich
(Hex) ₈ - H ₂ O	+H	1297.43	1297.42	0.611	0.001	333.8	0.8	0.2%	12	Derivative Signal	
Gamma-Cyclodextrin	+H	1297.43	1297.43	0.633	0.001	322.6	0.7	0.2%	12	Analytical Standard	Sigma-Aldrich
Gamma-Cyclodextrin	+Li	1303.44	1303.44	0.642	0.001	317.7	0.4	0.1%	12	Analytical Standard	Sigma-Aldrich
Gamma-Cyclodextrin	+Na	1319.41	1319.42	0.633	0.001	322.1	0.5	0.2%	12	Analytical Standard	Sigma-Aldrich
Gamma-Cyclodextrin	+K	1335.39	1335.39	0.628	0.001	324.8	0.5	0.2%	12	Analytical Standard	Sigma-Aldrich
(Hex) ₈ (peak 1)	+Na	1337.42	1337.42	0.636	0.003	320.9	1.3	0.4%	7	Derivative Signal	
(Hex) ₈ (peak 2)	+Na	1337.42	1337.42	0.602	0.001	338.8	0.7	0.2%	10	Derivative Signal	
HexNAc-(Hex) ₇ (peak 1)	+Na	1378.45	1378.45	0.612	0.003	333.4	1.7	0.5%	11	Derivative Signal	
HexNAc-(Hex) ₇ (peak 2)	+Na	1378.45	1378.45	0.593	0.001	343.7	0.8	0.2%	10	Derivative Signal	
Gamma-Cyclodextrin	+Rb	1381.33	1381.33	0.623	0.001	327.3	0.6	0.2%	12	Analytical Standard	Sigma-Aldrich
Gamma-Cyclodextrin	+Cs	1429.33	1429.33	0.603	0.001	338.2	0.6	0.2%	10	Analytical Standard	Sigma-Aldrich
(Hex) ₉ - H ₂ O	+H	1459.48	1459.48	0.577	0.002	353.3	1.2	0.4%	10	Derivative Signal	
(Hex) ₉ (peak 1)	+Na	1499.48	1499.48	0.598	0.003	340.5	1.6	0.5%	10	Derivative Signal	
(Hex) ₉ (peak 2)	+Na	1499.48	1499.48	0.579	0.002	351.9	1.5	0.4%	10	Derivative Signal	
HexNAc-(Hex) ₈	+H	1518.52	1518.52	0.586	0.003	347.8	1.5	0.4%	10	Derivative Signal	
HexNAc-(Hex) ₈ (peak 1)	+Na	1540.50	1540.50	0.575	0.003	354.2	1.7	0.5%	10	Derivative Signal	
HexNAc-(Hex) ₈ (peak 2)	+Na	1540.50	1540.50	0.579	0.003	351.6	1.5	0.4%	8	Derivative Signal	
(Hex) ₁₀ - H ₂ O	+H	1621.54	1621.54	0.531	0.001	383.4	0.9	0.2%	8	Derivative Signal	

HexNAc-(Fuc) ₂ - (Hex) ₇ - H ₂ O	+H	1630.57	1630.58	0.556	0.001	366.1	0.8	0.2%	10	Derivative Signal	
(Hex) ₁₀ (peak 1)	+H	1639.55	1639.55	0.558	0.002	365.1	1.4	0.4%	9	Derivative Signal	
(Hex) ₁₀ (peak 2)	+H	1639.55	1639.55	0.522	0.001	390.3	0.8	0.2%	8	Derivative Signal	
(Hex) ₁₀ (peak 1)	+Na	1661.53	1661.53	0.558	0.002	365.1	1.3	0.4%	10	Derivative Signal	
(Hex) ₁₀ (peak 2)	+Na	1661.53	1661.53	0.545	0.002	373.8	1.1	0.3%	8	Derivative Signal	
(Hex) ₁₁ - H ₂ O	+H	1783.59	1783.60	0.537	0.002	379.1	1.5	0.4%	6	Derivative Signal	
(Hex) ₁₁	+Li	1807.61	1807.59	0.546	0.002	372.4	1.1	0.3%	8	Derivative Signal	
(Hex) ₁₁	+Na	1823.58	1823.60	0.529	0.002	384.6	1.4	0.4%	8	Derivative Signal	
(Hex) ₁₁ (peak 1)	+K	1839.56	1839.53	0.554	0.002	367.4	1.6	0.4%	7	Derivative Signal	
(Hex) ₁₁ (peak 2)	+K	1839.56	1839.53	0.550	0.002	369.7	1.4	0.4%	8	Derivative Signal	
(Hex) ₁₁ (peak 1)	+Rb	1885.50	1885.48	0.556	0.002	365.7	1.3	0.4%	8	Derivative Signal	
(Hex) ₁₁ (peak 2)	+Rb	1885.50	1885.48	0.546	0.002	372.5	1.5	0.4%	6	Derivative Signal	
(Hex) ₁₂ - H ₂ O (peak 1)	+H	1945.64	1945.65	0.508	0.001	400.3	0.6	0.1%	8	Derivative Signal	
(Hex) ₁₂ - H ₂ O (peak 2)	+H	1945.64	1945.65	0.481	0.001	422.9	1.3	0.3%	6	Derivative Signal	
(Hex) ₁₂ - H ₂ O (peak 1)	+Na	1967.62	1967.63	0.520	0.001	390.6	0.9	0.2%	8	Derivative Signal	
(Hex) ₁₂ - H ₂ O (peak 2)	+Na	1967.62	1967.63	0.496	0.002	410.0	1.4	0.4%	6	Derivative Signal	
(Hex) ₁₃ (peak 1)	+Na	2147.69	2147.72	0.504	0.001	402.7	1.0	0.2%	6	Derivative Signal	
(Hex) ₁₃ (peak 2)	+Na	2147.69	2147.72	0.494	0.001	411.6	1.1	0.3%	6	Derivative Signal	

Table C.3 Collision Cross-Section Database of Peptides. Adapted from Jody C. May, Cody R. Goodwin, Nichole M. Lareau, Katrina L. Leaptrot, Caleb B. Morris, Ruwan T. Kurulugama, A. Mordehai, C. Klein, W. Barry, E. Darland, G. Overney, K. Imatani, George C. Stafford, John C. Fjeldsted, John A. McLean, “Conformational Ordering of Biomolecules in the Gas Phase: Nitrogen Collision Cross Sections Measured on a Prototype High Resolution Drift Tube Ion Mobility-Mass Spectrometer,” *Analytical Chemistry* 2014, 86 (4), 2107-2116. (<https://pubs.acs.org/doi/10.1021/ac4038448>) Note that further permissions related to the material excerpted should be directed to the ACS.

Analyte	z	Exact m/z	Measured m/z	K_0	$K_0 \sigma$	CCS	CCS σ	RSD (%)	N	Analyte Source	Vendor Source	Source Protein
DGDK	+H	434.19	434.19	1.064	0.004	195.8	0.7	0.3%	7	Analytical Standard	Waters	ENOLASE_YST
YVR	+H	437.25	437.25	1.006	0.002	207.0	0.4	0.2%	8	Analytical Standard	Waters	ADH_YST
DVCK	+H	464.22	464.22	1.016	0.004	204.7	0.7	0.4%	7	Analytical Standard	Waters	ALBUMIN_BOV
WIR	+H	474.28	474.27	0.964	0.003	215.4	0.7	0.3%	8	Analytical Standard	Waters	PHOSPH_RAB
GVFR	+H	478.28	478.28	0.967	0.001	214.8	0.3	0.1%	7	Analytical Standard	Waters	ENOLASE_YST
SDGRG	+H	491.22	491.22	1.015	0.003	204.6	0.5	0.3%	11	Analytical Standard	Sigma-Aldrich	SYNTHET_IC
GRGDS	+H	491.22	491.22	1.008	0.001	205.9	0.2	0.1%	14	Analytical Standard	Sigma-Aldrich	SYNTHET_IC
FGER	+H	508.25	508.24	0.955	0.002	217.1	0.4	0.2%	8	Analytical Standard	Waters	ENOLASE_YST
VYAR	+H	508.29	508.29	0.912	0.001	227.2	0.3	0.1%	7	Analytical Standard	Waters	PHOSPH_RAB
SDGRG	+Na	513.20	513.20	1.018	0.002	203.5	0.5	0.2%	11	Analytical Standard	Sigma-Aldrich	SYNTHET_IC
GRGDS	+Na	513.20	513.20	0.996	0.002	208.2	0.3	0.2%	14	Analytical Standard	Sigma-Aldrich	SYNTHET_IC
ADLAK	+H	517.30	517.30	0.908	0.004	228.3	1.1	0.5%	7	Analytical Standard	Waters	ALBUMIN_BOV
QENK	+H	518.26	518.26	0.946	0.003	219.0	0.6	0.3%	6	Analytical Standard	Waters	PHOSPH_RAB
MVIR	+H	518.31	518.31	0.906	0.001	228.7	0.3	0.1%	7	Analytical Standard	Waters	PHOSPH_RAB
WMGK	+H	521.25	521.26	0.941	0.002	220.1	0.5	0.2%	7	Analytical Standard	Waters	ENOLASE_YST
SDGRG	+K	529.18	529.17	1.009	0.004	205.4	0.8	0.4%	10	Analytical Standard	Sigma-Aldrich	SYNTHET_IC
GRGDS	+K	529.18	529.18	0.984	0.001	210.4	0.2	0.1%	14	Analytical Standard	Sigma-Aldrich	SYNTHET_IC
FWGK	+H	537.28	537.28	0.896	0.003	231.0	0.8	0.3%	7	Analytical Standard	Waters	ALBUMIN_BOV
VASLR	+H	545.34	545.34	0.890	0.001	232.5	0.3	0.1%	7	Analytical Standard	Waters	ALBUMIN_BOV
QENK	+H	549.31	549.31	0.889	0.001	232.8	0.3	0.1%	7	Analytical Standard	Waters	PHOSPH_RAB
NFNR	+H	550.27	550.27	0.920	0.002	225.0	0.6	0.3%	7	Analytical Standard	Waters	PHOSPH_RAB
LEYK	+H	552.30	552.30	0.863	0.003	239.6	0.9	0.4%	7	Analytical Standard	Waters	ADH_YST
FQNK	+Na	559.27	559.27	0.848	0.005	243.9	1.4	0.6%	5	Analytical Standard	Waters	PHOSPH_RAB

FQNK	+Na	569.31	569.31	0.945	0.002	218.9	0.6	0.3%	7	Analytical Standard	Waters	ENOLASE_YST
EWTR	+H	591.29	591.29	0.885	0.001	233.4	0.4	0.2%	7	Analytical Standard	Waters	PHOSPH_RAB
AMGYR	+H	597.28	597.28	0.843	0.001	245.0	0.3	0.1%	7	Analytical Standard	Waters	ADH_YST
QISVR	+H	602.36	602.36	0.855	0.001	241.4	0.3	0.1%	7	Analytical Standard	Waters	PHOSPH_RAB
LWSAK	+H	604.35	604.34	0.865	0.001	238.6	0.3	0.1%	7	Analytical Standard	Waters	PHOSPH_RAB
AFDEK	+H	609.29	609.29	0.867	0.001	238.3	0.3	0.1%	7	Analytical Standard	Waters	ALBUMIN_BOV
FSSDR	+H	611.28	611.28	0.870	0.001	237.3	0.3	0.1%	7	Analytical Standard	Waters	PHOSPH_RAB
FVVPR (peak 1)	+H	617.38	617.37	0.810	0.002	254.7	0.7	0.3%	7	Analytical Standard	Waters	PHOSPH_RAB
FVVPR (peak2)	+H	617.38	617.37	0.828	0.001	249.3	0.4	0.1%	7	Analytical Standard	Waters	PHOSPH_RAB
GQIVGR	+H	629.37	629.37	0.840	0.001	245.5	0.3	0.1%	7	Analytical Standard	Waters	ADH_YST
VSLAEK	+H	646.38	646.38	0.828	0.001	249.0	0.3	0.1%	7	Analytical Standard	Waters	PHOSPH_RAB
IETMR or CASIQK	+H	649.33	649.33	0.815	0.001	252.8	0.4	0.2%	7	Analytical Standard	Waters	ALBUMIN_BOV
AAGHDGK	+H	655.32	655.32	0.828	0.002	249.0	0.5	0.2%	7	Analytical Standard	Waters	ENOLASE_YST
NVATPR	+H	657.37	657.37	0.811	0.001	254.0	0.3	0.1%	7	Analytical Standard	Waters	PHOSPH_RAB
ANIDVK	+H	659.37	659.37	0.831	0.001	248.1	0.4	0.2%	7	Analytical Standard	Waters	ENOLASE_YST
VSALYK (peak 1)	+H	680.40	680.40	0.787	0.001	261.8	0.3	0.1%	7	Analytical Standard	Waters	PHOSPH_RAB
VSALYK (peak 2)	+H	680.40	680.40	0.811	0.001	254.0	0.4	0.2%	7	Analytical Standard	Waters	PHOSPH_RAB
IHEYK	+H	689.36	689.37	0.797	0.001	258.5	0.2	0.1%	7	Analytical Standard	Waters	PHOSPH_RAB
NIATSGK	+H	690.38	690.38	0.801	0.001	257.2	0.3	0.1%	8	Analytical Standard	Waters	PHOSPH_RAB
EELFR	+H	693.36	693.35	0.810	0.001	254.1	0.3	0.1%	8	Analytical Standard	Waters	ADH_YST
DHLVGR	+H	696.38	696.38	0.826	0.002	249.4	0.6	0.2%	8	Analytical Standard	Waters	PHOSPH_RAB
TVMIGGK	+H	705.40	705.40	0.785	0.001	262.2	0.4	0.2%	7	Analytical Standard	Waters	PHOSPH_RAB
GVLHAVK	+H	723.45	723.45	0.762	0.001	269.9	0.4	0.2%	7	Analytical Standard	Waters	ENOLASE_YST
SVYDSR	+H	726.34	726.34	0.796	0.002	258.4	0.6	0.2%	7	Analytical Standard	Waters	ENOLASE_YST
VEDVDR	+H	732.35	732.35	0.801	0.001	256.6	0.5	0.2%	8	Analytical Standard	Waters	PHOSPH_RAB
NVPLYK	+H	733.42	733.42	0.756	0.001	272.2	0.4	0.1%	7	Analytical Standard	Waters	ENOLASE_YST
QPDLFK	+H	745.45	745.44	0.746	0.001	275.5	0.3	0.1%	7	Analytical Standard	Waters	ENOLASE_YST
LNQLLR	+H	756.47	756.47	0.746	0.001	275.6	0.4	0.1%	7	Analytical Standard	Waters	ENOLASE_YST
TNGITPR (peak 1)	+H	758.42	758.41	0.733	0.001	280.4	0.3	0.1%	7	Analytical Standard	Waters	PHOSPH_RAB
TNGITPR (peak 2)	+H	758.42	758.41	0.762	0.001	269.8	0.5	0.2%	7	Analytical Standard	Waters	PHOSPH_RAB
TNGITPR (peak 3)	+H	758.42	758.41	0.795	0.001	258.4	0.4	0.1%	7	Analytical Standard	Waters	PHOSPH_RAB
HLADLSK	+H	783.44	783.43	0.752	0.001	273.3	0.5	0.2%	6	Analytical Standard	Waters	ENOLASE_YST
LVTDLTK	+H	789.47	789.47	0.743	0.001	276.6	0.5	0.2%	7	Analytical Standard	Waters	ALBUMIN_BOV
YDLDFK	+H	800.38	800.38	0.754	0.001	272.4	0.5	0.2%	7	Analytical Standard	Waters	ENOLASE_YST

TFAEALR	+H	807.44	807.43	0.724	0.001	283.5	0.5	0.2%	7	Analytical Standard	Waters	ENOLASE_YST
YVVDTSK	+H	811.42	811.42	0.746	0.001	275.2	0.3	0.1%	7	Analytical Standard	Waters	ADH_YST
AADALLK or DIVGAVLK	+H	814.50	814.50	0.704	0.001	291.8	0.4	0.1%	7	Analytical Standard	Waters	ENOLASE_YST or ADH_YST
AADALLK or DIVGAVLK	+H	814.50	814.50	0.739	0.001	277.8	0.3	0.1%	7	Analytical Standard	Waters	ENOLASE_YST or ADH_YST
ATEEQLK	+H	818.43	818.42	0.730	0.001	281.3	0.5	0.2%	7	Analytical Standard	Waters	ALBUMIN_BOV
TIAQYAR	+H	822.45	822.45	0.729	0.001	281.6	0.5	0.2%	7	Analytical Standard	Waters	PHOSPH_RAB
AWEVTVK	+H	832.46	832.45	0.736	0.000	279.0	0.7	0.2%	7	Analytical Standard	Waters	PHOSPH_RAB
IGDYAGIK	+H	836.45	836.45	0.718	0.001	285.9	0.3	0.1%	6	Analytical Standard	Waters	ADH_YST
VLVDLER	+H	843.49	843.49	0.718	0.001	285.7	0.4	0.1%	7	Analytical Standard	Waters	PHOSPH_RAB
FAAYLER	+H	869.45	869.45	0.694	0.001	295.5	0.4	0.1%	7	Analytical Standard	Waters	PHOSPH_RAB
YGNPWEK	+H	893.42	893.41	0.722	0.001	283.8	0.6	0.2%	7	Analytical Standard	Waters	PHOSPH_RAB
DIPVPKPK	+H	893.55	893.54	0.697	0.002	294.2	0.7	0.2%	7	Analytical Standard	Waters	ADH_YST
NLAENISR	+H	916.48	916.48	0.703	0.001	291.7	0.6	0.2%	7	Analytical Standard	Waters	PHOSPH_RAB
APNDFNLK	+H	918.47	918.46	0.683	0.001	300.0	0.6	0.2%	7	Analytical Standard	Waters	PHOSPH_RAB
AEFVEVTK	+H	922.49	922.49	0.693	0.001	295.7	0.5	0.2%	7	Analytical Standard	Waters	ALBUMIN_BOV
YLIEIAR	+H	927.49	927.49	0.672	0.001	305.0	0.5	0.2%	7	Analytical Standard	Waters	ALBUMIN_BOV
VLGIDGEGEK	+H	944.50	944.50	0.703	0.000	291.2	0.2	0.1%	7	Analytical Standard	Waters	ADH_YST
NNVNTMR	+H	947.47	947.47	0.681	0.001	300.7	0.6	0.2%	8	Analytical Standard	Waters	PHOSPH_RAB
EALDFAR	+H	968.48	968.48	0.669	0.001	305.9	0.4	0.1%	7	Analytical Standard	Waters	ADH_YST
LVVSTQATALA	+H	1002.58	1002.58	0.649	0.001	315.6	0.3	0.1%	6	Analytical Standard	Waters	ALBUMIN_BOV
ANELINVK	+H	1013.60	1013.60	0.626	0.001	326.8	0.3	0.1%	6	Analytical Standard	Waters	ADH_YST
VIFLENYR	+H	1053.57	1053.57	0.643	0.001	318.3	0.4	0.1%	7	Analytical Standard	Waters	PHOSPH_RAB
EIWGVEPSR	+H	1072.54	1072.54	0.639	0.001	320.2	0.6	0.2%	7	Analytical Standard	Waters	PHOSPH_RAB
VAAAFPGDVDR (peak1)	+H	1117.56	1117.56	0.626	0.001	326.7	0.5	0.2%	5	Analytical Standard	Waters	PHOSPH_RAB
VAAAFPGDVDR (peak 2)	+H	1117.56	1117.56	0.630	0.001	324.3	0.4	0.1%	6	Analytical Standard	Waters	PHOSPH_RAB
GVIFYESHGK	+H	1136.57	1136.57	0.614	0.001	332.9	0.5	0.2%	5	Analytical Standard	Waters	ADH_YST
IGSEVYHNLK	+H	1159.61	1159.61	0.586	0.001	348.4	0.7	0.2%	5	Analytical Standard	Waters	ENOLASE_YST
LVNELTEFAK	+H	1163.63	1163.63	0.593	0.000	344.4	0.2	0.1%	5	Analytical Standard	Waters	ALBUMIN_BOV
SISIVGSYVGNR	+H	1251.67	1251.67	0.585	0.001	349.1	0.8	0.2%	6	Analytical Standard	Waters	ADH_YST
VFADYEEYVK	+H	1262.59	1262.59	0.557	0.002	366.4	1.2	0.3%	6	Analytical Standard	Waters	PHOSPH_RAB
VNQGTLSESIK	+H	1288.71	1288.71	0.569	0.001	358.7	0.5	0.1%	5	Analytical Standard	Waters	ENOLASE_YST
SIGGEVDFIDFTK	+H	1312.68	1312.68	0.534	0.001	382.3	0.9	0.2%	5	Analytical Standard	Waters	ADH_YST
TVMENFVAFVDK	+H	1399.69	1399.69	0.522	0.003	390.2	1.9	0.5%	5	Analytical Standard	Waters	ALBUMIN_BOV

AVDDFLISLDGTA NK	+H	1578.80	1578.80	0.474	0.001	429.7	0.7	0.2%	6	Analytical Standard	Waters	ENOLASE _YST
TAGIQIVADDLTV TNPk	+H	1755.95	1755.95	0.452	0.000	450.6	0.5	0.1%	4	Analytical Standard	Waters	ENOLASE _YST

Table C.4 Collision Cross-Section Database of Lipids. Adapted from Jody C. May, Cody R. Goodwin, Nichole M. Lareau, Katrina L. Leaptrot, Caleb B. Morris, Ruwan T. Kurulugama, A. Mordehai, C. Klein, W. Barry, E. Darland, G. Overney, K. Imatani, George C. Stafford, John C. Fjeldsted, John A. McLean, “Conformational Ordering of Biomolecules in the Gas Phase: Nitrogen Collision Cross Sections Measured on a Prototype High Resolution Drift Tube Ion Mobility-Mass Spectrometer,” *Analytical Chemistry* 2014, 86 (4), 2107-2116. (<https://pubs.acs.org/doi/10.1021/ac4038448>) Note that further permissions related to the material excerpted should be directed to the ACS.

Analyte	z	Exact m/z	Measured m/z	K_0	$K_0 \sigma$	CCS	CCS σ	RSD (%)	N	Analyte Source	Vendor Source
GlcCer 34:01	+Na	722.55	722.55	0.742	0.002	277.3	0.8	0.3%	15	Analytical Standard	Avanti Polar Lipids
GlcCer 34:00	+Na	724.57	724.56	0.730	0.002	281.7	0.7	0.2%	14	Analytical Standard	Avanti Polar Lipids
GlcCer 36:02	+Na	748.57	748.56	0.727	0.002	282.6	0.6	0.2%	14	Analytical Standard	Avanti Polar Lipids
GlcCer 36:01	+Na	750.59	750.58	0.717	0.001	286.7	0.4	0.1%	14	Analytical Standard	Avanti Polar Lipids
GlcCer 37:01	+Na	764.60	764.59	0.717	0.002	286.8	0.9	0.3%	14	Analytical Standard	Avanti Polar Lipids
GlcCer 36:01 h	+Na	766.58	766.58	0.705	0.001	291.5	0.4	0.1%	14	Analytical Standard	Avanti Polar Lipids
GlcCer 38:02	+Na	776.60	776.60	0.705	0.002	291.4	1.0	0.3%	14	Analytical Standard	Avanti Polar Lipids
GlcCer 38:01	+Na	778.62	778.61	0.699	0.001	293.8	0.4	0.1%	14	Analytical Standard	Avanti Polar Lipids
GlcCer 38:00	+Na	780.63	780.63	0.695	0.001	295.6	0.5	0.2%	14	Analytical Standard	Avanti Polar Lipids
GlcCer 38:02 h	+Na	792.60	792.59	0.692	0.002	296.6	0.8	0.3%	14	Analytical Standard	Avanti Polar Lipids
GlcCer 38:01 h	+Na	794.61	794.61	0.690	0.001	297.7	0.5	0.2%	14	Analytical Standard	Avanti Polar Lipids
GlcCer 40:03	+Na	802.62	802.61	0.694	0.003	295.8	1.3	0.4%	14	Analytical Standard	Avanti Polar Lipids
GlcCer 40:02	+Na	804.63	804.63	0.691	0.002	297.1	0.6	0.2%	14	Analytical Standard	Avanti Polar Lipids
GlcCer 40:01	+Na	806.65	806.65	0.682	0.001	301.1	0.5	0.2%	14	Analytical Standard	Avanti Polar Lipids
GlcCer 40:00	+Na	808.66	808.66	0.679	0.001	302.3	0.5	0.2%	14	Analytical Standard	Avanti Polar Lipids
GlcCer 41:02	+Na	818.65	818.64	0.685	0.001	299.6	0.6	0.2%	14	Analytical Standard	Avanti Polar Lipids
GlcCer 41:01	+Na	820.66	820.65	0.679	0.001	302.5	0.5	0.2%	14	Analytical Standard	Avanti Polar Lipids
GlcCer 40:01 h	+Na	822.64	822.64	0.677	0.001	303.4	0.4	0.1%	14	Analytical Standard	Avanti Polar Lipids
GlcCer 40:00 h	+Na	824.66	824.65	0.671	0.001	306.1	0.6	0.2%	14	Analytical Standard	Avanti Polar Lipids
GlcCer 42:03	+Na	830.65	830.64	0.679	0.001	302.3	0.4	0.1%	14	Analytical Standard	Avanti Polar Lipids
GlcCer 42:02	+Na	832.66	832.67	0.672	0.001	305.2	0.5	0.1%	14	Analytical Standard	Avanti Polar Lipids
GlcCer 42:01	+Na	834.68	834.68	0.667	0.001	307.5	0.4	0.1%	14	Analytical Standard	Avanti Polar Lipids
GlcCer 42:00	+Na	836.70	836.68	0.666	0.001	308.2	0.5	0.2%	14	Analytical Standard	Avanti Polar Lipids
GlcCer 43:03	+Na	844.66	844.65	0.670	0.002	306.1	0.7	0.2%	14	Analytical Standard	Avanti Polar Lipids
GlcCer 43:02	+Na	846.68	846.67	0.667	0.002	307.8	1.0	0.3%	14	Analytical Standard	Avanti Polar Lipids
GlcCer 42:02 h	+Na	848.66	848.66	0.664	0.001	309.0	0.4	0.1%	14	Analytical Standard	Avanti Polar Lipids
GlcCer 42:01 h	+Na	850.67	850.68	0.656	0.001	312.7	0.4	0.1%	12	Analytical Standard	Avanti Polar Lipids
GlcCer 44:03	+Na	858.68	858.67	0.660	0.001	310.7	0.7	0.2%	12	Analytical Standard	Avanti Polar Lipids
GlcCer 44:02	+Na	860.70	860.69	0.651	0.001	315.3	0.4	0.1%	12	Analytical Standard	Avanti Polar Lipids
GlcCer 43:02 h	+Na	862.67	862.69	0.652	0.001	314.6	0.4	0.1%	12	Analytical Standard	Avanti Polar Lipids
GlcCer 43:01 h	+Na	864.69	864.68	0.654	0.001	313.7	0.4	0.1%	12	Analytical Standard	Avanti Polar Lipids
GlcCer 44:04 h	+Na	872.66	872.65	0.652	0.001	314.7	0.4	0.1%	12	Analytical Standard	Avanti Polar Lipids
GlcCer 44:03 h	+Na	874.67	874.67	0.653	0.001	314.0	0.6	0.2%	12	Analytical Standard	Avanti Polar Lipids
GlcCer 44:02 h	+Na	876.69	876.69	0.644	0.001	318.4	0.4	0.1%	12	Analytical Standard	Avanti Polar Lipids

GlcCer 44:01 h	+Na	878.71	878.70	0.642	0.001	319.5	0.4	0.1%	12	Analytical Standard	Avanti Polar Lipids
GlcCer 44:02 h	+K	892.66	892.68	0.639	0.001	321.1	0.7	0.2%	12	Analytical Standard	Avanti Polar Lipids
GlcCer 47:09	+K	904.61	904.60	0.648	0.001	316.4	0.6	0.2%	12	Analytical Standard	Avanti Polar Lipids
GlcCer 46:02 h	+Na	904.72	904.72	0.633	0.001	323.8	0.6	0.2%	12	Analytical Standard	Avanti Polar Lipids
GlcCer 47:10 h	+K	918.59	918.59	0.643	0.001	318.6	0.5	0.2%	12	Analytical Standard	Avanti Polar Lipids
PC 31:02	+K	754.48	754.48	0.725	0.002	283.6	0.8	0.3%	8	Analytical Standard	Avanti Polar Lipids
PC 31:01	+K	756.49	756.50	0.718	0.002	286.5	0.7	0.2%	8	Analytical Standard	Avanti Polar Lipids
PC 32:03	+K	766.48	766.49	0.711	0.001	288.9	0.6	0.2%	8	Analytical Standard	Avanti Polar Lipids
PC 32:02	+K	768.49	768.50	0.711	0.001	289.2	0.5	0.2%	8	Analytical Standard	Avanti Polar Lipids
PC 33:04	+K	778.48	778.48	0.715	0.002	287.5	0.7	0.3%	10	Analytical Standard	Avanti Polar Lipids
PC 33:03	+K	780.49	780.50	0.708	0.001	290.1	0.5	0.2%	8	Analytical Standard	Avanti Polar Lipids
PC 33:02	+K	782.51	782.52	0.705	0.001	291.5	0.6	0.2%	9	Analytical Standard	Avanti Polar Lipids
PC 34:04	+K	792.49	792.50	0.711	0.002	289.0	1.0	0.3%	10	Analytical Standard	Avanti Polar Lipids
PC 34:03	+K	794.51	794.51	0.702	0.002	292.4	0.8	0.3%	10	Analytical Standard	Avanti Polar Lipids
PC 34:02	+K	796.53	796.53	0.705	0.001	291.3	0.6	0.2%	8	Analytical Standard	Avanti Polar Lipids
PC 36:07	+Na	798.50	798.51	0.702	0.002	292.5	0.7	0.2%	9	Analytical Standard	Avanti Polar Lipids
PC 35:06	+K	802.48	802.48	0.704	0.002	291.8	1.0	0.3%	10	Analytical Standard	Avanti Polar Lipids
PC 35:05	+K	804.49	804.50	0.699	0.001	293.8	0.6	0.2%	9	Analytical Standard	Avanti Polar Lipids
PC 35:04	+K	806.51	806.51	0.697	0.002	294.5	0.7	0.2%	10	Analytical Standard	Avanti Polar Lipids
PC 35:03	+K	808.53	808.53	0.693	0.001	296.1	0.6	0.2%	10	Analytical Standard	Avanti Polar Lipids
PC 35:02	+K	810.54	810.54	0.690	0.001	297.7	0.6	0.2%	10	Analytical Standard	Avanti Polar Lipids
PC 38:10	+Na	820.49	820.50	0.694	0.001	295.9	0.6	0.2%	9	Analytical Standard	Avanti Polar Lipids
PC 38:09	+Na	822.50	822.51	0.689	0.001	297.8	0.6	0.2%	10	Analytical Standard	Avanti Polar Lipids
PC 38:08	+Na	824.52	824.52	0.684	0.002	299.9	0.7	0.2%	10	Analytical Standard	Avanti Polar Lipids
PC 37:07	+K	828.49	828.50	0.692	0.001	296.6	0.6	0.2%	10	Analytical Standard	Avanti Polar Lipids
PC 37:06	+K	830.51	830.51	0.688	0.001	298.2	0.5	0.2%	10	Analytical Standard	Avanti Polar Lipids
PC 37:05	+K	832.53	832.53	0.686	0.001	299.0	0.6	0.2%	8	Analytical Standard	Avanti Polar Lipids
PC 40:15	+Na	838.44	838.45	0.699	0.002	293.5	1.0	0.3%	9	Analytical Standard	Avanti Polar Lipids
PC 40:14	+Na	840.46	840.46	0.700	0.001	293.3	0.6	0.2%	8	Analytical Standard	Avanti Polar Lipids
PC 40:13	+Na	842.47	842.47	0.692	0.002	296.6	0.8	0.3%	8	Analytical Standard	Avanti Polar Lipids
PC 40:12	+Na	844.49	844.49	0.683	0.001	300.6	0.6	0.2%	8	Analytical Standard	Avanti Polar Lipids
PC 40:11	+Na	846.50	846.50	0.682	0.002	300.7	0.7	0.2%	9	Analytical Standard	Avanti Polar Lipids
PC 40:10	+Na	848.52	848.52	0.680	0.001	301.5	0.5	0.2%	8	Analytical Standard	Avanti Polar Lipids
PC 40:10	+Na	850.54	850.53	0.679	0.002	302.2	0.7	0.2%	10	Analytical Standard	Avanti Polar Lipids
PC 39:07	+K	856.53	856.53	0.675	0.002	303.8	0.7	0.2%	10	Analytical Standard	Avanti Polar Lipids
PC 39:06	+K	858.54	858.54	0.676	0.001	303.4	0.7	0.2%	9	Analytical Standard	Avanti Polar Lipids
PC 39:05	+K	860.56	860.55	0.673	0.002	304.7	0.7	0.2%	9	Analytical Standard	Avanti Polar Lipids
PC 42:15	+Na	866.47	866.47	0.679	0.003	301.9	1.1	0.4%	10	Analytical Standard	Avanti Polar Lipids
PC 42:14	+Na	868.49	868.49	0.686	0.002	299.0	0.7	0.2%	10	Analytical Standard	Avanti Polar Lipids
PC 42:13	+Na	870.50	870.50	0.673	0.002	304.9	0.7	0.2%	9	Analytical Standard	Avanti Polar Lipids
PC 42:12	+Na	872.52	872.52	0.675	0.002	303.9	0.7	0.2%	9	Analytical Standard	Avanti Polar Lipids
PC 43:17	+K	892.43	892.44	0.675	0.001	303.5	0.5	0.2%	8	Analytical Standard	Avanti Polar Lipids
PC 43:16	+K	894.45	894.44	0.674	0.002	304.1	0.7	0.2%	10	Analytical Standard	Avanti Polar Lipids
PE O-18:03/0:00	+Na	498.26	498.26	0.941	0.003	220.5	0.6	0.3%	11	Analytical Standard	Avanti Polar Lipids
PE O-20:05	+Na	522.26	522.26	0.956	0.004	216.8	0.9	0.4%	11	Analytical Standard	Avanti Polar Lipids
PE O-20:04	+Na	524.28	524.27	0.913	0.002	226.9	0.5	0.2%	11	Analytical Standard	Avanti Polar Lipids
PE O-20:03	+Na	526.29	526.29	0.906	0.002	228.7	0.6	0.3%	11	Analytical Standard	Avanti Polar Lipids
PE O-22:07	+Na	546.26	546.26	0.938	0.007	220.6	1.7	0.8%	11	Analytical Standard	Avanti Polar Lipids

PE O-22:06	+Na	548.28	548.27	0.907	0.003	228.1	0.7	0.3%	8	Analytical Standard	Avanti Polar Lipids
PE 21:03	+K	570.26	570.26	0.908	0.003	227.8	0.7	0.3%	8	Analytical Standard	Avanti Polar Lipids
PE 21:02	+K	572.28	572.27	0.902	0.001	229.3	0.3	0.2%	8	Analytical Standard	Avanti Polar Lipids
PE O-26:05	+K	622.33	622.31	0.851	0.002	242.4	0.4	0.2%	8	Analytical Standard	Avanti Polar Lipids
PE 26:06	+K	634.29	634.27	0.854	0.003	241.7	1.0	0.4%	8	Analytical Standard	Avanti Polar Lipids
PE 26:05	+K	636.31	636.29	0.850	0.003	242.6	0.8	0.3%	8	Analytical Standard	Avanti Polar Lipids
PE 26:04	+K	638.32	638.30	0.841	0.003	245.4	1.0	0.4%	8	Analytical Standard	Avanti Polar Lipids
PE 28:07	+K	660.31	660.29	0.843	0.003	244.4	0.8	0.3%	8	Analytical Standard	Avanti Polar Lipids
PE 28:06	+K	662.32	662.30	0.829	0.002	248.7	0.7	0.3%	8	Analytical Standard	Avanti Polar Lipids
PE 28:05	+K	664.34	664.32	0.821	0.002	250.9	0.5	0.2%	8	Analytical Standard	Avanti Polar Lipids
PE O-31:06	+K	690.39	690.37	0.799	0.002	257.8	0.5	0.2%	13	Analytical Standard	Avanti Polar Lipids
PE 32:01	+Na	712.49	712.49	0.751	0.002	274.1	0.7	0.3%	8	Analytical Standard	Avanti Polar Lipids
PE O-34:04	+Na	720.49	720.49	0.746	0.002	275.9	0.7	0.2%	11	Analytical Standard	Avanti Polar Lipids
PE O-34:03	+Na	722.51	722.51	0.740	0.003	278.0	0.9	0.3%	12	Analytical Standard	Avanti Polar Lipids
PE O-34:02	+Na	724.53	724.52	0.735	0.002	279.7	0.8	0.3%	12	Analytical Standard	Avanti Polar Lipids
PE 34:04	+Na	734.47	734.47	0.752	0.003	273.6	1.2	0.5%	8	Analytical Standard	Avanti Polar Lipids
PE O-O-36:04	+Na	734.55	734.55	0.736	0.003	279.3	1.2	0.4%	8	Analytical Standard	Avanti Polar Lipids
PE 34:03	+Na	736.49	736.49	0.745	0.003	276.1	1.0	0.4%	10	Analytical Standard	Avanti Polar Lipids
PE 34:02	+Na	738.50	738.51	0.739	0.001	278.3	0.6	0.2%	11	Analytical Standard	Avanti Polar Lipids
PE 34:01	+Na	740.52	740.52	0.731	0.002	281.3	0.6	0.2%	11	Analytical Standard	Avanti Polar Lipids
PE 33:00	+K	744.49	744.49	0.742	0.003	277.2	1.2	0.4%	11	Analytical Standard	Avanti Polar Lipids
PE O-36:05	+Na	746.51	746.51	0.736	0.002	279.2	0.7	0.3%	11	Analytical Standard	Avanti Polar Lipids
PE O-36:04	+Na	748.53	748.52	0.730	0.002	281.6	0.6	0.2%	11	Analytical Standard	Avanti Polar Lipids
PE O-36:03	+Na	750.54	750.54	0.720	0.003	285.4	1.1	0.4%	11	Analytical Standard	Avanti Polar Lipids
PE 35:02	+Na	752.52	752.52	0.731	0.001	281.3	0.3	0.1%	8	Analytical Standard	Avanti Polar Lipids
PE O-36:02	+Na	752.56	752.55	0.716	0.001	287.3	0.6	0.2%	12	Analytical Standard	Avanti Polar Lipids
PE 35:01	+Na	754.54	754.54	0.727	0.001	282.9	0.6	0.2%	11	Analytical Standard	Avanti Polar Lipids
PE 36:06	+Na	758.47	758.47	0.744	0.001	276.3	0.5	0.2%	11	Analytical Standard	Avanti Polar Lipids
PE 36:05	+Na	760.49	760.49	0.739	0.001	278.2	0.5	0.2%	11	Analytical Standard	Avanti Polar Lipids
PE 36:04	+Na	762.50	762.51	0.732	0.001	280.6	0.5	0.2%	11	Analytical Standard	Avanti Polar Lipids
PE 36:02	+Na	766.54	766.54	0.719	0.001	285.7	0.4	0.2%	11	Analytical Standard	Avanti Polar Lipids
PE 35:02	+K	768.49	768.49	0.728	0.002	282.5	0.7	0.2%	12	Analytical Standard	Avanti Polar Lipids
PE 36:01	+Na	768.55	768.55	0.712	0.001	288.5	0.6	0.2%	11	Analytical Standard	Avanti Polar Lipids
PE 35:01	+K	770.51	770.51	0.725	0.001	283.6	0.6	0.2%	10	Analytical Standard	Avanti Polar Lipids
PE 35:00	+K	772.53	772.53	0.718	0.002	286.2	0.7	0.2%	11	Analytical Standard	Avanti Polar Lipids
PE O-38:05	+Na	774.54	774.54	0.714	0.001	287.7	0.3	0.1%	11	Analytical Standard	Avanti Polar Lipids
PE O-O-38:05	+K	776.54	776.53	0.720	0.003	285.6	1.0	0.4%	10	Analytical Standard	Avanti Polar Lipids
PE 37:03	+Na	778.54	778.54	0.718	0.002	286.2	0.7	0.2%	12	Analytical Standard	Avanti Polar Lipids
PE 37:02	+Na	780.55	780.55	0.713	0.001	288.2	0.4	0.2%	12	Analytical Standard	Avanti Polar Lipids
PE 38:08	+Na	782.47	782.46	0.729	0.002	281.9	0.7	0.2%	13	Analytical Standard	Avanti Polar Lipids
PE 37:01	+Na	782.57	782.56	0.703	0.002	292.2	0.9	0.3%	12	Analytical Standard	Avanti Polar Lipids
PE 38:07	+Na	784.49	784.49	0.724	0.001	283.7	0.5	0.2%	11	Analytical Standard	Avanti Polar Lipids
PE 38:06	+Na	786.50	786.50	0.721	0.001	285.0	0.5	0.2%	11	Analytical Standard	Avanti Polar Lipids
PE 38:05	+Na	788.52	788.52	0.715	0.001	287.2	0.5	0.2%	11	Analytical Standard	Avanti Polar Lipids
PE 38:04	+Na	790.54	790.54	0.708	0.001	290.0	0.5	0.2%	12	Analytical Standard	Avanti Polar Lipids
PE 37:04	+K	792.49	792.49	0.721	0.002	284.7	0.7	0.2%	11	Analytical Standard	Avanti Polar Lipids
PE 38:03	+Na	792.55	792.54	0.710	0.002	289.3	0.7	0.2%	11	Analytical Standard	Avanti Polar Lipids
PE 37:03	+K	794.51	794.51	0.717	0.001	286.5	0.4	0.2%	11	Analytical Standard	Avanti Polar Lipids

PE 37:02	+K	796.53	796.52	0.709	0.001	289.8	0.6	0.2%	11	Analytical Standard	Avanti Polar Lipids
PE 37:01	+K	798.54	798.54	0.696	0.001	295.0	0.5	0.2%	11	Analytical Standard	Avanti Polar Lipids
PE 38:07	+K	800.46	800.48	0.716	0.001	287.0	0.5	0.2%	11	Analytical Standard	Avanti Polar Lipids
PE 39:06	+Na	800.52	800.52	0.717	0.002	286.4	0.7	0.3%	11	Analytical Standard	Avanti Polar Lipids
PE 37:00	+K	800.56	800.56	0.690	0.001	297.8	0.5	0.2%	10	Analytical Standard	Avanti Polar Lipids
PE 38:06	+K	802.48	802.48	0.711	0.001	288.7	0.5	0.2%	12	Analytical Standard	Avanti Polar Lipids
PE O-39:06	+K	802.52	802.52	0.706	0.001	290.9	0.5	0.2%	12	Analytical Standard	Avanti Polar Lipids
PE O-O-40:06	+K	802.55	802.55	0.700	0.000	293.3	0.7	0.2%	11	Analytical Standard	Avanti Polar Lipids
PE 39:04	+Na	804.55	804.55	0.701	0.002	292.8	0.8	0.3%	11	Analytical Standard	Avanti Polar Lipids
PE 40:09	+Na	808.49	808.49	0.717	0.001	286.6	0.5	0.2%	10	Analytical Standard	Avanti Polar Lipids
PE 40:08	+Na	810.50	810.50	0.710	0.001	289.2	0.3	0.1%	10	Analytical Standard	Avanti Polar Lipids
PE 40:07	+Na	812.52	812.52	0.706	0.001	290.8	0.6	0.2%	11	Analytical Standard	Avanti Polar Lipids
PE 40:05	+Na	816.55	816.55	0.696	0.002	294.8	0.7	0.2%	11	Analytical Standard	Avanti Polar Lipids
PE O-O-42:11	+K	818.49	818.50	0.708	0.002	289.8	0.9	0.3%	12	Analytical Standard	Avanti Polar Lipids
PE O-O-42:10	+K	820.50	820.51	0.702	0.001	292.6	0.6	0.2%	11	Analytical Standard	Avanti Polar Lipids
PE 39:03	+K	822.54	822.54	0.700	0.002	293.4	0.8	0.3%	11	Analytical Standard	Avanti Polar Lipids
PE O-O-44:14	+Na	824.50	824.48	0.712	0.002	288.2	1.0	0.3%	11	Analytical Standard	Avanti Polar Lipids
PE 39:02	+K	824.56	824.55	0.694	0.001	295.9	0.6	0.2%	11	Analytical Standard	Avanti Polar Lipids
PE O-O-44:13	+Na	826.52	826.50	0.709	0.001	289.4	0.6	0.2%	10	Analytical Standard	Avanti Polar Lipids
PE O-O-42:08	+K	826.55	826.56	0.691	0.002	297.0	0.7	0.2%	11	Analytical Standard	Avanti Polar Lipids
PE O-O-44:12	+Na	828.53	828.51	0.707	0.002	290.4	0.8	0.3%	11	Analytical Standard	Avanti Polar Lipids
PE 40:06	+K	830.51	830.53	0.696	0.002	294.7	0.8	0.3%	11	Analytical Standard	Avanti Polar Lipids
PE 42:10	+Na	834.50	834.50	0.705	0.002	291.0	0.7	0.2%	12	Analytical Standard	Avanti Polar Lipids
PE 42:09	+Na	836.52	836.52	0.694	0.001	295.6	0.4	0.1%	12	Analytical Standard	Avanti Polar Lipids
PE 42:08	+Na	838.54	838.53	0.690	0.001	297.3	0.5	0.2%	11	Analytical Standard	Avanti Polar Lipids
PE O-O-44:14	+K	842.49	842.49	0.704	0.002	291.4	0.7	0.3%	11	Analytical Standard	Avanti Polar Lipids
PE O-O-44:13	+K	844.50	844.51	0.696	0.001	294.7	0.6	0.2%	12	Analytical Standard	Avanti Polar Lipids
PE O-O-44:12	+K	846.52	846.52	0.691	0.001	297.0	0.6	0.2%	12	Analytical Standard	Avanti Polar Lipids
PE 42:10	+K	848.46	848.48	0.705	0.001	290.8	0.5	0.2%	11	Analytical Standard	Avanti Polar Lipids
PE O-O-44:11	+K	848.54	848.53	0.691	0.002	297.1	0.9	0.3%	11	Analytical Standard	Avanti Polar Lipids
PE O-O-46:15	+Na	850.52	850.50	0.701	0.002	292.7	0.7	0.2%	11	Analytical Standard	Avanti Polar Lipids
PE 42:08	+K	852.49	852.51	0.693	0.002	296.1	0.8	0.3%	11	Analytical Standard	Avanti Polar Lipids
PE O-O-45:14	+K	856.50	856.51	0.690	0.002	297.2	1.0	0.3%	11	Analytical Standard	Avanti Polar Lipids
PE 44:12	+Na	858.50	858.51	0.685	0.002	299.7	1.0	0.3%	8	Analytical Standard	Avanti Polar Lipids
PE 44:11	+Na	860.52	860.51	0.683	0.002	300.3	1.0	0.3%	8	Analytical Standard	Avanti Polar Lipids
PE O-O-46:16	+K	866.49	866.49	0.689	0.002	297.7	1.1	0.4%	12	Analytical Standard	Avanti Polar Lipids
PE O-O-46:15	+K	868.50	868.51	0.682	0.002	300.8	0.7	0.2%	11	Analytical Standard	Avanti Polar Lipids
PE O-O-46:14	+K	870.52	870.52	0.677	0.001	302.9	0.5	0.2%	10	Analytical Standard	Avanti Polar Lipids
PE O-45:12	+K	874.52	874.51	0.685	0.002	299.3	1.0	0.3%	7	Analytical Standard	Avanti Polar Lipids
PE 44:11	+K	876.49	876.50	0.685	0.001	299.3	0.5	0.2%	10	Analytical Standard	Avanti Polar Lipids
PE O-47:16	+Na	878.51	878.51	0.684	0.002	299.7	0.9	0.3%	11	Analytical Standard	Avanti Polar Lipids
PE O-O-47:16	+K	880.50	880.51	0.681	0.002	301.3	0.8	0.3%	11	Analytical Standard	Avanti Polar Lipids
PE O-46:14	+K	884.50	884.51	0.684	0.003	299.8	1.4	0.5%	8	Analytical Standard	Avanti Polar Lipids
PE O-46:13	+K	886.52	886.52	0.670	0.002	306.0	1.1	0.4%	8	Analytical Standard	Avanti Polar Lipids
PE O-O-48:16	+K	894.52	894.52	0.672	0.001	305.1	0.7	0.2%	11	Analytical Standard	Avanti Polar Lipids
PE O-47:14	+K	898.52	898.52	0.680	0.001	301.2	0.5	0.2%	11	Analytical Standard	Avanti Polar Lipids
PE O-47:13	+K	900.53	900.53	0.684	0.003	299.9	1.2	0.4%	11	Analytical Standard	Avanti Polar Lipids
PE 46:11	+K	904.53	904.51	0.678	0.002	302.4	0.9	0.3%	8	Analytical Standard	Avanti Polar Lipids

PE O-O-49:17	+K	906.52	906.52	0.672	0.002	304.9	0.9	0.3%	9	Analytical Standard	Avanti Polar Lipids
PE O-48:16	+K	908.50	908.49	0.675	0.002	303.5	0.9	0.3%	9	Analytical Standard	Avanti Polar Lipids
PE O-O-49:15	+K	910.52	910.52	0.672	0.001	304.9	0.6	0.2%	9	Analytical Standard	Avanti Polar Lipids
PE O-49:17	+K	920.50	920.50	0.670	0.002	306.1	1.0	0.3%	8	Analytical Standard	Avanti Polar Lipids
PE O-49:16	+K	922.52	922.52	0.682	0.002	300.6	1.1	0.4%	9	Analytical Standard	Avanti Polar Lipids
PE O-49:15	+K	924.53	924.53	0.673	0.003	304.7	1.2	0.4%	12	Analytical Standard	Avanti Polar Lipids
PE O-49:14	+K	926.55	926.55	0.665	0.002	308.1	1.0	0.3%	10	Analytical Standard	Avanti Polar Lipids
PE O-50:17	+K	934.52	934.51	0.658	0.002	311.2	1.0	0.3%	9	Analytical Standard	Avanti Polar Lipids
PE O-51:16	+K	950.55	950.54	0.659	0.002	311.0	0.7	0.2%	11	Analytical Standard	Avanti Polar Lipids
PE (1008.51)	--	1008.51	1008.51	0.637	0.002	321.2	0.8	0.3%	11	Analytical Standard	Avanti Polar Lipids
PE O-O-62:19	+K	1084.69	1084.69	0.600	0.001	340.5	0.8	0.2%	10	Analytical Standard	Avanti Polar Lipids
PE O-O-62:18	+K	1086.71	1086.71	0.598	0.001	341.8	0.7	0.2%	10	Analytical Standard	Avanti Polar Lipids
PE O-O-64:19	+K	1112.72	1112.72	0.589	0.002	347.3	1.1	0.3%	10	Analytical Standard	Avanti Polar Lipids
PE O-O-66:21	+K	1136.72	1136.73	0.586	0.001	348.9	0.7	0.2%	10	Analytical Standard	Avanti Polar Lipids
PE Dimer 36:05+36:04	+Na	1500.00	1500.00	0.481	0.001	423.9	0.8	0.2%	10	Analytical Standard	Avanti Polar Lipids
PE Dimer 36:04	+Na	1502.02	1502.02	0.477	0.001	426.9	0.8	0.2%	10	Analytical Standard	Avanti Polar Lipids
PE Dimer 36:05+38:05	+Na	1526.02	1526.02	0.474	0.001	429.9	0.7	0.2%	10	Analytical Standard	Avanti Polar Lipids
PE Dimer 36:05+38:04	+Na	1528.04	1528.04	0.473	0.001	430.3	0.6	0.1%	10	Analytical Standard	Avanti Polar Lipids
PE Dimer 38:06	+Na	1550.02	1550.03	0.472	0.001	431.8	0.9	0.2%	10	Analytical Standard	Avanti Polar Lipids
PE Dimer 38:06+38:05	+Na	1552.04	1552.04	0.470	0.001	433.5	0.6	0.1%	10	Analytical Standard	Avanti Polar Lipids
PE Dimer 39:06	+Na	1578.05	1578.06	0.460	0.000	443.1	0.3	0.1%	8	Analytical Standard	Avanti Polar Lipids
PE Dimer 40:07	+Na	1602.05	1602.05	0.460	0.001	442.8	0.8	0.2%	8	Analytical Standard	Avanti Polar Lipids
PS O-O-36:03	+Na	780.55	780.55	0.707	0.002	290.6	0.6	0.2%	11	Analytical Standard	Avanti Polar Lipids
PS O-O-36:02	+Na	782.57	782.57	0.703	0.002	292.2	0.7	0.3%	10	Analytical Standard	Avanti Polar Lipids
PS O-36:05	+Na	804.52	804.52	0.708	0.002	290.2	0.9	0.3%	10	Analytical Standard	Avanti Polar Lipids
PS 36:04	+Na	806.49	806.50	0.713	0.003	287.8	1.0	0.4%	13	Analytical Standard	Avanti Polar Lipids
PS 37:04	+Na	820.51	820.51	0.696	0.002	295.0	1.0	0.3%	11	Analytical Standard	Avanti Polar Lipids
PS 38:07	+Na	828.48	828.48	0.707	0.001	290.2	0.4	0.1%	11	Analytical Standard	Avanti Polar Lipids
PS 38:06	+Na	832.51	832.51	0.698	0.001	294.0	0.6	0.2%	10	Analytical Standard	Avanti Polar Lipids
PS 38:05	+Na	834.53	834.53	0.698	0.002	294.2	0.8	0.3%	12	Analytical Standard	Avanti Polar Lipids
PS 37:02	+K	840.52	840.51	0.700	0.002	293.0	0.9	0.3%	10	Analytical Standard	Avanti Polar Lipids
PS 39:07	+Na	842.49	842.50	0.700	0.002	293.1	1.0	0.3%	11	Analytical Standard	Avanti Polar Lipids
PS 39:06	+Na	846.53	846.52	0.689	0.002	297.7	1.0	0.3%	9	Analytical Standard	Avanti Polar Lipids
PS 39:05	+Na	848.54	848.54	0.677	0.002	303.3	0.9	0.3%	11	Analytical Standard	Avanti Polar Lipids
PE 38:04	+K	850.50	850.50	0.683	0.002	300.5	1.0	0.3%	11	Analytical Standard	Avanti Polar Lipids
PS O-O-41:10	+K	852.49	852.49	0.692	0.002	296.6	0.6	0.2%	7	Analytical Standard	Avanti Polar Lipids
PS 40:08	+Na	854.49	854.49	0.699	0.002	293.6	0.8	0.3%	11	Analytical Standard	Avanti Polar Lipids
PS 40:07	+Na	856.51	856.51	0.694	0.001	295.6	0.6	0.2%	10	Analytical Standard	Avanti Polar Lipids
PS 40:06	+Na	860.54	860.54	0.684	0.002	299.9	0.9	0.3%	10	Analytical Standard	Avanti Polar Lipids
PS 40:05	+Na	862.56	862.56	0.679	0.002	302.2	0.8	0.3%	10	Analytical Standard	Avanti Polar Lipids
PS 41:07	+Na	870.53	870.52	0.686	0.002	299.2	0.9	0.3%	11	Analytical Standard	Avanti Polar Lipids
PS O-O-44:13	+Na	872.52	872.51	0.687	0.002	298.4	1.0	0.3%	8	Analytical Standard	Avanti Polar Lipids
PS 41:06	+Na	872.54	872.54	0.676	0.002	303.3	1.1	0.4%	11	Analytical Standard	Avanti Polar Lipids
PS 42:12	+Na	874.46	874.46	0.698	0.003	293.7	1.1	0.4%	10	Analytical Standard	Avanti Polar Lipids
PS 42:11	+Na	876.48	876.48	0.697	0.002	294.2	0.7	0.2%	10	Analytical Standard	Avanti Polar Lipids
PS 42:10	+Na	878.49	878.49	0.690	0.001	297.1	0.6	0.2%	10	Analytical Standard	Avanti Polar Lipids

PS 42:09	+Na	880.51	880.51	0.679	0.002	302.0	0.7	0.2%	10	Analytical Standard	Avanti Polar Lipids
PS 42:08	+Na	882.53	882.53	0.681	0.002	301.3	0.9	0.3%	12	Analytical Standard	Avanti Polar Lipids
PS 42:07	+Na	884.54	884.54	0.673	0.001	304.7	0.6	0.2%	10	Analytical Standard	Avanti Polar Lipids
PS 42:05	+Na	888.57	888.57	0.668	0.001	307.0	0.6	0.2%	10	Analytical Standard	Avanti Polar Lipids
PS 43:09	+Na	894.53	894.52	0.676	0.002	303.2	1.0	0.3%	10	Analytical Standard	Avanti Polar Lipids
PS 43:08	+Na	896.54	896.53	0.672	0.001	305.2	0.6	0.2%	10	Analytical Standard	Avanti Polar Lipids
PS 44:13	+Na	900.48	900.48	0.695	0.002	294.9	0.8	0.3%	8	Analytical Standard	Avanti Polar Lipids
PS 44:12	+Na	902.49	902.50	0.684	0.001	299.7	0.5	0.2%	10	Analytical Standard	Avanti Polar Lipids
PS 44:11	+Na	904.51	904.51	0.679	0.001	302.1	0.6	0.2%	10	Analytical Standard	Avanti Polar Lipids
PS 44:10	+Na	906.53	906.52	0.675	0.001	303.5	0.6	0.2%	10	Analytical Standard	Avanti Polar Lipids
PS 44:09	+Na	908.54	908.54	0.675	0.002	303.7	0.7	0.2%	10	Analytical Standard	Avanti Polar Lipids
PS 44:08	+Na	910.56	910.56	0.668	0.001	306.8	0.5	0.2%	10	Analytical Standard	Avanti Polar Lipids
PS 45:15	+K	912.52	912.51	0.683	0.002	300.2	0.9	0.3%	8	Analytical Standard	Avanti Polar Lipids
PS 44:07	+Na	912.57	912.58	0.657	0.002	311.8	1.0	0.3%	13	Analytical Standard	Avanti Polar Lipids
PS 45:14	+K	914.47	914.47	0.677	0.002	302.6	1.0	0.3%	11	Analytical Standard	Avanti Polar Lipids
PS 43:07	+K	914.53	914.53	0.675	0.002	303.6	0.7	0.2%	8	Analytical Standard	Avanti Polar Lipids
PS 44:05	+Na	916.60	916.62	0.658	0.002	311.5	0.8	0.3%	10	Analytical Standard	Avanti Polar Lipids
PS O-45:12	+K	918.51	918.51	0.674	0.001	304.0	0.6	0.2%	10	Analytical Standard	Avanti Polar Lipids
PS 44:09	+K	924.52	924.52	0.667	0.002	307.0	0.7	0.2%	10	Analytical Standard	Avanti Polar Lipids
PS 46:12	+Na	930.53	930.53	0.662	0.002	309.5	0.8	0.3%	10	Analytical Standard	Avanti Polar Lipids
PS 46:11	+Na	932.54	932.54	0.666	0.002	307.7	0.8	0.3%	10	Analytical Standard	Avanti Polar Lipids
PS 46:10	+Na	934.56	934.56	0.663	0.002	309.2	0.8	0.3%	11	Analytical Standard	Avanti Polar Lipids
PS 45:10	+K	936.52	936.52	0.654	0.002	313.2	0.9	0.3%	10	Analytical Standard	Avanti Polar Lipids
PS 45:09	+K	938.53	938.53	0.659	0.002	310.6	1.1	0.4%	12	Analytical Standard	Avanti Polar Lipids
PS 46:08	+Na	938.59	938.60	0.654	0.002	313.2	0.8	0.2%	8	Analytical Standard	Avanti Polar Lipids
PS O-47:14	+K	942.51	942.51	0.670	0.002	305.9	0.7	0.2%	11	Analytical Standard	Avanti Polar Lipids
PS O-47:13	+K	944.52	944.52	0.665	0.002	308.1	1.0	0.3%	12	Analytical Standard	Avanti Polar Lipids
PS O-47:12	+K	946.54	946.53	0.662	0.002	309.2	1.0	0.3%	11	Analytical Standard	Avanti Polar Lipids
PS 46:10	+K	950.53	950.52	0.669	0.002	306.3	1.0	0.3%	12	Analytical Standard	Avanti Polar Lipids
PS 48:15	+Na	952.51	952.52	0.666	0.002	307.8	0.8	0.3%	10	Analytical Standard	Avanti Polar Lipids
PS 48:14	+Na	954.53	954.53	0.657	0.002	312.0	0.8	0.3%	10	Analytical Standard	Avanti Polar Lipids
PS 49:18	+Na	960.48	960.47	0.665	0.001	307.7	0.5	0.2%	8	Analytical Standard	Avanti Polar Lipids
PS 47:12	+K	960.52	960.52	0.665	0.002	307.8	0.8	0.3%	11	Analytical Standard	Avanti Polar Lipids
PS 47:11	+K	962.53	962.53	0.659	0.000	311.0	0.2	0.1%	9	Analytical Standard	Avanti Polar Lipids
PS 49:16	+Na	964.51	964.50	0.661	0.001	309.6	0.7	0.2%	7	Analytical Standard	Avanti Polar Lipids
PS O-50:16	+Na	964.55	964.54	0.655	0.001	312.4	0.6	0.2%	11	Analytical Standard	Avanti Polar Lipids
PS 49:15	+Na	966.53	966.52	0.656	0.000	312.3	1.2	0.4%	12	Analytical Standard	Avanti Polar Lipids
PS 49:14	+Na	968.54	968.54	0.651	0.002	314.6	0.8	0.3%	10	Analytical Standard	Avanti Polar Lipids
PS 48:14	+K	970.50	970.50	0.658	0.001	311.0	0.6	0.2%	10	Analytical Standard	Avanti Polar Lipids
PS 48:13	+K	972.52	972.52	0.654	0.002	313.0	0.9	0.3%	10	Analytical Standard	Avanti Polar Lipids
PS 48:12	+K	974.53	974.53	0.653	0.002	313.6	0.9	0.3%	10	Analytical Standard	Avanti Polar Lipids
PS 51:16	+Na	992.54	992.54	0.645	0.002	317.3	0.8	0.3%	10	Analytical Standard	Avanti Polar Lipids
PS 51:15	+Na	994.56	994.56	0.634	0.001	322.8	0.8	0.2%	10	Analytical Standard	Avanti Polar Lipids
PS 52:19	+Na	1000.51	1000.51	0.646	0.002	316.7	0.9	0.3%	10	Analytical Standard	Avanti Polar Lipids
PS 52:18	+Na	1002.53	1002.53	0.641	0.001	319.1	0.7	0.2%	10	Analytical Standard	Avanti Polar Lipids
PS 52:17	+Na	1004.54	1004.54	0.637	0.001	321.4	0.6	0.2%	10	Analytical Standard	Avanti Polar Lipids
PS 52:16	+Na	1006.56	1006.57	0.635	0.001	322.2	0.4	0.1%	7	Analytical Standard	Avanti Polar Lipids
PS O-51:10	+K	1006.63	1006.63	0.635	0.002	322.4	0.8	0.3%	9	Analytical Standard	Avanti Polar Lipids

PS 51:13	+K	1014.56	1014.55	0.626	0.002	326.8	1.0	0.3%	8	Analytical Standard	Avanti Polar Lipids
PS 51:12	+K	1016.58	1016.56	0.637	0.001	321.1	0.5	0.2%	8	Analytical Standard	Avanti Polar Lipids
PS 53:17	+Na	1018.56	1018.56	0.633	0.001	323.3	0.5	0.2%	7	Analytical Standard	Avanti Polar Lipids
PS 55:18	+Na	1044.57	1044.57	0.621	0.002	329.3	0.9	0.3%	7	Analytical Standard	Avanti Polar Lipids
SM 34:01	+Na	725.56	725.56	0.722	0.001	285.1	0.4	0.1%	10	Analytical Standard	Avanti Polar Lipids
SM O-36:03	+Na	735.58	735.57	0.708	0.001	290.4	0.6	0.2%	11	Analytical Standard	Avanti Polar Lipids
SM 35:01	+Na	739.57	739.57	0.711	0.002	289.1	0.8	0.3%	11	Analytical Standard	Avanti Polar Lipids
SM 36:02	+Na	751.57	751.57	0.707	0.001	290.9	0.2	0.1%	11	Analytical Standard	Avanti Polar Lipids
SM 36:01	+Na	753.59	753.59	0.703	0.001	292.4	0.2	0.1%	11	Analytical Standard	Avanti Polar Lipids
SM 37:01	+Na	767.60	767.60	0.697	0.001	294.8	0.6	0.2%	11	Analytical Standard	Avanti Polar Lipids
SM O-38:00	+Na	769.66	769.66	0.676	0.002	303.9	1.0	0.3%	11	Analytical Standard	Avanti Polar Lipids
SM 771.07	--	771.67	771.67	0.672	0.002	305.6	0.9	0.3%	10	Analytical Standard	Avanti Polar Lipids
SM 38:01	+Na	781.62	781.62	0.688	0.001	298.5	0.4	0.1%	10	Analytical Standard	Avanti Polar Lipids
SM 39:01	+Na	795.64	795.63	0.681	0.002	301.6	0.7	0.2%	11	Analytical Standard	Avanti Polar Lipids
SM O-40:00	+Na	797.69	797.69	0.670	0.002	306.7	0.7	0.2%	9	Analytical Standard	Avanti Polar Lipids
SM 40:03	+Na	805.62	805.62	0.685	0.002	299.9	0.9	0.3%	11	Analytical Standard	Avanti Polar Lipids
SM 40:02	+Na	807.64	807.63	0.681	0.001	301.7	0.3	0.1%	11	Analytical Standard	Avanti Polar Lipids
SM 40:01	+Na	809.65	809.65	0.676	0.001	303.9	0.5	0.2%	11	Analytical Standard	Avanti Polar Lipids
SM 40:00	+Na	811.67	811.66	0.672	0.001	305.7	0.5	0.1%	10	Analytical Standard	Avanti Polar Lipids
SM O-42:04	+Na	817.66	817.65	0.659	0.001	311.3	0.5	0.2%	9	Analytical Standard	Avanti Polar Lipids
SM 41:02	+Na	821.65	821.65	0.675	0.001	303.9	0.5	0.2%	11	Analytical Standard	Avanti Polar Lipids
SM 41:01	+Na	823.67	823.66	0.670	0.001	306.3	0.3	0.1%	9	Analytical Standard	Avanti Polar Lipids
SM 42:03	+Na	833.65	833.65	0.672	0.001	305.6	0.4	0.1%	11	Analytical Standard	Avanti Polar Lipids
SM 42:02	+Na	835.67	835.67	0.666	0.001	308.2	0.2	0.1%	10	Analytical Standard	Avanti Polar Lipids
SM 42:01	+Na	837.68	837.68	0.663	0.001	309.3	0.3	0.1%	9	Analytical Standard	Avanti Polar Lipids
SM 43:03	+Na	847.67	847.66	0.663	0.001	309.6	0.3	0.1%	10	Analytical Standard	Avanti Polar Lipids
SM 43:02	+Na	849.68	849.68	0.659	0.001	311.5	0.3	0.1%	8	Analytical Standard	Avanti Polar Lipids
SM 43:01	+Na	851.70	851.69	0.657	0.001	312.5	0.4	0.1%	9	Analytical Standard	Avanti Polar Lipids
SM O-43:01	+K	853.69	853.68	0.645	0.001	318.0	0.7	0.2%	9	Analytical Standard	Avanti Polar Lipids
SM 44:03	+Na	861.68	861.68	0.657	0.001	312.0	0.5	0.2%	8	Analytical Standard	Avanti Polar Lipids
SM 44:02	+Na	863.70	863.70	0.654	0.001	313.5	0.4	0.1%	10	Analytical Standard	Avanti Polar Lipids
SM 44:01	+Na	865.71	865.71	0.651	0.001	315.1	0.3	0.1%	9	Analytical Standard	Avanti Polar Lipids
SM dimer 35:01	+Na	1456.16	1456.17	0.459	0.001	444.2	0.8	0.2%	4	Analytical Standard	Avanti Polar Lipids
SM dimer 36:01+36:02	+Na	1482.17	1482.18	0.457	0.000	445.6	0.3	0.1%	4	Analytical Standard	Avanti Polar Lipids
SM dimer 36:01	+Na	1484.19	1484.20	0.465	0.000	438.1	0.1	0.0%	4	Analytical Standard	Avanti Polar Lipids
SM dimer 37:01	+Na	1512.22	1512.23	0.458	0.000	444.8	0.3	0.1%	4	Analytical Standard	Avanti Polar Lipids
SM dimer 38:01+38:02	+Na	1538.23	1538.25	0.469	0.000	433.9	0.3	0.1%	4	Analytical Standard	Avanti Polar Lipids
SM dimer 38:01	+Na	1540.25	1540.26	0.464	0.000	439.4	0.1	0.0%	4	Analytical Standard	Avanti Polar Lipids
SM dimer 38:01+39:02	+Na	1552.25	1552.26	0.441	0.001	461.7	0.8	0.2%	4	Analytical Standard	Avanti Polar Lipids
SM dimer 38:01+39:01	+Na	1554.27	1554.28	0.452	0.000	450.2	0.3	0.1%	4	Analytical Standard	Avanti Polar Lipids
SM dimer 39:02	+Na	1564.25	1564.27	0.464	0.001	438.5	0.6	0.1%	4	Analytical Standard	Avanti Polar Lipids
SM dimer 39:01 + 39:02	+Na	1566.27	1566.28	0.451	0.000	451.5	0.2	0.1%	4	Analytical Standard	Avanti Polar Lipids

Table C.5 CCS Values Measured in Both Helium and Nitrogen Drift Gas. Adapted from Jody C. May, Cody R. Goodwin, Nichole M. Lareau, Katrina L. Leaptrot, Caleb B. Morris, Ruwan T. Kurulugama, A. Mordehai, C. Klein, W. Barry, E. Darland, G. Overney, K. Imatani, George C. Stafford, John C. Fjeldsted, John A. McLean, “Conformational Ordering of Biomolecules in the Gas Phase: Nitrogen Collision Cross Sections Measured on a Prototype High Resolution Drift Tube Ion Mobility-Mass Spectrometer,” *Analytical Chemistry* 2014, 86 (4), 2107-2116. (<https://pubs.acs.org/doi/10.1021/ac4038448>) Note that further permissions related to the material excerpted should be directed to the ACS.

Analyte	Exact m/z	Nitrogen CCS (This Work) [Å ²]	Helium CCS (Literature) [Å ²]	Difference in CCS [Å ²]	Absolute Difference [%]	Literature Reference for Helium CCS Values	
Quaternary Ammonium Salts (N=8)							
Tetramethylammonium	TAA1	74.1	107.4*	48.5	58.9	76%	1
Tetraethylammonium	TAA2	130.3	123.3	65.9	57.4	61%	1
Tetrapropylammonium	TAA3	186.4	144.1	88.9	55.2	47%	1
Tetrabutylammonium	TAA4	242.5	166.6	111.2	55.4	40%	1
Tetrapentylammonium	TAA5	298.6	190.1	133.5	56.6	35%	1
Tetrahexylammonium	TAA6	354.7	213.5	154.9	58.6	32%	1
Tetraheptylammonium	TAA7	410.8	236.4	174.5	61.9	30%	1
Tetraoctylammonium	TAA8	466.5	256.6	194.3	62.3	28%	1
Carbohydrates (N=24)							
Lactose + Na		342.30	178.1	121.1	57.0	38%	2
Maltotetraose + Na		689.21	235.3	159.0	76.3	39%	2
Lacto-N-fucopentaose I + Li		860.32	269.6	203.1	66.5	28%	2
Lacto-N-fucopentaose I + Na		876.30	276.1	204.4	71.7	30%	2
Lacto-N-fucopentaose II + Na		876.30	271.1	201.3	69.8	30%	2
Lacto-N-fucopentaose I + K		892.27	274.7	205.0	69.7	29%	2
Lacto-N-fucopentaose II + K		892.27	267.2	202.6	64.6	28%	2
Lacto-N-fucopentaose I + Rb		938.22	275.2	198.4	76.8	32%	2
Lacto-N-fucopentaose II + Rb		938.22	278.4	197.5	80.9	34%	2
Lacto-N-fucopentaose I + Cs		986.21	275.6	204.0	71.6	30%	2
α-cyclodextrin + Na		995.31	285.5	200.7	84.8	35%	2
Lacto-N-difucohexaose I + Li		1006.38	301.4	225.9	75.5	29%	6
Maltohexaose + Na		1013.32	286.4	206.0	80.4	33%	2
Lacto-N-difucohexaose I + Na		1022.35	290.6	225.6	65.0	25%	2
Lacto-N-difucohexaose I + Na		1022.35	304.2	225.6	78.6	30%	2
Lacto-N-difucohexaose II + Na		1022.35	291.2	220.6	70.6	28%	2
Lacto-N-difucohexaose II + Na		1022.35	306.3	220.6	85.7	33%	2
Lacto-N-difucohexaose I + K		1038.33	303.5	229.8	73.8	28%	6
Lacto-N-difucohexaose II + K		1038.33	305.8	225.3	80.5	30%	6

Lacto-N-difucohexaose I + Rb	1084.28	303.2	230.0	73.2	27%	6
Lacto-N-difucohexaose I + Cs	1132.27	301.2	232.3	68.9	26%	6
β -cyclodextrin + Na	1157.36	319.7	231.4	88.3	32%	2
Maltoheptaose + Na	1175.37	303.1	236.4	66.7	25%	6
Maltoheptaose + K	1191.34	303.4	236.7	66.7	25%	6
Tryptic Peptides (N=38)						
YVR + H	437.3	207.0	140.2	66.8	38%	3
GVFR + H	478.3	214.8	146.8	68.1	38%	3
SDGRG + H	491.2	204.6	130.0	74.6	45%	4
GRGDS + H	491.2	205.9	132.0	73.9	44%	4
VYAR + H	508.3	217.1	157.1	60.1	32%	3
ADLAK + H	517.3	228.3	159.3	69.0	36%	3
WMGK + H	521.3	220.1	152.9	67.2	36%	3
FWGK + H	537.3	231.0	160.5	70.5	36%	3
VASLR + H	545.3	232.5	163.7	68.8	35%	3
AFDEK + H	609.3	238.3	168.4	69.9	34%	3
GQIVGR + H	629.4	245.5	173.6	71.9	34%	3
IETMR + H	649.3	252.8	181.3	71.5	33%	3
AAGHDGK + H	655.3	249.0	170.2	78.8	38%	3
ANIDVK + H	659.4	248.1	176.8	71.3	34%	3
GVLHAVK + H	723.5	269.9	199.2	70.7	30%	3
SVYDSR + H	726.3	258.4	184.2	74.3	34%	3
NVPLYK + H	733.4	272.2	195.3	76.9	33%	3
IATAIEK + H	745.4	275.5	202.9	72.6	30%	3
LNQLLR + H	756.5	275.6	205.0	70.6	29%	3
HLADLSK + H	783.4	273.3	201.8	71.6	30%	3
LVTDLTK + H	789.5	276.6	205.8	70.8	29%	3
YDLDFK + H	800.4	272.4	201.0	71.4	30%	3
TFAEALR + H	807.4	283.5	210.0	73.5	30%	3
AADALLK + H	814.5	291.8	223.9	68.0	26%	3
DIVGAVLK + H	814.5	277.8	206.1	71.7	30%	3
ATEEQLK + H	818.4	281.3	206.4	74.9	31%	3
IGDYAGIK + H	836.5	285.9	210.4	75.5	30%	3
DIPVPKPK + H	893.5	294.2	219.2	75.0	29%	3
AEFVEVTK + H	922.5	295.7	223.4	72.3	28%	3
LYEYIAR + H	927.5	305.0	228.0	76.9	29%	3
EALDFFAR + H	968.5	305.9	231.1	74.9	28%	3
LVVSTQTALA + H	1002.6	315.6	239.3	76.3	28%	3
ANELLINVK + H	1013.6	326.8	249.7	77.1	27%	3
GVIFYESHGK + H	1136.6	332.9	254.9	78.0	27%	3

IGSEVYHNLK + H	1159.6	348.4	269.7	78.7	25%	3
LVNELTEFAK + H	1163.6	344.4	267.5	76.9	25%	3
SISIVGSYVGNR + H	1251.7	349.1	267.8	81.3	26%	3
VNQIGTLSESIK + H	1288.7	358.7	278.8	80.0	25%	3
Lipids (N=49)						
PE 34:02 + Na	738.5	278.3	213.5	64.8	26%	2
PE 34:01 + Na	740.5	281.3	214.7	66.6	27%	2
SM (36:01) + Na	753.6	292.4	221.3	71.1	28%	2
PC 32:01 + Na [†]	754.5	283.6	217.6	66.0	26%	5
PC 32:00 + Na	756.6	286.5	217.4	69.1	27%	5
PE 36:04 + Na	762.5	280.6	214.4	66.2	27%	2
PE 36:02 + Na	766.5	285.7	220.9	64.8	26%	2
PE 35:02 + K [†]	768.6	282.5	221.7	60.8	24%	2
SM O-(38:00) + Na [†]	769.6	303.9	222.7	81.2	31%	2
PC 34:02 + Na	780.6	290.1	218.9	71.2	28%	2
SM (38:01) + Na	781.6	298.5	231.3	67.2	25%	2
PC 34:01 + Na	782.6	291.5	221.7	69.8	27%	2
PE 38:05 + Na	788.5	287.2	220.6	66.6	26%	2
PE 38:04 + Na	790.5	290.0	228.1	61.9	24%	2
SM O-(40:00) + Na [†]	797.6	306.7	227.9	78.8	29%	5
PC 34:01 + K	798.5	292.5	222.0	70.5	27%	5
PC 36:04 + Na	804.6	293.8	221.3	72.5	28%	5
PC 36:03 + Na [†]	806.6	294.5	220.6	73.9	29%	5
GlcCer 40:01 + Na	806.6	301.1	232.9	68.2	26%	2
PC 36:02 + Na	808.6	296.1	226.7	69.4	27%	2
GlcCer 40:00 + Na [†]	808.6	302.3	236.6	65.7	24%	2
SM (40:01) + Na [†]	809.7	303.9	225.4	78.5	30%	5
PC 36:01 + Na	810.6	297.7	228.1	69.6	26%	2
GlcCer 41:01 + Na [†]	820.6	302.5	236.2	66.3	25%	2
PC 36:03 + K	822.5	297.8	222.9	74.9	29%	5
GlcCer 40:01 h + Na	822.6	303.4	234.6	68.8	26%	2
PC 36:02 + K	824.6	299.9	226.2	73.7	28%	2
GlcCer 40:00 h + Na [†]	824.6	306.1	237.9	68.2	25%	2
PC 38:05 + Na	830.6	298.2	222.2	76.0	29%	2
PC 38:04 + Na	832.6	299.0	228.5	70.5	27%	2
GlcCer 42:02 + Na	832.7	305.2	238.8	66.4	24%	2
PS 38:05 + Na [†]	834.5	294.2	225.5	68.7	26%	2
GlcCer 42:01 + Na	834.7	307.5	239.3	68.2	25%	2
SM (42:02) + Na	835.7	308.2	239.4	68.8	25%	2
GlcCer 42:00 + Na [†]	836.7	308.2	240.2	68.0	25%	2

SM (42:01) + Na	837.7	309.3	239.3	70.0	26%	2
PS 37:02 + K [†]	840.6	293.0	222.6	70.4	27%	2
PC 38:06 + K	844.5	300.6	224.6	76.0	29%	5
GlcCer 43:02 + Na [†]	846.6	307.8	238.8	69.0	25%	2
PC 38:04 + K	848.6	301.5	230.0	71.5	27%	5
GlcCer 42:02 h + Na	848.7	309.0	240.3	68.7	25%	2
GlcCer 42:01 h + Na [†]	850.6	312.7	242.8	69.9	25%	5
SM O-(43:01) + K [†]	853.7	318.0	241.2	76.8	27%	5
GlcCer 44:02 + Na	860.7	315.3	245.9	69.4	25%	5
GlcCer 43:02 h + Na [†]	862.7	314.6	244.3	70.3	25%	5
GlcCer 43:01 h + Na [†]	864.6	313.7	245.2	68.5	25%	2
GlcCer 44:02 h + Na	876.7	318.4	246.7	71.7	25%	5
PS 42:09 + Na	880.5	302.0	238.0	64.0	24%	2
PS 42:08 + Na	882.5	301.3	230.8	70.5	26%	2

* TAA1 nitrogen CCS value obtained from Reference 1.

[†] Denotes lipid identifications which are different than originally reported in literature, due to the higher mass accuracy measurements obtained in this study.

References:

1. I. Campuzano, M.F. Bush, C.V. Robinson, C. Beaumont, K. Richardson, H. Kim, H.I. Kim, *Analytical Chemistry* 2012, 84(2), 1026-33.
2. L.S. Fenn, M. Kliman, A. Mahsut, S. Zhao, J.A. McLean, *Analytical and Bioanalytical Chemistry* 2009, 394, 235-244.
3. S.J. Valentine, A.E. Counterman, D.E. Clemmer, *Journal of the American Society for Mass Spectrometry* 1999, 10, 1188-1211.
4. M.F. Bush, Z. Hall, K. Giles, J. Hoyes, C.V. Robinson, B.T. Ruotolo, *Analytical Chemistry* 2010, 82(22), 9557-9565.
5. W.B. Ridenour, M. Kliman, J.A. McLean, R.M. Caprioli, *Analytical Chemistry* 2010, 82(5), 1881-1889.
6. Unpublished values measured in helium on a uniform field IM-MS instrument (Vanderbilt drift tube). For instrumentation details, see: S. Sundarapandian, J.C. May, J.A. McLean, *Analytical Chemistry* 2010, 82, 3247-3254.

C.4 Carbohydrate Nomenclature

Lacto-N-fucopentaose I	Fuc α 1-2Gal β 1-3GlcNAc β 1-3Gal β 1-4Glc
Lacto-N-fucopentaose II	Gal β 1-3[Fuc α 1-4]GlcNAc β 1-3Gal β 1-4Glc
Lacto-N-difucohexaose I	Fuc α 1-2Gal β 1-3[Fuc α 1-4]GlcNAc β 1-3Gal β 1-4Glc
Lacto-N-difucohexaose II	Gal β 1-3[Fuc α 1-4]GlcNAc β 1-3Gal β 1-4[Fuc α 1-3]Glc
α -cyclodextrin	cyclomaltohexaose
β -cyclodextrin	cyclomaltoheptaose

Hex – Hexose (Hexose assignments in the database are based on exact mass measurement. The exact type of hexose is uncertain)

Fuc – Fucose (All pentose identifications are assigned as fucose in the database as this is the only pentose present in the samples)

HexNAc – N-acetylated hexosamine (the exact type of hexose is uncertain).

Gal – Galactose

Glc – Glucose

GlcNAc – N-acetylglucosamine

C.5 Lipid Nomenclature

Glycerophospholipids:

Ex. PC x:y

PC, PE, PS = abbreviated names for phosphatidylcholine, phosphatidylethanolamine, phosphatidylserine respectively

x = total number of carbons in fatty acid chains

y = total number of double bonds in fatty acid chains

Sphingolipids:

Ex. SM x:y

SM, GlcCer = abbreviated names for sphingomyelin and cerebroside respectively

x = total number of carbons in the amide linked fatty acid of the ceramide plus eighteen carbons from the sphingosine backbone

y = total number of double bonds, one trans double bond in the sphingosine backbone plus the number of double bonds in the amide

linked fatty acid of the ceramide

Hydroxylation on Cerebrosides:

Ex. GlcCer x:y h

h = denotes hydroxylation on the number two carbon (from the carbonyl) of the amide linked fatty acid

Alkyl Ether Linkage

Ex. PS O-x:y

x = total number of carbons in fatty acid chains

y = total number of double bonds in fatty acid chains

O = alkyl ether substituent

O-O = alkyl ether substituent occurs on both chains

APPENDIX D

SUPPLEMENTAL INFORMATION FOR CHAPTER 5

D.1 Equations used to calculate the various analytical figures-of-merit in this work

Single-peak resolving power (R_p) is calculated in this work as

$$R_p = \frac{CCS}{\Delta CCS} \quad (D.1)$$

Here, CCS is the collision cross section, and ΔCCS is the full width at half maximum (FWHM) in CCS for the peak.

Two-peak resolution (R_{pp}) is calculated in this work as

$$R_{pp} = 1.18 * \frac{(t_2 - t_1)}{(\Delta t_2 + \Delta t_1)} \quad (D.2)$$

Here, t_1 is the centroid drift time of the first analyte peak, t_2 is the centroid drift time of the second analyte peak, Δt_1 is the FWHM for the first analyte peak, and Δt_2 is the FWHM for the second analyte peak.

Peak capacity is calculated in this work as

$$Peak\ Capacity = \frac{CCS_2 - CCS_1}{\frac{1}{2}(\Delta CCS_1 + \Delta CCS_2)} \quad (D.3)$$

Here, CCS_1 is the collision cross section for the most compact structure in a given mass range, CCS_2 is the collision cross section for the most loosely packed structure, ΔCCS_1 is the FWHM of the peak for the most compact CCS, and ΔCCS_2 is the FWHM of the peak for the most loosely packed CCS. In this work, the mass range selected is a ca. 100 Da wide mass window that contains four small mass analytes from the different chemical classes investigated (c.f., the insets in Figure 5.4 of the main text).

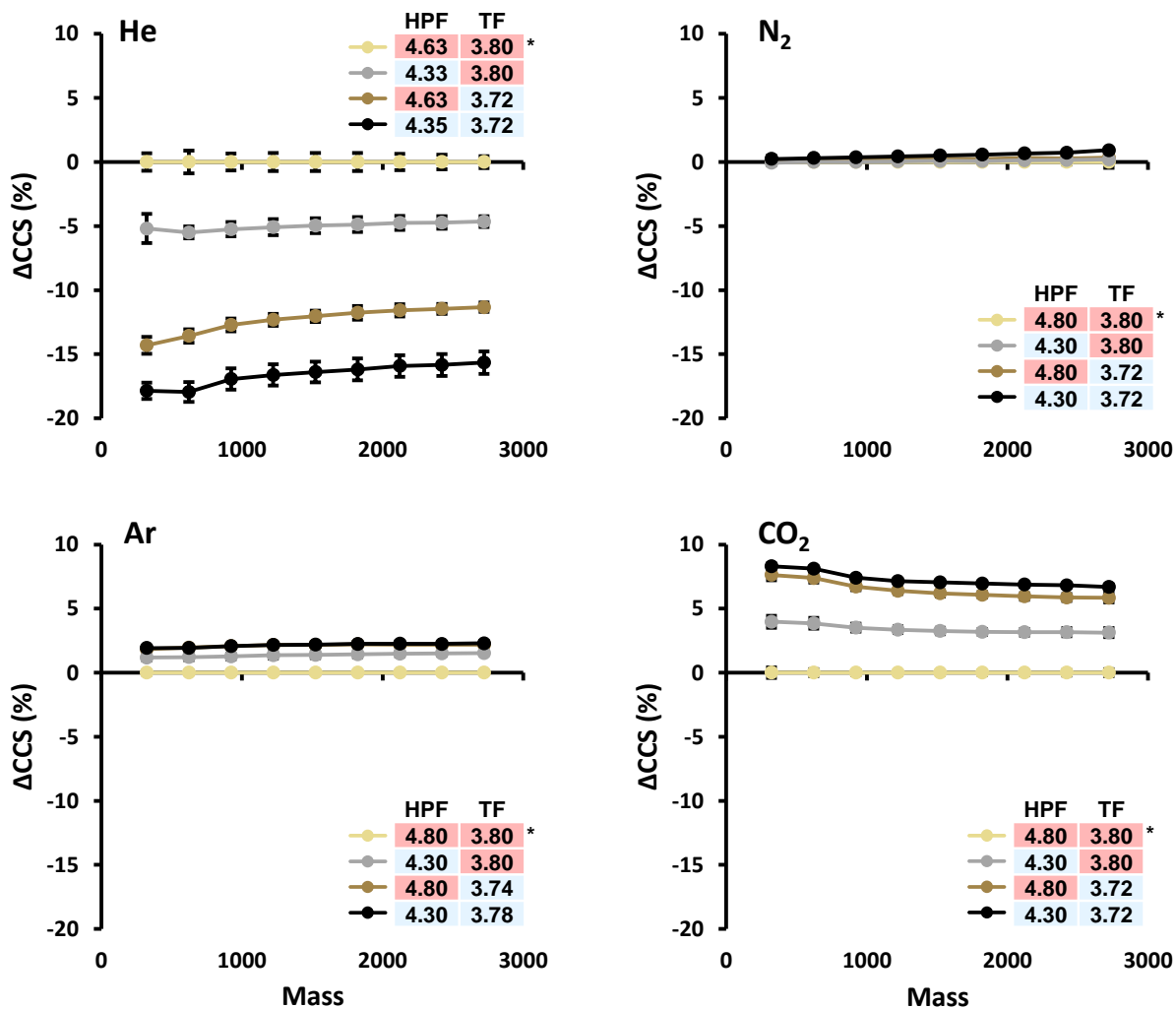


Figure D.1 The effect of the operational pressure of the two front funnel regions (HPF and TF) on the measured CCS of HFAP ions. Mass (in Da) is projected on the x-axis, whereas the y-axis represents the change in CCS relative to high pressure operational conditions (denoted with the asterisk in each legend). Error bars represent five replicate measurements. Red and blue shading in the legends indicate high or low relative pressure conditions for HPF and TF. Lower HPF and TF operational pressures had minimal effect on the CCS in N₂, but increased CCS in Ar and CO₂ and decreased the measured CCS in He. These results are interpreted as a DT gas intrusion effect caused when operating at the higher pressures. Adapted from Caleb B. Morris, Jody C. May, Katrina L. Leaptrot, and John A. McLean, "Evaluating Separation Selectivity and Collision Cross Section Measurement Reproducibility in Helium, Nitrogen, Argon, and Carbon Dioxide Drift Gases for Drift Tube Ion Mobility-Mass Spectrometry," *Journal of the American Society for Mass Spectrometry* 2019 (in press).

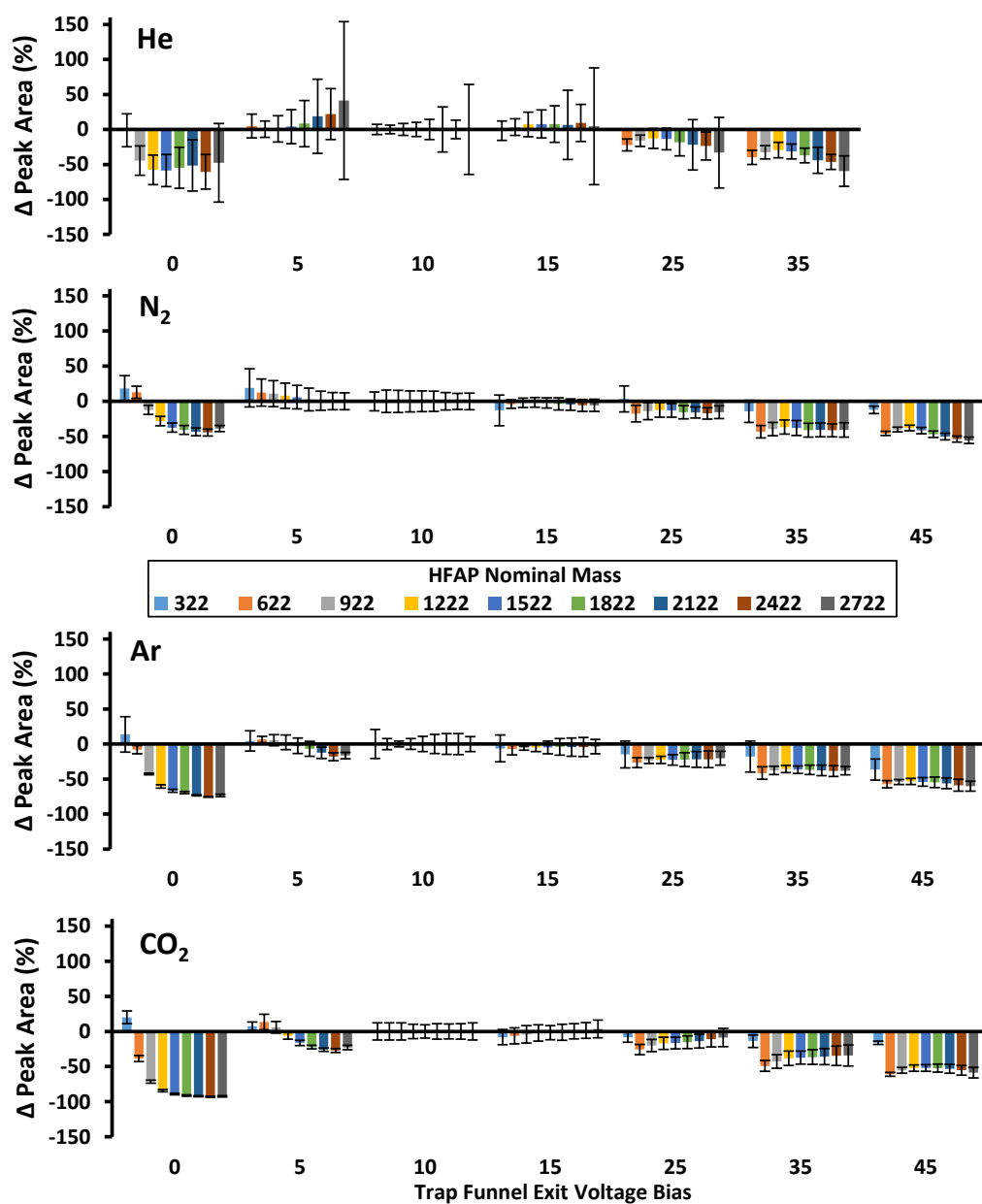


Figure D.2 The effect of the ion injection voltage (trap exit voltage) on the ion intensity (relative peak areas) of HFAP ions. The y-axis is the percent change in peak area relative to the vendor-recommended setting of 10 V at each trap funnel exit voltage bias (x-axis, in volts). All error bars are based on five replicate measurements. The highest ion abundances were observed at around 10 V. Data for voltages above 35V in helium was not obtained due to electrical breakdown issues. Adapted from Caleb B. Morris, Jody C. May, Katrina L. Leaptrot, and John A. McLean, “Evaluating Separation Selectivity and Collision Cross Section Measurement Reproducibility in Helium, Nitrogen, Argon, and Carbon Dioxide Drift Gases for Drift Tube Ion Mobility-Mass Spectrometry,” *Journal of the American Society for Mass Spectrometry* 2019 (in press).

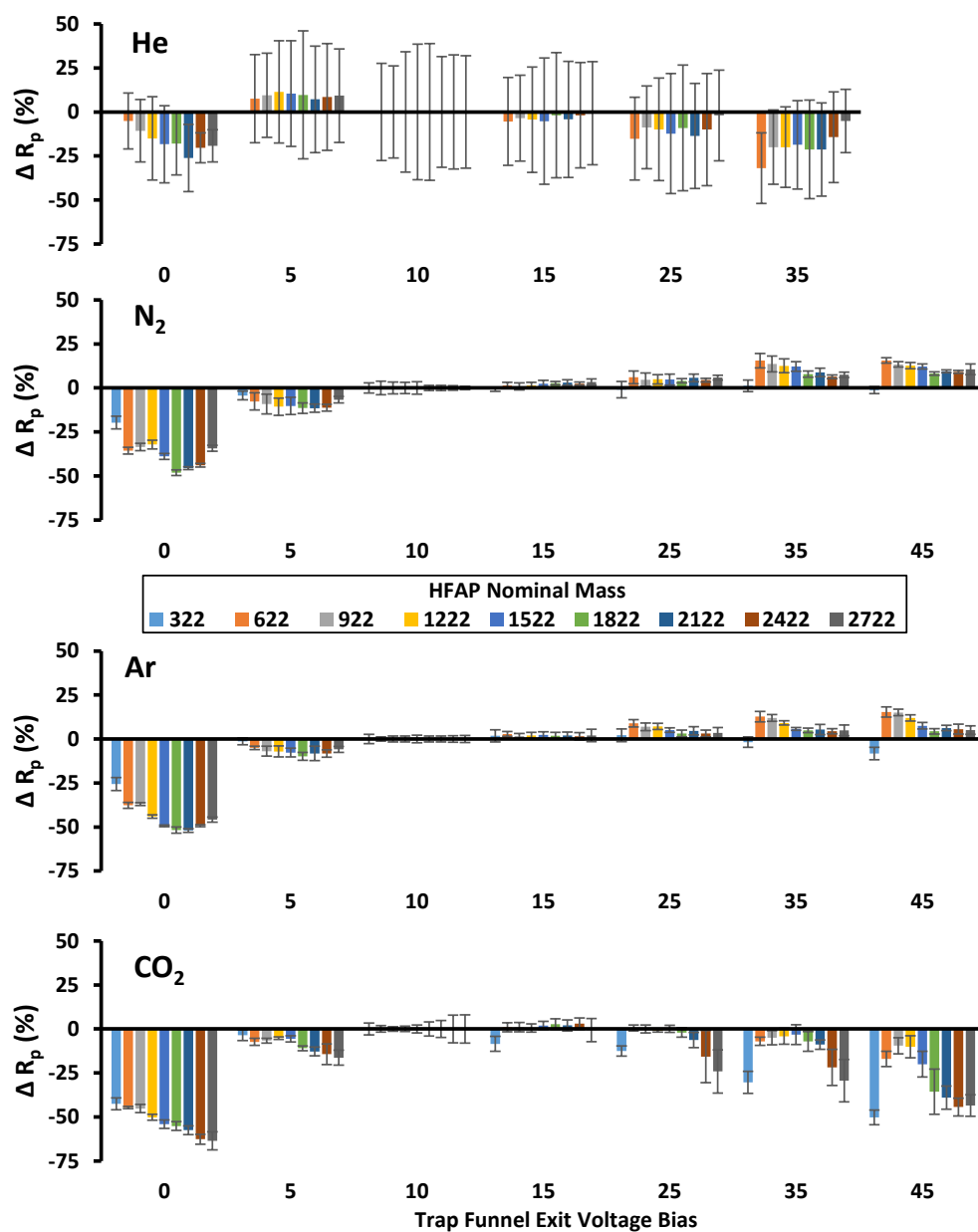


Figure D.3 The effect of the ion injection voltage (trap funnel exit bias, in volts) on the single-peak resolving power (R_p) for all HFAP ions. The y-axis is the change in R_p as compared to the vendor default setting of 10 V. All error bars are based on five replicate measurements. Increasing the ion injection voltage modestly increased ($\sim 15\%$) the resolving power in N₂ and Ar, however CO₂ exhibited a maximum resolving power at 10 to 15 V, whereas He saw no R_p difference outside of error. Data for voltages above 35V in helium was not obtained due to electrical breakdown issues. Adapted from Caleb B. Morris, Jody C. May, Katrina L. Leaptrot, and John A. McLean, “Evaluating Separation Selectivity and Collision Cross Section Measurement Reproducibility in Helium, Nitrogen, Argon, and Carbon Dioxide Drift Gases for Drift Tube Ion Mobility-Mass Spectrometry,” *Journal of the American Society for Mass Spectrometry* 2019 (in press).

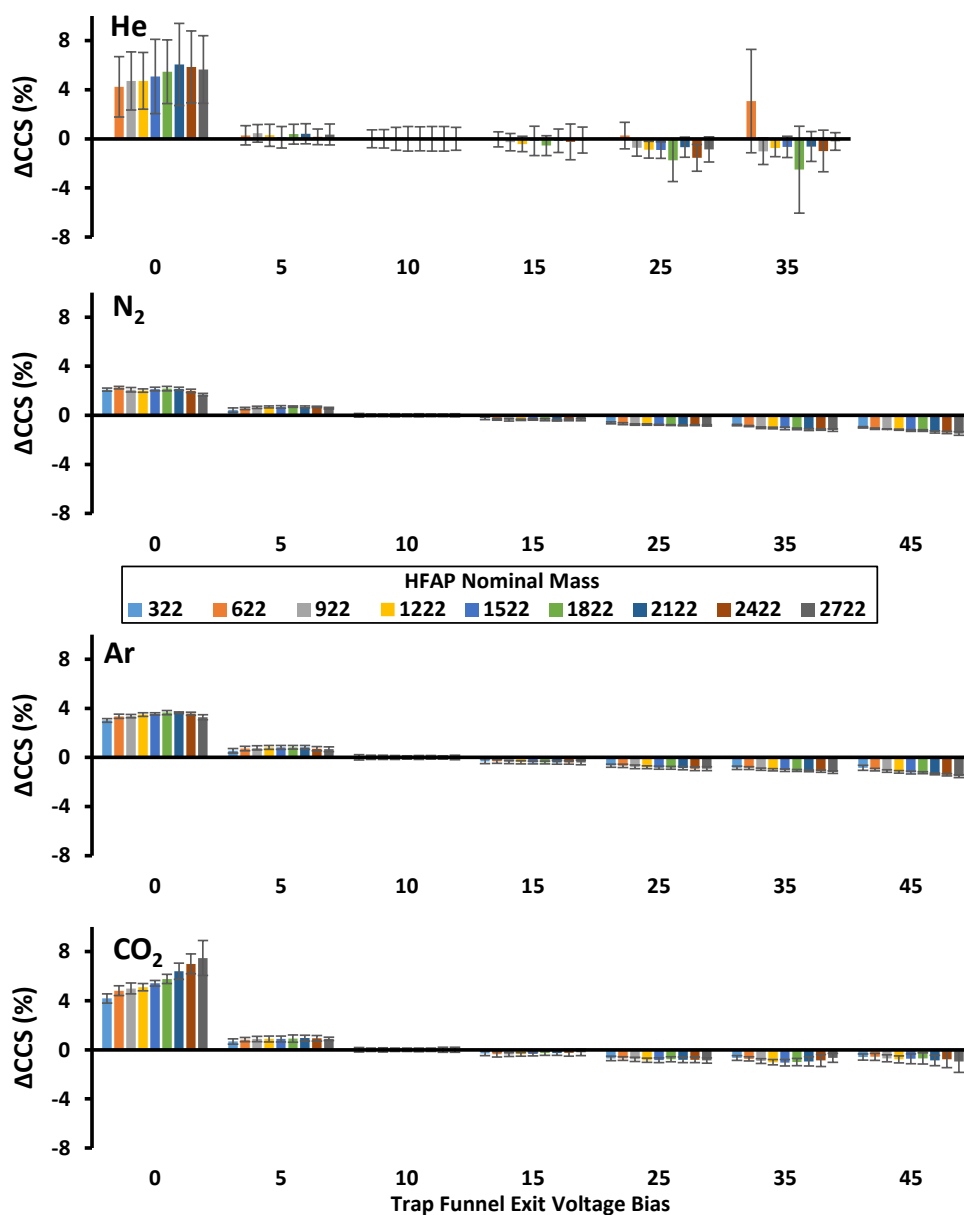


Figure D.4 The effect of the ion injection voltage (trap exit voltage) on the measured CCS for HFAP ions. The y-axis is the change in CCS relative to the vendor-recommended setting of 10 V at each trap funnel exit voltage bias (x-axis, in volts). All error bars are based on five replicate measurements. Increasing the ion injection voltage decreases the CCS for all but helium, which saw no difference outside of error. Data for voltages above 35V in helium was not obtained due to electrical breakdown issues. Adapted from Caleb B. Morris, Jody C. May, Katrina L. Leaptrout, and John A. McLean, "Evaluating Separation Selectivity and Collision Cross Section Measurement Reproducibility in Helium, Nitrogen, Argon, and Carbon Dioxide Drift Gases for Drift Tube Ion Mobility-Mass Spectrometry," *Journal of the American Society for Mass Spectrometry* 2019 (in press).

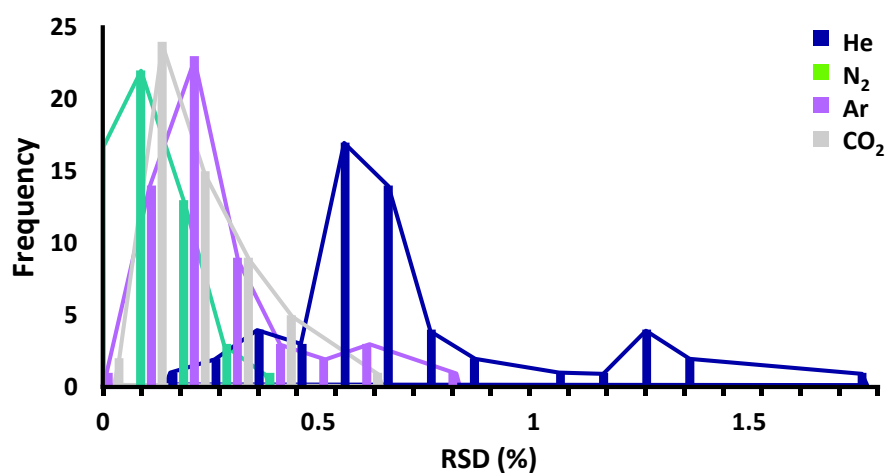


Figure D.5 Histogram of the empirical relative standard deviations (RSD) in CCS observed in each drift gas, based on five measurements for each analyte. The average %RSD observed for N₂, Ar, and CO₂ was ~0.2%, whereas in He, the RSD was ~0.6% on average, but deviations >1% were also observed. Adapted from Caleb B. Morris, Jody C. May, Katrina L. Leaptrot, and John A. McLean, “Evaluating Separation Selectivity and Collision Cross Section Measurement Reproducibility in Helium, Nitrogen, Argon, and Carbon Dioxide Drift Gases for Drift Tube Ion Mobility-Mass Spectrometry,” *Journal of the American Society for Mass Spectrometry* 2019 (in press).

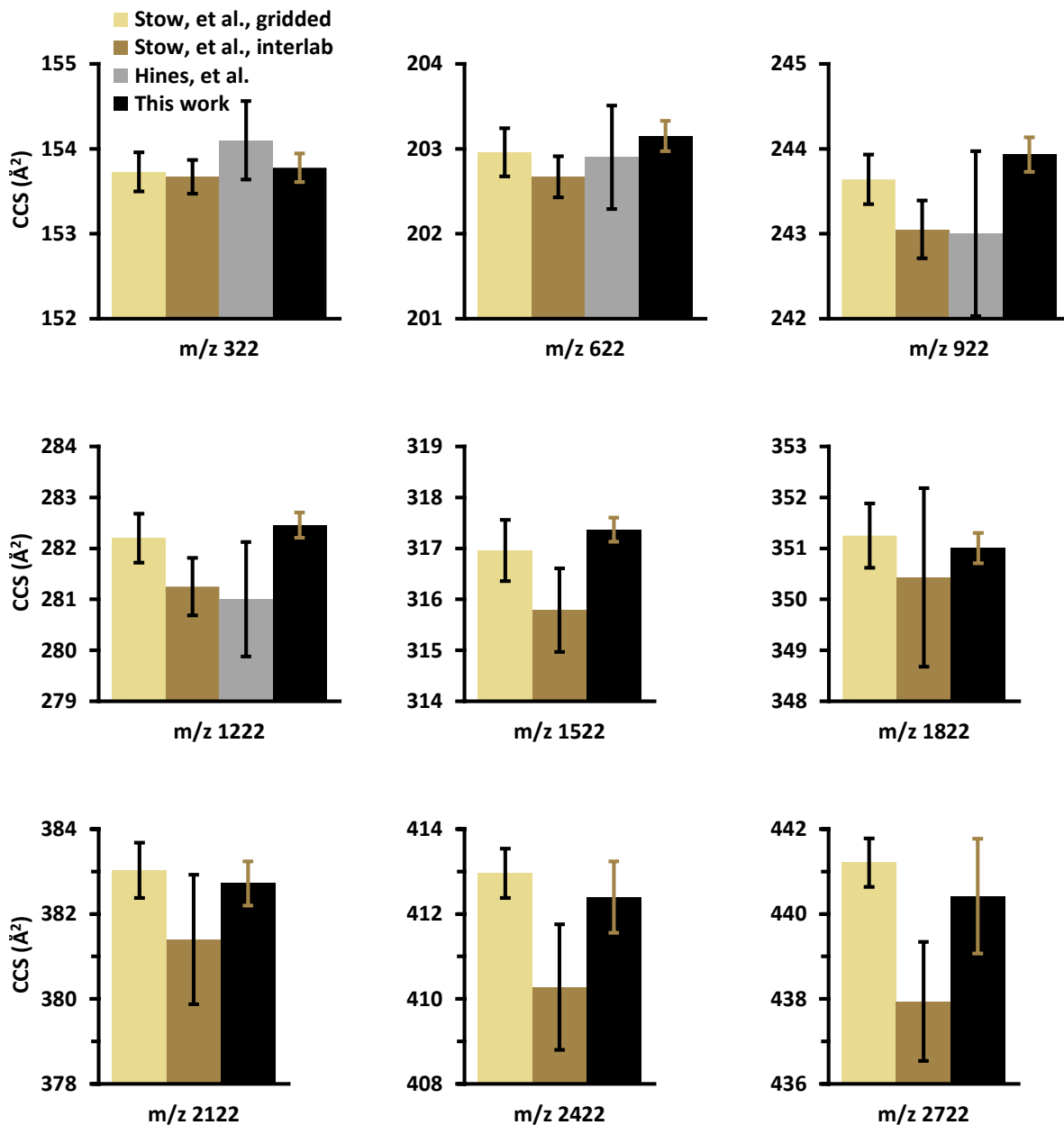


Figure D.6 Tuning mixture (HFAP) CCS measurements obtained in nitrogen, for this work and compared to previously published values.^{1,2} Measurements in tan (Stow et al., gridded¹) were obtained on a gridded reference drift tube instrument, while the measurements in brown (Stow et al., interlab¹) represent the averaged ^{DT}CCS_{N₂} values reported in a recent interlaboratory study Adapted from Caleb B. Morris, Jody C. May, Katrina L. Leaptrot, and John A. McLean, “Evaluating Separation Selectivity and Collision Cross Section Measurement Reproducibility in Helium, Nitrogen, Argon, and Carbon Dioxide Drift Gases for Drift Tube Ion Mobility-Mass Spectrometry,” *Journal of the American Society for Mass Spectrometry* 2019 (in press).

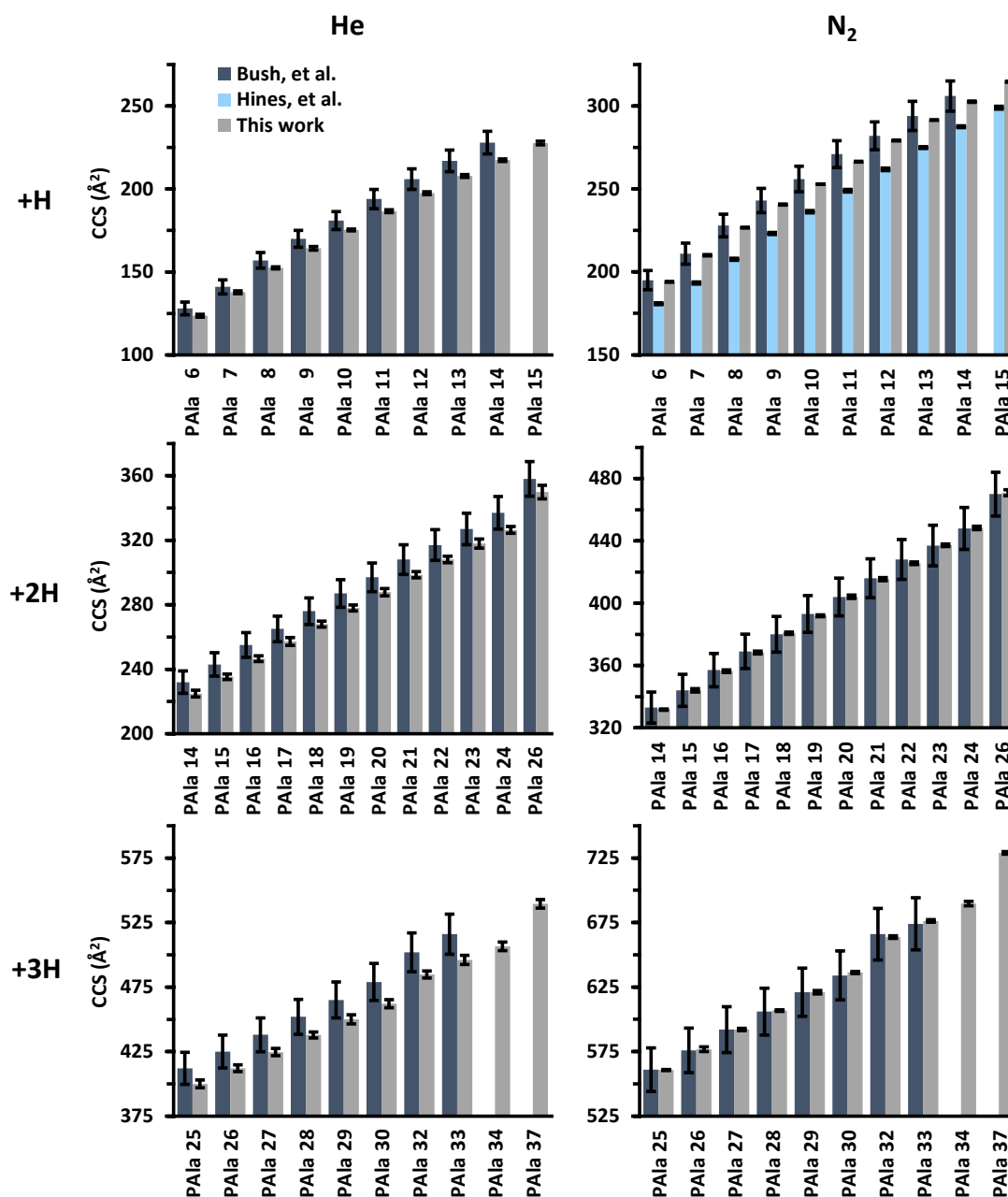


Figure D.7 Polyalanine values compared to previously published values^{2,3} for helium (left column) and nitrogen (right column) drift gases. Each row represents a different charge state family. The values reported from this work were calculated using a drift tube effective length that was determined from comparison of tune mix values in nitrogen to values gathered on a gridded instrument also operated in nitrogen¹. Adapted from Caleb B. Morris, Jody C. May, Katrina L. Leaprot, and John A. McLean, “Evaluating Separation Selectivity and Collision Cross Section Measurement Reproducibility in Helium, Nitrogen, Argon, and Carbon Dioxide Drift Gases for Drift Tube Ion Mobility-Mass Spectrometry,” *Journal of the American Society for Mass Spectrometry* 2019 (in press).

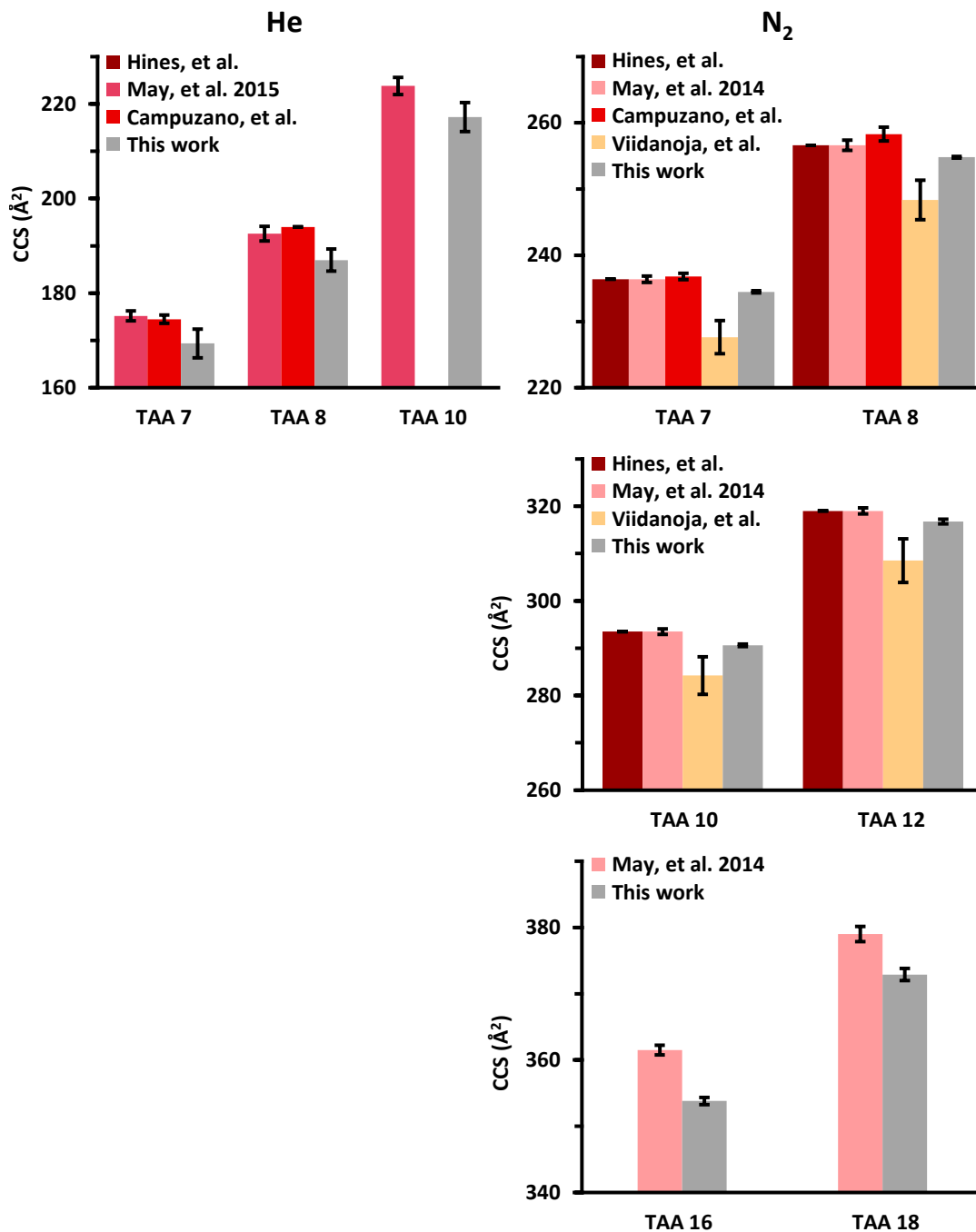


Figure D.8 TAA values compared to previously published values²⁻⁷ for helium (left column) and nitrogen (right column) drift gases. The effective length used in this work was the same as used to for the measurements in Figure D.7. Adapted from Caleb B. Morris, Jody C. May, Katrina L. Leaptrot, and John A. McLean, "Evaluating Separation Selectivity and Collision Cross Section Measurement Reproducibility in Helium, Nitrogen, Argon, and Carbon Dioxide Drift Gases for Drift Tube Ion Mobility-Mass Spectrometry," *Journal of the American Society for Mass Spectrometry* 2019 (in press).

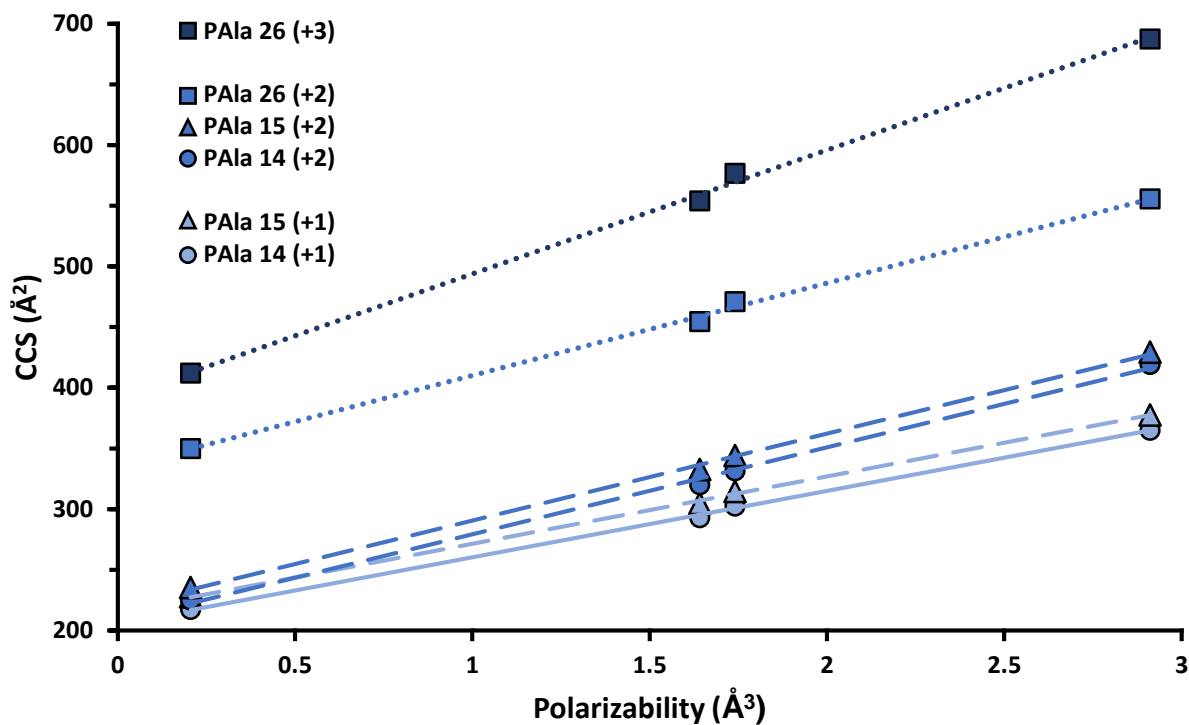


Figure D.9 CCS values (in square angstroms) plotted as a function of drift gas polarizability (in cubic angstroms) for multiple charge states of poly-DL-alanine, with linear fits for each analyte ion. The linear fits within each charge state exhibit similar slopes, whereas the slopes increase as the charge state increases, indicating a stronger contribution to the drift gas polarizability. Adapted from Caleb B. Morris, Jody C. May, Katrina L. Leaptrot, and John A. McLean, "Evaluating Separation Selectivity and Collision Cross Section Measurement Reproducibility in Helium, Nitrogen, Argon, and Carbon Dioxide Drift Gases for Drift Tube Ion Mobility-Mass Spectrometry," *Journal of the American Society for Mass Spectrometry* 2019 (in press).

Table D.1 Gas-specific instrument parameters which yield CCS measurements exhibiting high reproducibility and correspondence to literature. The header titles correspond to the names of the tabs and instrument controls found in the vendor acquisition software. For all gases, data is acquired at each drift field for 30 seconds. Adapted from Caleb B. Morris, Jody C. May, Katrina L. Leaprot, and John A. McLean, "Evaluating Separation Selectivity and Collision Cross Section Measurement Reproducibility in Helium, Nitrogen, Argon, and Carbon Dioxide Drift Gases for Drift Tube Ion Mobility-Mass Spectrometry," Journal of the American Society for Mass Spectrometry 2019 (in press).

	Source					IM Trap	
	Gas Temp. (°C)	Drying Gas (L/min)	Nebulizer (psig)	Sheath Gas Temp. (°C)	Sheath Gas Flow (L/min)	Trap Fill Time (μs)	Trap Release Time (μs)
Helium	325	13	20	275	12	40000	100
Nitrogen							
Argon							
Carbon Dioxide							

	IM-FrontFunnel			IM-DriftTube		Pressure		
	Trap Funnel Delta (V)	Trap Funnel RF (V _{pp})	Trap Funnel Exit (V)	Drift Tube Entrance Voltage (V)	Drift Tube Exit Voltage (V)	High Pressure Funnel (Torr)	Trap Funnel (Torr)	Drift Tube (Torr)
Helium	180	150	10	874, 974, 1074, 1174, 1274, 1374, 1474	224	4.35	3.72	3.95
Nitrogen				1074, 1174, 1274, 1374, 1474, 1574, 1674		4.80	3.80	
Argon						3.74		
Carbon Dioxide						4.30	3.72	

Table D.2 CCS measurements for all analyte ions investigated in this work. CCS values are reported as an average of five replicate measurements made on multiple days. Analytes are reported in this table if they were consistently observed across all drift gases and days and had a %RSD of 0.7% or less in helium and 0.5% or less in other drift gases. The values reported here were calculated from an effective length of 78.06 cm determined for this instrument by comparison of HFAP ^{DT}CCS_{N₂} values to measurements obtained on a specially-modified reference instrument.¹ Adapted from Caleb B. Morris, Jody C. May, Katrina L. Leaprot, and John A. McLean, “Evaluating Separation Selectivity and Collision Cross Section Measurement Reproducibility in Helium, Nitrogen, Argon, and Carbon Dioxide Drift Gases for Drift Tube Ion Mobility-Mass Spectrometry,” *Journal of the American Society for Mass Spectrometry* 2019 (in press).

Name	Ion Exact Mass	Charge State	Adduct	He		N ₂		Ar		CO ₂	
				CCS	%RSD	CCS	%RSD	CCS	%RSD	CCS	%RSD
HFAP 322	322.0487	1	+H	96.30	1.38	153.78	0.11	148.00	0.20	203.74	0.21
HFAP 622	622.0295	1	+H	135.27	0.77	203.15	0.09	194.29	0.21	259.98	0.13
HFAP 922	922.0103	1	+H	171.74	0.81	243.93	0.08	234.31	0.16	294.68	0.11
HFAP 1222	1221.9911	1	+H	204.10	0.76	282.46	0.09	271.81	0.11	332.82	0.11
HFAP 1522	1521.9720	1	+H	234.01	0.70	317.37	0.07	305.92	0.11	367.98	0.12
HFAP 1822	1821.9529	1	+H	262.79	0.73	351.00	0.09	338.52	0.09	402.55	0.16
HFAP 2122	2121.9337	1	+H	290.34	0.72	382.72	0.14	369.96	0.13	435.67	0.13
HFAP 2422	2421.9145	1	+H	316.49	0.73	412.40	0.21	399.70	0.12	467.25	0.14
HFAP 2722	2721.8954	1	+H	341.79	0.73	440.42	0.31	428.90	0.15	498.08	0.11
D-(+)-Maltose	365.1060	1	+Na	99.54	1.34	179.72	0.09	167.24	0.23	246.97	0.10
D-(+)-Maltose	381.0799	1	+K	103.12	0.83	181.89	0.11	170.03	0.21	251.92	0.36
Maltotriose	527.1588	1	+Na	132.14	0.77	211.11	0.12	199.90	0.20	278.33	0.21
Maltotriose	543.1327	1	+K	132.47	0.70	212.07	0.08	200.66	0.22	280.84	0.25
Maltotetraose	689.2116	1	+Na	147.88	0.67	231.29	0.13	220.17	0.27	301.80	0.31
Maltopentaose	851.2644	1	+Na	171.04	0.58	257.24	0.15	246.32	0.30	330.98	0.29
Maltopentaose	867.2384	1	+K	171.50	0.74	258.17	0.28	247.33	0.25	333.73	0.49
Maltohexaose	1013.3173	1	+Na	189.94	0.70	281.45	0.17	270.63	0.29	359.44	0.24
Maltoheptaose	1175.3701	1	+Na	206.45	0.66	299.65	0.15	288.22	0.29	377.75	0.32
PAIa 6	445.2411	1	+H	123.68	0.70	194.02	0.15	186.07	0.23	250.40	0.42
PAIa 7	516.2782	1	+H	137.76	0.61	210.05	0.16	201.61	0.15	266.97	0.27
PAIa 8	587.3153	1	+H	152.45	0.39	226.70	0.10	217.87	0.17	283.87	0.21
PAIa 9	658.3524	1	+H	164.28	0.66	240.58	0.14	231.75	0.16	298.05	0.06
PAIa 10	729.3895	1	+H	175.32	0.29	252.98	0.05	243.80	0.27	310.86	0.12
PAIa 11	800.4266	1	+H	186.58	0.47	266.43	0.09	256.93	0.14	325.31	0.21
PAIa 12	871.4637	1	+H	197.46	0.42	279.19	0.10	269.64	0.19	339.30	0.21
PAIa 13	942.5008	1	+H	207.83	0.42	291.49	0.07	281.80	0.20	352.52	0.26
PAIa 14	1013.5380	1	+H	217.38	0.35	302.56	0.13	292.99	0.18	365.12	0.18
PAIa 15	1084.5751	1	+H	227.72	0.46	314.62	0.08	304.72	0.12	377.70	0.30

PAIa 14	1014.5457	2	+H	224.89	0.96	331.65	0.13	320.03	0.49	419.08	0.32
PAIa 15	1085.5829	2	+H	235.31	0.71	344.05	0.31	332.61	0.67	429.48	0.17
PAIa 16	1156.6200	2	+H	246.53	0.73	356.30	0.23	343.25	0.45	442.25	0.17
PAIa 17	1227.6571	2	+H	257.17	0.94	368.24	0.24	354.66	0.21	452.93	0.13
PAIa 18	1298.6942	2	+H	268.00	0.70	380.74	0.21	366.49	0.33	464.61	0.25
PAIa 19	1369.7313	2	+H	278.02	0.65	391.89	0.14	377.18	0.26	476.48	0.16
PAIa 20	1440.7685	2	+H	287.80	0.81	404.15	0.27	388.87	0.23	487.54	0.16
PAIa 21	1511.8056	2	+H	298.57	0.65	415.35	0.24	400.82	0.83	498.36	0.19
PAIa 22	1582.8427	2	+H	308.06	0.67	425.66	0.20	409.75	0.33	509.95	0.28
PAIa 23	1653.8798	2	+H	317.95	0.88	437.18	0.21	420.10	0.54	521.70	0.17
PAIa 24	1724.9169	2	+H	326.39	0.65	448.33	0.24	432.49	0.62	531.52	0.18
PAIa 26	1866.9911	2	+H	349.89	1.20	470.87	0.40	454.44	0.33	555.51	0.28
PAIa 25	1796.9618	3	+H	399.94	0.76	560.74	0.07	539.10	0.34	672.22	0.34
PAIa 26	1867.9990	3	+H	412.11	0.63	576.82	0.31	554.01	0.27	687.38	0.40
PAIa 27	1939.0361	3	+H	424.61	0.67	592.10	0.15	567.88	0.31	702.88	0.67
PAIa 28	2010.0732	3	+H	437.84	0.54	606.82	0.10	582.61	0.38	721.15	0.37
PAIa 29	2081.1103	3	+H	449.98	0.79	620.94	0.21	598.68	0.34	732.70	0.14
PAIa 30	2152.1474	3	+H	462.05	0.68	636.26	0.14	610.94	0.31	749.72	0.46
PAIa 32	2294.2216	3	+H	484.79	0.57	663.67	0.15	637.58	0.25	774.74	0.34
PAIa 33	2365.2587	3	+H	496.05	0.71	676.23	0.15	650.47	0.70	787.85	0.30
PAIa 34	2436.2958	3	+H	506.59	0.66	689.67	0.24	665.06	0.54	804.93	0.49
PAIa 37	2649.4072	3	+H	539.58	0.62	729.03	0.14	700.89	0.42	845.26	0.44
TAA 7	410.4726	1	+	169.38	1.80	234.48	0.07	225.76	0.33	284.26	0.17
TAA 8	466.5351	1	+	187.00	1.25	254.81	0.05	245.32	0.29	305.61	0.17
TAA 10	578.6603	1	+	217.24	1.42	290.58	0.09	280.59	0.24	344.70	0.16
TAA 12	690.7855	1	+	240.42	1.39	316.77	0.16	307.00	0.24	373.60	0.15
TAA 16	915.0359	1	+	273.51	1.32	353.81	0.15	343.15	0.23	412.76	0.21
TAA 18	1027.1611	1	+	290.49	1.48	372.90	0.25	362.38	0.26	433.63	0.19

Table D.3 CCS measurements for analytes that were not observed across all drift gases and days but still had a %RSD of 0.7% or less in helium and 0.5% or less in other drift gases. Relative standard deviations are based on three to five runs. Adapted from Caleb B. Morris, Jody C. May, Katrina L. Leaptrot, and John A. McLean, “Evaluating Separation Selectivity and Collision Cross Section Measurement Reproducibility in Helium, Nitrogen, Argon, and Carbon Dioxide Drift Gases for Drift Tube Ion Mobility-Mass Spectrometry,” *Journal of the American Society for Mass Spectrometry* 2019 (in press).

Name	Ion Exact Mass	Charge State	Adduct	He		N ₂		Ar		CO ₂	
				CCS	%RSD	CCS	%RSD	CCS	%RSD	CCS	%RSD
α-D-Glucose	203.05	1	+Na	-	-	147.15	0.11	-	-	-	-
PAIa 5	374.20	1	+H	-	-	179.77	0.16	172.05	0.43	238.16	0.69
PAIa 13	471.75	2	+H	212.79	0.70	318.71	0.11	304.81	0.29	406.59	0.70
PAIa 25	897.98	2	+H	335.15	0.76	456.95	0.33	440.81	0.53	542.60	0.52
PAIa 27	969.01	2	+H	356.01	1.33	479.65	0.82	466.32	1.38	561.03	0.88
PAIa 29	1040.05	2	+H	379.87	0.74	505.68	0.33	489.84	1.58	-	-
PAIa 30	1075.57	2	+H	389.40	0.92	518.75	0.72	-	-	-	-
PAIa 24	575.31	3	+H	385.00	0.73	543.79	0.21	523.53	0.40	656.03	0.21
PAIa 31	741.06	3	+H	471.40	0.77	646.84	0.21	623.48	0.30	758.37	0.33
PAIa 35	835.78	3	+H	517.05	0.68	699.31	0.35	671.81	0.46	813.57	0.19
PAIa 36	859.46	3	+H	526.31	0.77	712.14	0.18	692.38	0.76	829.33	0.52
PAIa 38	906.81	3	+H	547.16	0.82	735.72	0.33	716.79	1.75	849.94	0.69
PAIa 39	930.49	3	+H	559.58	0.58	749.15	0.46	728.90	1.44	-	-
PAIa 40	954.17	3	+H	572.00	0.63	760.07	0.43	-	-	882.56	1.20
PAIa 41	977.85	3	+H	580.28	0.53	775.36	0.21	755.62	2.03	892.86	0.66
TAA 2	130.16	1	+	-	-	124.64	0.14	120.34	0.68	176.85	0.66
TAA 3	186.22	1	+	87.47	1.06	145.44	0.07	140.41	0.25	196.31	0.24
TAA 4	242.28	1	+	109.60	0.33	166.52	0.09	161.00	0.25	216.48	0.21
TAA 5	298.35	1	+	130.81	2.45	189.59	0.09	183.17	0.33	238.53	0.26
TAA 6	354.41	1	+	149.68	0.93	212.05	0.11	204.54	0.30	261.02	0.19

Table D.4 Chemical standards used in this work, their vendor sources, product numbers, and CAS numbers. Adapted from Caleb B. Morris, Jody C. May, Katrina L. Leaptrot, and John A. McLean, "Evaluating Separation Selectivity and Collision Cross Section Measurement Reproducibility in Helium, Nitrogen, Argon, and Carbon Dioxide Drift Gases for Drift Tube Ion Mobility-Mass Spectrometry," *Journal of the American Society for Mass Spectrometry* 2019 (in press).

Analyte	Source	Product#	CAS#
HFAPs (ESI Tuning Mixture)	Agilent Technologies	G1969-85000	(321 Da) 957-13-1 (621 Da) 186817-57-2 (921 Da) 58943-98-9 (1221 Da) 186406-47-3 (1521 Da) 16059-16-8 (1821 Da) 186406-48-4 (2121 Da) 3830-74-8 (2421 Da) 186406-49-5 (2721 Da) 186043-67-4
D-(+)-Maltose	Sigma-Aldrich	63419	6363-53-7
Isomaltotriose	Sigma-Aldrich (Supelco)	4-7884	3371-50-4
Maltotetraose	Sigma-Aldrich (Supelco)	4-7877	34612-38-9
Maltopentaose	Sigma-Aldrich (Supelco)	4-7876	34620-76-3
Maltohexaose	Sigma-Aldrich (Supelco)	4-7873	34620-77-4
Maltoheptaose	Sigma-Aldrich	M7753	34620-78-5
Poly-DL-Alanine	Sigma-Aldrich	P9003	25281-63-4
TAA 7 (Tetraheptylammonium Bromide)	Sigma-Aldrich	87301	4368-51-8
TAA 8 (Tetraoctylammonium Bromide)	Acros Organics	352100050	14866-33-2
TAA 10 (Tetradecylammonium Bromide)	Sigma-Aldrich	87578	14937-42-9
TAA 12 (Tetradodecylammonium Bromide)	Sigma-Aldrich	87249	14866-34-3
TAA 16 (Tetrahexadecylammonium Bromide)	Sigma-Aldrich	367524	139653-55-7
TAA 18 (Tetraoctadecylammonium Bromide)	Alfa Aesar	20582	63462-99-7

Table D.5 Slope, intercept, and regression coefficient values corresponding to the linear fits in Figure 5.6 of the main text. Adapted from Caleb B. Morris, Jody C. May, Katrina L. Leaptrot, and John A. McLean, "Evaluating Separation Selectivity and Collision Cross Section Measurement Reproducibility in Helium, Nitrogen, Argon, and Carbon Dioxide Drift Gases for Drift Tube Ion Mobility-Mass Spectrometry," *Journal of the American Society for Mass Spectrometry* 2019 (in press).

	Slope (\AA^{-1})	Intercept (\AA^2)	R^2
HFAP m/z 322 (+1)	39.389	85.779	0.996
HFAP m/z 922 (+1)	45.290	161.512	0.998
Maltose (+1)	54.075	84.732	0.993
Maltohexaose (+1)	62.163	173.122	0.996
PAIa 6 (+1)	46.544	112.071	0.998
PAIa 13 (+1)	53.261	195.594	0.999
PAIa 14 (+2)	71.291	206.624	0.998
TAA 7 (+1)	42.235	158.816	0.998
TAA 16 (+1)	51.246	260.976	0.998

D.2 References

1. Stow, S. M.; Causon, T. J.; Zheng, X. Y.; Kurulugama, R. T.; Mairinger, T.; May, J. C.; Rennie, E. E.; Baker, E. S.; Smith, R. D.; McLean, J. A.; Hann, S.; Fjeldsted, J. C. *Anal. Chem.* 2017, 89 (17), 9048-9055.
2. Hines, K. M.; May, J. C.; McLean, J. A.; Xu, L. B. *Anal. Chem.* 2016, 88 (14), 7329-7336.
3. Bush, M. F.; Campuzano, I. D. G.; Robinson, C. V. *Anal. Chem.* 2012, 84 (16), 7124-7130.
4. May, J. C.; McLean, J. A. *Proteomics* 2015, 15 (16), 2862-2871.
5. May, J. C.; Goodwin, C. R.; Lareau, N. M.; Leaptrot, K. L.; Morris, C. B.; Kurulugama, R. T.; Mordehai, A.; Klein, C.; Barry, W.; Darland, E.; Overney, G.; Imatani, K.; Stafford, G. C.; Fjeldsted, J. C.; McLean, J. A. *Anal. Chem.* 2014, 86 (4), 2107-2116.
6. Campuzano, I.; Bush, M. F.; Robinson, C. V.; Beaumont, C.; Richardson, K.; Kim, H.; Kim, H. I. *Anal. Chem.* 2012, 84 (2), 1026-1033.
7. Viidanoja, J.; Sysoev, A.; Adamov, A.; Kotiaho, T. *Rapid Commun. Mass Spectrom.* 2005, 19 (21), 3051-3055.

APPENDIX E

CURRICULUM VITAE

Caleb B. Morris

Vanderbilt University Department of Chemistry | 7330 Stevenson Center, Station B 35-1822,
Nashville, TN 37235 | Lab: (615) 343-4563 | caleb.morris@vanderbilt.edu

Education

Ph.D. Chemistry | May 2019 | Vanderbilt University: Nashville, TN

- Dissertation: Molecular Descriptor on the Basis of Structural Analysis in Ion Mobility-Mass Spectrometry
- Research Director: Prof. John A. McLean (Chemistry)

B.S. Chemistry | May 2012 | University of Kentucky: Lexington, KY

- Research Director: Prof. Kevin Schey (Biochemistry)
- Research Director: Prof. Jurgen Rohr (Chemistry)
- Research Director: Prof. Robert Yokel (Pharmacology)

Publications

- Morris, C. B.; May, J. C.; Leaptrot, K. L.; McLean, J. A. "Evaluating Separation Selectivity and Collision Cross Section Measurement Reproducibility in Helium, Nitrogen, Argon, and Carbon Dioxide Drift Gases for Drift Tube Ion Mobility-Mass Spectrometry." *Anal. Chem.* (in press)
- Morris, C. B.; Poland, J. C.; May, J. C.; McLean, J. A. "Fundamentals of Ion Mobility Mass Spectrometry for the Analysis of Biomolecules," Book Chapter in *Ion Mobility Mass Spectrometry – Methods and Protocols*, Springer Nature (to be published in 2019)
- Nichols, C. M.; Dodds, J. N.; Rose, B. S.; Picache, J. A.; Morris, C. B.; Codreanu, S. G.; May, J. C.; Sherrod, S. D.; McLean, J. A. "Untargeted Molecular Discovery in Primary Metabolism: Collision Cross Section as a Molecular Descriptor in Ion Mobility-Mass Spectrometry." *Anal. Chem.* **2018**, *90* (24), 14484-14492.
- May, J. C.; Morris, C. B.; McLean, J. A. "Ion Mobility Collision Cross Section Compendium." *Anal. Chem.* **2017**, *89* (2), 1032-1044.
- May, J. C.; Goodwin, C. R.; Lareau, N. M.; Leaptrot, K. L.; Morris, C. B.; Kurulugama, R. T.; Mordehai, A.; Klein, C.; Barry, W.; Darland, E.; Overney, G.; Imatani, K.; Stafford, G. C.; Fjeldsted, J. C.; McLean, J. A. "Conformational Ordering of Biomolecules in the Gas Phase: Nitrogen Collision

Cross Sections Measured on a Prototype High Resolution Drift Tube Ion Mobility-Mass Spectrometer.” *Anal. Chem.* **2014**, 86 (4), 2107-2116.

Presentations

Orals

- Morris, C. B.; May, J. C.; McLean, J. A. “Evaluation and Prediction of Biomolecular Class in Ion Mobility-Mass Spectrometry.” 37th Area Collegiate Chemistry Meeting, Martin, TN (Spring 2014).

Posters

- May, J. C.; Morris, C. B.; McLean, J. A. “A Canonical Conformational Space Map of Over 10,000 Collision Cross Section Values.” 63rd ASMS, St. Louis, MO (Summer 2015).
- Morris, C. B.; May, J. C.; McLean, J. A. “Predictive Mathematical Descriptors of Biological Class Trends in Ion Mobility-Mass Spectrometry Analysis.” 62nd ASMS, Baltimore, MD (Summer 2014)

Research Experience

- **Ph.D. Advisor: John A. McLean, Ph.D. | 2013 – 2019 | Analytical Chemistry** – Mathematical descriptor development for ion mobility trends/Creation of collision cross section databases/Establishment of instrument parameters for alternate drift gases for a drift tube ion mobility-mass spectrometer (Agilent 6560 w/ gas kit)
- **Undergraduate Advisor: Kevin Schey, Ph.D. | 2012 | Biochemistry** – Integral membrane protein tissue extraction and digestion/Triple quad analysis with reverse phase chromatography/Fragmentation spectra analysis of tryptic digests
- **Undergraduate Advisor: Jurgen Rohr, Ph.D. | 2011 | Organic Chemistry** – Bacteria culture/Protein and secondary metabolite purification
- **Undergraduate Advisor: Robert Yokel, Ph.D. | 2010-2011 | Pharmacology** – Preparation of rat tissue for mass spectrometry analysis/Development of inline aluminum chelation device for total parenteral nutrition packs

Teaching Experience

- **Recitation Teaching Fellow for General Chemistry Lecture | 3 semesters** – Taught 6 recitation sections per semester/created and administered quizzes/assisted students with challenge problems (~25 students/section).
- **Head Teaching Assistant for General Chemistry Laboratory Courses | 6 semesters** – Managed other teaching assistants and ensured their duties were fulfilled (12-18 teaching assistants/semester).
- **Teaching Assistant for General Chemistry Laboratory Course | 8 semesters** – Taught 2 sections per week or 1 section when Head Teaching Assistant (~24 students per section).
- **Teaching Assistant for General Chemistry for Non-Science Majors Laboratory Course | 3 semesters** – Taught 1 section per week and assisted with course development (15-20 students).